The neural basis of motor control and learning in the vestibulocerebellar system

The neural basis of motor control and learning in the vestibulocerebellar system

Bin Wu

The research described in this thesis was performed at the department of Neuroscience, Erasmus Medical Center Rotterdam.

The research in this thesis was financially supported by European Research Council (ERC-Stg, ERC-Adv and ERC-PoC), China Scholarship Council (CSC), Netherlands Organization for Scientific Research (NOW-ALW) and Dutch Organization for Medical Sciences (ZonMW) grants.

ISBN: 978-94-6361-288-3

Layout: Optima Grafische Communicatie
Cover design: the author of this book (image adapted from www.fengniao.com)
Printed by: Optima Grafische Communicatie

The author appreciates the kind financial support for printing this thesis from: Erasmus University Rotterdam and Scientifica.

The neural basis of motor control and learning in the vestibulocerebellar system

De neurale basis van motor controle en motorisch leren in het vestibulocerebellaire systeem

Proefschrift

ter verkrijging van de graad van doctor aan de
Erasmus Universiteit Rotterdam
op gezag van rector magnificus

Prof. Dr. R.C.M.E. Engels

en volgens besluit van het College voor Promoties

De openbare verdediging zal plaatsvinden op

dinsdag 2 juli 2019
om 15:30 uur

Bin Wu

geboren te Qingdao, China

Erasmus University Rotterdam

Erasmus

PROMOTIECOMMISSIE

Promotor:	Prof. Dr. C.I. De Zeeuw
Overige leden:	Dr. T.J.H. Ruigrok Prof. Dr. S.A. Kushner Prof. Dr. F.E. Hoebeek
Co-promotor:	Dr. M. Schonewille

To my parents

献给我的父母

TABLE OF CONTENTS

Chapter 1

Introduction

The human brain has 100 billion neurons, each neuron connected to 10,000 other neurons. Sitting on your shoulders is the most complicated object in the known universe.

— Michio Kaku (American physicist)

The brain, the most complex and important organ in the nervous system, gives rise to our ability to sense, think, remember, and act. It consists of billions of neurons communicating with one another by means of axons, which carry trains of action potentials and convey either sensory or motor information to other parts of the body. A fundamental challenge nowadays in neuroscience is to understand how our brain processes sensory information in order to generate accurate perception and guide appropriate behavioral responses.

Intriguingly, although the mammalian cerebellum accounts for only approximately 10% of the total brain weight and volume, it contains at least 50% of all neurons[1-3], thereby outnumbering all other brain areas combined. With this thesis, I focus on the multiple aspects of the neural activities within the cerebellum, including the development, anatomy, physiology and function. By using the vestibulocerebellar system as a model, I try to understand how the cerebellum processes sensory information to drive motor behaviors and learning.

Chapter 1.1

The neuronal machine of the cerebellum

Anatomy and structure

The cerebellum, meaning "little brain" in Latin, is a highly organized brain area located dorsally to the pons and medulla of the brainstem (**Fig.1**).

It is symmetrically connected with the rest of the brain through three peduncles: superior, middle, and inferior. The superior peduncle contains most of cerebellar output fibers, projecting to the brain stem, red nucleus, hypothalamus, and thalamus; the middle peduncle contains exclusively afferents from the both ipsilateral and contralateral pontine nuclei; and the inferior cerebellar peduncle contains afferent fibers from the brain stem including inferior olive and the spinal cord, as well as cerebellar efferent fibers to the vestibular nuclei.

Longitudinally, the cerebellum is composed of three regions from medial to lateral: the vermis, the paravermis and the hemisphere, which are further divided into 10 lobules (**Fig. 2A**). In the sagittal plane, based on zebrin expression, the vermis of cerebellum is further divided into 4 zones: anterior, central, posterior and the nodular zone (**Fig. 2B**). There are three pairs of nuclei embedded in the white matter (see descriptions in the following section).

In the cerebellum, the flocculonodular lobe is the most conserved part in terms of phylogenesis. The vestibular nuclei (VN) are situated downstream of the flocculonodular output. These two areas constitute the larger part of the vestibulocerebellar system, which is thought to be in charge of regulating balance, coordination as well as eye movements.

Cyto-architecture and neural circuitry

The cerebellum comprises three anatomical components: cerebellar cortex, white matter and cerebellar nuclei.

Cerebellar cortex

The cerebellar cortex is made up of stereotyped three stereotyped layers that are well-organized: the molecular layer, the granular layer and the Purkinje cell layer[6,7] (**Fig. 3**). The molecular layer is the outermost layer, containing two types of inhibitory interneurons: the stellate cells (SC) and the basket cells (BC), collectively referred to as molecular layer interneurons (MLIs). The granular layer is located at the most inner part, which contains thousands of small excitatory granule cells (GrC) as well as a few inhibitory Golgi cells (GoC). The same layer also includes the unipolar brush cells (UBC), which are mainly found in the vestibulocerebellum. The intermediate layer, or Purkinje cell (PC) layer, is only composed of PCs, the largest cells in the cerebellum, forming the sole inhibitory output of the cerebellar cortex.

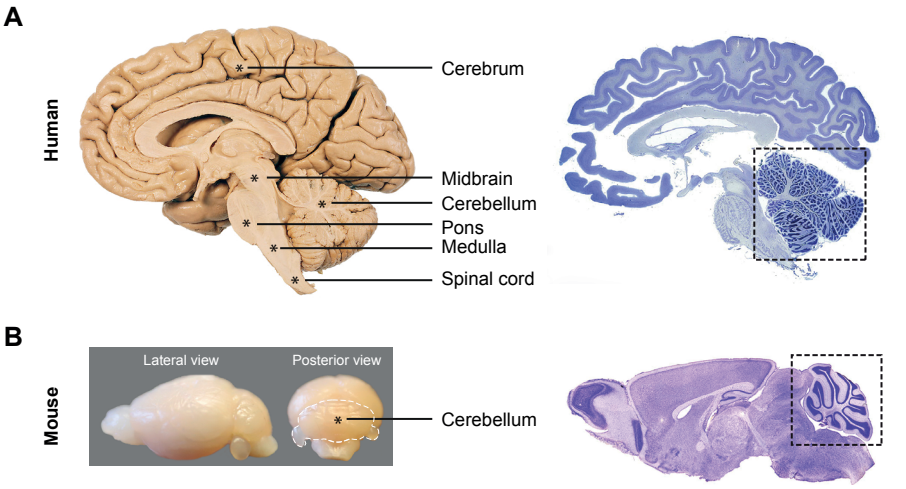

Figure 1. Location of the cerebellum in the human (A) and mouse (B) brain. Nissl staining of sagittal sections are shown on the right, with highlighted cerebellum in the black squares, adapted from the Human Brain Atlas (Brain Biodiversity Bank, Michigan state university) and Paxinos Mouse Atlas (Academic Press,2001).

There are predominantly two types of inputs in the cerebellar cortex: the mossy fibers (MF), carrying sensorimotor information, and the climbing fibers (CF), primarily relaying motor error signals (**Fig. 4**). MFs are derived from various sources including the brainstem as well as the spinal cord and supply extensive excitatory inputs to the granule cell layer. The ascending GrC axons bifurcate in the molecular layer and form parallel fibers (PF). PFs run transversely to the PC dendritic trees, but parallel to each other, thus forming an extensive network innervating PCs, GoCs and MLIs. The other major input, the CF, originating from the contralateral inferior olive (IO), passes through the granule cell layer and terminates on Purkinje cell dendrites.

Cerebellar Nuclei

Cerebellar nuclei (CN), consisting of three pairs of sub-nuclei, are embedded in the middle of cerebellar white matter. From medial to lateral, they are the medial cerebellar nuclei (MCN) (fastigial nuclei in humans), the anterior and posterior interposed nuclei (AIN and PIN) (emboliform and globose nuclei in humans) and the lateral nuclei (LCN) (dentate nuclei in humans) [9], subsequently (**Fig. 2**). CN receives substantial inhibitory inputs of PCs and few excitatory inputs from MFs and CFs collaterals[10,11]. Each nucleus targets different brain areas: MCN targets the brainstem and the spinal cord; AIN and PIN project to the thalamus and mid-brain; LCN also contacts thalamus. Interestingly, the olivo-cortico-nuclear system is highly organized: specific longitudinal zones in the cerebellar cortex connect specific areas in the CN and IO, thus forming 12 functional cerebellar modules[12] (**Fig. 5**). CN neurons, together with vestibular nuclei (VN, see more details in **Chapter 1.2**), form the ultimate

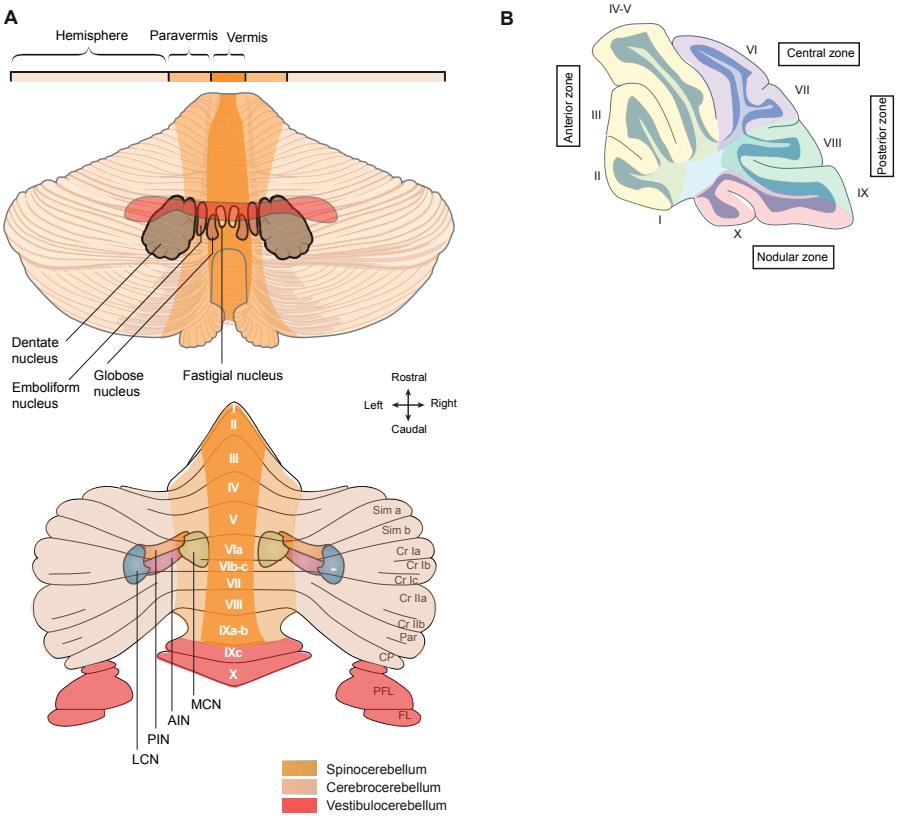

Figure 2. Gross anatomical segmentation of the cerebellum. A, Schematic representation of a dorsal view of the human cerebellum (top) and unfolded mouse (bottom) cerebellum, as well as the superimposed deep cerebellar nuclei. The functional regions, named vestibulocerebellum, spinocerebellum and cerebrocerebellum, are indicated in three different colors. Note that the widest folia are found in the lateral part (hemispheres). The hemispheres spread overtly more widely than that in the mice, while the flocculonodular lobe (vestibulocerebellum) is relatively larger in the latter. Adapted from (Principles of Neural Science, 5th edition Kandel et al. 2012)[4] and (Sugihara et al. 2007)[5]. **B**, Sagittal view of the mouse cerebellum revealing 10 different lobules (I-X), which can be classified into 4 zones: the anterior zone (lobules I-V), the central zone (lobule VI-VII), the posterior zone (lobules VIII to dorsal IX), and the nodular zone (ventral lobule IX and lobule X). Sim, simplex; Cr, Crus; Par, paramedian lobule; CP, Copula Pyramidis; PFL, paraflocculus; PL, flocculus.

output of the cerebellar cortex; however, the exact wiring circuitry and how the input convergence occurs during motor performance and learning are still elusive[13].

Physiology in the cerebellar cortex

PCs are featured with a striking pace-making activity, which is presumably mediated by a specific mixture of various Na+ currents and K+ current channels[14]. This property of PCs is so robust that it will generate spontaneous action potentials even in dissociated cells.

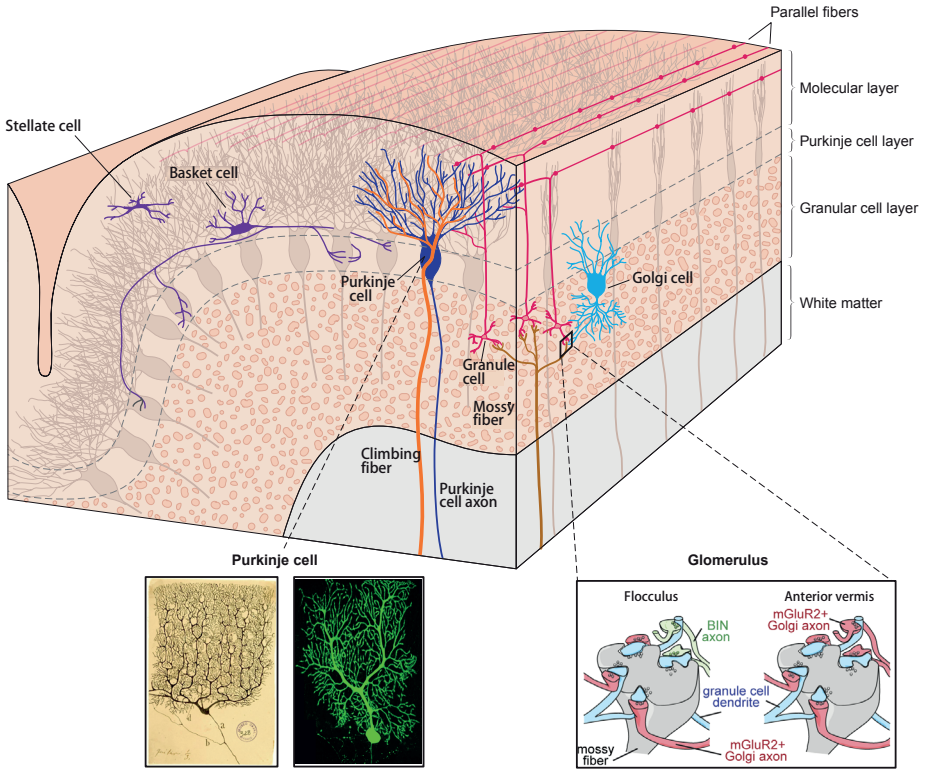

Figure 3. Scheme of the cerebellar cortex with the most important neurons organized into three layers. Purkinje cells (PC), the biggest neurons in the cerebellum, form the sole output of the cerebellar cortex. Parallel fibers run transversely to PCs and innervate PCs and molecular layer interneurons. Note that PC dendrites are prone to spread out in the parasagittal plane, but not in the transverse plane. Inhibitory stellate cells are located at more distal parts of the PC dendritic tree. Basket cells make contacts with PC somata. Granule cells, which are inhibited by Golgi cells, contact PCs through their ascending axons and parallel fibers. The glomerulus is formed by the terminals of mossy fibers (see inset), granule and Golgi cells. Climbing fibers, originating from the inferior olive (not shown), contact PCs in a one-on-one manner. Inset on the left shows Purkinje cell morphology drawn by Santiago Ramón y Cajal (1852-1934) and a mouse Purkinje cell stained with biocytin (middle inset). Right inset shows the detail of glomeruli in the granular layer or BIN cell (see **Chapter 4**). Adapted from (Principles of Neural Science, 5th edition, Kandel et al. 2012)[4]

There are two unique forms of action potential evoked by PC: simple spikes and complex spikes (**Fig. 5**). This specific spiking pattern makes single unit PC signals easy to identify in extracellular recordings[15] (see **Chapter 2** for methodology).

Simple spikes

Simple spikes are predominantly mediated by various cations, such as sodium, calcium and potassium ions[16] and can be observed even in slice without synaptic input[14,17,18]. It is commonly accepted that the interplay between transient, persistent, and resurgent Na^+

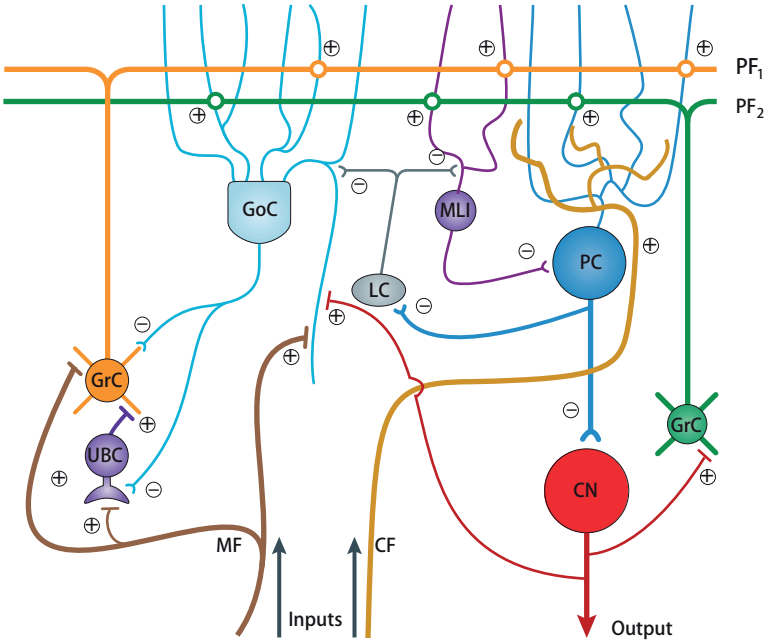

Figure 4. Synaptic connectivity of the cerebellar microcircuit. The two excitatory inputs to the cerebellum are the mossy fibers (MF) and climbing fibers (CF). Granule cells (GrC) with their PF together with PCs form the major throughput in the cerebellar cortex, whereas stellate and basket cells (collectively called MLI), send inhibitory innervation to the PCs. Golgi cells (GoC) also are innervated by parallel fibers and provide inhibitory feedback to the GrC dendrites. PCs inhibit neurons in the cerebellar nuclei (CN), which in turn excite GoC and GrC through an internal feedback pathway. In addition, excitatory unipolar brush cells (UBCs) and inhibitory Lugaro cells (LC) are superimposed into the networks. "+" and "-" indicate excitatory and inhibitory synapse respectively. Adapted from (Gao et al. 2012 & 2016)[7,8].

currents, and voltage-gated K^+ currents generate PCs' pace-making activity[19,20], while the firing rate and the regularity of PCs in vivo are mainly influenced by the convergence of excitatory and inhibitory synaptic inputs[21,22]. It has been shown that, when presynaptic PFs are activated, the α-amino-3-hydroxy-5-methyl-4-isoxazolepropionic acid (AMPA) receptors and metabotropic glutamate type 1 (mGluR1) receptors in the postsynaptic PCs, will lead to fast and slow excitatory postsynaptic currents (EPSCs), respectively. More importantly, the activation of mGluR1 triggers two different forms of synaptic signalling cascades: 1) IP3R-mediated Ca^{2+} release[23], 2) transient receptor potential cation channel, subfamily C, member 3 (TRPC3) mediated cation currents (see **Chapter 3**), to increase the intracellular calcium concentration. This increased intracellular calcium subsequently activates the voltage-gated calcium channels (VGCCs) that are located in PC dendritic spines, which will then cause the depolarization in the dendrite and spread towards the soma. Eventually, when the current spreads to the axon hillock and surpasses the threshold levels, voltage-gated sodium channels in this area will turn open. Consequently, a simple spike is evoked[24,25].

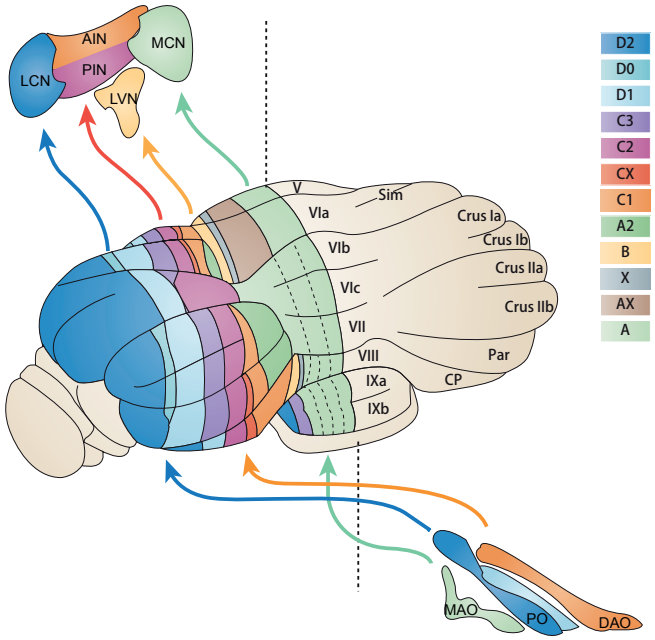

Figure 5. Modular organization of the olivo-cortico-nuclear system. Olivo-cerebellar projections are arranged in longitudinal bands in the cerebellar cortex, which are receiving input from a circumscribed sub-nucleus of the inferior olive and projecting to a confined area in the cerebellar nuclei. Regions in the inferior olive: DAO (Dorsal accessory olive), PO (Principal olive), MAO (Medial accessory olive) and regions in the DCN: MCN (Medial Nuclei), PIN (posterior Interposed Nuclei), AIN (anterior Interposed Nuclei) and LCN (Lateral Nuclei). Depending on the CF inputs and outputs, the cerebellar cortex is divided into twelve longitudinal zones (from lateral to medial): D2, D0, D1, C3, C2, CX, C1, A2, B, X, AX, A, and each is 1-2 mm wide. Adapted from (Apps and Hawkes, 2009)[12].

Complex spikes The complex spikes (CS), evoked through CF activation, is characterized as a somatic sodium spike and a few spikelets riding on a depolarization plateau[26]. The average spontaneous CS firing rate is about 1 Hz, but can increase to 10 Hz due to the specific conductances in the olivary neurons[27]. PCs that are contacted by neurons from the same olivary subnucleus can be activated synchronously due to the gap-junction-mediated electronic coupling in the IO[28]. In vivo, each CS is followed by a pause, so-called "climbing fiber pause", in the simple spike activity, which has not yet fully been explained[29].

The CS is initiated by glutamate release from numerous CF contact sites on a single PC, thus leading to a robust postsynaptic depolarization[30]. This process is mainly mediated by AMPAR, a NMDA and kainate receptors[31,32]. Subsequently, dendritic P/Q and T-type VGCCs are activated, and lead to the generation of the dendritic calcium spikes[33]. Similar to the simple spike, when the dendritic current propagates to the axon hillock, a fast sodium conductance will be inducted, leading to the initial spike in the CS waveform[34]. Following this is the plateau phase

which is putatively due to the de-inactivation of dendritic calcium channels and/or somatic resurgent sodium channels. It should be noted that after the first fast spike, there are several slow components, namely repolarization and after-hyperpolarization phase, which probably attribute to large (BK) and small (SK2) voltage-gated potassium channels, respectively[18,33]. (Also see introductions of the thesis of E. Galliano, 2013 and K. Zhou, 2017, EUR)[35,36].

Zebrin-identity

The apparent homogeneity of the cerebellum's crystalline cortical structure and the absence of clear structure-function relationships have long nourished the assumption that the cerebellar cortex was, for all practical purposes, physiologically uniform. This concept of a homogenous cortex existed despite accumulating evidence for the presence of a sub-organization in the cerebellar cortex. However, the cerebellar cortex can be further divided into smaller compartments in the sagittal plane by the expression of a molecular marker called zebrin II, a glycolytic enzyme aldolase C which is selectively expressed in PCs[5,37-39]. In particular, zebrin II is differentially expressed by symmetric bands of zebrin-positive and alternative zebrin-negative PCs (**Fig. 6**), and this kind of striped-organization is highly conserved in all vertebrate classes, varying from birds and mice up to primates including humans[12,40-42]. The CF input adheres to the zebrin-identified modules, and in turn, PCs with the same zebrin identity converge to designated parts of the cerebellar nuclei[5,43] (**Fig. 5**). Moreover, both the firing rate of simple spikes and complex spikes of cerebellar PCs were recently found to be selectively higher in zebrin-negative modules, which was proved subsequently to be the result of the intrinsic properties of PCs[44]. Given these features, it is becoming increasingly clear that zebrin-identified modules as more fundamental architecture not only differ in their input and output relations but also differ in operational capabilities and may play differential roles in distinct cerebellar function. Yet, how these well-defined cerebellar modules can give rise to differential forms of cerebellar learning remains to be elucidated. Recent technical developments that are available to tackle this question are addressed in **Chapter 3**.

Behavioral paradigms of motor control and learning

The cerebellum has mainly been implicated in various forms of motor behaviors and learning. Disruptions of cerebellar functioning, e.g. through stroke or neurodegenerative disorders, affect coordination and adaption of many types of behaviors such as gait, eye movements and even speech[45,46]. Thus, the key function of the cerebellum is sensorimotor control.

Compensatory eye movements

In the cerebellar field, many behavioral models have been developed in the laboratory in attempts to unravel the underlying neural principles of motor control and motor learning,

among which compensatory eye movements is likely to be one of the best-studied. Foveal species, like humans, are capable of capturing the image of a moving target by smooth pursuit. However, afoveal animals, such as the mouse, cannot stabilize the image on the retina in this way. Instead, they have to rely on compensatory eye movements which can be induced by the visual stimulation in light (OKR), vestibular stimulation in the dark (VOR) or in the light (visually enhanced VOR, VVOR) (**Fig. 7A**).

Motor performance in response to these stimulations was evaluated by calculating the gain (ratio of eye velocity to stimulus velocity) and phase (the lag of eye to stimulus in degrees) of the response. Motor learning was studied by subjecting mice to mismatched visual and vestibular input. Rotating the visual and vestibular stimuli in the same direction simultaneously in the light will induce a decrease of the gain of the VOR (gain-decrease), whereas if visual and vestibular stimuli are rotated out of phase, the gain of VOR will be increased (gain-increase) (see more in **Chapter 1.2**).

The flocculus and ventral part of paraflocculus, located in the ventrolateral cerebellum, are thought to be the anatomical structures responsible for the compensatory eye movements. More specifically, the flocculus mainly consists of 4 vestibular input-related zones based on the modulation of both simple and complex spikes with respect to optokinetic stimulation[48]. PCs in zone 2 and 4 respond best to the visual stimulation induced by horizontal rotation (vertical axis, so-called VA cells), and both the simple spike and complex spike exhibit clear discharge modulation changes relative to the horizontal optokinetic stimulation. While PCs in zone 1 and 3 respond optimally to the rotation around the horizontal

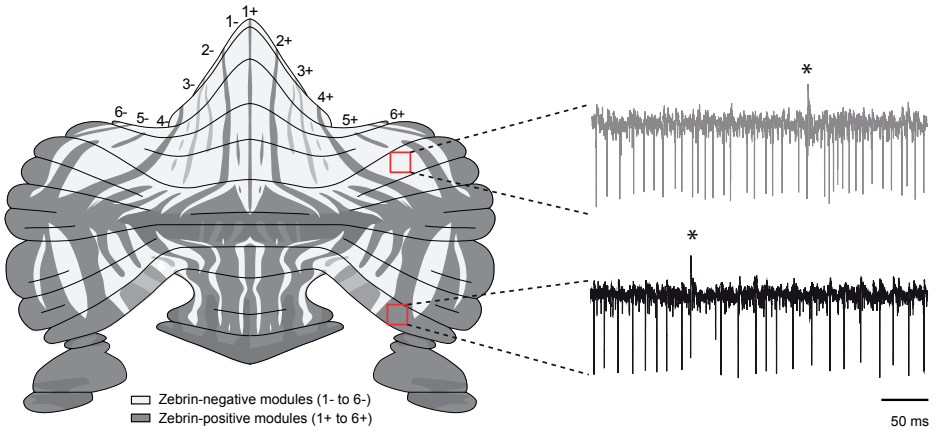

Figure 6. Purkinje cell activity differs based on zebrin identity. The alternation of zebrin-positive (gray) and zebrin-negative (white) zones gives rise to a striped pattern on the cerebellum cortex. Right, example traces of single unit Purkinje cell activity by extracellular recording in zebrin-positive and negative zones, respectively. Asterisks indicate complex spikes.

axis (so-called HA cells), and the discharge modulation predominantly exists under the vertical optokinetic stimulation. Notably, the multisensory information from both PFs and CFs reciprocally regulate the firing configuration of PC simple and complex spikes[49-52](**Fig. 7B**).

Eyeblink conditioning

The other most extensively studied form of motor learning is eyeblink conditioning. In a typical eyeblink conditioning experiment, a conditioned stimulus (CS), which usually is an auditory tone or a light stimulus, precedes the unconditioned stimulus (US), typically peri-ocular stimulation such as an air puff. The US is usually presented with several hundreds of milliseconds delay and co-terminates with the CS. Repeated CS-US pairings will gradually elicit an eyelid closure in response to the CS only, termed the conditioned response (CR) (**Fig. 8A-B**).

Importantly, eyeblink CR is not just a matter of all or none, but rather is a optimally timed motor response. In well-trained mice, the elicited CR just precedes and peaks at the onset of the US[53,54]. This finding emphasizes the most pronounced feature of the cerebellum – precise timing control. Although the eye movements and eyelid movement are very simple movements, they provide prime model systems for measurement of motor properties, like timing, amplitude, duration, velocity and so forth.

Molecular pathways and mechanisms for motor learning

The most fascinating property unique to neurons is their ability to adapt their structure or function in response to previous experience. These adaptive modifications can exist in the morphological changes of spines and boutons, the intrinsic excitability, and the synaptic plasticity. Among them, the synaptic plasticity is postulated by Donald Hebb (1904-1985), consists of two forms: long term potentiation (LTP) and long term depression (LTD), which have been extensively studied during the last decades for their involvement in various forms of learning and memory.

It has been shown that both types of synaptic plasticity exist in PCs and their interconnected networks (**Figure 9**). The PF-PC synapse is thought to be the core of cerebellar dependent learning, because of its important locus and highly communicating efficiency within the cerebellar neuronal circuits. In nearly half century, the Marr-Albus-Ito theory for cerebellar motor learning has prevailed through the scientific community, which deems the role of PF-PC LTD as the main mechanism underlying motor learning.[56-58]. Various mechanisms of this LTD have been since proposed. Importantly, when the PF is activated through high-frequency stimulation without CF co-activation[59,60], LTP, instead of LTD will be generated. Therefore, the plasticity is bidirectional in vitro. However, the opposite learning process

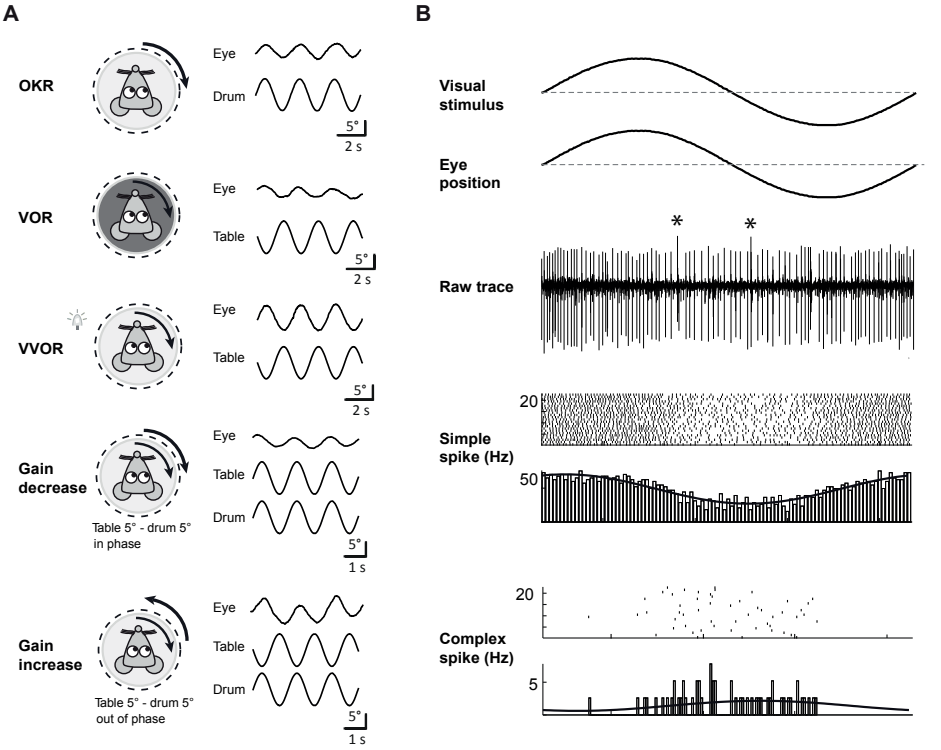

Figure 7. Behavioral paradigms to study compensatory eye movements. **A,** The mouse is placed in the center of a turntable (vestibular stimulus) and surrounded with a random dotted drum (visual stimulus). Baseline performances of compensatory eye movements consist of OKR, VOR and VVOR. Motor learning was studied by subjecting mice to mismatched visual and vestibular input. Rotating the drum and table simultaneously, in phase or out of phase (at 0.6 Hz, both with an amplitude of 5°) in the light will induce an decrease or increase of the gain of the VOR, respectively. **B,** Recording of a floccular Purkinje cell (VA cell) during sinusoidal optokinetic stimulation, shows modulation of both simple and complex spikes (asterisks). Ipsilateral rotation (here: down slope of the sine curve) is related to a decrease in simple spike firing rate, and an increase in complex spikes. Histograms and raster plots further demonstrate this reciprocal relationship. Adapted from (Galliano E et al, 2018)[47] and **Chapter 5.1** of this thesis.

cannot be reversed in the behaving mice in vivo, i.e., VOR gain-increase and gain-decrease learning, which questions the symmetricity of LTP and LTD (see **Chapter 1.2**). Nowadays, it is a common view that the increase in intracellular calcium is involved in the induction both LTD and LTP. Specifically, LTD is correlated with high calcium induced by co-stimulation of CF and PF, whereas LTP is correlated with low calcium provoked by alone PF stimulation[7,61]. Downstream of the calcium signaling cascade, lots of molecules supporting the plastic synaptic changes, for instance, PLC, PKC, PKG, PP2B, CaMKII and so on (**Figure 9**), eventually trigger the dynamic changes of ligand-gated receptors on the membrane, thus thereby conjuring the regulation of the direction of synaptic plasticity[35,62-64].

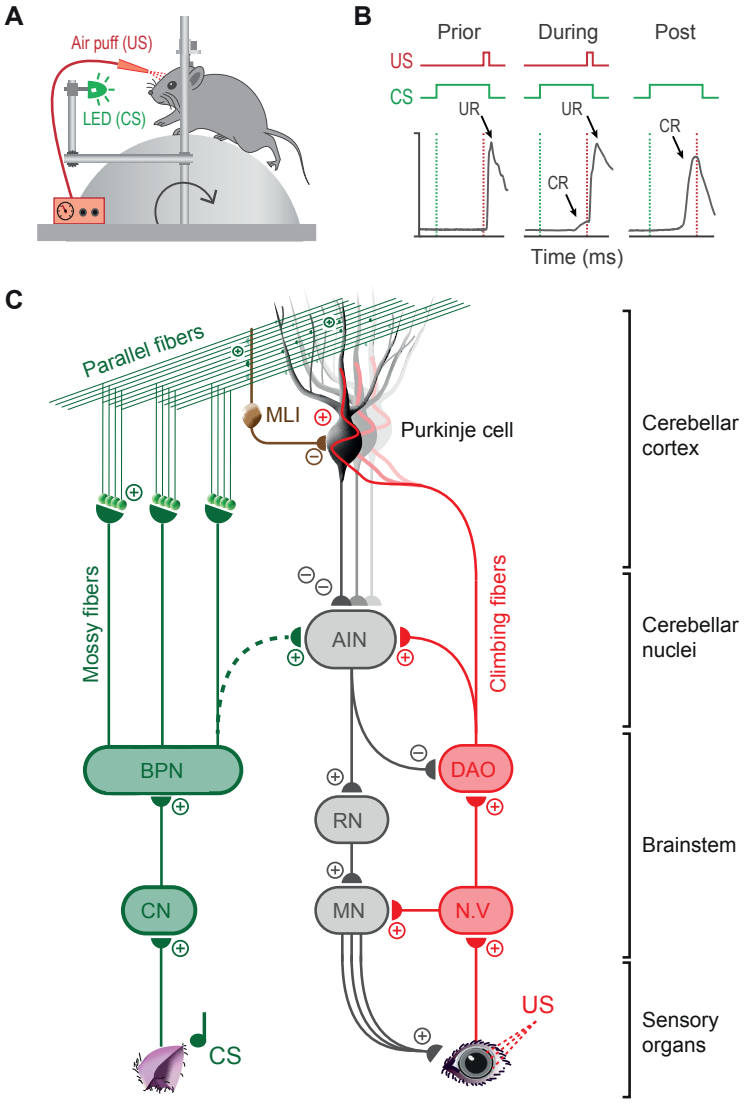

Figure 8. Behavioral paradigms to study eyeblink conditioning. **A,** Two stimuli, the unconditioned stimulus (US, here is an air puff) and the conditioned stimulus (CS, here is an LED light) are presented to the recording mouse. **B,** the CR responses prior to, during and post-training. **C,** Neuronal circuits involved in eyeblink conditioning. PCs in the cerebellar lobule HVI are responsible for the learning. They receive CF inputs from the dorsal accessory olive (DAO), which transmits the information from the peri-orbital facial region. Also, the same PCs receive information from tons of PFs, deriving from MFs from various brainstem nuclei including the basilar pontine nuclei (BPN). These Purkinje cells ultimately send outputs to the anterior interposed nucleus (AIN), which in turn innervates, via the red nucleus (RN), the motor neurons that control the eyeblink. CN, Cochlear Nucleus, MN, Motor Neurons innervating the eyeblink muscles, including oculomotor nucleus (III), accessory nucleus (VI), and facial nucleus (VII), N.V Trigeminal nucleus (V). Note that US, CS and CR pathways are shown in red, green and gray, respectively. Adapted from (the thesis of MM ten Brinke, 2017, EUR) [55]

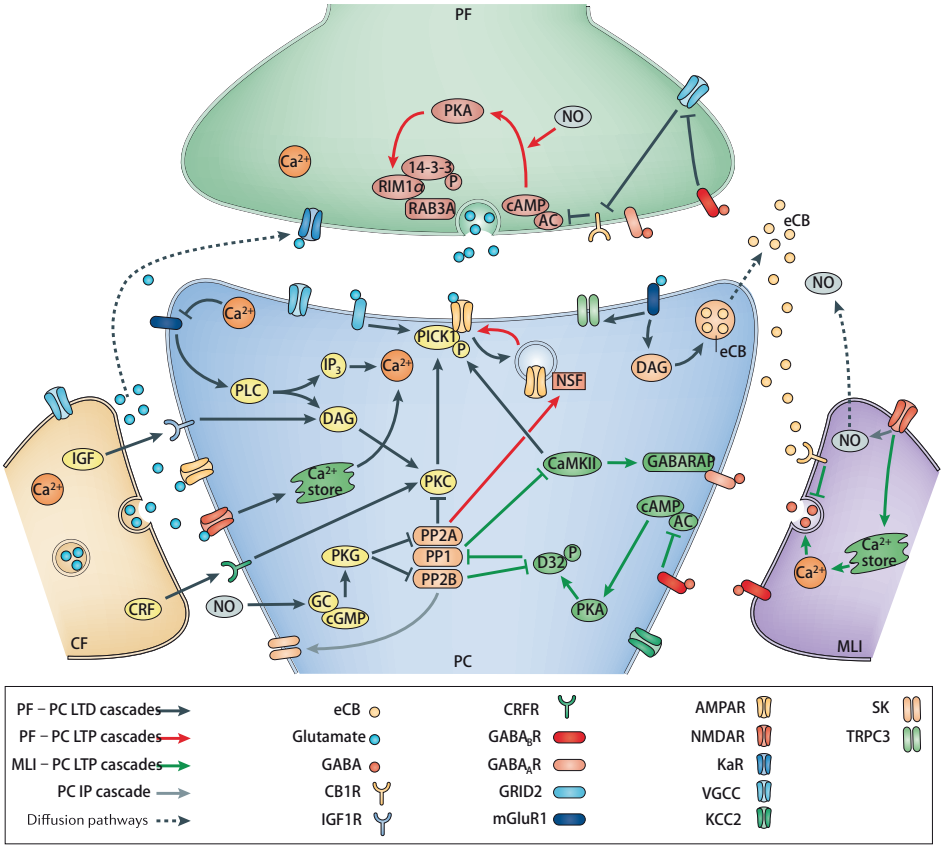

Figure 9. Molecular pathways involved in multiple types of synaptic plasticity that occur at synaptic connections between PFs, CFs or MLIs and PCs. PF–PC LTD, PF–PC LTP, MLI–PC LTP and intrinsic plasticity (IP) pathways are depicted in black, red, green and grey, respectively. Freely diffusing messengers are shown in dashed arrows. Figure from (Gao et al. 2012)[7].

Chapter 1.3

Scope of the thesis

The goal of the research in this thesis is to elucidate the fundamental neural basis of motor control and motor learning. More specifically, focusing on the vestibulocerebellar system, we make use of in vitro and in vivo electrophysiological, imaging, optogenetic, and specific behavioral techniques combined with mouse genetic and molecular methods, to probe how the unitary architectures and functional modules of the cerebellum process information and give rise to the pluriformity of behavioral features.

Chapter 2 describes a targeted approach of recording electrophysiological activity in the cerebellum, particular that of Purkinje cells, in vivo in the awake, active animal.

In **Chapter 3** we set out to address the question how the homogeneous cyto-architecture of the cerebellar cortex gives rise to variety of behavioral consequences and where the zebrin-related differentiation come from at the cellular level. Our results show that TRPC3 is essential for the cellular heterogeneity that introduces distinct physiological properties in an otherwise homogeneous population of Purkinje cells, conjuring functional heterogeneity in cerebellar sensorimotor integration.

In **Chapter 4** we clarify the characteristics of the basal interstitial nucleus in the vestibulocerebellum, which may contribute to controlling compensatory and smooth pursuit eye movements.

In **Chapter 5** we lay emphasis on the electrophysiological investigation of spike responses in individual Purkinje cell in the context of compensatory eye movement performance and adaptation. In **Chapter 5.1** we identify that modulation depths might be a form of neural code underlying the process of motor learning; in **Chapter 5.2** we use direction-specific visuovestibular mismatch training to evoke VOR gain adaptation in relation to movement direction, and show that asymmetries in the magnitude of adaptation depends on movement direction.

In **Chapter 6** we investigate the role of several synaptic proteins during motor learning and cerebellar development. In **Chapter 6.1** through genetic manipulation of PP2B, we investigate the hypothesis that cerebellar development plays a crucial role in the emergence of motor behaviors and learning. In **Chapter 6.2** we demonstrate that PP2B plays a crucial role in controlling the PSD structure at the parallel fiber to Purkinje cell synapse and this function contributes to behavioral learning. In **Chapter 6.3** we report that Shisa6 is crucial for Purkinje cell AMPA-receptor function, synaptic plasticity, and cerebellar motor learning.

In **Chapter 7** we expand the argument for the role of cerebellum in autism by presenting evidence on cerebellar malfunction due to the deletion of shank2 gene.

In **Chapter 8** we discuss the results described in this thesis.

REFERENCES

1 Herculano-Houzel, S. The human brain in numbers: a linearly scaled-up primate brain. *Front Hum Neurosci*. 2009; 3, 31.

2 Williams, R. W. & Herrup, K. The control of neuron number. *Annu Rev Neurosci*. 1988; 11, 423-53.

3 Herculano-Houzel, S. Coordinated scaling of cortical and cerebellar numbers of neurons. *Front Neuroanat*. 2010; 4, 12.

4 E.R. Kandel, e. a. Principles of Neural Science, 5th edition. *McGraw-Hill Companies*. 2012.

5 Sugihara, I. & Quy, P. N. Identification of aldolase C compartments in the mouse cerebellar cortex by olivocerebellar labeling. *J Comp Neurol*. 2007; 500, 1076-92.

6 De Zeeuw, C. I., Hoebeek, F. E., Bosman, L. W. *et al.* Spatiotemporal firing patterns in the cerebellum. *Nat Rev Neurosci*. 2011; 12, 327-44.

7 Gao, Z., van Beugen, B. J. & De Zeeuw, C. I. Distributed synergistic plasticity and cerebellar learning. *Nat Rev Neurosci*. 2012; 13, 619-35.

8 Gao, Z., Proietti-Onori, M., Lin, Z. *et al.* Excitatory Cerebellar Nucleocortical Circuit Provides Internal Amplification during Associative Conditioning. *Neuron*. 2016; 89, 645-57.

9 Apps, R. & Garwicz, M. Anatomical and physiological foundations of cerebellar information processing. *Nat Rev Neurosci*. 2005; 6, 297-311.

10 Ruigrok, T. J. & Voogd, J. Organization of projections from the inferior olive to the cerebellar nuclei in the rat. *J Comp Neurol*. 2000; 426, 209-28.

11 Wu, H. S., Sugihara, I. & Shinoda, Y. Projection patterns of single mossy fibers originating from the lateral reticular nucleus in the rat cerebellar cortex and nuclei. *J Comp Neurol*. 1999; 411, 97-118.

12 Apps, R. & Hawkes, R. Cerebellar cortical organization: a one-map hypothesis. *Nat Rev Neurosci*. 2009; 10, 670-81.

13 Person, A. L. & Raman, I. M. Synchrony and neural coding in cerebellar circuits. *Front Neural Circuits*. 2012; 6, 97.

14 Raman, I. M. & Bean, B. P. Ionic currents underlying spontaneous action potentials in isolated cerebellar Purkinje neurons. *J Neurosci*. 1999; 19, 1663-74.

15 Wu, B. & Schonewille, M. (2018). Targeted Electrophysiological Recordings In Vivo in the Mouse Cerebellum. *Extracellular Recording Approaches, Roy Sillitoe, ed. (New York: Humana Press)*, pp. 19-37.

16 Llinas, R. & Sugimori, M. Electrophysiological properties of in vitro Purkinje cell somata in mammalian cerebellar slices. *J Physiol*. 1980; 305, 171-95.

17 Hausser, M. & Clark, B. A. Tonic synaptic inhibition modulates neuronal output pattern and spatiotemporal synaptic integration. *Neuron*. 1997; 19, 665-78.

18 Raman, I. M. & Bean, B. P. Resurgent sodium current and action potential formation in dissociated cerebellar Purkinje neurons. *J Neurosci*. 1997; 17, 4517-26.

19 Edgerton, J. R. & Reinhart, P. H. Distinct contributions of small and large conductance Ca2+-activated K+ channels to rat Purkinje neuron function. *J Physiol*. 2003; 548, 53-69.

20 Womack, M. D., Chevez, C. & Khodakhah, K. Calcium-activated potassium channels are selectively coupled to P/Q-type calcium channels in cerebellar Purkinje neurons. *J Neurosci*. 2004; 24, 8818-22.

21 Galliano, E., Gao, Z., Schonewille, M. *et al.* Silencing the majority of cerebellar granule cells uncovers their essential role in motor learning and consolidation. *Cell Rep*. 2013; 3, 1239-51.

22 Wulff, P., Schonewille, M., Renzi, M. *et al.* Synaptic inhibition of Purkinje cells mediates consolidation of vestibulo-cerebellar motor learning. *Nat Neurosci*. 2009; 12, 1042-9.

23 Finch, E. A. & Augustine, G. J. Local calcium signalling by inositol-1,4,5-trisphosphate in Purkinje cell dendrites. *Nature*. 1998; 396, 753-6.

24 Callaway, J. C. & Ross, W. N. Spatial distribution of synaptically activated sodium concentration changes in cerebellar Purkinje neurons. *J Neurophysiol*. 1997; 77, 145-52.

25 Kuruma, A., Inoue, T. & Mikoshiba, K. Dynamics of Ca(2+) and Na(+) in the dendrites of mouse cerebellar Purkinje cells evoked by parallel fibre stimulation. *Eur J Neurosci*. 2003; 18, 2677-89.

26 Eccles, J. C., Llinas, R. & Sasaki, K. The excitatory synaptic action of climbing fibres on the purinje cells of the cerebellum. *J Physiol*. 1966; 182, 268-96.

27 Llinas, R. & Yarom, Y. Properties and distribution of ionic conductances generating electroresponsiveness of mammalian inferior olivary neurones in vitro. *J Physiol*. 1981; 315, 569-84.

28 Llinas, R., Baker, R. & Sotelo, C. Electrotonic coupling between neurons in cat inferior olive. *J Neurophysiol*. 1974; 37, 560-71.

29 Simpson, J. I., Wylie, D.R., and DeZeeuw, C.I. in *Behavioral and brain sciences* Ch. 19, 384-98 (Cambridge University Press, 1996).

30 Sugihara, I., Wu, H. & Shinoda, Y. Morphology of single olivocerebellar axons labeled with biotinylated dextran amine in the rat. *J Comp Neurol*. 1999; 414, 131-48.

31 Perkel, D. J., Hestrin, S., Sah, P. *et al.* Excitatory synaptic currents in Purkinje cells. *Proc Biol Sci*. 1990; 241, 116-21.

32 Piochon, C., Levenes, C., Ohtsuki, G. *et al.* Purkinje cell NMDA receptors assume a key role in synaptic gain control in the mature cerebellum. *J Neurosci*. 2010; 30, 15330-5.

33 Schmolesky, M. T., Weber, J. T., De Zeeuw, C. I. *et al.* The making of a complex spike: ionic composition and plasticity. *Ann N Y Acad Sci*. 2002; 978, 359-90.

34 Stuart, G. & Hausser, M. Initiation and spread of sodium action potentials in cerebellar Purkinje cells. *Neuron*. 1994; 13, 703-12.

35 Galliano, E. Questioning the cerebellar doctrine. *EUR*. 2013.

36 Zhou, K. Fundamental principles underlying motro reflexes. *EUR*. 2017.

37 Brochu, G., Maler, L. & Hawkes, R. Zebrin II: a polypeptide antigen expressed selectively by Purkinje cells reveals compartments in rat and fish cerebellum. *J Comp Neurol*. 1990; 291, 538-52.

38 Sugihara, I. & Shinoda, Y. Molecular, topographic, and functional organization of the cerebellar cortex: a study with combined aldolase C and olivocerebellar labeling. *J Neurosci*. 2004; 24, 8771-85.

39 Sugihara, I., Fujita, H., Na, J. *et al.* Projection of reconstructed single Purkinje cell axons in relation to the cortical and nuclear aldolase C compartments of the rat cerebellum. *J Comp Neurol*. 2009; 512, 282-304.

40 Graham, D. J. & Wylie, D. R. Zebrin-immunopositive and -immunonegative stripe pairs represent functional units in the pigeon vestibulocerebellum. *J Neurosci*. 2012; 32, 12769-79.

41 Marzban, H. & Hawkes, R. On the architecture of the posterior zone of the cerebellum. *Cerebellum*. 2011; 10, 422-34.

42 Caffe, A. R., Von Schantz, M., Szel, A. *et al.* Distribution of Purkinje cell-specific Zebrin-II/aldolase C immunoreactivity in the mouse, rat, rabbit, and human retina. *J Comp Neurol*. 1994; 348, 291-7.

43 Ruigrok, T. J. Ins and outs of cerebellar modules. *Cerebellum*. 2011; 10, 464-74.

44 Zhou, H., Lin, Z., Voges, K. *et al.* Cerebellar modules operate at different frequencies. *Elife*. 2014; 3, e02536.

45 Bodranghien, F., Bastian, A., Casali, C. *et al.* Consensus Paper: Revisiting the Symptoms and Signs of Cerebellar Syndrome. *Cerebellum*. 2016; 15, 369-91.

46 Ackermann, H., Vogel, M., Petersen, D. *et al.* Speech deficits in ischaemic cerebellar lesions. *J Neurol*. 1992; 239, 223-7.

47 Galliano, E., Schonewille, M., Peter, S. *et al.* Impact of NMDA Receptor Overexpression on Cerebellar Purkinje Cell Activity and Motor Learning. *eNeuro*. 2018; 5.

48 Schonewille, M., Luo, C., Ruigrok, T. J. *et al.* Zonal organization of the mouse flocculus: physiology, input, and output. *J Comp Neurol*. 2006; 497, 670-82.

49 Simpson, J. I., Wylie, D. R. & De Zeeuw, C. I. On climbing fiber signals and their consequence(s). *Beh.Brain Sciences*. 1996; 19, 380-94.

50 Yakhnitsa, V. & Barmack, N. H. Antiphasic Purkinje cell responses in mouse uvula-nodulus are sensitive to static roll-tilt and topographically organized. *Neuroscience*. 2006; 143, 615-26.

51 Barmack, N. H. & Yakhnitsa, V. Vestibularly evoked climbing-fiber responses modulate simple spikes in rabbit cerebellar Purkinje neurons. *Ann N Y Acad Sci*. 2002; 978, 237-54.

52 Raymond, J. L. & Lisberger, S. G. Error signals in horizontal gaze velocity Purkinje cells under stimulus conditions that cause learning in the VOR. *Ann N Y Acad Sci*. 1996; 781, 686-9.

53 Gormezano, I., Schneiderman, N., Deaux, E. *et al.* Nictitating membrane: classical conditioning and exctinction in the albino rabbit. *Science*. 1962; 138, 33-4.

54 Ivarsson, M. & Svensson, P. Conditioned eyeblink response consists of two distinct components. *J Neurophysiol*. 2000; 83, 796-807.

55 Brinke, M. M. t. Sprezzatura: on olivocerebellar activity and function. *EUR*. 2017.

56 Marr, D. A theory of cerebellar cortex. *J Physiol*. 1969; 202, 437-70.

57 Albus, J. S. A theory of cerebellar function. *Math. Biosci*. 1971; 10, 25-61.

58 Ito, M., Jastreboff, P. J. & Miyashita, Y. Specific effects of unilateral lesions in the flocculus upon eye movements in albino rabbits. *Exp Brain Res*. 1982; 45, 233-42.

59 Lev-Ram, V., Wong, S. T., Storm, D. R. *et al.* A new form of cerebellar long-term potentiation is postsynaptic and depends on nitric oxide but not cAMP. *Proc Natl Acad Sci U S A*. 2002; 99, 8389-93.

60 Salin, P. A., Malenka, R. C. & Nicoll, R. A. Cyclic AMP mediates a presynaptic form of LTP at cerebellar parallel fiber synapses. *Neuron*. 1996; 16, 797-803.

61 Coesmans, M., Weber, J. T., De Zeeuw, C. I. *et al.* Bidirectional parallel fiber plasticity in the cerebellum under climbing fiber control. *Neuron*. 2004; 44, 691-700.

62 Schonewille, M., Belmeguenai, A., Koekkoek, S. K. *et al.* Purkinje cell-specific knockout of the protein phosphatase PP2B impairs potentiation and cerebellar motor learning. *Neuron*. 2010; 67, 618-28.

63 van Woerden, G. M., Hoebeek, F. E., Gao, Z. *et al.* betaCaMKII controls the direction of plasticity at parallel fiber-Purkinje cell synapses. *Nat Neurosci*. 2009; 12, 823-5.

64 De Zeeuw, C. I., Hansel, C., Bian, F. *et al.* Expression of a protein kinase C inhibitor in Purkinje cells blocks cerebellar LTD and adaptation of the vestibulo-ocular reflex. *Neuron*. 1998; 20, 495-508.

65 Yarrow, K., Brown, P. & Krakauer, J. W. Inside the brain of an elite athlete: the neural processes that support high achievement in sports. *Nat Rev Neurosci*. 2009; 10, 585-96.

66 Huang, V. S., Haith, A., Mazzoni, P. *et al.* Rethinking motor learning and savings in adaptation paradigms: model-free memory for successful actions combines with internal models. *Neuron*. 2011; 70, 787-801.

67 Hess, G. & Donoghue, J. P. Long-term depression of horizontal connections in rat motor cortex. *Eur J Neurosci*. 1996; 8, 658-65.

68 Ito, M. Neural design of the cerebellar motor control system. *Brain Res*. 1972; 40, 81-4.

69 Shutoh, F., Katoh, A., Ohki, M. *et al.* Role of protein kinase C family in the cerebellum-dependent adaptive learning of horizontal optokinetic response eye movements in mice. *Eur J Neurosci*. 2003; 18, 134-42.

70 De Zeeuw, C. I. & Yeo, C. H. Time and tide in cerebellar memory formation. *Curr Opin Neurobiol*. 2005; 15, 667-74.

71 Highstein, S. M. & Holstein, G. R. The anatomy of the vestibular nuclei. *Prog Brain Res*. 2006; 151, 157-203.

72 Ito, M. The modifiable neuronal network of the cerebellum. *Jpn J Physiol*. 1984; 34, 781-92.

73 Dash, S., Yan, X., Wang, H. *et al.* Continuous updating of visuospatial memory in superior colliculus during slow eye movements. *Curr Biol*. 2015; 25, 267-74.

74 Miles, F. A. & Lisberger, S. G. The "error" signals subserving adaptive gain control in the primate vestibulo-ocular reflex. *Ann N Y Acad Sci*. 1981; 374, 513-25.

75 Blazquez, P. M., Hirata, Y. & Highstein, S. M. The vestibulo-ocular reflex as a model system for motor learning: what is the role of the cerebellum? *Cerebellum*. 2004; 3, 188-92.

76 Boyden, E. S., Katoh, A. & Raymond, J. L. Cerebellum-dependent learning: the role of multiple plasticity mechanisms. *Annu Rev Neurosci*. 2004; 27, 581-609.

77 Mitchell, D. E., Della Santina, C. C. & Cullen, K. E. Plasticity within excitatory and inhibitory pathways of the vestibulo-spinal circuitry guides changes in motor performance. *Sci Rep*. 2017; 7, 853.

78 Huterer, M. & Cullen, K. E. Vestibuloocular reflex dynamics during high-frequency and high-acceleration rotations of the head on body in rhesus monkey. *J Neurophysiol*. 2002; 88, 13-28.

79 Szentágothai, J. The elementary vestibulo-ocular reflex arc. *J Neurophysiol*. 1950; 13, 395-407.

80 Lorente de Nó, R. Vestibulo-ocular reflex arc. *Arch. Neurol. Psychiat.* 1933; 30, 245-91.

81 De Zeeuw, C. I., Koekkoek, S. K., van Alphen, A. M. *et al.* in *Handbook of auditory research* 375-422 (Springer Verlag, 2003).

82 Barmack, N. H., Baughman, R. W., Eckenstein, F. P. *et al.* Secondary vestibular cholinergic projection to the cerebellum of rabbit and rat as revealed by choline acetyltransferase immunohistochemistry, retrograde and orthograde tracers. *J Comp Neurol*. 1992; 317, 250-70.

83 Chubb, M. C., Fuchs, A. F. & Scudder, C. A. Neuron activity in monkey vestibular nuclei during vertical vestibular stimulation and eye movements. *J Neurophysiol*. 1984; 52, 724-42.

84 Scudder, C. A. & Fuchs, A. F. Physiological and behavioral identification of vestibular nucleus neurons mediating the horizontal vestibuloocular reflex in trained rhesus monkeys. *J Neurophysiol*. 1992; 68, 244-64.

85 Cullen, K. E. & McCrea, R. A. Firing behavior of brain stem neurons during voluntary cancellation of the horizontal vestibuloocular reflex. I. Secondary vestibular neurons. *J Neurophysiol*. 1993; 70, 828-43.

86 Partsalis, A. M., Zhang, Y. & Highstein, S. M. Dorsal Y group in the squirrel monkey. II. Contribution of the cerebellar flocculus to neuronal responses in normal and adapted animals. *J Neurophysiol*. 1995; 73, 632-50.

87 Dickman, J. D. & Angelaki, D. E. Dynamics of vestibular neurons during rotational motion in alert rhesus monkeys. *Exp Brain Res*. 2004; 155, 91-101.

88 Ito, M., Nisimaru, N. & Yamamoto, M. Specific patterns of neuronal connections involved in the control of the rabbit's vestibulo-ocular reflexes by the cerebellar flocculus. *J Physiol*. 1977; 265, 833-54.

89 du Lac, S. & Lisberger, S. G. Eye movements and brainstem neuronal responses evoked by cerebellar and vestibular stimulation in chicks. *J Comp Physiol [A]*. 1992; 171, 629-38.

90 Sekirnjak, C., Vissel, B., Bollinger, J. *et al.* Purkinje cell synapses target physiologically unique brainstem neurons. *J Neurosci*. 2003; 23, 6392-8.

91 Ramachandran, R. & Lisberger, S. G. Neural substrate of modified and unmodified pathways for learning in monkey vestibuloocular reflex. *J Neurophysiol*. 2008; 100, 1868-78.

92 McCrea, R. A., Strassman, A., May, E. *et al.* Anatomical and physiological characteristics of vestibular neurons mediating the horizontal vestibulo-ocular reflex of the squirrel monkey. *J Comp Neurol*. 1987; 264, 547-70.

93 Broussard, D. M., DeCharms, R. C. & Lisberger, S. G. Inputs from the ipsilateral and contralateral vestibular apparatus to behaviorally characterized abducens neurons in rhesus monkeys. *J Neurophysiol*. 1995; 74, 2445-59.

94 Lisberger, S. G., Pavelko, T. A., Bronte-Stewart, H. M. *et al.* Neural basis for motor learning in the vestibuloocular reflex of primates. II. Changes in the responses of horizontal gaze velocity Purkinje cells in the cerebellar flocculus and ventral paraflocculus. *J Neurophysiol*. 1994; 72, 954-73.

95 Langer, T., Fuchs, A. F., Chubb, M. C. *et al.* Floccular efferents in the rhesus macaque as revealed by autoradiography and horseradish peroxidase. *J Comp Neurol*. 1985; 235, 26-37.

96 Broussard, D. M. & Lisberger, S. G. Vestibular inputs to brain stem neurons that participate in motor learning in the primate vestibuloocular reflex. *J Neurophysiol*. 1992; 68, 1906-9.

97 Lisberger, S. G. & Pavelko, T. A. Brain stem neurons in modified pathways for motor learning in the primate vestibulo-ocular reflex. *Science*. 1988; 242, 771-3.

98 Sato, Y., Kanda, K. & Kawasaki, T. Target neurons of floccular middle zone inhibition in medial vestibular nucleus. *Brain Res*. 1988; 446, 225-35.

99 Stahl, J. S. & Simpson, J. I. Dynamics of abducens nucleus neurons in the awake rabbit. *J Neurophysiol*. 1995; 73, 1383-95.

100 McElvain, L. E., Bagnall, M. W., Sakatos, A. *et al.* Bidirectional plasticity gated by hyperpolarization controls the gain of postsynaptic firing responses at central vestibular nerve synapses. *Neuron*. 2010; 68, 763-75.

101 Maekawa, K. & Takeda, T. Electrophysiological identification of the climbing and mossy fiber pathways from the rabbit's retina to the contralateral cerebellar flocculus. *Brain Res*. 1976; 109, 169-74.

102 Maekawa, K. & Takeda, T. Origin of descending afferents to the rostral part of dorsal cap of inferior olive which transfers contralateral optic activities to the flocculus. A horseradish peroxidase study. *Brain Res*. 1979; 172, 393-405.

103 Simpson, J. I., Leonard, C. S. & Soodak, R. E. The accessory optic system of rabbit. II. Spatial organization of direction selectivity. *J Neurophysiol*. 1988; 60, 2055-72.

104 Giolli, R. A., Torigoe, Y., Blanks, R. H. *et al.* Projections of the dorsal and lateral terminal accessory optic nuclei and of the interstitial nucleus of the superior fasciculus (posterior fibers) in the rabbit and rat. *J Comp Neurol*. 1988; 277, 608-20.

105 Sugihara, I., Ebata, S. & Shinoda, Y. Functional compartmentalization in the flocculus and the ventral dentate and dorsal group y nuclei: an analysis of single olivocerebellar axonal morphology. *J Comp Neurol*. 2004; 470, 113-33.

106 Broussard, D. M. & Kassardjian, C. D. Learning in a simple motor system. *Learn Mem*. 2004; 11, 127-36.

107 Medina, J. F. The multiple roles of Purkinje cells in sensori-motor calibration: to predict, teach and command. *Curr Opin Neurobiol*. 2011; 21, 616-22.

108 Lisberger, S. G. & Sejnowski, T. J. Motor learning in a recurrent network model based on the vestibulo-ocular reflex [see comments]. *Nature*. 1992; 360, 159-61.

109 Medina, J. F. & Lisberger, S. G. Links from complex spikes to local plasticity and motor learning in the cerebellum of awake-behaving monkeys. *Nat Neurosci*. 2008; 11, 1185-92.

110 Kassardjian, C. D., Tan, Y. F., Chung, J. Y. *et al.* The site of a motor memory shifts with consolidation. *J Neurosci*. 2005; 25, 7979-85.

111 McElligott, J. G., Beeton, P. & Polk, J. Effect of cerebellar inactivation by lidocaine microdialysis on the vestibuloocular reflex in goldfish. *J Neurophysiol*. 1998; 79, 1286-94.

112 Anzai, M., Kitazawa, H. & Nagao, S. Effects of reversible pharmacological shutdown of cerebellar flocculus on the memory of long-term horizontal vestibulo-ocular reflex adaptation in monkeys. *Neurosci Res*. 2010; 68, 191-8.

113 Ito, M., Shida, T., Yagi, N. *et al.* The cerebellar modification of rabbit's horizontal vestibulo-ocular reflex induced by sustained head rotation combined with visual stimulation. *Proc Jpn Acad*. 1974; 50, 85-9.

114 Zee, D. S., Yamazaki, A., Butler, P. H. *et al.* Effects of ablation of flocculus and paraflocculus of eye movements in primate. *J Neurophysiol*. 1981; 46, 878-99.

115 Nagao, S. Effects of vestibulocerebellar lesions upon dynamic characteristics and adaptation of vestibulo-ocular and optokinetic responses in pigmented rabbits. *Exp Brain Res*. 1983; 53, 36-46.

116 Torte, M. P., Courjon, J. H., Flandrin, J. M. *et al.* Anatomical segregation of different adaptative processes within the vestibulocerebellum of the cat. *Exp Brain Res*. 1994; 99, 441-54.

117 Rambold, H., Churchland, A., Selig, Y. *et al.* Partial Ablations of the Flocculus and Ventral Paraflocculus in Monkeys Cause Linked Deficits in Smooth Pursuit Eye Movements and Adaptive Modification of the VOR. *J Neurophysiol*. 2002; 87, 912-24.

118 Ito, M. The vestibulo--cerebellar relationships: vestibulo-ocular reflex arc and flocculus. pp 129-46. *In: Naunton RF, ed. The vestibular system. New York, Academic Press*. 1975; 255.

119 Haddad, G. M., Demer, J. L. & Robinson, D. A. The effect of lesions of the dorsal cap of the inferior olive on the vestibulo-ocular and optokinetic systems of the cat. *Brain Res*. 1980; 185, 265-75.

120 Tempia, F., Dieringer, N. & Strata, P. Adaptation and habituation of the vestibulo-ocular reflex in intact and inferior olive-lesioned rats. *Exp Brain Res*. 1991; 86, 568-78.

121 Yakushin, S. B., Reisine, H., Buttner-Ennever, J. *et al.* Functions of the nucleus of the optic tract (NOT). I. Adaptation of the gain of the horizontal vestibulo-ocular reflex. *Exp Brain Res*. 2000; 131, 416-32.

122 Gonshor, A. & Jones, G. M. Extreme vestibulo-ocular adaptation induced by prolonged optical reversal of vision. *J Physiol*. 1976; 256, 381-414.

123 Ghelarducci, B., Ito, M. & Yagi, N. Impulse discharges from flocculus Purkinje cells of alert rabbits during visual stimulation combined with horizontal head rotation. *Brain Res*. 1975; 87, 66-72.

124 Dufosse, M., Ito, M., Jastreboff, P. J. *et al.* A neuronal correlate in rabbit's cerebellum to adaptive modification of the vestibulo-ocular reflex. *Brain Res*. 1978; 150, 611-6.

125 Watanabe, E. Role of the primate flocculus in adaptation of the vestibulo-ocular reflex. *Neurosci Res*. 1985; 3, 20-38.

126 Nagao, S. Role of cerebellar flocculus in adaptive interaction between optokinetic eye movement response and vestibulo-ocular reflex in pigmented rabbits. *Exp Brain Res*. 1989; 77, 541-51.

127 Miles, F. A. & Lisberger, S. G. Plasticity in the vestibulo-ocular reflex: a new hypothesis. *Annu Rev Neurosci*. 1981; 4, 273-99.

128 Miles, F. A., Braitman, D. J. & Dow, B. M. Long-term adaptive changes in primate vestibuloocular reflex. IV. Electrophysiological observations in flocculus of adapted monkeys. *J Neurophysiol*. 1980; 43, 1477-93.

129 Lisberger, S. G., Pavelko, T. A. & Broussard, D. M. Neural basis for motor learning in the vestibuloocular reflex of primates. I. Changes in the responses of brain stem neurons. *J Neurophysiol*. 1994; 72, 928-53.

130 Luebke, A. E. & Robinson, D. A. Gain changes of the cat's vestibulo-ocular reflex after flocculus deactivation. *Exp Brain Res*. 1994; 98, 379-90.

131 Ke, M. C., Guo, C. C. & Raymond, J. L. Elimination of climbing fiber instructive signals during motor learning. *Nat Neurosci*. 2009; 12, 1171-9.

132 Watanabe, E. Neuronal events correlated with long-term adaptation of the horizontal vestibulo-ocular reflex in the primate flocculus. *Brain Res*. 1984; 297, 169-74.

133 Blazquez, P. M., Hirata, Y., Heiney, S. A. *et al.* Cerebellar signatures of vestibulo-ocular reflex motor learning. *J Neurosci*. 2003; 23, 9742-51.

134 Hirata, Y. & Highstein, S. M. Acute adaptation of the vestibuloocular reflex: signal processing by floccular and ventral parafloccular purkinje cells. *J Neurophysiol*. 2001; 85, 2267-88.

135 Nagao, S. & Kitazawa, H. Effects of reversible shutdown of the monkey flocculus on the retention of adaptation of the horizontal vestibulo-ocular reflex. *Neuroscience*. 2003; 118, 563-70.

136 Barmack, N. H. & Simpson, J. I. Effects of microlesions of dorsal cap of inferior olive of rabbits on optokinetic and vestibuloocular reflexes. *J Neurophysiol*. 1980; 43, 182-206.

137 Ito, M., Jastreboff, P. J. & Miyashita, Y. Retrograde influence of surgical and chemical flocculectomy upon dorsal cap neurons of the inferior olive. *Neurosci Lett*. 1980; 20, 45-8.

138 Simpson, J. I. & Alley, K. E. Visual climbing fiber input to rabbit vestibulo-cerebellum: a source of direction-specific information. *Brain Res*. 1974; 82, 302-8.

139 Wylie, D. R., De Zeeuw, C. I., DiGiorgi, P. L. *et al.* Projections of individual Purkinje cells of identified zones in the ventral nodulus to the vestibular and cerebellar nuclei in the rabbit. *J Comp Neurol*. 1994; 349, 448-63.

140 De Zeeuw, C. I., Wylie, D. R., Stahl, J. S. *et al.* Phase Relations of Purkinje Cells in the Rabbit Flocculus During Compensatory Eye Movements. *J of Neurophysiol.* 1995; 74, 2051-63.

141 Graf, W., Simpson, J. I. & Leonard, C. S. Spatial organization of visual messages of the rabbit's cerebellar flocculus. II. Complex and simple spike responses of Purkinje cells. *J Neurophysiol*. 1988; 60, 2091-121.

142 Voges, K., Wu, B., Post, L. *et al.* Mechanisms underlying vestibulo-cerebellar motor learning in mice depend on movement direction. *J Physiol*. 2017; 595, 5301-26.

143 Li, J., Smith, S. S. & McElligott, J. G. Cerebellar nitric oxide is necessary for vestibulo-ocular reflex adaptation, a sensorimotor model of learning. *J Neurophysiol*. 1995; 74, 489-94.

144 Titley, H. K., Heskin-Sweezie, R. & Broussard, D. M. The bidirectionality of motor learning in the vestibulo-ocular reflex is a function of cerebellar mGluR1 receptors. *J Neurophysiol*. 2010; 104, 3657-66.

145 Schonewille, M., Gao, Z., Boele, H. J. *et al.* Reevaluating the role of LTD in cerebellar motor learning. *Neuron*. 2011; 70, 43-50.

146 Boyden, E. S., Katoh, A., Pyle, J. L. *et al.* Selective engagement of plasticity mechanisms for motor memory storage. *Neuron*. 2006; 51, 823-34.

147 Seja, P., Schonewille, M., Spitzmaul, G. *et al.* Raising cytosolic Cl- in cerebellar granule cells affects their excitability and vestibulo-ocular learning. *EMBO J*. 2012; 31, 1217-30.

148 Miles, F. A. & Eighmy, B. B. Long-term adaptive changes in primate vestibuloocular reflex. I. Behavioral observations. *J Neurophysiol*. 1980; 43, 1406-25.

149 Kuki, Y., Hirata, Y., Blazquez, P. M. *et al.* Memory retention of vestibuloocular reflex motor learning in squirrel monkeys. *Neuroreport*. 2004; 15, 1007-11.

150 Boyden, E. S. & Raymond, J. L. Active reversal of motor memories reveals rules governing memory encoding. *Neuron*. 2003; 39, 1031-42.

151 Kimpo, R. R., Boyden, E. S., Katoh, A. *et al.* Distinct patterns of stimulus generalization of increases and decreases in VOR gain. *J Neurophysiol*. 2005; 94, 3092-100.

152 Broussard, D. M., Titley, H. K., Antflick, J. *et al.* Motor learning in the VOR: the cerebellar component. *Exp Brain Res*. 2011; 210, 451-63.
153 Titley, H. K. & Hansel, C. Asymmetries in Cerebellar Plasticity and Motor Learning. *Cerebellum*. 2016; 15, 87-92.
154 Dash, S., Catz, N., Dicke, P. W. *et al.* Specific vermal complex spike responses build up during the course of smooth-pursuit adaptation, paralleling the decrease of performance error. *Exp Brain Res*. 2010; 205, 41-55.
155 Mitchell, D. E., Della Santina, C. C. & Cullen, K. E. Plasticity within non-cerebellar pathways rapidly shapes motor performance in vivo. *Nat Commun*. 2016; 7, 11238.
156 Bagnall, M. W., McElvain, L. E., Faulstich, M. *et al.* Frequency-independent synaptic transmission supports a linear vestibular behavior. *Neuron*. 2008; 60, 343-52.
157 Hansel, C., Linden, D. J. & D'Angelo, E. Beyond parallel fiber LTD: the diversity of synaptic and non-synaptic plasticity in the cerebellum. *Nat Neurosci.* 2001; 4, 467-75.
158 Nagao, S. & Ito, M. Subdural application of hemoglobin to the cerebellum blocks vestibuloocular reflex adaptation. *Neuroreport*. 1991; 2, 193-6.
159 Hansel, C., de Jeu, M., Belmeguenai, A. *et al.* alphaCaMKII Is essential for cerebellar LTD and motor learning. *Neuron*. 2006; 51, 835-43.
160 Kakegawa, W., Katoh, A., Narumi, S. *et al.* Optogenetic Control of Synaptic AMPA Receptor Endocytosis Reveals Roles of LTD in Motor Learning. *Neuron*. 2018; 99, 985-98 e6.
161 Ito, M. Cerebellar learning in the vestibulo-ocular reflex. *Trends Cogn Sci*. 1998; 1998, 305-71.
162 Ito, M. Long-term depression. *Annu Rev Neurosci*. 1989; 12, 85-102.
163 Nguyen-Vu, T. D., Kimpo, R. R., Rinaldi, J. M. *et al.* Cerebellar Purkinje cell activity drives motor learning. *Nat Neurosci*. 2013; 16, 1734-6.
164 Miyashita, Y. & Nagao, S. Contribution of cerebellar intracortical inhibition to Purkinje cell response during vestibulo-ocular reflex of alert rabbits. *J Physiol*. 1984; 351, 251-62.
165 Shin, M., Moghadam, S. H., Sekirnjak, C. *et al.* Multiple types of cerebellar target neurons and their circuitry in the vestibulo-ocular reflex. *J Neurosci.* 2011; 31, 10776-86.
166 Spencer, R. F., Wenthold, R. J. & Baker, R. Evidence for glycine as an inhibitory neurotransmitter of vestibular, reticular, and prepositus hypoglossi neurons that project to the cat abducens nucleus. *J Neurosci*. 1989; 9, 2718-36.
167 Capocchi, G., Della Torre, G., Grassi, S. *et al.* NMDA receptor-mediated long term modulation of electrically evoked field potentials in the rat medial vestibular nuclei. *Exp Brain Res*. 1992; 90, 546-50.
168 Grassi, S., Pettorossi, V. E. & Zampolini, M. Low-frequency stimulation cancels the high-frequency-induced long- lasting effects in the rat medial vestibular nuclei. *J Neurosci.* 1996; 16, 3373-80.
169 Scarduzio, M., Panichi, R., Pettorossi, V. E. *et al.* The repetition timing of high frequency afferent stimulation drives the bidirectional plasticity at central synapses in the rat medial vestibular nuclei. *Neuroscience*. 2012; 223, 1-11.
170 Straka, H., Biesdorf, S. & Dieringer, N. Canal-specific excitation and inhibition of frog second-order vestibular neurons. *J Neurophysiol*. 1997; 78, 1363-72.
171 Bagnall, M. W., Stevens, R. J. & du Lac, S. Transgenic mouse lines subdivide medial vestibular nucleus neurons into discrete, neurochemically distinct populations. *J Neurosci*. 2007; 27, 2318-30.
172 Malinvaud, D., Vassias, I., Reichenberger, I. *et al.* Functional organization of vestibular commissural connections in frog. *J Neurosci*. 2010; 30, 3310-25.
173 Cullen, K. E. & Roy, J. E. Signal processing in the vestibular system during active versus passive head movements. *J Neurophysiol*. 2004; 91, 1919-33.
174 du Lac, S. Candidate cellular mechanisms of vestibulo-ocular reflex plasticity. *Ann N Y Acad Sci*. 1996; 781, 489-98.
175 Zhang, W. & Linden, D. J. The other side of the engram: experience-driven changes in neuronal intrinsic excitability. *Nat Rev Neurosci*. 2003; 4, 885-900.
176 Nelson, A. B., Krispel, C. M., Sekirnjak, C. *et al.* Long-lasting increases in intrinsic excitability triggered by inhibition. *Neuron*. 2003; 40, 609-20.

Chapter 2

Targeted electrophysiological recordings in vivo in the mouse cerebellum

Bin Wu and Martijn Schonewille

Department of Neuroscience, Erasmus Medical Center, Rotterdam, The Netherlands

Published in Extracellular Recording Approaches (2018), Ch.2

ABSTRACT

Single unit recordings *in vivo* are the unitary elements in the processing of the brain, and as such essential in systems physiology to understand brain functioning. In the cerebellum, a structure with high levels of intrinsic activity, studying these elements *in vivo* in an awake animal is imperative to obtain information regarding the processing features of these units in action. In this chapter we address the rationale and the approach of recording electrophysiological activity in the cerebellum, particular that of Purkinje cells, *in vivo* in the awake, active animal. In line with the developing appreciation for the diversity within populations of the cells of the same type, there is a growing interest in the differentiation within the population of Purkinje cells. Here we describe a successful approach to analyzing the activity of two populations of Purkinje cells, which differ in connectivity and the expression of several genes. By driving the expression of a fluorescent marker with the promotor of one of the differentiating genes, the presence of a fluorescence signal could be used to recognize and approach Purkinje cells, while the strength of the signal can be used as a marker to identify the two subpopulations. Finally, the drawbacks and the advantages of this technique are discussed, and placed into a future perspective.

INTRODUCTION

Single unit recordings in vivo

Understanding what goes on in the most studied black box we know, the brain, is the essence of neuroscience. Brain physiology traditionally has been studied at several levels, varying from broad view approaches using EEGs or fMRI to that of individual cell structures such as axons, dendrites or even synapses using patch clamp recordings. Analysis at this level of detail has provided a wealth of knowledge regarding the cellular activity underlying concepts such as sensory processing, motor coding and learning. Top down, non-invasive approaches have taught us about functionalities, somatotopy, or about temporal aspects of activity and about the connectivity between areas. To bridge the gap between molecular processes occurring at the (sub)cellular level and the activity observed using non-invasive techniques, several electrophysiological approaches are used. Local field potential recordings indicate activity in a particular volume of recording area, while imaging -at the expense of temporal resolution- adds or increases spatial resolution. These forms of recording population code will help us understand the information passing through and processed by the ensemble, but are less informative regarding the individual units. For detailed information on the specific activity of individual units, the neurons, single unit recordings are required. Neuronal activity presents itself predominantly in the form of rapid fluctuation of the electrical membrane potential, also known as action potentials. Whereas the membrane potential can only be recorded inside the cell with patch clamp recordings or voltage sensitive dyes, the currents underlying the action potential are significantly large enough to reliably be recorded in the extracellular space. The potential of this technique has been known and used for a long time, including, for instance, in the landmark scientific discovery of the direction selectivity of neurons in the cat striatum [1]. But even today the technique is still used in many key studies[2,3], in part driven by the revival of systems physiology. New technical developments such as optogenetic manipulations of cellular activity require, to assure appropriate manipulation, a cell-specific read-out of the change in the firing rate induced by the light.

Targeted recordings in vivo: why and how?

Although the local environment of neurons in slice preparations is thought to remain intact, features such as sensory input, extracellular chemical configuration and axons of projecting neurons are typically disrupted. Switching to recording *in vivo* circumvents these issues, but at the expense of the possibility to use visual information for guidance. In many instances recordings can be somewhat directed based on neuroanatomy or known cellular activity patterns, or is simply not needed. If information on cell-type is essential but not needed to direct sampling, cells can also be labeled and classified post mortem. In all other situations, whether it is to minimize variation or to zoom in on the properties of specific

cell types, the ability to target recordings can be essential. This technique was pioneered by Margrie and colleagues, who performed *in vivo* electrophysiological recordings based on images generated by two-photon excitation laser-scanning microscopy[4], a technique they named two-photon targeted patching, or TPTP[5]. Transgenic mice expressing enhanced green fluorescent protein (eGFP) under control of the parvalbumin promotor to label cortical interneurons were anesthetized and placed under a two-photon microscope. With the cells labeled in green, and with the pipette filled with red Alexa594 the approach could be visualized and directed, and the success rate of patching was >50% per animal and over >10% per penetration[4]. Following the TPTP approach describe above an alternative, inverse method was developed. Kitamura and colleagues demonstrated that by labeling the extracellular space with a fluorescent dye, the neurons can be 'visualized' as a negative image[6]. By perfusing the extracellular space with the same Alexa594, which is not taken up by neurons, the authors were able to identify neurons as shadows and either electroporate or recorded from them. The success rate of obtaining a giga-seal and whole cell configuration was >60% for pyramidal cells and interneurons per attempt. Despite promising success rates both approaches are, however, used quite rarely, as whole cell recordings *in vivo* remain labor intensive with relatively low success rates and hence their use in today's neuroscience is limited.

Cerebellar wiring and physiology

The cerebellum holds a special place in neuroscience, not in the least due to its electrophysiological properties. The 'little brain' presents a combination of central nuclei surrounded by a highly organized, crystalline cortical structure (**Fig. 1**), with a sole principal output neuron, the Purkinje cell, that uses GABA as a neurotransmitter and has an immense, two-dimensional dendritic tree [7]. Information enters the cerebellum predominantly via two sources: mossy fibers and climbing fibers. Mossy fibers carry information about sensory stimulation and ongoing motor activities in the form of efference copies, or corollary discharges[8], and contact excitatory granule cells and inhibitory Golgi cells[9,10]. In contrast, a single climbing fiber provide excitatory input to each Purkinje cells resulting in a complex spike[11,12] and are commonly thought to carry error signals[13,14], but other potential functions have also been described[15,16]. Granule cells send their axon into the molecular layer, where they bifurcate and provide a direct excitatory drive to the Purkinje cell's extensive dendritic tree via parallel fibers and an indirect inhibitory input via the molecular layer interneurons, stellate cells and basket cells, which predominantly contact the Purkinje cell's dendrite and the soma, respectively [17]. Granule cells typically fire action potentials in bursts [18]. Purkinje cells are intrinsically active and integrate excitatory and inhibitory input into a GABAergic output onto cerebellar nuclear neurons. Most inhibitory interneurons have an intermediate firing rate, with less pronounced differences amongst them[19]. Together the mossy fiber and climbing fiber system create a matrix-like configuration. Parallel fibers run horizontally for

millimeters, contacting spines on the dendrites of numerous Purkinje cells in the coronal plane. In contrast, the Purkinje cell dendrite is oriented sagittally and the inferior olive with its climbing fibers connects to multiple Purkinje cells in a sagittal plane, with each Purkinje cell receiving hundreds of inputs from only a single climbing fiber in the adult stage (**Fig. 1c**). This typical configuration sparked the interest of computational neuroscientists to generate a theory for cerebellar learning[20,21], which is still the topic of discussion today[22-27].

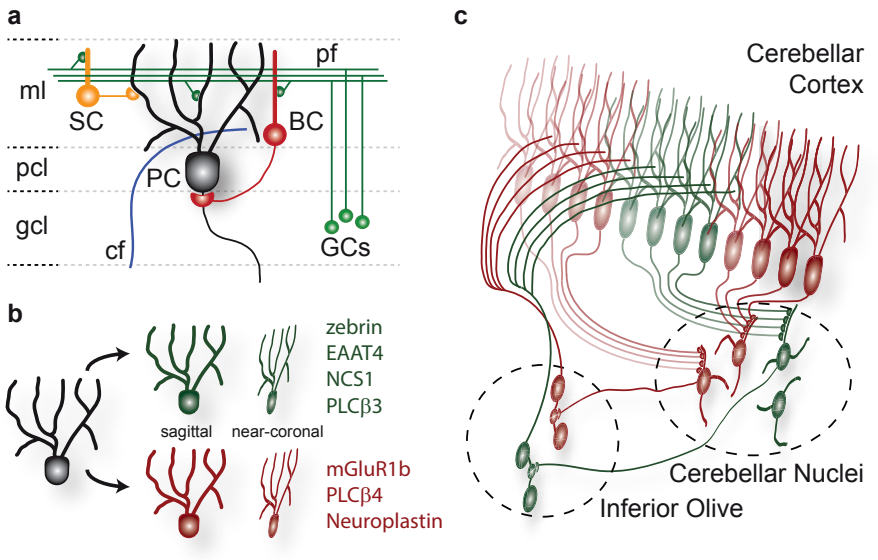

Figure 1. The olivo-cerebellar circuit is constructed of modules with distinct cytochemical signatures. **a**) Schematic drawing of the main cortical cell types, including granule (GC), stellate (SC), basket (BC) and Purkinje cells (PC) with parallel (pf) and climbing fibers (cf) in their respective layers: gcl, pcl and molecular layer. **b**) Purkinje cells can be subdivided based on the expression pattern of particular proteins, of which the most well-known is zebrin, or aldolase c. Purkinje cell dendritic trees are virtually two dimensional; in the vermis they can be fully visualized in a sagittal plane. **c**) Schematic representation of the three dimensional configuration and the inter-modular connectivity between the inferior olive, cerebellar cortex and cerebellar nuclei. Inferior olivary neurons typically project to Purkinje cells of the same zebrin-identity in similar modules, which in turn commonly project to the same regions in the cerebellar nuclei. As a result, the cerebellar nuclei can be divided into zebrin-positive and –negative parts too, based on zebrin stained Purkinje cell axons. In contrast to this organisation in the sagittal plane, parallel fibers (not depicted) run horizontally, i.e. perpendicular to the orientation of the virtually flat Purkinje cell dendritic tree.

Electrophysiological recordings in the cerebellum in vivo

The cerebellum is characterized by several features that facilitate convenient, reliable *in vivo* electrophysiological recordings. First there is the location; as the cerebellum is situated in the back of the skull there is ample space to place an immobilizing construct on the more frontal parts, assuring a preparation that is solid enough for chronic experiments.

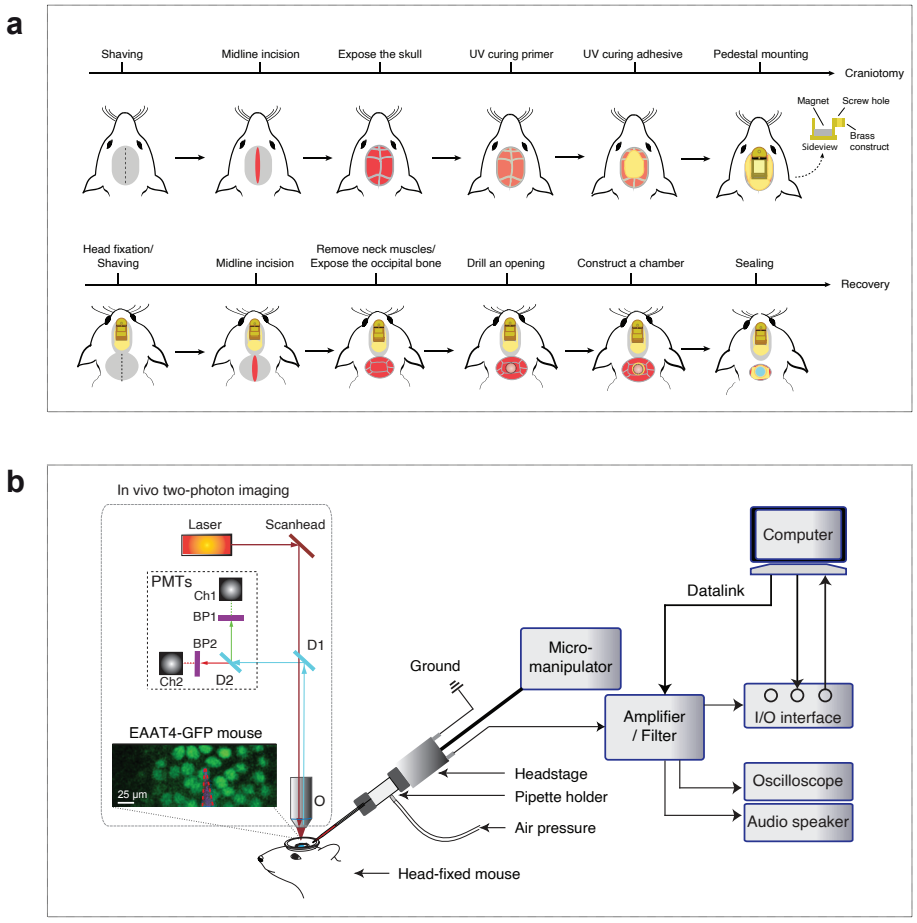

Figure 2. Outline of preparational surgery and recording setup. a) Diagram of procedures for installation of pedestal and craniotomy surgeries in anesthetized mice. **b**) Schematic drawing of the configuration for combined electrophysiological (right) and two-photon imaging to allow targeted recordings in vivo (left). In short, the mouse is head-fixed in the restrainer. Electrical signals are recorded by a microelectrode and amplified by the headstage, which is attached to a three-axis micromanipulator to, and forwarded to the main amplifier. The signal is then sent to a sound monitor and/or oscilloscope for rapid monitoring of the recorded signals, digitized by the I/O interface and stored on the computer controlling the recording settings and stimulations. Left, scheme of two-photon microscope for imaging the eGFP labelled neurons and the electrode. PMT, photomultiplier tube; D1, dichroic 1 (695 nm split); D2, dichroic 2 (585 nm split); BP1, band-pass filter 1 (500-550 nm); BP2, band-pass filter 2 (584-676 nm); O, water immersion objective. Inset with image: a glass pipette containing Alexa Fluor 594 (10 µM in 2M Nacl, depicted in red) is targeted towards Purkinje cells (green circles) using the eGFP signal from the EAAT4-positive cells, and cell-population specific extracellular recordings are obtained.

Secondly, the layered, cyto-architectural organization, due to its predictable pattern, allows for online reconstructions of the trajectory and thereby makes it possible to determine in which lobules recordings are made, even without post mortem analysis (**Fig. 3a**).

Moreover, due to the two types of inputs, parallel fibers and climbing fibers, the cells that integrate all inputs and form the only output of the cerebellar cortex, the Purkinje cells, can be readily identified by their two types of action potentials. Activation of the hundreds of synapses from a single climbing fiber onto a Purkinje cell results in a massive, prolonged depolarization, also known as the 'complex' spike [12]. This signature response can also be observed in extracellular recordings, here too as a complex shape (**Fig. 3a**), and as such forms a landmark feature to identify cerebellar Purkinje cells. Hence it has been possible for decades, and thus since long before two-photon imaging became available, to perform cell-type specific targeted recordings of Purkinje cells. The 'visualization' here, however, comes in the form of recorded electrical signal, which is commonly converted into an auditory signal that allows the experimenter to 'hear' Purkinje cells, rather than see them. Finally, combining the advantages elements described above, the ability to record cell-specific activity at relatively deep locations in the cerebellar with long tapered pipettes brings the advantage of increased stability due to the intimate and extended contact between pipette and brain. The relevance of the technique in neuroscience is substantiated by the list of animal types (and labs) that have been used to perform cerebellar extracellular recordings in vivo. Originally technical limitation prohibited the use of smaller animals, and experiments were done in larger mammals, e.g. in monkeys[28-31], cats[32-35], rabbits [36-39] and less conventional animal models including fish[40,41], birds [42] and amphibians [43]. More recent work has been done on rats[19,44,45] and ferrets [46,47], but the mouse has rapidly move into the spot of the most popular animal for extracellular recordings in vivo, also in the cerebellum[3,13,48-51].

Cerebellar genetics and connectivity

With its crystalline architecture, the cerebellum has attracted the attention from neuroanatomists since the early days of neuroscience[52,53]. Particularly the cerebellar cortex attracted attention, with its apparent highly homogenously present layered organization (**Fig. 1c**). Over the years, or even decades, this image of a homogeneous structure has been contested at different levels. The first evidence against the uniform nature is the description of a patterned expression of 5'-nucleotidase, more than half a century ago[54]. Since then, numerous protein have been found to expressed in particular patterns, with the most well-known example being , identified in rats, the zebrins: zebrin I and II [55,56]. Zebrins owe their name to the peculiar pattern of expression, consisting of sagittal stripes of stained, 'positive' and non-stained, 'negative' Purkinje cells (**Fig. 1b**). This pattern of stripes of varying width is not unique to rats, but has been observed in various species of different classes ranging from pigeons[57], via e.g. hedgehogs[58] to humans. It has been observed for numerous proteins since, including for instance: mGlur1b[59], EAAT4[60], PLCβ3 and β4[61], PKCδ[62], NCS-1[63], IP3R1[64] and Neuroplastin[65] (**Fig. 1b**). Interestingly, the differentiation does not only exist in the genetic profile, but also in morphology and connectivity.

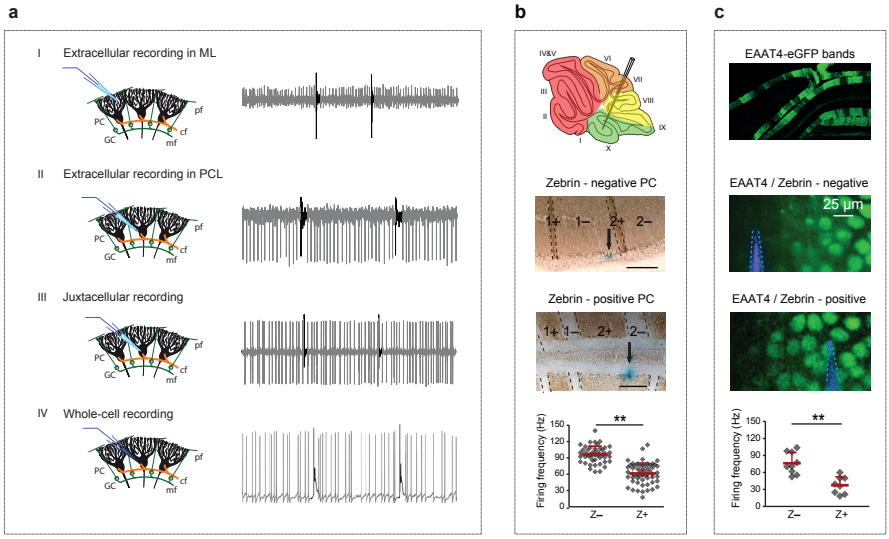

Figure 3. In vivo recording configurations and example data from labelled and targeted Purkinje cell recordings. a) The position of the recording electrode relative to the Purkinje cell determines the observed signals. Liquid filled glass pipette electrodes are used to record single cell activity from PCs. In the molecular layer only complex spikes are observed, seen as slow, negative deflections (I). Towards the soma complex spike signals become predominantly positive with slower elements, while simple spikes appear as negative or more bidirectional deflections (II). When the tip of the electrode is placed even more intimately with the soma, this is referred to as juxtacellular, a configuration that allows cell-specific labelling (III). Ultimately, using suction, followed by sealing and breaking in, the configuration can be converted into a whole-cell patch clamp recording (IV). **b**) Schematic representation in sagittal plane of the electrode path. Micrographs show coronal sections of recorded Purkinje cells labelled with Alcian blue after staining against zebrin; top: zebrin-negative Purkinje cell in the anterior cerebellum, bottom: zebrin-positive in the posterior cerebellum. The bottom graph depicts the difference in simple spike firing rate between modules observed using this technique. **c**) Confocal image of a coronal section of an EAAT4-eGFP brain, showing the typical EAAT4/zebrin pattern. Two-photon images (approx. the same location, shifted about 25 µm) with the pipette recording a negative (top) and a positive (bottom) Purkinje cell. The bottom graph shows how the targeted recordings confirmed the difference observed in b, with a lower number of cells. Results in b and c are adapted from Zhou et al., 2014. PC, Purkinje cell. GC, granule cell. PF, parallel fiber. CF, climbing fiber. MF, mossy fiber.

For instance, Altman and Bayer in 1977 described cell-type that is abundantly present, but almost only in the granule cell layer of vestibule-cerebellum[66], later to be recognized and named by its peculiar shape as the unipolar brush cell (UBC)[67]. This discovery signifies the more general notion that despite its homogeneous appearance, the cerebellar cortex has regional variations in composition.

Apart from the variations, cumulative research indicates that the connectivity of the cerebellum adheres to particular patterns as well. PCs with the same zebrin II-identity form a cerebellar module, in that they receive CF inputs from a the same subnucleus of the

inferior olive, and send their output to the parts of the cerebellar nuclei (**Fig. 1c**)[68-73]. In fact, even mossy fibers can adhere to the zebrin signatur [68], although there is integration of different modalities at the input stage already [74]. Hence, one could argue that zebrin is a marker identifying cerebellar cortical regions, or modules, that form a functional unit that integrates particular mossy and climbing information[68,70,75].

Differential cerebellar physiology

The presence of differential gene expression profiles between distinct Purkinje cell populations could implicate that there are related differences in physiology as well. The first evidence supporting this concept came from Wadiche and Jahr, who demonstrated that the presence of EAAT4, which has an expression pattern very similar to that of Zebrin, inhibits the activation of metabotropic glutamate receptors. As a result, EAAT4-negative (and thus zebrin-negative) Purkinje cells in lobule III exhibit long-term depression of the PF-PC synapse (PF-PC LTD), while zebrin/EAAT4-positive Purkinje cells in lobule X do not[76]. Similar differences between anterior and posterior lobules have been described for a depolarization-induced slow current, a current related to postsynaptic dopamine, released in an autocrine manner[77,78]. *In vitro* experiments also revealed differences in general excitability between Purkinje cells in anterior and posterior lobules, and related them to differences in specific K^+ and Na^+ currents[79]. Even the climbing fiber input itself has been suggested to be physiologically different between zebrin-positive and zebrin-negative Purkinje cells, although is not clear if these differences work in conjunction with or against those observed in Purkinje cells[80].

Taken together these results sparked our interest in the activity of individual zebrin-positive and zebrin-negative Purkinje cells in the awake, active mouse. This scientific question required exactly those recordings conditions, that allow insight into not only into the identity of the recorded cell in terms of cell-type, but also that in terms of genetic 'identity', a feature that can only be visualized by immunohistochemistry or genetically-encoded fluorescent markers. To determine the impact of these features or other differences in gene expression profiles, hundreds of Purkinje cells were recorded throughout the cerebellar cortex and the activity patterns were correlated to their location and zebrin-identity, either by postmortem analysis or by online identification based on two-photon imaging (**Fig. 3b-c**)[81,82], results that were confirmed by others [44].

METHODS

By preparing mice for in vivo recordings in the awake animal with the option for chronic recordings over several days, one can avoid side-effects of anesthetics or analgesics (see

e.g. Schonewille, et al.[48]). In this section we provide a detailed protocol for the surgical preparation of a craniotomy to access the cerebellum, followed by an overview of the experimental setup and the protocol for *in vivo* electrophysiological recording in an awake mouse, and the data analysis. These methods have been successfully developed and applied in our laboratory over the last decade to record neuronal activities in an anesthetized[19,48], or alert [81,83,84], or behaving mouse[85,86].

Surgical procedures

Mice are commonly prepared for experiments with a preparational surgery, as also described by White, et al.[87]. During the surgery a "pedestal" for immobilization of the head and a chamber for a single or multiple electrophysiological recording session(s) will be placed as follows (see also **Fig. 2a**). Mice are anaesthetized by a mixture of isoflurane and oxygen (initial concentration: 4% V/V in O_2, maintenance concentration: 1.5-2% V/V in O_2) in a gas chamber. Once the mouse no longer has a foot pinching reflex, the mouth is opened and the tongue is pulled out with tweezers. Next, the bar of a stereotaxic apparatus (Bilaney, Germany) is gently inserted into the mouth. When in the proper position, the screw is fastened to fix the head horizontally. To assure that body temperature is maintained at 37 °C, the anal thermosensor is carefully placed and connected to a heating pad (FHC, Bowdoinham, ME). The eyes are protected by covering them with an eye ointment (duratears, Alcon, Belgium). The dorsal cranial fur is shaven with soap and a scalpel, a midline incision is made to expose the skull, and the periost is cleared and cleaned with cotton swabs **(Fig. 2a)**. A drop of OptiBond all-in-one (Kerr, Salerno, Italy) is applied to the dorsal cranial surface of the skull from bregma to lambda and cure with light for 60 seconds. The adhesive layer is covered with a thin layer of Charisma composite (Heraeus Kulzer, Germany) and the pedestal is embedded in the composite and cured it immediately. Additional layers of composite are added to surround the base of the pedestal and cured with light, to complete the pedestal placement part of the surgery **(Fig. 2a)**.

From here on, the mouse can be fixed by either the pedestal or the mouth bar. The skin over the skull is opened until the foramen magnum and the three layers of medial neck muscles overlying the occipital bone and foramen magnum are removed. A craniotomy is made by drilling an opening (max. Ø < 3 mm) in the interparietal or occipital bone, overlying the cerebellar part of interest. Size and location of the craniotomy can be adapted to the experimental approach. Smaller craniotomies are preferable for reasons of stability and the dura mater should be preserved to keep the brain intact and healthy, if possible **(Fig. 2b)**. A recording chamber is constructed around the craniotomy with Charisma composite again and sealed with self-curing silicone composite (Twinsil speed 22, Picodent, Germany). The mouse preferably is allowed to recover in its home cage for at least 3 days after the surgery before starting electrophysiological recordings.

Anesthesia, analgesia and anti-inflammatory drugs for experimental mice

Discomfort to the mice is limited by the use of several anesthetics, analgesics and anti-inflammatory drugs given pre-, peri- and post-surgery. A balanced combination could include isoflurane (4% induction, 1.5-2% maintenance), lidocaine (in Xylocain 10%, drop of 100mg/ml), Bupivacaine (Bupivacaine Actavis, drop of 2.5mg/ml), buprenorphine (Temgesic, 0.3 mg/ml) and rimadyl (Carprofen, 50 mg/ml). Isoflurane is given as indicated in the experimental approach, lidocaine and bupivacaine are administered locally as analgesic on the skull and buprenorphine (diluted to 0.02 mg/kg) and Rimadyl (5 mg/kg) are injected intraperitoneally for post-operative analgesia and to prevent inflammation.

The equipment and recording procedures

There is no golden standard for in vivo electrophysiological recordings. Below the method that has been developed over several years of using this technique is detailed. First, to assure that the animal is comfortable with the experimental conditions including the restraining of the head, mice are habituated by placing them in the experimental setup for 30–60 min for one or two days before the first experimental session. For habituation and experiments the mice are immobilized using a custom-made restrainer, by bolting the head holder to a head fixation post. Prior to experiments, the dental mixture should be removed to expose the craniotomy. Tissue can accumulate on top of the dura, which needs to be removed to allow a clean entrance and easy penetration for the recording and stimulation probes. Using a hypodermic needle an incision is made in the dura to facilitate the penetration of glass pipettes (only needed for sharper tips) and the exposed cortex is rinsed with saline to remove blood. During the recording, the brain surface is covered with saline in order to prevent dehydration. Glass pipettes (OD 1.5 mm, ID 0.86 mm, borosilicate, Sutter Instruments, USA; 1-2 µm tips, 4-8 MΩ) are pulled (P-1000, Sutter Instruments, USA) and filled with 2 M NaCl solution and Alcian Blue (for pressure injections) or 2–3% solution of biotin (Vector Laboratories). The pipette is lowered slowly into the cerebellar cortex by either an analogue, hydraulic Microdrive (Trent Wells, TX, USA) or a digital Microdrive (in final approach set to 2–4-µm step size, step every 2–3 s). The recorded signals are pre-amplified (custom-made preamplifier, 1000x DC), filtered and digitized (either CyberAmp320, Molecular Devices, with Power1401, CED, Cambridge, UK or Axon Multiclamp 700B with Digidata 1440A, Molecular Devices, Sunnyvale, CA, USA) and stored on disk (using Spike2, CED or pClamp10, Molecular Devices) for offline analysis (**Fig. 2c**). To mark the recording location, brief air pulses (MPPI-3, ASI, USA) or iontophoresis (custom-made device, 4-8 µA, 7 s on – 7 s off) can be used locally deliver the Alcian Blue or biotin, respectively. After the recording session the animal will be sacrificed if the experiment is completed or the brain is covered with an ointment (Duratears, Alcon, Belgium) and the chamber is sealed using self-curing silicone composite (Twindil speed 22, Picodent, Germany) to continue the next day.

Targeted recordings using two-photon imaging

Described above is the general surgical preparation for in vivo recording in awake mice. For *in vivo* two-photon targeted recordings the approach is similar to these procedures, but the construction for immobilization and craniotomy is adapted to the requirements of the microscope. For these experiments a rectangular metal plate is used and placed perpendicular to the midline of the mouse, with grooves for solid fixation and a larger opening for imaging and recordings.

Images are acquired using a TriM Scope II (LaVision BioTec, Bielefeld, Germany) attached to an upright microscope with a 40x/0.8 NA water-immersion objective (Olympus, Tokyo, Japan). Laser illumination is provided by a Chameleon Ultra titanium sapphire laser (Coherent, Santa Clara, CA) and to detect fluorescent emissions, two photomultiplier tubes (Hamamatsu, Iwata City, Japan) are used. The recording pipette is filled with Alexa-594 (10 μM in 2 M NaCl; Life Technologies, Carlsbad, CA) and visualized with an excitation wavelength of 800 nm. Images from eGFP and Alexa-594 are filtered using a Gaussian kernel, contrast-optimized and subsequently merged in Photoshop (Adobe, San Jose, CA). A typical recording sampled 40 x 200 μM with a frame rate of approximately 25Hz [81] (**Fig. 2c**).

Selecting cells for recording

In contrast to *in vitro techniques*, *in vivo* approaches can be used to study neurons in physiological conditions with normal inputs and intact axon, and in their virtually natural ambience of neuronal circuits, thus resulting in more realistic characterization that can be more easily extrapolated than *in vitro* recordings. However, in an intact animal, it is not easy to determine the type and location of the neuron that is being recorded. Fortunately, there are several ways to identify the cell type and location in the cerebellum.

Spike waveform. Even when recorded extracellularly, different types of cells present distinct spike waveforms. For instance, Purkinje cells are identified by the presence of simple and complex spikes and are confirmed to be a single unit by the presence of a pause in simple spikes after each complex spike[88]. Interestingly, the signal recorded when approaching a Purkinje cell depends on the location relative to the orientation of the cell. When approached from the molecular layer, the first signal that can be identified visually (and heard if the recordings signals are converted to audio) is that of the complex spikes. These large, slow spikes (lower tones) appear as negative deflections from the baseline, at ~1 Hz (**Fig. 3a, top**). Continuing in the direction of the soma will slowly reveal the ~50-100 Hz firing rate (a soft hum) of the simple spikes, also as negative deflections, while the complex spike signal slowly changes into a predominantly positive signal (See **Fig. 3a, middle**). Close to the soma, the spike waveform indicates the distance between the tip of pipette and neuron**.**

In extracellular recordings, the tip of an electrode is positioned adjacent to, but outside of a neuron, as depicted in **(Fig. 3a, upper middle)**. With a clean tip one can, in optimal circumstances and -if needed- aided by a little negative pressure, establish a juxtacellular recording **(Fig. 3a, lower middle)**. The ultimate step would be to proceed to whole cell patch clamp recording configuration, the most commonly used patch-clamp mode where the membrane patch is disrupted by briefly applying strong suction to establish electrical and molecular access to the intracellular space. It is the gold standard for high-fidelity analysis of the electrical properties and functional connectivity of neurons, but its success rate is much lower than extracellular and juxtacellular recording (**Fig. 3a, bottom**)[2,3,89].

Firing pattern. In the cerebellar cortex other cell types can identified, apart from Purkinje cells. Separating these is more complicated, but can be done quite reliably based on wave forms and firing characteristics under anesthesia as indicated by Ruigrok, et al.[19], although this is debated[90]. In this manner, granule cells can be identified by their high irregularity and low average firing rate; unipolar brush cells have a signature low CV2 (see "data analysis"); molecular layer interneurons typically stand out by their irregularity and intermediate to high firing rate, while Golgi cells have an intermediate firing rate and are more regular [19]. Due to the poor level of somatotopy in the cerebellar cortex, the potential to identify the recording area based on responses to sensory input is limited[91]. Nonetheless there are several exception of well-studied areas including: the (para)flocculus, which responds with reciprocal modulation of simple and complex spikes to visual and vestibular input[28,85], the saccade-related area in lobule VI and VII in which Purkinje cells respond to saccadic eye movements [29] and a designated area in the transitions between the vermis and the hemispheres and (the hemispheral parts of) lobules IV-V and lobule VI - simple lobule [24,35].

Labeling. To know the exact recording location when recording deeper in the brain, it is imperative to label the cell individually after completing the recording. The two most common forms of labeling with glass pipettes are iontophoresis and pressure injections, whereas with metal electrodes often lesions are placed to mark recording location. Iontophoresis results in minimal tissue damage, but requires a charged tracer or dye and has limited control over injection volume or concentration. Several tracers are very suitable for iontophoresis, including biotinylated dextran amines (i.e., BDA-3000), as they can be used for visualization of long-range axonal projections and hence require intact structures and up to a few days of survival after labeling[92,93]. Alternatively, an uncharged dye can be injected with controlled back-pressure on the glass pipette, such as Alcian Blue (0.1-2 % solution in saline, Sigma-Aldrich, USA) by air pressure[81,94]. Ideal for these injection are double barrel or septum borosilicate glass pipettes (e.g. theta septum, 1.5 OD, 1.02 ID, USA), one half of the pipette is filled with 2 M NaCl for recording, the other half barrel is filled with a blue dye for labeling. Although the immunohistological procedures are time-

consuming, iontophoresis-based injections allow for the most controlled small injections that, by controlling the amount of current and duration, ideally label only one cell.

Imaging. With the growing understanding of the complexity of the brain, there is also a growing appreciation for the diversity present, even within populations of a particular cell-type. To be able to characterize this diversity *in vivo*, tools are required to identify this subdivision within cell-types, either offline with immunohistochemistry, or online with fluorescent markers. Hence, to be able to identify the different cerebellar modules, based on the expression of zebrin, we used EAAT4-promotor driven eGFP expressing, or EAAT4-eGFP, mice[95]. EAAT4, or Excitatory Amino Acid Transporter 4, is expressed in a pattern similar to that of zebrin[96]. Alternatively, one could also use a zebrin (aldolase c) promotor driven expression of a fluorescent marker[97]. The strong expression of eGFP in both the dendrite and the soma readily identifies zebrin / EAAT4 positive Purkinje cells, but the weak expression in zebrin / EAAT4 negative cells helps localizing also those, and thus facilitates targeted recordings of both types, with a single genetic manipulation[81]. By visualizing also the recording pipette with Alexa-594 both the pipette and the preferred area can be made visible, allowing for selection of and careful, precise approaches to the chosen cells.

Data analysis

Several commercial software packages are available to analyze the recorded traces. Off-line analysis is performed here using SpikeTrain (Neurasmus B.V., Rotterdam, The Netherlands, www.neurasmus.com), running under Matlab (Mathworks, MA, USA). SpikeTrain is an object oriented program code that can use either superparamagnetic clustering[98] or on principal component analysis . After automated SS and CS detection and discrimination of simple spike and complex spike the assigned codes can be manually checked and corrected, if needed. Histograms of SS trigger on the occurrence of a CS (bin width 1 ms) can be used to verify that each isolated Purkinje cell shows a clean climbing fiber pause (i.e. no simple spikes for the duration of each complex spikes, see also **Fig. 3a**). The absence of a climbing fiber pause, the minimum duration between a complex spike and the following simple spike, is taken to indicate that the isolation is imperfect and there is a second unit present. For each cell several parameters for simple and complex spikes can be calculated, including: firing rate, CV and mean CV2, as well as the climbing fiber pause [84]. CV is the standard deviation of inter-spike intervals (ISI) divided by the mean, the mean CV2 is calculated as the mean of $2\cdot|(ISI)n+1 - ISIn|/(ISIn+1 + ISIn)$[99]. Both are measures for the regularity of the firing, also referred to as precision[50], with CV reflecting that of the entire recording and mean CV2 that of adjacent intervals, making the latter a measure of regularity on small timescales. In addition to auto-correlograms, which also illustrates the regularity, the presence of complex spikes also allows for cross-correlograms[100], of which the shape correlates with the cerebellar region[81,82].

Technical considerations

Several aspects need to be taken into account when performing recordings in vivo and when using fluorescent signals. First, when experimental procedures and ethical considerations allow doing so, recording in awake animals is preferable. Generalize anesthesia significantly reduces the discomfort of the animal and enhances the stability of the preparation, especially if the slower and deeper breathing can be properly controlled to avoid movement of the brain. However, anesthesia significantly impacts for instance Purkinje cells, and changes various properties of its firing activity, depending also on the type of anesthetic[48]. The effects of anesthetics are comprehendible, as the cerebellum is a sensorimotor integrator [101] and under anesthesia at least the motor part is disrupted. Isoflurane had a more pronounced effect on Purkinje cell activity then ketamine/xylazine in that it increased the pausing time and other parameters related to inter-spike intervals more severely[48].

Moreover, both in anesthetized and in awake animals it is essential to consider the role of temperature. It is common knowledge that in *in vitro* experiments temperature has a substantial influence on activity and plasticity. Similar effects can be predicted in vivo, but it is less clear to what extent they are present[102]. Using a miniature probe in vivo we found that the temperature drops dramatically at the surface of the craniotomy in the absence of any form of heating. In fact, we observed a temperature difference of up to 5°C compared to deeper parts of the cerebellum that correlated with a lower Purkinje cell simple spike firing rate in the first 0.5 to 1 mm of tissue[82]. Two-photon imaging only reaches to first couple of hundred micrometers, implicating that recordings under these conditions can be affected (compare **Fig. 3b vs. 3c**). A perfusion system, similar to that used in *in vitro* recordings, could potentially solve the issue, which is of particular relevance in studies that also include a behavioral component[103]. Conversely, during two-photon imaging photostimulation can hamper the success rate of obtaining patch recordings *in vivo*, possibly due to photo-damage or interactions with the pipette solution[4].

CONCLUSIONS

In this chapter we describe the use of extracellular recordings in mice during quiet wakefulness combined with methods to target specific subpopulations. We focus on cerebellar Purkinje cells and describe the approach to targeted recordings from specific sub-types of Purkinje cells. In addition to post-mortem labelling we detailed the approach to imaging based recordings of specific Purkinje cells. In mice expressing a fluorescent protein under a cell sub-type specific promotor (so-called zebrin-positive or negative neurons), we used two-photon imaging to identify the target neurons and subdivide them based on the

intensity of fluorescence. By visualizing the pipette tip with a fluorescent dye we assure an optimal approach to the identified neuron and create the potential to even do dual or multiple, side-by-side recordings. In this time of increasing appreciation for the heterogeneity within particular cell-types, the ability to make targeted recordings of specific sub-types will become more and more relevant.

REFERENCES

1 Hubel, D. H. & Wiesel, T. N. Receptive fields of single neurones in the cat's striate cortex. *J Physiol*. 1959; 148, 574-91.

2 van Welie, I., Roth, A., Ho, S. S. *et al.* Conditional Spike Transmission Mediated by Electrical Coupling Ensures Millisecond Precision-Correlated Activity among Interneurons In Vivo. *Neuron*. 2016; 90, 810-23.

3 Chen, S., Augustine, G. J. & Chadderton, P. The cerebellum linearly encodes whisker position during voluntary movement. *Elife*. 2016; 5, e10509.

4 Margrie, T. W., Meyer, A. H., Caputi, A. *et al.* Targeted whole-cell recordings in the mammalian brain in vivo. *Neuron*. 2003; 39, 911-8.

5 Komai, S., Denk, W., Osten, P. *et al.* Two-photon targeted patching (TPTP) in vivo. *Nat Protoc*. 2006; 1, 647-52.

6 Kitamura, K., Judkewitz, B., Kano, M. *et al.* Targeted patch-clamp recordings and single-cell electroporation of unlabeled neurons in vivo. *Nat Methods*. 2008; 5, 61-7.

7 Palay, S. L. & Chan-Palay, V. *Cerebellar cortex: cytology and organization*. 180-336 (Springer Verlag, 1974).

8 Kennedy, A., Wayne, G., Kaifosh, P. *et al.* A temporal basis for predicting the sensory consequences of motor commands in an electric fish. *Nat Neurosci*. 2014; 17, 416-22.

9 Eccles, J., Llinas, R. & Sasaki, K. Golgi Cell Inhibition in the Cerebellar Cortex. *Nature*. 1964; 204, 1265-6.

10 Eccles, J. C., Llinas, R. & Sasaki, K. The mossy fibre-granule cell relay of the cerebellum and its inhibitory control by Golgi cells. *Exp Brain Res*. 1966; 1, 82-101.

11 Eccles, J. C., Llinas, R. & Sasaki, K. The excitatory synaptic action of climbing fibres on the Purkinje cells of the cerebellum. *J Physiol*. 1966; 182, 268-96.

12 Schmolesky, M. T., Weber, J. T., De Zeeuw, C. I. *et al.* The making of a complex spike: ionic composition and plasticity. *Ann N Y Acad Sci*. 2002; 978, 359-90.

13 Najafi, F. & Medina, J. F. Beyond "all-or-nothing" climbing fibers: graded representation of teaching signals in Purkinje cells. *Front Neural Circuits*. 2013; 7, 115.

14 Ito, M. Cerebellar long-term depression: characterization, signal transduction, and functional roles. *Physiol Rev*. 2001; 81, 1143-95.

15 Winkelman, B. & Frens, M. Motor coding in floccular climbing fibers. *J Neurophysiol*. 2006; 95, 2342-51.

16 Yarom, Y. & Cohen, D. The olivocerebellar system as a generator of temporal patterns. *Ann N Y Acad Sci*. 2002; 978, 122-34.

17 Andersen, P., Eccles, J. & Voorhoeve, P. E. Inhibitory Synapses on Somas of Purkinje Cells in the Cerebellum. *Nature*. 1963; 199, 655-6.

18 van Beugen, B. J., Gao, Z., Boele, H. J. *et al.* High frequency burst firing of granule cells ensures transmission at the parallel fiber to purkinje cell synapse at the cost of temporal coding. *Front Neural Circuits*. 2013; 7, 95.

19 Ruigrok, T. J., Hensbroek, R. A. & Simpson, J. I. Spontaneous activity signatures of morphologically identified interneurons in the vestibulocerebellum. *J Neurosci*. 2011; 31, 712-24.

20 Albus, J. S. A theory of cerebellar function. *Math. Biosci.* 1971; 10, 25-61.

21 Marr, D. A theory of cerebellar cortex. *J Physiol*. 1969; 202, 437-70.

22 Ito, M., Sakurai, M. & Tongroach, P. Climbing fibre induced depression of both mossy fibre responsiveness and glutamate sensitivity of cerebellar Purkinje cells. *J Physiol*. 1982; 324, 113-34.

23 Schonewille, M., Gao, Z., Boele, H. J. *et al.* Reevaluating the role of LTD in cerebellar motor learning. *Neuron*. 2011; 70, 43-50.

24 ten Brinke, M. M., Boele, H. J., Spanke, J. K. *et al.* Evolving Models of Pavlovian Conditioning: Cerebellar Cortical Dynamics in Awake Behaving Mice. *Cell Rep*. 2015; 13, 1977-88.

25 Boyden, E. S., Katoh, A. & Raymond, J. L. Cerebellum-dependent learning: the role of multiple plasticity mechanisms. *Annu Rev Neurosci*. 2004; 27, 581-609.

26 Gao, Z., van Beugen, B. J. & De Zeeuw, C. I. Distributed synergistic plasticity and cerebellar learning. *Nat Rev Neurosci*. 2012; 13, 619-35.

27 Ito, M., Yamaguchi, K., Nagao, S. *et al.* Long-term depression as a model of cerebellar plasticity. *Prog Brain Res*. 2014; 210, 1-30.

28 Lisberger, S. G. & Fuchs, A. F. Response of flocculus Purkinje cells to adequate vestibular stimulation in the alert monkey: fixation vs. compensatory eye movements. *Brain Res*. 1974; 69, 347-53.

29 Thier, P., Dicke, P. W., Haas, R. *et al.* Encoding of movement time by populations of cerebellar Purkinje cells. *Nature*. 2000; 405, 72-6.

30 Pasalar, S., Roitman, A. V., Durfee, W. K. *et al.* Force field effects on cerebellar Purkinje cell discharge with implications for internal models. *Nat Neurosci*. 2006; 9, 1404-11.

31 Roy, J. E. & Cullen, K. E. A neural correlate for vestibulo-ocular reflex suppression during voluntary eye-head gaze shifts. *Nat Neurosci*. 1998; 1, 404-10.

32 Sato, Y., Miura, A., Fushiki, H. *et al.* Complex spike responses of cerebellar Purkinje cells to constant velocity optokinetic stimuli in the cat flocculus. *Acta Otolaryngol Suppl*. 1993; 504, 13-6.

33 Jorntell, H. & Ekerot, C. F. Reciprocal bidirectional plasticity of parallel fiber receptive fields in cerebellar Purkinje cells and their afferent interneurons. *Neuron*. 2002; 34, 797-806.

34 Yartsev, M. M., Givon-Mayo, R., Maller, M. *et al.* Pausing purkinje cells in the cerebellum of the awake cat. *Front Syst Neurosci*. 2009; 3, 2.

35 Hesslow, G. Inhibition of classically conditioned eyeblink responses by stimulation of the cerebellar cortex in the decerebrate cat. *J Physiol (Lond)*. 1994; 476, 245-56.

36 Ekerot, C. F. & Kano, M. Stimulation parameters influencing climbing fibre induced long-term depression of parallel fibre synapses. *Neurosci Res*. 1989; 6, 264-8.

37 Simpson, J. I. & Alley, K. E. Visual climbing fiber input to rabbit vestibulo-cerebellum: a source of direction-specific information. *Brain Res*. 1974; 82, 302-8.

38 Yagi, N., Chikamori, Y. & Matsuoka, I. Response of single Purkinje neurons in the flocculus of albino rabbits to caloric stimulation. *Acta Otolaryngol*. 1977; 84, 98-104.

39 Miyashita, Y. Eye velocity responsiveness and its proprioceptive component in the floccular Purkinje cells of the alert pigmented rabbit. *Exp Brain Res*. 1984; 55, 81-90.

40 Yoshida, M. & Kondo, H. Fear conditioning-related changes in cerebellar Purkinje cell activities in goldfish. *Behav Brain Funct*. 2012; 8, 52.

41 Sawtell, N. B., Williams, A. & Bell, C. C. Central control of dendritic spikes shapes the responses of Purkinje-like cells through spike timing-dependent synaptic plasticity. *J Neurosci*. 2007; 27, 1552-65.

42 Wylie, D. R. & Frost, B. J. Purkinje cells in the vestibulocerebellum of the pigeon respond best to either translational or rotational wholefield visual motion. *Exp Brain Res*. 1991; 86, 229-32.

43 Llinas, R., Bloedel, J. R. & Hillman, D. E. Functional characterization of neuronal circuitry of frog cerebellar cortex. *J Neurophysiol*. 1969; 32, 847-70.

44 Xiao, J., Cerminara, N. L., Kotsurovskyy, Y. *et al.* Systematic regional variations in Purkinje cell spiking patterns. *PLoS One*. 2014; 9, e105633.

45 Shin, S. L., Hoebeek, F. E., Schonewille, M. *et al.* Regular patterns in cerebellar Purkinje cell simple spike trains. *PLoS ONE*. 2007; 2, e485.

46 Hesslow, G. & Ivarsson, M. Suppression of cerebellar Purkinje cells during conditioned responses in ferrets. *Neuroreport*. 1994; 5, 649-52.

47 Lou, J. S. & Bloedel, J. R. The responses of simultaneously recorded Purkinje cells to the perturbations of the step cycle in the walking ferret: a study using a new analytical method--the real-time postsynaptic response (RTPR). *Brain Res*. 1986; 365, 340-4.

48 Schonewille, M., Khosrovani, S., Winkelman, B. H. *et al.* Purkinje cells in awake behaving animals operate at the upstate membrane potential. *Nat Neurosci*. 2006; 9, 459-61; author reply 61.

49 Arancillo, M., White, J. J., Lin, T. *et al.* In vivo analysis of Purkinje cell firing properties during postnatal mouse development. *J Neurophysiol*. 2015; 113, 578-91.

50 Walter, J. T., Alvina, K., Womack, M. D. *et al.* Decreases in the precision of Purkinje cell pacemaking cause cerebellar dysfunction and ataxia. *Nat Neurosci*. 2006; 9, 389-97.

51 Barmack, N. H. & Yakhnitsa, V. Functions of interneurons in mouse cerebellum. *J Neurosci*. 2008; 28, 1140-52.

52 Cajal, S. R. y. *Histologie du Système Nerveux de l'Homme et des Vertébrés*. Vol. I-II (1911).

53 Henle, J. *Handbuch der Nervenlehre des Menschen*. (Fachbuchverlag Dresden, 1879).

54 Scott, T. G. A Unique Pattern of Localization within the Cerebellum. *Nature*. 1963; 200, 793.

55 Leclerc, N., Dore, L., Parent, A. *et al.* The compartmentalization of the monkey and rat cerebellar cortex: zebrin I and cytochrome oxidase. *Brain Res*. 1990; 506, 70-8.

56 Brochu, G., Maler, L. & Hawkes, R. Zebrin II: a polypeptide antigen expressed selectively by Purkinje cells reveals compartments in rat and fish cerebellum. *J Comp Neurol*. 1990; 291, 538-52.

57 Graham, D. J. & Wylie, D. R. Zebrin-immunopositive and -immunonegative stripe pairs represent functional units in the pigeon vestibulocerebellum. *J Neurosci*. 2012; 32, 12769-79.

58 Sillitoe, R. V., Kunzle, H. & Hawkes, R. Zebrin II compartmentation of the cerebellum in a basal insectivore, the Madagascan hedgehog tenrec Echinops telfairi. *J Anat*. 2003; 203, 283-96.

59 Grandes, P., Mateos, J. M., Ruegg, D. *et al.* Differential cellular localization of three splice variants of the mGluR1 metabotropic glutamate receptor in rat cerebellum. *Neuroreport*. 1994; 5, 2249-52.

60 Nagao, S., Kwak, S. & Kanazawa, I. EAAT4, a glutamate transporter with properties of a chloride channel, is predominantly localized in Purkinje cell dendrites, and forms parasagittal compartments in rat cerebellum. *Neuroscience*. 1997; 78, 929-33.

61 Sarna, J. R., Marzban, H., Watanabe, M. *et al.* Complementary stripes of phospholipase Cbeta3 and Cbeta4 expression by Purkinje cell subsets in the mouse cerebellum. *J Comp Neurol*. 2006; 496, 303-13.

62 Barmack, N. H., Qian, Z. & Yoshimura, J. Regional and cellular distribution of protein kinase C in rat cerebellar purkinje cells [In Process Citation]. *J Comp Neurol*. 2000; 427, 235-54.

63 Jinno, S., Jeromin, A., Roder, J. *et al.* Compartmentation of the mouse cerebellar cortex by neuronal calcium sensor-1. *J Comp Neurol*. 2003; 458, 412-24.

64 Furutama, D., Morita, N., Takano, R. *et al.* Expression of the IP3R1 promoter-driven nls-lacZ transgene in Purkinje cell parasagittal arrays of developing mouse cerebellum. *J Neurosci Res*. 2010; 88, 2810-25.

65 Marzban, H., Khanzada, U., Shabir, S. *et al.* Expression of the immunoglobulin superfamily neuroplastin adhesion molecules in adult and developing mouse cerebellum and their localisation to parasagittal stripes. *J Comp Neurol*. 2003; 462, 286-301.

66 Altman, J. & Bayer, S. A. Time of origin and distribution of a new cell type in the rat cerebellar cortex. *Exp Brain Res*. 1977; 29, 265-74.

67 Harris, J., Moreno, S., Shaw, G. *et al.* Unusual neurofilament composition in cerebellar unipolar brush neurons. *J Neurocytol*. 1993; 22, 1039-59.

68 Pijpers, A., Apps, R., Pardoe, J. *et al.* Precise spatial relationships between mossy fibers and climbing fibers in rat cerebellar cortical zones. *J Neurosci*. 2006; 26, 12067-80.

69 Sugihara, I. & Shinoda, Y. Molecular, topographic, and functional organization of the cerebellar nuclei: analysis by three-dimensional mapping of the olivonuclear projection and aldolase C labeling. *J Neurosci*. 2007; 27, 9696-710.

70 Voogd, J. & Ruigrok, T. J. The organization of the corticonuclear and olivocerebellar climbing fiber projections to the rat cerebellar vermis: the congruence of projection zones and the zebrin pattern. *J Neurocytol*. 2004; 33, 5-21.

71 Apps, R. & Hawkes, R. Cerebellar cortical organization: a one-map hypothesis. *Nat Rev Neurosci*. 2009; 10, 670-81.

72 Sugihara, I. Compartmentalization of the deep cerebellar nuclei based on afferent projections and aldolase C expression. *Cerebellum*. 2011; 10, 449-63.

73 Sugihara, I., Fujita, H., Na, J. *et al.* Projection of reconstructed single Purkinje cell axons in relation to the cortical and nuclear aldolase C compartments of the rat cerebellum. *J Comp Neurol*. 2009; 512, 282-304.

74 Huang, C. C., Sugino, K., Shima, Y. *et al.* Convergence of pontine and proprioceptive streams onto multimodal cerebellar granule cells. *Elife*. 2013; 2, e00400.

75 Ruigrok, T. J. Ins and outs of cerebellar modules. *Cerebellum*. 2011; 10, 464-74.

76 Wadiche, J. I. & Jahr, C. E. Patterned expression of Purkinje cell glutamate transporters controls synaptic plasticity. *Nat Neurosci*. 2005; 8, 1329-34.

77 Shin, J. H., Kim, Y. S. & Linden, D. J. Dendritic glutamate release produces autocrine activation of mGluR1 in cerebellar Purkinje cells. *Proc Natl Acad Sci U S A*. 2008; 105, 746-50.

78 Kim, Y. S., Shin, J. H., Hall, F. S. *et al.* Dopamine signaling is required for depolarization-induced slow current in cerebellar Purkinje cells. *J Neurosci*. 2009; 29, 8530-8.

79 Kim, C. H., Oh, S. H., Lee, J. H. *et al.* Lobule-specific membrane excitability of cerebellar Purkinje cells. *J Physiol*. 2012; 590, 273-88.

80 Paukert, M., Huang, Y. H., Tanaka, K. *et al.* Zones of enhanced glutamate release from climbing fibers in the mammalian cerebellum. *J Neurosci*. 2010; 30, 7290-9.

81 Zhou, H., Lin, Z., Voges, K. *et al.* Cerebellar modules operate at different frequencies. *Elife*. 2014; 3, e02536.

82 Zhou, H., Voges, K., Lin, Z. *et al.* Differential Purkinje cell simple spike activity and pausing behavior related to cerebellar modules. *J Neurophysiol*. 2015; 113, 2524-36.

83 Peter, S., Ten Brinke, M. M., Stedehouder, J. *et al.* Dysfunctional cerebellar Purkinje cells contribute to autism-like behaviour in Shank2-deficient mice. *Nat Commun*. 2016; 7, 12627.

84 Goossens, J., Daniel, H., Rancillac, A. *et al.* Expression of protein kinase C inhibitor blocks cerebellar long-term depression without affecting Purkinje cell excitability in alert mice. *J Neurosci*. 2001; 21, 5813-23.

85 Schonewille, M., Luo, C., Ruigrok, T. J. *et al.* Zonal organization of the mouse flocculus: physiology, input, and output. *J Comp Neurol*. 2006; 497, 670-82.

86 Badura, A., Schonewille, M., Voges, K. *et al.* Climbing fiber input shapes reciprocity of Purkinje cell firing. *Neuron*. 2013.

87 White, J. J., Lin, T., Brown, A. M. *et al.* An optimized surgical approach for obtaining stable extracellular single-unit recordings from the cerebellum of head-fixed behaving mice. *J Neurosci Methods*. 2016; 262, 21-31.

88 Simpson, J. I., Wylie, D. R. & De Zeeuw, C. I. On climbing fiber signals and their consequence(s). *Beh.Brain Sciences*. 1996; 19, 380-94.

89 Bengtsson, F. & Jorntell, H. Specific relationship between excitatory inputs and climbing fiber receptive fields in deep cerebellar nuclear neurons. *PLoS One*. 2014; 9, e84616.

90 Haar, S., Givon-Mayo, R., Barmack, N. H. *et al.* Spontaneous activity does not predict morphological type in cerebellar interneurons. *J Neurosci*. 2015; 35, 1432-42.

91 Manni, E. & Petrosini, L. A century of cerebellar somatotopy: a debated representation. *Nat Rev Neurosci*. 2004; 5, 241-9.

92 Pinault, D. A novel single-cell staining procedure performed in vivo under electrophysiological control: morpho-functional features of juxtacellularly labeled thalamic cells and other central neurons with biocytin or Neurobiotin. *J Neurosci Methods*. 1996; 65, 113-36.

93 Boele, H. J., Koekkoek, S. K., De Zeeuw, C. I. *et al.* Axonal sprouting and formation of terminals in the adult cerebellum during associative motor learning. *J Neurosci*. 2013; 33, 17897-907.

94 Hoebeek, F. E., Stahl, J. S., van Alphen, A. M. *et al.* Increased noise level of purkinje cell activities minimizes impact of their modulation during sensorimotor control. *Neuron*. 2005; 45, 953-65.

95 Gincel, D., Regan, M. R., Jin, L. *et al.* Analysis of cerebellar Purkinje cells using EAAT4 glutamate transporter promoter reporter in mice generated via bacterial artificial chromosome-mediated transgenesis. *Exp Neurol*. 2007; 203, 205-12.

96 Dehnes, Y., Chaudhry, F. A., Ullensvang, K. *et al.* The glutamate transporter EAAT4 in rat cerebellar Purkinje cells: a glutamate-gated chloride channel concentrated near the synapse in parts of the dendritic membrane facing astroglia. *J Neurosci*. 1998; 18, 3606-19.

97 Fujita, H., Aoki, H., Ajioka, I. *et al.* Detailed expression pattern of aldolase C (Aldoc) in the cerebellum, retina and other areas of the CNS studied in Aldoc-Venus knock-in mice. *PLoS One*. 2014; 9, e86679.

98 Quiroga, R. Q., Nadasdy, Z. & Ben-Shaul, Y. Unsupervised spike detection and sorting with wavelets and superparamagnetic clustering. *Neural Comput*. 2004; 16, 1661-87.

99 Holt, G. R., Softky, W. R., Koch, C. *et al.* Comparison of discharge variability in vitro and in vivo in cat visual cortex neurons. *J Neurophysiol*. 1996; 75, 1806-14.

100 De Zeeuw, C. I., Wylie, D. R., Stahl, J. S. *et al.* Phase Relations of Purkinje Cells in the Rabbit Flocculus During Compensatory Eye Movements. *J of Neurophysiol.* 1995; 74, 2051-63.

101 De Zeeuw, C. I., Hoebeek, F. E., Bosman, L. W. *et al.* Spatiotemporal firing patterns in the cerebellum. *Nat Rev Neurosci*. 2011; 12, 327-44.

102 Kalmbach, A. S. & Waters, J. Brain surface temperature under a craniotomy. *J Neurophysiol*. 2012; 108, 3138-46.

103 Long, M. A. & Fee, M. S. Using temperature to analyse temporal dynamics in the songbird motor pathway. *Nature*. 2008; 456, 189-94.

Chapter 4

The basal interstitial nucleus (BIN) of the cerebellum provides diffuse ascending inhibitory input to the floccular granule cell layer

Dick Jaarsma[1]*, Francois Blot[1], Bin Wu[1], Subramanian Venkatesan [1], Jan Voogd[1], Dies Meijer[2], Tom J.H. Ruigrok[1], Zhenyu Gao[1], Martijn Schonewille[1], and Chris I. De Zeeuw[1,3]

1. Dept. of Neuroscience, Erasmus MC, Rotterdam, the Netherlands
2. Centre of neuroregeneration, University of Edinburgh, Edinburgh, UK
3. Netherlands Institute for Neuroscience, Amsterdam, the Netherlands

Published on Journal of Comparative neurology (2018)

ABSTRACT

The basal interstitial nucleus (BIN) in the white matter of the vestibulocerebellum has been defined more than three decades ago, but has since been largely ignored. It is still unclear which neurotransmitters are being used by BIN neurons, how these neurons are connected to the rest of the brain and what their activity patterns look like. Here, we studied BIN neurons in a range of mammals, including macaque, human, rat, mouse, rabbit and ferret, using tracing, immunohistological and electrophysiological approaches. We show that BIN neurons are GABAergic and glycinergic, that in primates they also express the marker for cholinergic neurons choline acetyl transferase (ChAT), that they project with beaded fibers to the glomeruli in the granular layer of the ipsilateral floccular complex, and that they are driven by excitation from the ipsilateral and contralateral medio-dorsal medullary gigantocellular reticular formation. Systematic analysis of co-distribution of the inhibitory synapse marker VIAAT, labeled BIN axons and Golgi cell marker mGluR2 indicate that BIN axon terminals complement Golgi cell axon terminals in glomeruli, accounting for a considerable proportion (> 20%) of the inhibitory terminals in the granule cell layer of the floccular complex. Together, these data show that BIN neurons represent a novel and relevant inhibitory input to the part of the vestibulocerebellum that controls compensatory and smooth pursuit eye movements.

INTRODUCTION

The cerebellar cortex is well known for its relatively simple stereotyped trilaminar histo-architecture and sagittally organized modules [1,2], and represents a powerful model system for investigating the organization and computations of complex central nervous system circuitries [3-5]. The cerebellar cortex receives two main types of excitatory afferent systems, the climbing fiber system and the mossy-parallel fiber system, that converge on a single output neuron, the Purkinje cell that in turn provides inhibitory control of the cerebellar and vestibular nuclei. Climbing fibers arise from the inferior olive and innervate about 8-15 Purkinje cells each, providing an exceptionally strong direct synaptic connection with well over ~1,000 release sites distributed over a large portion of the dendritic tree [5-7]. Mossy fibers originate from various sources in the brainstem and spinal cord and modulate Purkinje cell activity indirectly via the granule cells and inhibitory interneurons [8]. With about 100-200 rosettes per mossy fiber, each innervating about 10-20 granule cells that in turn may form synaptic terminals with more than 500 Purkinje cells, the mossy fibers represent a highly divergent system [5,9-11]. One of the key questions regarding the cerebello-cortical circuitry is how mossy fiber activity is translated into granule cell activity and subsequently integrated into Purkinje cell activity[12-14].

Mossy fibers are morphologically heterogeneous, encode diverse modalities and may evoke greatly distinct patterns of excitatory responses in granule cells across different parts of the cerebellar cortex[15-18]. Therefore, it is feasible that also the down-stream cerebellar cortical circuitries display modality and task-depending variabilities[12,15,19]. For example, the activity patterns and learning mechanisms of different cerebellar modules may be dominated by Purkinje cells with different intrinsic electrophysiological and biochemical properties[2,20,21]. In addition, the flocculus and nodulus of the vestibulocerebellum, which are involved in compensatory eye and body movements [22-25] show a marked enrichment of unipolar brush cells (UBCs), an excitatory granular layer interneuron, which can prolong the excitatory drive of the mossy fiber system [5,26-28]. Furthermore, there is evidence for heterogeneity of inhibitory granule cell layer interneurons across distinct lobules[29-32].

In the present study, we show that the granule cell layer of the flocculus receives an inhibitory input from a hitherto largely neglected population of neurons, the basal interstitial nucleus (BIN), which was originally identified by Langer in macaque [33,34]. We found that BIN cells in human, rodents, ferret and rabbit are, just like in macaque, mainly located in the white matter of the lateral vestibulocerebellum, and that they are GABAergic and glycinergic. In addition, we show in rodents that BIN neurons receive a relevant and unique excitatory input from the medio-rostral medullary reticular formation. Our data indicate that the BIN represents a novel inhibitory afferent system, which may play an essential role in the proper conversion of mossy fiber activity into Purkinje cell firing in the flocculus.

MATERIALS AND METHODS

Animals. GlyT2GFP transgenic mice that express enhanced green fluorescent protein under the control of the glycine transporter type 2 promoters were kindly provided by Dr. Fritschy [35] and maintained as hemizygotes in C57BL/6 background in the ErasmusMC animal core facility. VGluT2-ires-Cre knock-in mice, generated by Dr. Lowell [36], were obtained from Jackson Laboratories (JAX#016963, and maintained as homozygotes in the Erasmus MC animal core facility. Young (3-4 weeks) and adult (3-6 months) male Wistar rats were obtained from Charles River. Animals were group housed until surgery, fed ad libitum, and kept at 12:12 light/dark cycle. Cerebella from adult pigmented Dutch belted rabbits (n = 2), ferret (n = 2), and macaque monkey (n = 4) were derived from animals used in other studies [37-40].

Human tissue. Human cerebella were obtained via the Dutch National body donation program. Donors gave their informed and written consent to the donation of their bodies to the Erasmus MC for research and education purposes. In this study we used cerebellar tissue from two male donors who died at 74 and 78 years of age. Cerebellar specimens were dissected within 48 h following death and fixed in formalin for 6-8 weeks.

Stereotaxic injections. For stereotaxic injections of Cholera toxin B-subunit (CTB) in rat flocculus, animals (n = 2) were anesthetized with an intraperitoneal injection of thiazinehydrochloride (3 mg/kg) and ketamine (100 mg/kg), placed in a stereotactic frame, and their caudal vermis was exposed by removing overlying skin and neck muscles and opening of the atlanto-occipital membrane and dura. Carprofen (Rimadyl Cattle i.p. 5 mg/kg) and lidocaine (s.c. 0,4 mg/ml) were used to reduce perisurgical pain. The flocculus was approached by a glass micropipette (tip diameter 10 - 20 µm), placed horizontally at an angle of 50 degrees with the rostrocaudal axis, and penetrating the cerebellum 6.5 mm starting from the midline at the border of lobule IX-B and -C [41]. 100 nl CTB (1% w/v in phosphate buffered saline, pH 7.2, 0.1 M) was injected with mechanical pressure at a speed of 10 nl/min. After injection, the pipette was left in place for >10 minutes before being slowly withdrawn. After a survival period of 5 to 7 days, rats were deeply anesthetized with an overdose of Nembutal (200 mg/kg) and transcardially perfused with an initial flush of 500 ml 0.9% saline, followed by 1 liter of 4% paraformaldehyde (PFA) in 0.12 M phosphate buffer (PB, pH 7.4). Methods for stereotaxic injections in mice were largely as previously reported [18,24,42]. Mice were positioned on a custom-made mouse stereotaxic head-holding frame following the Paxinos mouse brain atlas [43], small craniotomies (diameter ~3 mm) were made in corresponding sites, and injections were performed using glass pipettes (tip opening 8 - 15 µm) with mechanical pressure or iontophoresis. Alternatively, anterograde tracing was performed using AAV viral vector

expressing enhanced GFP [44,45]: 50-100 nl purified AAV1.CAG.CI.eGFP.WPRE.rBG (AAV-GFP, 10^{12}-10^{13} GC/ml) or AAV1.CAG.Flex.eGFP.WPRE.bGH (AAV-Flex-GFP), purchased from UPenn Vector Core, were pressure injected. To examine BIN axons in the flocculus, AAV-GFP was injected in C57BL/6 mice (n=10) using the following coordinates: 1.4 posterior of Lambda, 2.4 mm lateral and 2.6 mm ventral of the pial surface. The same coordinates were used for CTB injections in the BIN of C57BL/6 mice (n=4) to characterize brain stem neurons that innervate BIN neurons. Coordinates of BDA injections in the medullary gigantocellular reticular nucleus that resulted in labeling of fibers innervating BIN neurons were 2,3-2,6 mm posterior of lambda, 0,2-0,4 mm lateral, 4,6 - 4,8 ventral of the pial surface. These coordinates were also used for AAV-Flex-GFP injections in VGluT2-Cre mice (n=2) to demonstrate that medullary gigantocellular reticular nucleus projections to BIN neurons were VGluT2+ neurons. For injection in the inferior olive, penetrations were made with reference to the obex and guided by electrophysiological recording, and injections were made using iontophoresis [46]. CTB injections in the floccular cortex were performed in alert, head-fixed restrained GlyT2GFP (n=3) and C57BL/6 (n=2) mice placed on a platform in the center of a random dotted drum to enable identification of floccular zones on the basis of complex spike modulation of Purkinje cells triggered by optokinetic stimulation [24]. In these mice, a head fixation pedestal was fixed to the skull with dental cement (Charisma, Heraeus Kulzer, NY, USA) 5 days prior to injection, and a recording chamber was made following craniotomy of the occipital bone [24].

Antibody characterization. Primary antibodies used for immunohistology were from commercial sources with the exception of a rat monoclonal antibody against Lgi2 The commercial primary antibodies have been well characterized in previous studies [18,30,39,47-49]. The labelling specificity for Lgi2 was determined using cerebellar sections from Lgi2 knockout mice, which did not show any labelling. Furthermore, the labelling pattern in the cerebellar cortex is consistent with the expected distribution based on mRNA expression in Allan Brain Atlas [50]. Further details of the production and validation of the rat-anti Lgi2 antibody will be reported elsewhere.

Immunohistology and Slice recording, for details refer to Methods in Chapter 3.
Immunoperoxidase histochemistry was used for mapping BIN neurons using the following antibodies: goat anti-ChAT (1:500; Millipore AB144P, RRID:AB_11214092), rabbit anti-Glutamic acid decarboxylase 65 and 67 (GAD; 1:2000; Millipore AB1511, RRID:AB_90715), mouse anti-GAD67 (1:1000; Millipore MAB5406), rabbit anti-Necab1 (1:1000; Sigma, HPA023629; RRID:AB_1848014), or mouse anti-NeuN (1:2000; Millipore, MAB377; RRID:AB2298772).

Analyse. To map and count BIN neurons in different species, series of sections processed for bright-field microscopy were examined and plotted using an Olympus microscope fitted with a Lucivid miniature monitor and Neurolucida software (MicroBrightField, Inc., Colchester, VT), while fluorescently-labeled section selected areas were scanned at a 0.625 x 0.625 x 2.5 µm (xyz) resolution using a LSM 700 confocal microscopes (Carl Zeiss, Jena, Germany) with Plan-Apochromat 20x (n.a. 0.8) objective and the tile function, and analyzed using ImageJ. To plot and count BIN neurons in macaque cerebellum we used 1 in 5 transverse thionin-stained serial sections (section thickness 40 µm, 160 µm interval between sections), and 1 in 10 GAD- and ChAT-immunoperoxidase stained series (360 µm between sections). Only cells with a visible nucleus were counted. In case of human cerebellum, ChAT-stained serial sections in a final frequency of 1 in 10 (section thickness 50 µm, 450 µm interval between section) were used for counting and plotting BIN neurons. For mapping the distribution of BIN neurons in rat, we used 1 in 4 CTB-immunoperoxidase/thionin stained series of transverse sections (120 µm interval) of previously documented (rat #798, rat #802, rat #836; [41] For mapping BIN neurons in rabbit, we used previously documented WGA-HRP experiments with tracer injections in the floccular cortex (K227, K244, K358, K360; [52]) and 40 µm GAD-immunoperoxidase stained sections at frequencies of 1 in 10 (360 µm interval between sections). To analyze anterograde BDA tracing experiments with injections made throughout the brainstem, 1 in 4 sections were processed for ABC peroxidase-DAB staining to map the injection area, and examine the floccular white matter for the presence of BDA+ beaded fibers contacting BIN neurons. BIN neurons were examined for the presence of BDA+VGluT2+ and BDA-VGluT2+ boutons using a LSM 700 confocal microscope with Plan-Apochromat 40x (n.a. 1.3) and 63x (n.a. 1.4) oil objectives. Only BDA+VGluT2+ and BDA-VGluT2+ boutons contacting BIN cell bodies and their proximal dendrites were analyzed.

Statistical analyses. Statistical analyzes were performed with Graphpad Prism using Student's t-test and ANOVA. Data are expressed as Means ± SE.

RESULTS

ChAT (choline acetyltransferase) immunostaining outlines the basal interstitial nucleus (BIN) in macaque cerebellum

While analyzing the distribution of immunoreactivity of choline acetyltransferase (ChAT, the terminal biosynthetic enzyme for acetylcholine) in macaque cerebellum, we identified a group of ChAT+ cells dispersed in the white matter ventrolateral of the cerebellar nuclei (Fig. 1a). The distribution and morphology of these ChAT+ neurons coincided with that of the basal interstitial nucleus (BIN), identified by Langer after retrograde tracing injections in the flocculus or the ventral paraflocculus [33,34]. Like BIN neurons, ChAT+ cells had relatively

large polymorphic cell bodies (area = 441 ± 18 μm^2, 251-720; mean ± SE, range, n=40 cells), and formed a cluster that extended from the hilus of the ventral paraflocculus to the white matter of the most rostral folium of the nodulus, respectively, with most ChAT+ cells in the white matter medial of the stalk of the flocculus (Fig. 1a,f). While most BIN neurons had a fusiform elongated morphology with dendrites emanating from each end, other BIN neurons showed pyramidal and polygonal morphologies (Fig. 1b). Notably, ChAT+ cells were also observed in Group Y, medial of the BIN, but these cells were much smaller (104 ± 5 μm^2, mean ± SE, n=10 cells) and clearly distinguishable from ChAT+ BIN cells (Fig. 1c).

In accord with the notion that BIN neurons innervate the flocculus/ventral paraflocculus (also referred to as the floccular complex; see [25], ChAT+ fibers in the BIN were oriented towards the white matter of the floccular complex, and a high density of ChAT+ fibers occurred in the white matter and granule cell layer of the floccular complex (Fig. 1a,d). In the granule cell layer, the ChAT+ fibers provided multiple beaded branches resulting in a dense plexus of ChAT+ varicose fibers (Figs 1d). These beaded ChAT+ fibers occurred throughout the floccular complex, but were absent in other cerebellar lobules, including the dorsal paraflocculus (Fig. 1e) and the nodulus. The density of ChAT+ fibers varied across different lobules of the floccular complex: grossly, ChAT+ fibers were more frequent in the flocculus than in the ventral paraflocculus and were denser in the basal than the apical part of individual folia (Fig.1f). Together, the data indicate that BIN neurons in macaque are ChAT+ and provide dense ChAT+ innervation of the granule cell layer in the floccular complex.

BIN neurons provide GABAergic input to the granule cell layer of the flocculus/ventral paraflocculus

Further characterization of the neurochemical identity of macaque BIN neurons showed that BIN neurons also stained positive with anti-glutamic acid decarboxylase (GAD) antibody. GAD/ChAT double labeling showed that all ChAT+ BIN neurons stained positive for GAD (Fig. 2a, b), while an additional population of neurons inside the macaque BIN territory was negative for ChAT, but stained positive for GAD (Fig. 2a, b). These GAD+ChAT- BIN neurons showed the same size and morphologies as those of GAD+ChAT+ BIN neurons. Thus, the BIN in macaque may comprise 2 neurochemically distinct populations of neurons, GAD+ChAT+ and GAD+ChAT- neurons. Counting of serial ChAT and GAD immunoperoxidase stained sections indicated that there were about 1000 (1.3 ± 0.3 $*10^3$, mean ± SE, n= 3) ChAT+ and 2000 (2.2 ± 0.2 $*10^3$, n= 3) GAD+ BIN cells per half macaque cerebellum.

GAD/ChAT double labelling also showed that the cell bodies and proximal dendrites of BIN neurons were only sparsely covered by GAD+ nerve terminals. In this respect, BIN neurons were distinct from cerebellar nuclear neurons, whose cell bodies and proximal dendrites are densely innervated by GAD+ synaptic terminals from Purkinje cells axons (compare Fig.

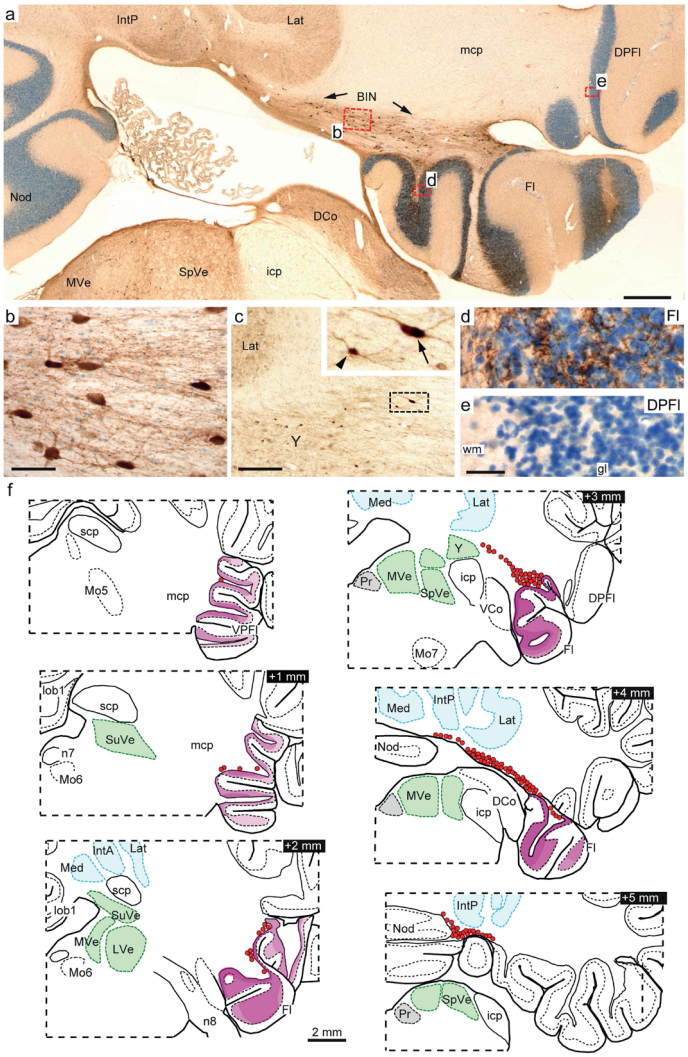

Figure 1. Choline Acetyltransferase (ChAT) immunostaining outlines the basal interstitial nucleus (BIN) in macaque cerebellum. a-e: Low-power (a) and high power (b-e) photomicrographs of ChAT immunoperoxidase diaminobenzidine (DAB) stained coronal sections of Macaque cerebellum illustrating intensely stained BIN neurons in the basal white matter between the flocculus and the cerebellar nuclei (a,b), and ChAT+ beaded fibers in the floccular granule cell layer (a,d). The photomicrograph in c illustrates that ChAT+ BIN neurons (arrow) are considerably larger than ChAT+ neurons in group Y (arrow head). No or minimal ChAT+ fibers occur in the dorsal paraflocculus (DPFl; a,e). Sections are counterstained with thionin (blue). f: Plots of ChAT+ BIN neurons (red dots) and relative density of ChAT+ beaded fibers (violet staining) in serial coronal macaque cerebellar sections. Cerebellar and vestibular nuclei are indicated in light blue and green, respectively. Abbreviations: DCo, dorsal cochlear nucleus; DPFl, Dorsal paraflocculus; Fl, Flocculus; icp, inferior cerebellar peduncle; IntA, anterior interposed cerebellar nucleus; IntP, posterior interposed nucleus; Lat, lateral cerebellar nucleus; mcp, middle cerebellar peduncle; LVe, lateral vestibular nucleus; MVe, medial vestibular nucleus; Nod, Nodulus; Pr, prepositus hypoglossi; SpVe, spinal vestibular nucleus; SuVe, Superior vestibular nucleus. Scale bars: a, 500 µm; c, 200 µm; b and e, 50 µm

2b and e). Analysis of GAD/ChAT double labelling in the floccular complex showed that ChAT+ axons in the granule cell layer were GAD+ (Fig. 2c), supporting the notion that ChAT+ fibers in these lobes are axons from BIN neurons. Moreover, these GAD+ChAT+ labeled axonal projections were morphologically distinct from ChAT+ mossy fibers in the nodulus that were GAD-negative (Fig. 2e). In contrast to previous monkey studies suggesting that ChAT+ fibers in the flocculus represent mossy fibers from the medial vestibular and the prepositus hypoglossal nuclei [53,54], we found virtually no ChAT+ fibers in the macaque flocculus that showed the typical mossy fiber morphology.

ChAT+ boutons in the flocculus/ventral paraflocculus did not stain positive for the mGluR2 metabotropic glutamate receptor (Fig. 2f), which is expressed by the majority of cerebellar Golgi cells, and is present on a large proportion of the GABAergic nerve terminals in the glomeruli [29,30,55]. Notably, glomeruli with ChAT+ boutons always also contained mGluR2+ boutons (Fig. 2f), indicating that BIN axon terminals complement Golgi cell axonal terminals in the same glomeruli. Triple staining of ChAT and mGluR2 with antibodies against VIAAT (vesicular inhibitory amino acid transporter, also termed vesicular GABA transporter, VGAT) to outline GABAergic/glycinergic inhibitory nerve terminals, showed that ChAT+ boutons, like mGluR2+ boutons, were VIAAT+ (Fig. 2g), further indicating that ChAT+ fibers in the macaque flocculus are GABAergic. In addition to ChAT+mGluR2-VIAAT+ and ChAT-mGluR2+VIAAT+ boutons we also found ChAT-mGluR2-VIAAT+ boutons in the floccular glomeruli (Fig. 2g). Analysis of 50 floccular glomeruli in ChAT/VIAAT/mGluR2 triple-stained sections showed that about two-thirds (64 ± 2 %; mean ± SE) of the VIAAT+ boutons were ChAT-mGluR2+, while about one-third of the VIAAT+ boutons were mGluR2-, consisting of ChAT+mGluR2- (21 ± 1.4%) and ChAT-mGluR2- (15 ± 1.7%) boutons. We also performed triple staining of ChAT and VIAAT with VGluT1 to outline mossy fiber nerve endings (rosettes). This staining indicated that the distribution of ChAT+VIAAT+ boutons in floccular glomeruli resembles that of ChAT-VIAAT+ boutons (Fig. 2h). Together these data indicate that a portion of inhibitory boutons in the macaque floccular glomeruli does not arise from mGluR2+ Golgi cells, and that about half of these mGluR2- boutons represent axon terminals from ChAT+ BIN neurons. For comparison, in the dorsal paraflocculus, which is not innervated by BIN afferents, we found more than 90% (94 ± 1%) of VIAAT+ boutons in the glomeruli to be mGluR2+.

In ChAT/VIAAT/mGluR2 stained sections we also noted ChAT+VIAAT+ boutons in glomeruli with a dendritic brush of unipolar brush cells (UBCs), which also may stain positive for mGluR2 [56]. Double labeling for ChAT and calretinin, which outlines a subset of UBCs [27], showed the presence of ChAT+ boutons surrounding calretinin+ UBC brushes (Fig. 2i). However, we also found calretinin+ brushes that were not surrounded by ChAT+ boutons. This was particularly evident in a region of the ventral paraflocculus that shows a dramatic

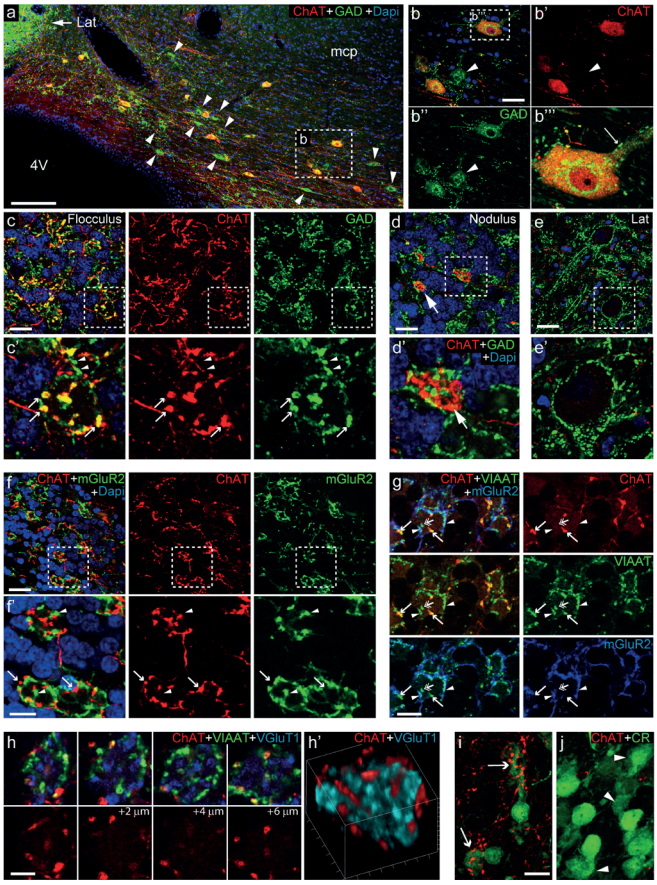

Figure 2. Macaque BIN neurons provide GABAergic input to the granule cell layer of the flocculus. a-e: Double labelling confocal immunofluorescence for ChAT and glutamic acid decarboxylase 65/67 (GAD) shows that ChAT+ neurons in the BIN (a,b) and ChAT+ axonal terminals in the granule cell layer of the flocculus (arrows in c) are also positive for GAD, while ChAT+ mossy fibers in the granule cell layer of the nodulus are negative for GAD (arrow in d). Note in panel a and b, that the BIN also contains ChAT-GAD+ neurons (arrow heads in a, b). Also note that both ChAT+ and ChAT- BIN neurons are only sparsely covered by GAD+ nerve terminals (thin arrow in b'''), which differs from deep cerebellar nuclear neurons whose cell bodies and proximal dendrites are densely innervated by GAD+ synaptic terminals (e). Note in c' that ChAT+GAD+ boutons (arrows) complement ChAT-GAD+ boutons (arrow heads) in the same glomerulus. f, g: ChAT/mGluR2 double staining (f) and ChAT/mGluR2/VIAAT triple staining (g), shows that ChAT+ fibers and boutons (arrows in f and g) are always mGluR2-, and complement mGluR2+ boutons (arrow heads in f and g) in glomeruli in the floccular granule cell layer. Both ChAT+ and mGluR2+ boutons stain positive for VIAAT. In g, also note the presence of ChAT-mGluR2-VIAAT+ nerve terminals (double-headed arrow). h: Serial confocal optical sections and 3D-reconstructions of an exemplary mossy fiber ending labeled by VGluT1 that is surrounded by ChAT+VIAAT+ and ChAT-VIAAT+ nerve endings. i, j: High magnifications of ChAT/calretinin (CR) double staining in the granule cell layer of the ventral paraflocculus showing examples of CR+ UBCs with a substantial number of ChAT+ nerve endings surrounding their brush-like dendritic arbor (arrows in i) as well as CR+ UBCs with virtually no ChAT+ nerve endings surrounding the 'brush' (arrow heads in j). Scale bars: a, 100 µm; b-f, 25 µm; g, 10 µm; h, 5 µm; i, 20 µm.

enrichment of UBCs and virtually no ChAT+ fibers (Fig. 2j). These data indicate that ChAT+ boutons do not have a simple all or none relationship with glomeruli containing UBC dendritic brushes.

ChAT-staining outlines the BIN in human cerebellum

To examine whether a BIN-like population of neurons also occurs in other species, we first examined human cerebellum. Using ChAT staining, we found a population of ChAT+ neurons in the basal white matter, reminiscent of BIN neurons in macaque (Fig. 3a,b). ChAT+ neurons were distributed in an area extending from the nodulus to the peduncles of the flocculus and the accessory paraflocculus (i.e. the human homologue of the macaque ventral paraflocculus;[25], ChAT+ neurons being most abundant near the base of the floccular peduncle (Fig. 3a,b). As in macaque, these ChAT+ neurons showed variable morphologies, had moderately large cell bodies (area = 533 ± 31 μm^2, 281-770; mean ± SE, range, n=20 cells), and stained positive for GAD (Fig. 3c,d). These data indicate that also in human cerebellum the BIN can be outlined using ChAT and GAD staining. Based on analysis of 1 out of 10 sections we estimate that about 5000 ($4.6 \pm 0.7*10^3$; Mean ± SE, n= 2) ChAT+ BIN neurons occur on each side of the cerebellum in human. The quality of the GAD staining did not allow counting of GAD+ BIN cells in human series.

As in macaque, ChAT+ fibers emanating from the human BIN were oriented towards the white matter of the flocculus and the accessory paraflocculus, and the flocculus/accessory paraflocculus showed a correspondingly high density of ChAT+ fibers in the white matter as well as a dense network of ChAT+ beaded fibers in the granule cell layer (Fig. 3e,f). However, in contrast to macaque, the human cerebellum also showed a subset of Golgi cells that were ChAT+ (Fig. 3f,g; see also [57]), and, hence, ChAT+ innervation in the human flocculus/accessory paraflocculus may also derive from Golgi cells. The overall density of granular layer ChAT+ innervation in these lobules was higher than in other lobules. A particularly high density of ChAT+ fibers occurred in the areas of the floccular granule cell layer that contained ChAT+ Golgi cells (Fig. 3f), suggesting that in these areas ChAT+ axons are from both BIN neurons and Golgi cells. We were not able to further characterize the identities of ChAT+ boutons in the human floccular complex with reliable mGluR2 and VIAAT immuno-staining, probably due to limited possibilities of fixation and antigen epitope preservation of our human brain specimen.

Retrograde tracing and GAD-staining outlines the BIN in rat cerebellum

To further examine the occurrence of BIN neurons in other species we moved to rat. No ChAT+ neurons are present in the white matter of rat cerebellum [47,58]. However, following floccular cortical injections with cholera toxin B subunit (CTB) [41], we identified retrogradely labeled neurons in the hilus and the white matter of the ipsilateral flocculus (Fig. 4a-c).

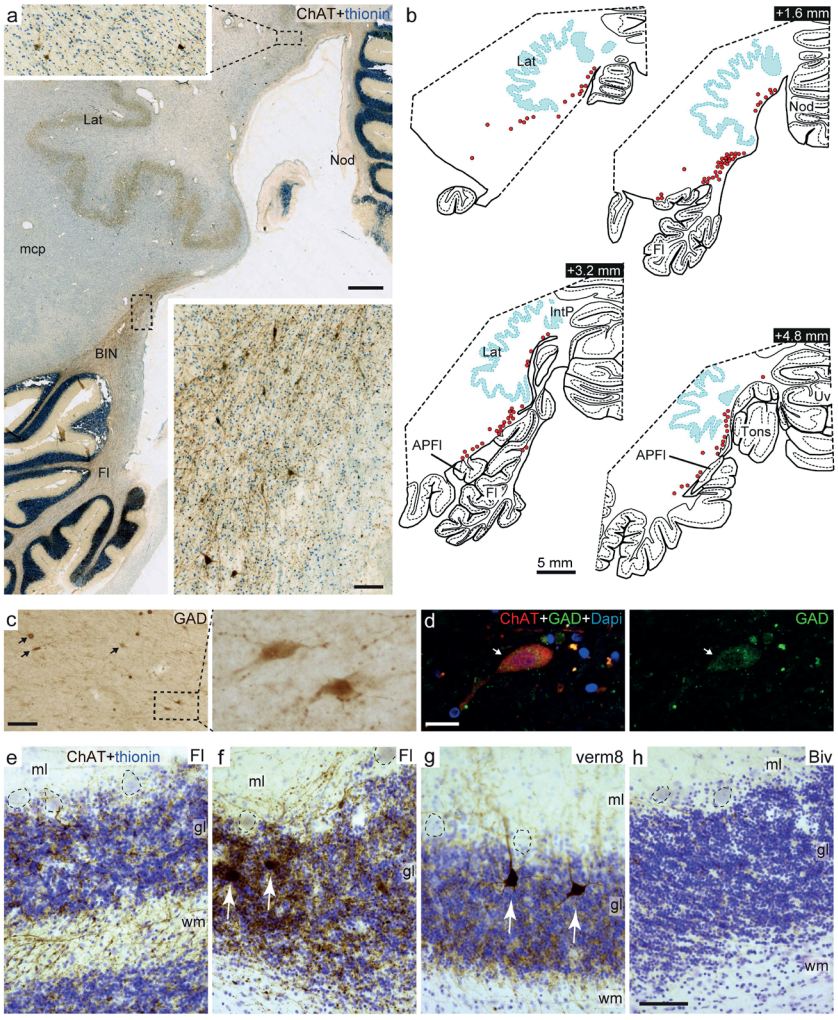

Figure 3. ChAT-staining outlines the BIN in human cerebellum. a: Low- and high-power (inserts) photomicrographs of ChAT immunoperoxidase diaminobenzidine (DAB) stained coronal sections of human cerebellum showing a cluster of ChAT stained neurons in the white matter between the flocculus and the lateral cerebellar nucleus (Lat) that is reminiscent of the BIN in macaque. b: Plots of ChAT+ neurons in the basal white matter of human cerebellum. ChAT+ neurons are most abundant in the white matter, extending from the ventrolateral aspect of the lateral cerebellar nucleus (Lat) to the peduncles of the flocculus and the accessory paraflocculus (APFl). c, d: GAD immunoperoxidase-DAB (c) and immunofluorescent (d) staining of BIN neurons arrows in c and d. The BIN neuron shown in d (arrow) also is ChAT+. e-h: ChAT immunoperoxidase-DAB staining reveals variable densities of ChAT+ beaded fibers in the granule cell layer of different lobules that correlate with the presence of ChAT+ Golgi cells: in the flocculus, high densities of ChAT+ fibers occurs in parts of the granule cell layer containing ChAT+ Golgi cells (white arrows in f, g), while moderate levels of ChAT+ fibers occur in parts without ChAT+ Golgi cells (e). Moderate levels of ChAT+ fibers also occur in lobules with ChAT+ Golgi cells, e.g. lobule 8 of the vermis (g). Lobules of the hemispheres with no ChAT+ Golgi cells do not show ChAT+ fibers (h, biventral lobule). Scale bars: a, 1 mm (overview) and 100 µm (insert); c and h, 100 µm (also for e-g); d, 20 µm.

These retrogradely labeled neurons occurred throughout the rostro-caudal extent of the floccular white matter (Fig. 4a), were moderately large in size, and had multipolar and fusiform morphologies (Fig. 4b,c) reminiscent of macaque BIN neurons. Furthermore, these retrogradely labeled white matter neurons were all GAD+ (Fig. 4d). Based on their localization in the white matter and their similarities with macaque BIN neurons, we designate these neurons the rat homologues of macaque BIN neurons [41]. Notably, no retrogradely labeled BIN neurons occurred in an animal where the injection was centered in the ventral paraflocculus (e.g. case 902 in [41].)

The rat BIN neurons could also be identified in thionin and NeuN stained sections, based on their size and localization in the white matter (Fig. 4c,e). Based on CTB tracing, GAD/NeuN staining and morphological criteria we propose that the BIN area in rat is rostro-medially delimited by the medial and inferior cerebellar peduncles, and more caudo-medially by the lateral cerebellar nuclei and group Y (Fig. 4a). Ventro-medially some BIN neurons may populate the cochlear nuclear superficial granule cell layer that borders the floccular white matter (Fig. 4a,b). Based on counting of GAD/NeuN and thionin stained serial sections, we estimate that in rat there are about 600-700 ($0.66 \pm 0.06 * 10^3$; Mean ± SE, n= 3) BIN neurons per side. We also estimated the number of retrogradely labeled BIN neurons in three animals following CTB injections in the floccular cortex (rat #798, rat #802 and rat #836; [41]). Importantly, although injection areas covered less than 20% (15 ± 2%, mean ± SE) of the floccular granule cell layer, more than 70% (78 ± 5%) of BIN neurons were retrogradely labeled. These data suggest that projections from multiple BIN neurons converge on the same portion of the granule cell layer.

Electrophysiological characterization of rat BIN neurons in acute slices

To electrophysiologically characterize the BIN cells, we performed whole cell recording in acute transverse slices of rat cerebellar cortex. After recordings, cells were filled with neurobiotin for morphological analysis (Fig. 5a,b). Consistent with immunohistological data neurobiotin-filled BIN neurons showed fusiform or polygonal cell bodies with long dendrites that extend in the white matter from opposite poles of the cell. In 3 of 7 cells dendritic branches also extended into the granule cell layer to reach the Purkinje cell layer (Fig. 5a,b). The axon extended from the cell body or a proximal dendrite and produced multiple branches, many of which left the slice. In 2 of 7 cells we could trace several axonal branches innervating a substantial portion of the granule cell layer within the slice (Fig. 5a,b). The axonal branches produced a network of fine beaded fibers with multiple ramifications (Fig. 5b-d). Co-staining for mGluR2 and VGluT1 confirmed that the neurobiotin-labeled axons do not stain for mGluR2, but co-distribute with mGluR2+ axonal profiles in glomeruli identified with VGluT1-staining of the mossy fiber rosettes (Fig. 5c,d). Typically, individual branchlets of the BIN-axon innervated 10-20 glomeruli with 2-5 bou-

tons/per glomerulus (Fig. 5c,d). These data are consistent with the notion emerging from our tracing experiments that individual BIN neurons have diffuse widespread projections, innervating large proportions of the floccular granule cell layer.

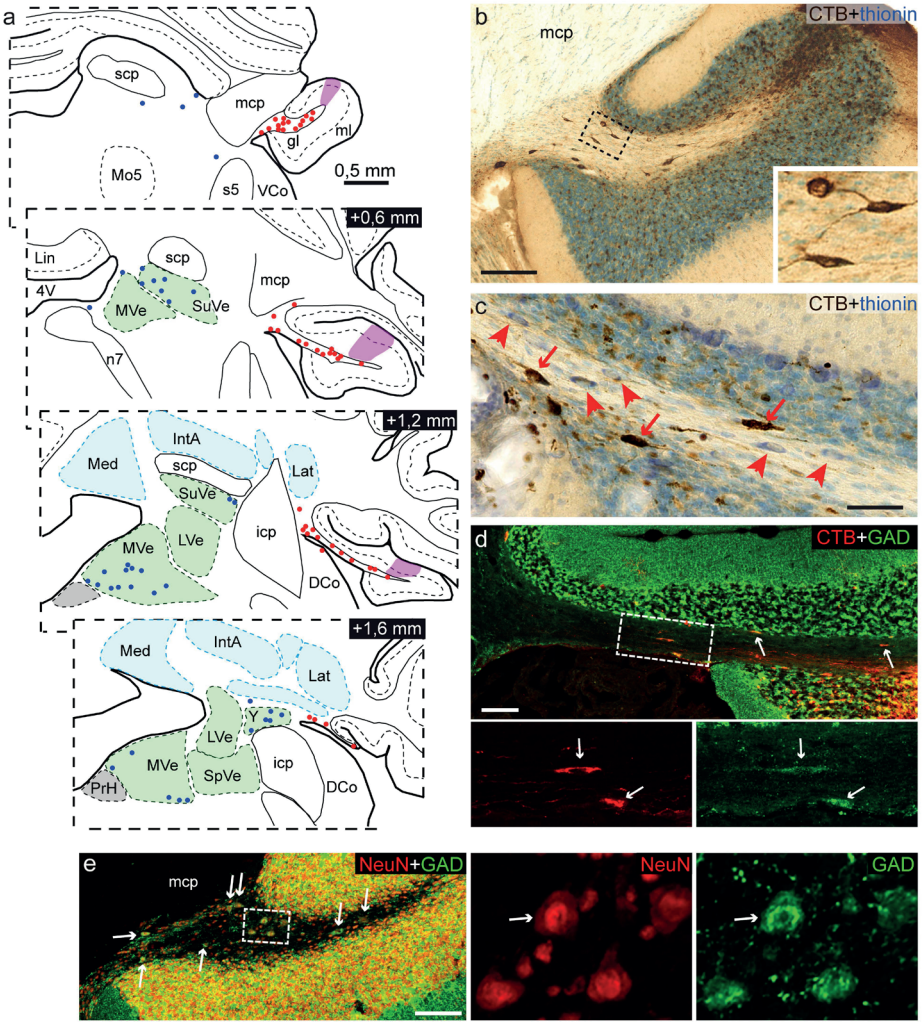

Figure 4. BIN neurons in rat. a-c: Plot (a) and photomicrographs (b, c) of retrogradely cholera toxin ß subunit (CTB) labeled BIN neurons (red dots in a; red arrows in c) following a small CTB injection in the flocculus (purple area in a); sections and plots are from rat 836 described in [41]. Note that retrogradely CTB labeled neurons also occur in the vestibular nuclei (blue dots in a). Arrowheads in c point to unlabeled BIN neurons. d: Double labelling confocal immunofluorescence for GAD and CTB shows that retrogradely CTB labeled BIN neurons (arrows) are GAD+. e: Double labelling confocal immunofluorescence for GAD and NeuN shows that GAD+ BIN neurons in the rat floccular white matter (arrows) are NeuN+. Scale bars: b,d and e 100 µm; c, 50 µm.

Cell attached recordings from 7 morphologically validated BIN neurons indicated that they were silent (n=5) or fired at low frequency (8.4 and 5.6 Hz respectively). The capacitance of the cells was 48 ± 10 pF (15-88; Mean ± SE, ranges, n = 7). We next determined their excitability in current clamp mode. Increasing depolarizing current injections with 20 pA increment triggered increased firing rates (Fig. 5e,f) with a rheobase current of 50 ± 10 pA (Mean ± SE, n=7), action potential (AP) threshold of -43 ± 2 mV (Fig. 5g), peak AP amplitude of 93 ± 6 mV, AP rise and decay times of 0.55 ± 0.02 and 1.18 ± 0.05 ms, respectively, and afterhyperpolarization amplitude of 12 ± 1 mV. Whole-cell voltage-clamp recoding uncovered spontaneous EPSC (sEPSC) in BIN cells (Fig. 5h-j), with sEPSC amplitudes of 17.69 ± 3.13 pA and frequencies of 3.93 ± 1.14 Hz. Together the data indicate that BIN neurons are readily excitable, receive excitatory input (see below), but show a low level of intrinsic firing activity in acute slices.

Necab1outlines BIN neurons in mouse flocculus

To further characterize the BIN in rodents we performed retrograde CTB tracing in GlyT-2GFP mice that express GFP under control of the GlyT2 gene promoter to label glycinergic neurons [35]. We found that all retrogradely labeled BIN neurons were GFP+, indicating that BIN neurons are also glycinergic (Fig. 6a, b). Counting of serial GlyT2GFP sections indicated that mice have about 300 ($0.33 \pm 0.02 * 10^3$, mean ± SE, n = 6 flocculi from 3 animals) BIN neurons per side. Consistent with data from rat, CTB retrograde tracing in mouse showed that, while the injection areas covered less than 20%, (12 ± 3%, n = 3) of the floccular granule cell layer, more than 60% (63 ± 2%) of GFP+ BIN neurons were retrogradely labeled, indicative of widespread overlapping projection of BIN neurons. Together the data indicate that also in mice BIN neurons are distributed throughout the hilus and white matter of the flocculus.

As in macaque and rat, BIN neurons in the floccular white matter mice can be differentiated from Golgi cells in the floccular granule cell layer based on the absence of mGluR2 immunoreactivity (Fig. 6c). BIN neurons stained positive for the cholinergic muscarinic M2 receptor (Fig. 6d), which is expressed in cerebellar Golgi cells in multiple mammalian species [39,58]. To further identify genes that are expressed by BIN neurons, we used the AGEA (Anatomic Gene Expression Atlas) viewer modus of Allen Brain Atlas that examines gene expression in user defined neuroanatomical areas. We screened nearly 2000 genes for distinct signal in intermediate-large cells in the white matter of the anterior flocculus. In accord with our immunohistological data, no visible signal occurs in the floccular white matter of *mGluR2* mRNA labeled sections, whereas sections stained for *Gad1 (Gad67)*, *Gad2 (Gad65)*, *GlyT2 (Slc6A5)* and *ChRM2* mRNA show labelling of intermediate-sized cells in the floccular white matter, indicative of labelling of BIN neurons (Fig. 6e). Of 89 genes with distinct labelling of BIN neurons identified in our screen, the majority (85 of

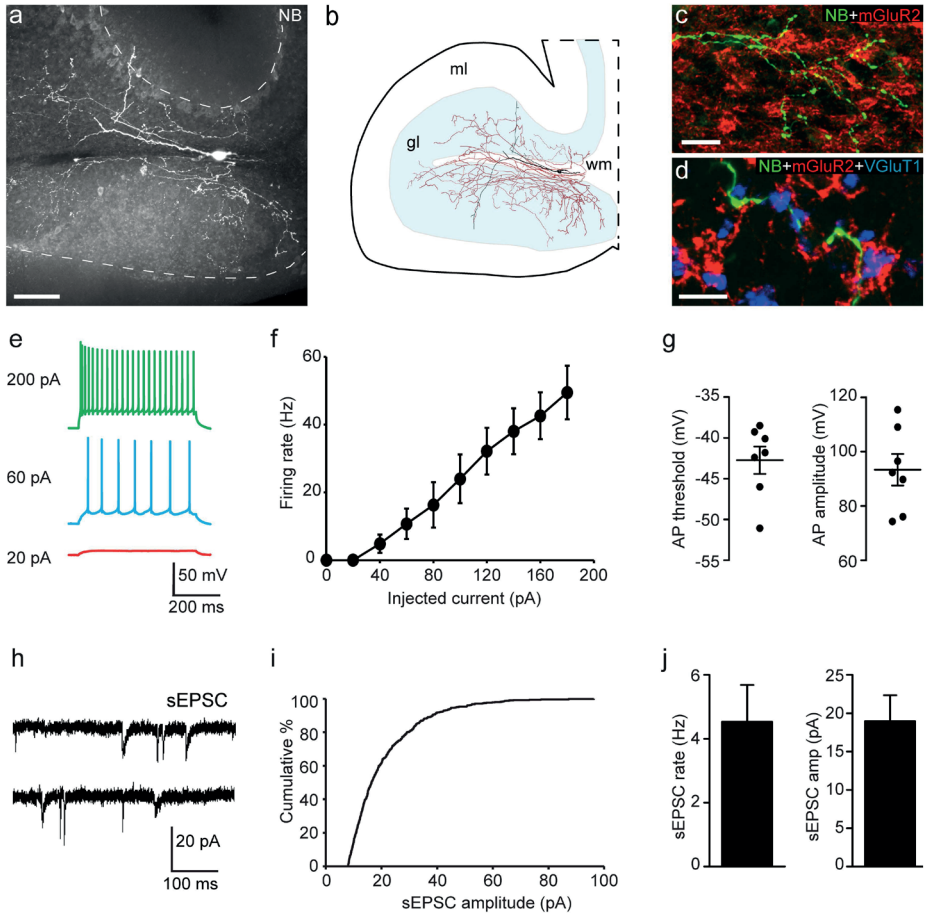

Figure 5. Evoked action potentials and spontaneous EPSC in rat BIN neurons. a-d: Example of a recorded BIN neuron filled with 1% neurobiotin (NB) visualized with A488-streptavidin. NB filling reveals an extensive axonal tree, and dendritic branches that may extend in the granule cell layer. Axonal branches are mGluR2- and contact multiple glomeruli characterized by the presence of VGluT1+ mossy fiber endings and mGluR2+ Golgi cell axons (c, d). Scale bars: b, 100 µm; c, 25 µm; d, 10 µm. e: Example traces of subthreshold depolarization of and evoked action potentials with increasing depolarizing current injection. f: Average firing rate of BIN neurons (mean ± SE, n=7 cells) as a function of the injected current during the depolarizing step. g: Action potential threshold and amplitudes (individual values and means ±SE). h-j: Example traces (h), cumulative distribution of sEPSC activity from an exemplary BIN neuron (i), and mean ± SE of sEPSC frequencies and amplitudes (j) of recorded BIN neurons (n=6).

89) showed similar expression in granule cell layer interneurons, while showing variable expression in other cerebello-cortical neuronal populations. Examples of genes that like *GlyT2* and *ChRM2* are expressed in both BIN neurons and granule cell layer interneurons, include acetylcholine esterase (*AChE*) and *Lgi2* (Fig. 6e). Out of the 2000 genes examined, we identified only four genes with distinct expression in BIN neurons and no apparent expression in granule cell layer interneurons in the flocculus. For one of these, *Necab1* (N-

terminal EF-hand calcium Binding protein 1) expression in BIN neurons was confirmed by immunohistology (Fig. 6f,g): Analysis of Necab1 immunostaining in GlyT2GFP mice shows that all GFP+ neurons in the floccular hilus and white matter, stain positive for Necab1, while other floccular cells, including GlyT2+ Golgi and Lugaro cells show no or very weak staining for Necab1 (Fig. 6f). Accordingly, BIN neurons identified by retrograde CTB-tracing were always strongly Necab1+ (Fig. 6g). Necab1 immunohistology also showed that BIN neurons may have one or more dendritic branches extending into the granule cell layer (Fig. 6f), consistent with data from rat neurobiotin-filled BIN neurons. Together, the data indicate that Necab1 selectively outlines BIN neurons in the mouse flocculus, consistent with the idea that they represent a specific class of floccular neurons.

Absence of Necab1+ and Neurogranin+ Golgi cells in mouse flocculus

While granule cell layer interneurons in the flocculus show no or very weak Necab1 expression, a substantial subset of granule cell layer interneurons in other cerebellar lobules stained positive for Necab1 (Fig. 6f). The Necab1+ granule cell layer interneurons included both GlyT2GFP+ and GlyT2GFP- neurons (Fig. 6f). These data indicate that Necab1 outlines one or more subclasses of granule cell layer interneurons that are absent in the flocculus. To further characterize Necab1+ granule cell layer interneurons, and differences between the flocculus and other cerebellar lobules we compared the distribution of Necab1 with that of mGluR2 and neurogranin in sections from GlyT2GFP mice. A previous study focusing on lobules 4-6 of the vermis [30] showed that several subclasses of granule cell layer interneurons can be differentiated on the basis of differential expression of these markers, including a population of GlyT2GFP+mGluR2+neurogranin+ cells (designated type 1 Golgi cells), two populations that are GlyT2GFP+mGluR2+, but neurogranin- (type 2 and 3 Golgi cells), GlyT2GFP-GluR2-neurogranin+ cells (type 4 Golgi cells), and GlyT2GFP+ cells that are neurogranin-mGluR2- (representing Lugaro and globular cells). Consistent with this classification we found that in lobule 4-5 of the vermis (verm4/5) neurogranin occurred in GlyT2GFP+ as well as GlyT2GFP- Golgi cells (Fig. 7a), and that GlyT2GFP-/neurogranin+ cells were negative for mGluR2 (type 4 Golgi cells), while GlyT2GFP+/neurogranin+ Golgi cells were mGluR2+ (type 1 Golgi cells). However, no neurogranin+ Golgi cells occurred in the flocculus, and furthermore also BIN neurons stained negative for neurogranin (Fig. 7b). Like neurogranin, Necab1 in verm4/5 occurred in either GlyT2GFP-/mGluR2- (potentially type 4 Golgi cells) or GlyT2GFP+/mGluR2+ (potentially type 1 Golgi cells), but not in GlyT2GFP+/mGluR2- cells (Lugaro/globular cells) (data not shown). Double labeling for Necab1 and neurogranin showed consistent codistribution of neurogranin and Necab1 in GlyT2GFP- (type 4) Golgi cells, but incomplete colocalization in GlyT2GFP+ Golgi cells (Fig. 7c). These data indicate that Necab1 is expressed in type 4 Golgi cells, to variable extent is expressed by other Golgi cell subtypes, but is not expressed in Lugaro/globular cells.

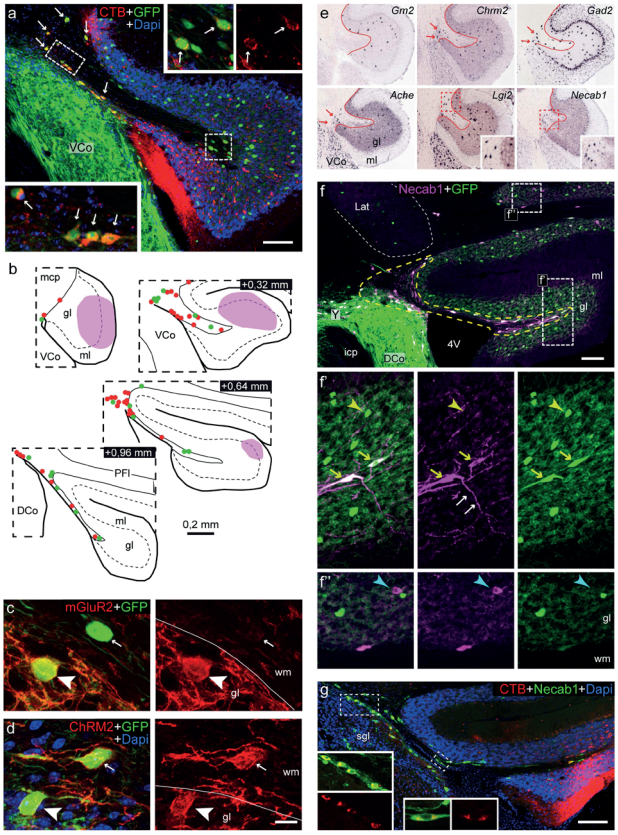

Figure 6. BIN neurons in mouse flocculus identified by retrograde CTB tracing and Necab1 immunostaining. a, b: Double labelling confocal immunofluorescent image (a) and plot (b) of CTB-labeled BIN neurons (arrows in a; red dots in b) following CTB injection in the flocculus (purple area in b outline the injection area) of GlyT2GFP transgenic mice (a is from mouse Gly1; b is from mouse Gly4). All retrogradely CTB labeled BIN neurons are also positive for GFP (arrows in a). GlyT2-GFP+ BIN neurons that are not positive for CTB are indicated by green dots in b. c, d: Confocal immunofluorescence of mGluR2 (c) and muscarinic M2 receptor (d) in the flocculus of a GlyT2GFP transgenic mouse. GlyT2+ Golgi cells in the granule cell layer (gl) stain positive for mGluR2 (arrow heads in c) and muscarinic M2 receptor (arrow heads in d), while GlyT2GFP BIN neurons are M2+ and mGluR2- (small arrows in c and d). wm, white matte. e: In situ hybridization image from Allan Brain Atlas showing that mGluR2 (Gm2) mRNA is expressed in granule cell layer (gl) but not in white matter cells of the flocculus, while muscarinic M2 receptor (Chrm2), GAD65 (Gad2), AChE and Lgi2 mRNA occur cells in both the granule cell layer and the white matter (red arrows). Necab1 mRNA, instead, is expressed in cells in the floccular white matter, but not in the granule cell layer. f, g: Confocal images of Necab1 immunostaining in the flocculus of a GlyT2GFP mouse (f), and a non-trangenic mouse receiving a CTB tracer injection in the flocculus (g). Intense Necab1 staining is present in GlyT2GFP+ neurons (yellow arrows in f) and CTB-traced BIN neurons (g, see inserts). Note in f', that dendrites of some Necab1+ BIN neurons may extend in the granule cell layer (white arrows in f'). Also note in f, a population of Necab1+ neurons in the granule cell layer of the paraflocculus (cyan arrow head in f''), while no Necab1+ neurons occur in the granule cell layer of the flocculus (yellow arrow head in f' points to a GlyT2GFP+ Golgi cell in the flocculus). Scale bars: a,f and g, 100 µm; d, 10 µm.

We further characterized differences in Golgi cells between the flocculus and verm4/5 using an antibody against Lgi2. Lgi2-immunostaining occurred in granule cell layer interneurons as well as BIN neurons, in accord with mRNA expression data from Allan brain atlas (Fig. 6e). Lgi2/mGluR2 and Lgi2/neurogranin double labeling in GlyT2GFP mice indicated that in verm4/5 Lgi2 is expressed in all Golgi cells, but not in Lugaro/globular cells: thus, in Lgi2/mGluR2 labeled sections, Lgi2-immunostaining outlines GlyT2GFP+mGluR2+ cells (type 1-3 Golgi cells) and GlyT2GFP-mGluR2- cells (potentially type 4 Golgi cells), but is not present in GlyT2GFP+mGluR2- cells (Lugaro/globular cells) (data not shown). Lgi2/neurogranin staining showed that GlyT2GFP-Lgi2+ cells all stain positive for neurogranin (Fig. 7d,e) and indeed represent type 4 Golgi cells. Consistent with the notion that type 4 Golgi cells do not occur in the flocculus we found that all Lgi2+ cells in the floccular granule cell layer were GlyT2+mGluR2+, with the exception of sporadic GlyT2GFP+ cells that like BIN neurons are Necab1+ (Fig. 7f,g). Cell counts in Lgi2/Necab1/GlyT2GFP and Lgi2/neurogranin/GlyT2GFP labeled sections indicated that the density of Lgi2+ Golgi cells is slightly, but non-significantly ($p = 0.09$; unpaired 2-tailed *t*-test) higher in verm4/5 compared to the flocculus, with 227 ± 17 (Mean ± SE, n=3 animals) Lgi2+ cells/mm^2 in verm4/5 and 187 ± 11 (n=4) Lgi2+ cells/mm^2 in the floccular granule cell layer, respectively. In verm4/5 87% (197 ± 15) of the Lgi2+ Golgi cells were GlyT2GFP+ representing type 1-3 Golgi cells, whereas in the flocculus all Lgi2+ cells were GlyT2+. In sum, our comparison of Golgi cells between verm4-5 and flocculus using established (mGluR2, neurogranin, GlyT2) and novel markers (Lgi2, Necab1) of (subsets of) Golgi cells, uncovered differences in the neurochemical identities of Golgi cells in the flocculus versus the anterior vermis [30]. In particular, the absence of neurogranin+, Necab1+, and Lgi2+GlyT2GFP- Golgi cells in the flocculus indicates that type 4 Golgi cells are not present in the flocculus, all Golgi cells being mGluR2+GlyT2+.

BIN neurons innervate granule cells dendrites in floccular glomeruli

Based on analysis of BIN nerve terminals in macaque and rat, we anticipate that BIN axons provide inhibitory input to granule cell dendrites, and complement inhibitory input from Golgi cells in floccular glomeruli. To further examine the axonal projections of BIN neurons we injected AAV-GFP viral particles into the white matter and hilus of the flocculus of mice (Fig. 8a). We obtained 7 injections centered in the hilus of the flocculus infecting BIN neurons and resulting in a variable degree of axonal labelling in the ipsilateral flocculus (Fig. 8b,c). Labeled axons were morphologically distinct from mossy fibers, and form a plexus of thin fibers with multiple VIAAT-positive nerve terminals (Fig. 8c) resembling BIN fibers in macaque (Fig. 2) and rat (Fig. 5a-c). No GFP+VIAAT+ labeled axons occurred in the flocculus in case of more dorsal and medial injections that targeted the cerebellar nuclei, but did not target BIN neurons. The highest densities of labeled fibers occurred in experiments, where also BIN neurons in the floccular white matter were infected (Fig. 8b).

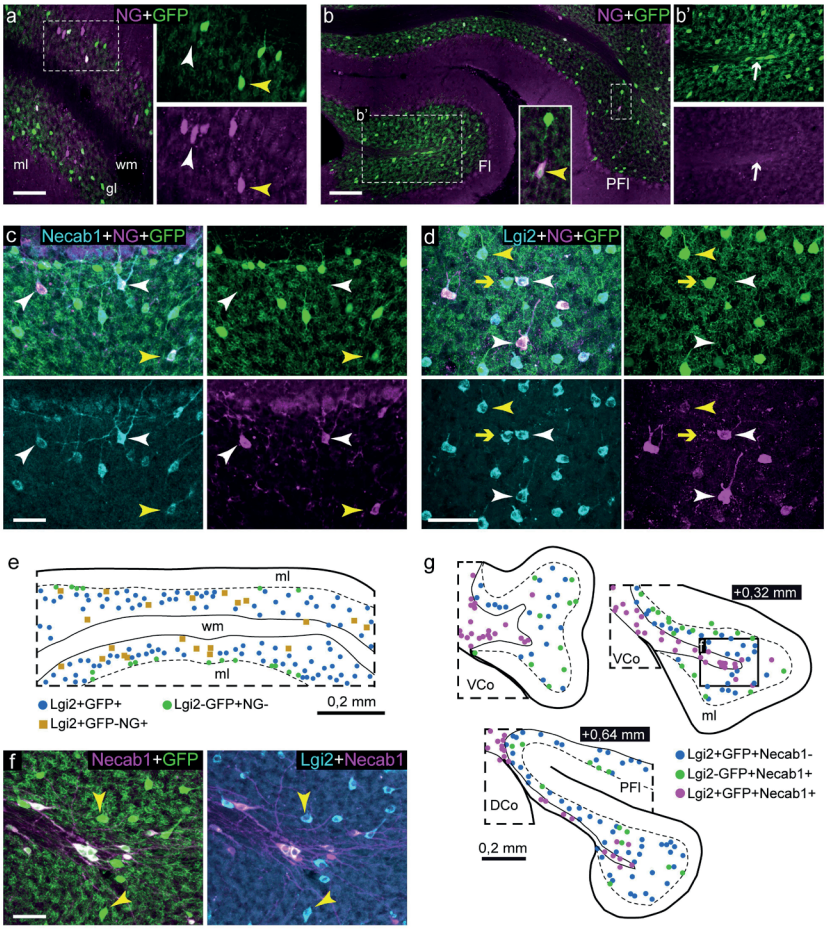

Figure 7. Absence of Necab1+ and Neurogranin+ Golgi cells in mouse flocculus. a,b: Confocal images of neurogranin-immunostaining in GlyT2GFP mouse cerebellar cortex, showing that in lobule 4-5 of the vermis (a) neurogranin (NG, rabbit antibody) labelling occurs in GFP- (white arrow head) and GFP+ Golgi cells (yellow arrow head), while in the flocculus (Fl in b) there are no neurogranin+ Golgi cells. Note in flocculus, that BIN neurons (white arrow in b') do not stain for neurogranin, while sporadic neurogranin+ cells can be observed in the adjacent ventral paraflocculus (PFl, yellow arrow head in insert in b). c: Staining for neurogranin (mouse antibody) and Necab1 in vermis 4-5 of GlyT2GFP mouse illustrates that neurogranin and Necab1coditribute in GFP- Golgi cells (white arrow heads), and show variable codistribution in GFP+ Golgi cells (e.g. yellow arrow head points to GlyT+neurogranin+Necab1+ cell). d: Staining for neurogranin (rabbit antibody) and Lgi2 in vermis 4-5 of GlyT2GFP mice shows that Lgi2 is present in neurogranin+GFP- (white arrow heads), neurogranin+GFP+ (yellow arrow heads), and neurogranin-GFP+ Golgi cells (yellow arrow). e: Plot of vermis 4-5 in coronal section of GlyT2GFP mouse stained for Lgi2 and neurogranin; the plot outlines the distribution of type 1-3 Golgi cells (blue dots, Lgi2+GFP+), type 4 Golgi cells (light brown squares, Lgi2+GFP-NG+) and Lugaro/globular cells (green dots, Lgi2+GFP-NG-). Lgi2+GFP- cells always were also positive for neurogranin. f,g: Confocal image (f) and plot (g) illustrating the distribution of Golgi cells (Lgi2+GFP+Necab1-, yellow arrow heads in f, blue dots in g), Lugaro/globular cells (green dots, Lgi2+GFP-Necab1-), and BIN neurons (magenta dots, Lgi2+GFP+Necab1+) in coronal sections of the flocculus. Scale bars: a, 100 µm; b, 200 µm; c, d, f, 50 µm.

To characterize the post-synaptic target of AAV-GFP labeled BIN axons, we performed transmission electron microscopy of anti-GFP immunoperoxidase histochemistry with diaminobenzidine (DAB) as a substrate. Consistent with GFP fluorescence, DAB precipitate was associated with thin axonal profiles and presynaptic boutons with diameters ranging from 1 to 2 µm. Labeled axon terminals were localized in glomeruli (Fig. 8d). Analysis of 40 labeled axon terminals, revealed multiple synaptic contacts with granule cell dendrites (Fig. 8d). Post-embedding immunogold labelling for GABA showed that DAB-labeled profiles in all occasions (n=30) are enriched in GABA-immunoreactivity (Fig. 8e,f) Together the data indicate that BIN axons like Golgi cell axon terminals [6,59-61] primarily innervate granule cell dendrites.

BIN inhibitory input complements mGluR2+ Golgi axon terminals in glomeruli in the mouse flocculus

Immunostaining of AAV-GFP labeled sections for VIAAT, mGluR2 and VGluT1 showed that GFP+ BIN axon terminals always are mGluR2-negative, but co-distribute with VIAAT+mGluR2+ boutons in the same glomeruli (Fig. 8g,h). In addition, the same glomeruli also contained VIAAT+ terminals that are both mGluR2- and GFP-negative (Fig. 8g). To obtain an estimate of the proportion of mGluR2+ Golgi versus BIN axon terminals in the floccular granule cell layer we determined the proportion of VIAAT+ boutons labeled by either GFP or mGluR2 in confocal stacks from the three AAV-GFP injections that yielded the highest level of BIN axonal labelling (i.e. VBIN2, VBIN3, VBIN5). This analysis showed that 10-20% of the area labeled by VIAAT was GFP+ whereas 50-60% of the VIAAT+ area was mGluR2+ (Fig. 8i). For comparison, we analyzed the proportion of mGluR2+ VIAAT+ boutons in the nodulus and lobules 3 and 4/5 of the anterior vermis (Fig. 8j,k). In the anterior vermis, more than 90-95% of VIAAT+ area was mGluR2+ (Fig. 8j,k), consistent with the notion that inhibitory axons in the glomeruli primarily derive from mGluR2+ Golgi cells [30,55,62], while in the nodulus about 70% of the VIAAT+ area van mGluR2+ (Fig. 8k). The large proportion (40-50%) of VIAAT+mGluR2- boutons in the floccular granule cell layer as compared to the anterior vermis and the nodulus, can at least in part be explained by the presence of innervation from BIN neurons. In accord with data from macaque flocculus, these data indicate that BIN inhibitory input represents a significant complement of inhibitory input from Golgi cells in the floccular granule cell layer (Fig. 8l).

Rodent BIN neurons receive excitatory input from the rostro-medial medullary reticular formation

Staining for markers of inhibitory (VIAAT, GAD) and excitatory (VGluT1, VGluT2) nerve terminals, revealed that BIN neurons have a large number of VGluT2-positive boutons contacting their cell body and proximal dendrites (Fig. 9a) consistent with our electrophysiological analysis showing sEPSC in BIN neurons (Fig. 5h-j). To learn about the origin of this

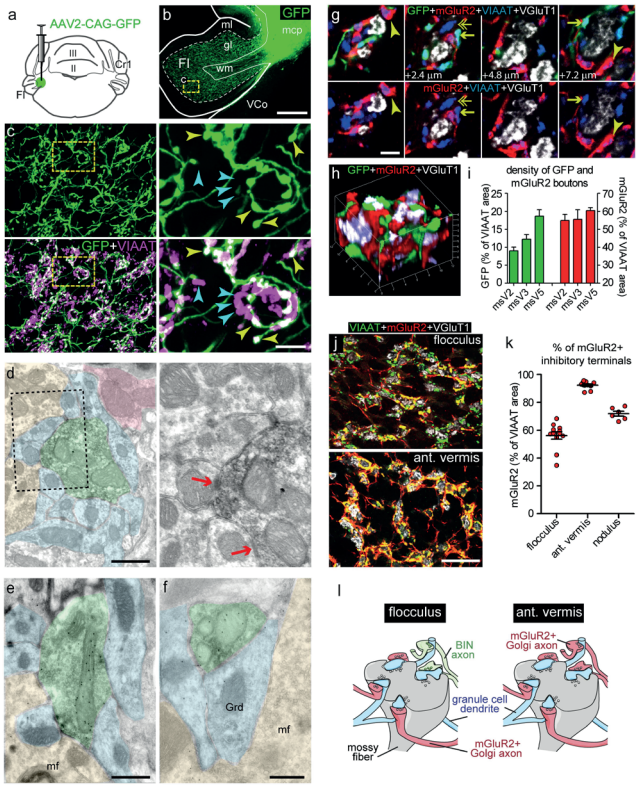

Figure 8. BIN neurons innervate granule cell dendrites in glomeruli in mouse flocculus. a-c: Injection of AAV2-CAG-eGFP virus in the white matter and the hilus of the flocculus (a,b) results in labelling of BIN neurons and their axons in the floccular granule cell layer (b,c). Co-immunostaining for VIAAT shows that GFP+ axons display VIAAT+ varicosities (white boutons, e.g. yellow arrow heads in c). Double-labeled GFP+VIAAT+ varicosities are intermingled with GFP-VIAAT+ boutons (magenta boutons, cyan arrow heads in c). d-f: Transmission electron microscopy of anti-GFP immunoperoxidase-DAB precipitate in the floccular granule cell layer following AAV2-CAG-eGFP infection of BIN neurons. DAB precipitate is associated with presynaptic boutons (outlined by green color coding) that form synapses (red arrows in d) with granule cell dendrites (Grd, blue color coding). Post-embedding anti-GABA immunogold-labeling shows that DAB+ axon terminals are also enriched in GABA (e, f). Mossy fiber endings and putative Golgi cell axons are coded in yellow and red, respectively. g,h: Series of optical sections (g) and 3-dimensional reconstruction (h) of a glomerulus innervated by GFP-labeled BIN axons and labeled for mGluR2, VIAAT and VGluT1. Note that the VGluT1+ mossy fiber rosette is surrounded by GFP+mGluR2-VIAAT+ (small arrows), GFP-mGluR2+VIAAT+ (arrow heads) and single-labeled GFP-mGluR2-VIAAT+ boutons (double-headed arrow). i: Bar graph showing the area of VIAAT+ nerve endings in floccular granule cell layer that co-distribute with GFP labeled BIN axon endings (green bars) or mGluR2 staining (red bars). Analyzed sections are from 3 mice with AAV2-CAG-GFP virus injections in the BIN showing the highest amount of BIN axonal labeling in the flocculus (mouseV2, mouseV3, mouseV5; see material and methods for details). j,k: Exemplary confocal images (j) and graph (k) showing that in the anterior vermis more than 90% of the VIAAT+ axon endings is mGluR2+, whereas in the flocculus the proportion is 60%, as illustrated by the large proportion of single labeled VIAAT+ terminals (green boutons in upper panel in j). l: Cartoon illustrating how BIN axon terminals may complement mGluR2+ Golgi axon terminals in floccular glomeruli. Scale bars: b, 250 µm; c, 5 µm; d -f, 500 nm; g, 2 µm; j, 50 µm.

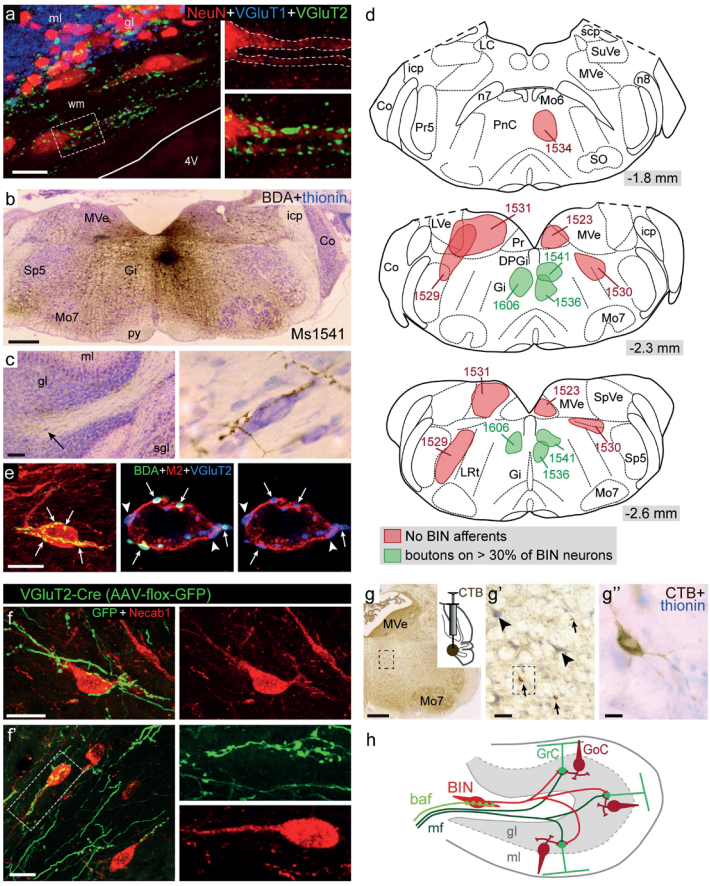

Figure 9. BIN neurons are innervated by VGluT2+ axons arising in the medial medullary reticular formation. a: Confocal image of NeuN/VGluT1/VGluT2 triple staining in rat flocculus showing that cell body and proximal dendrites of BIN neurons are covered by VGluT2+ axon terminals. b-d: Representative images of injection spot (b) and anterogradely-labeled fibers in the floccular white matter (c), and map of injection areas of selected BDA (biotinylated dextran amine) anterograde tracing experiments (d) showing that injections targeting the gigantocellular reticular nucleus (Gi) in the rostral medullary reticular formation result in labelling of fibers contacting BIN neurons. Injections in surrounding areas (indicated in red) did not result in labeling of fibers innervating BIN neurons, but to variable extend produced labeling of mossy fibers innervating floccular granule cell layer. e: Maximal projection (left panel, total thickness = 12 µm) and single optical section (middle and right panel, z = 1 µm) illustrating a BDA-labeled fiber from the Gi innervating a BIN neuron (labeled with anti-muscarinic M2 receptor antibody). Arrows in maximal projection and single optical section point to the same nerve endings. Co-staining for VGluT2+ shows that nerve endings from labeled fibers are VGluT2+, and that this cell is innervated by additional VGluT2+ nerve endings from non-labeled fibers (arrow heads). f: Maximal projections of exemplary BIN neurons identified by (Necab1-immunostaining) innervated by GFP+-beaded fibers following AAV-floxed-GFP injection in the Gi of VGluT2-Cre mouse. g: Immunoperoxidase-DAB staining of retrogradely labeled medium-sized neurons (arrows in G') in the Gi following CTB injection in hilus of the flocculus. Note that the large Gi neurons (arrow heads) are not labeled for CTB. h: Schematic representation of BIN neurons and glutamatergic BIN afferent fibers (baf) from the Gi in the floccular circuitry. Scale bars: a and f', 20 µm; b and g, 500 µm; c, 100 µm; d and g'', 10 µm; g', 50 µm.

excitatory input, we set out tracing experiments in mouse. VGluT2 is present in climbing fibers and multiple populations of mossy fibers [63] raising the possibility that BIN neurons are innervated by collaterals of climbing or mossy fibers. To test this possibility, we injected anterograde tracer (biotin dextran amine 10 kDa, BDA) in the inferior olive, i.e. the source of climbing fibers, and in brainstem nuclei known to provide mossy fiber input to the flocculus, including the vestibular nuclei and the prepositus hypoglossal nucleus [41]. However, none of these injections resulted in labelling of fibers contacting BIN neurons, despite abundant climbing fiber and mossy fiber labelling, respectively (data not shown). Instead a systematic anterograde tracing approach with injections throughout the medulla oblongata and the pontine reticular formation, revealed that BDA injection in the rostro-medial medullary reticular formation resulted in labeling of fibers innervating BIN neurons (Fig. 9b-e). We obtained 7 BDA injections that resulted in labeling of beaded fibers contacting the cell bodies and proximal dendrites of a substantial portion (>30%) of BIN neurons. These injections all targeted the medio-dorsal aspect of the medullary gigantocellular reticular nucleus (Gi). In 4 of 7 cases injections also included the dorsal paragigantocellular reticular nucleus (DPGi) dorsal of the Gi. However, 2 injection that targeted the DPGi, but not the Gi, resulted in labeled fibers on less than 4% of BIN neurons, indicating that afferents predominantly arise in the Gi. Similarly, BDA injections in the ventral aspect of the Gi, the pontine reticular formation rostral of the Gi, or the caudal aspect of the Gi resulted in no or minimal labeling of BIN afferents, substantiating the medio-dorsal Gi as the main source of BIN afferents. Importantly, the injections restricted to the medio-dorsal Gi that resulted in substantial labelling of BIN afferents (e.g. experiments #1541, #1606 and #1536) all produced negligible mossy fiber staining, supporting the notion that fibers innervating the cell bodies of BIN neurons do not represent mossy fiber collaterals. In all experiments labeled BIN afferent fibers were observed bilaterally, even when the injection was clearly unilateral. In addition, we observed that individual afferents may innervate several BIN neurons, and typically produce multiple (5-32) consecutive swellings on the cell body and proximal dendrites of individual BIN neurons (Fig. 9c,e). Double labelling for VGluT2 indicated that these axonal swellings in all occasions were VGluT2+ (Fig. 9e). In all neurons systematically examined for codistribution of BDA and VGluT2 (30 of 30 cells) we found that BDA+VGluT2+ boutons on BIN neurons were complemented by BDA-VGluT2+ boutons (Fig. 9e). This observation indicates that individual BIN neurons are innervated by multiple excitatory axons. To further demonstrate that VGluT2+ axon terminals innervating BIN neurons arise from neurons in the medio-dorsal Gi, we injected AAV-flex-GFP viral particles in the Gi of VGluT2-Cre mice in order to express GFP selectively in VGluT2 expressing neurons. Consistent with BDA tracing these injections resulted in bilateral GFP+ beaded fibers that made multiple synaptic connections with BIN neurons (Fig. 9f).

Next, to visualize the cells of origin of the BIN afferents in the Gi, we performed retrograde tracing with cholera toxin ß subunit (CTB). Comparison of CTB injections centered in the hilus of the flocculus (n=2) with injections in the floccular cortex (n=4), uncovered a population of intermediate-size (length =14 to 22 µm) polygonal CTB-labeled neurons in the dorsal Gi following hilar, but not cortical CTB injections (Fig. 9g). Consistent with anterograde tracing experiments, retrogradely-labeled neurons occurred both ipsi- and contralateral. Large neurons, characteristic for the Gi were not retrogradely labeled. The presence of intermediately sized VGluT2+ neurons in the Gi is consistent with *VGluT2* mRNA expression data documented in Allen brain atlas [50] showing high levels of *VGluT2* mRNA staining in both very large and small-to-intermediate size neurons in the Gi. We therefore propose that BIN neurons receive bilateral excitatory input from intermediately sized neurons in the dorsal Gi. Together the data indicate that the BIN is part of a disynaptic afferent pathway to the floccular granule cell layer, consisting of glutamatergic fibers from the medullary reticular formation innervating BIN neurons that in turn provide inhibitory input to granule cells (Fig. 9h).

Variability in the distribution of BIN neurons across mammalian species.

On the basis of data from primates and rodent, the BIN can be defined as a population of GABA/glycinergic neurons in the white matter, that innervate the floccular granule cell layer. However, BIN neurons show a differential distribution in rodents and primates, i.e. a preferential localization in the floccular white matter in rodents, versus a more widespread and distant distribution in the white matter between the floccular peduncle and the cerebellar nuclei in macaque and human. This raises questions about the presence and distribution of BIN neurons in other mammalian species. Our search for BIN neurons in rabbit cerebellum indicates that their identification in other species is not always straightforward. Thionin and GAD staining shows that in rabbit a low number of neurons is present in the white matter within and dorso-medial of the flocculus. Accordingly, analysis of sections from previous tracer experiments with small injections of the anterograde/retrograde tracer WGA-HRP in the floccular cortex (rabbits K227, K244, K358, K360; [52] revealed no or sporadic retrogradely labeled cells in this area. However, further analysis of these experiments revealed retrogradely labeled cells in the white matter medial of the medial cerebellar peduncle (mcp), rostral of the cerebellar nuclei (Fig. 10a,b). Retrogradely labeled cells only occurred ipsilateral. Notably, in several occasions labeled cells occurred close to the granule cell layer of the anterior vermis (Fig. 10b). Importantly, GAD staining revealed GAD+ neurons with similar size and distribution in this region of the white matter (Fig. 10c,d). The GAD+ neurons showed morphologies reminiscent of BIN neurons in primates and rodent. Based on counting of serial sections, we estimate that on each side there are about 800 ($0.8 \pm 0.2 * 10^3$, mean ± SE, n=2) of these GAD+ neurons populating either the floccular or the anterior vermis white matter (Fig. 10c,d).

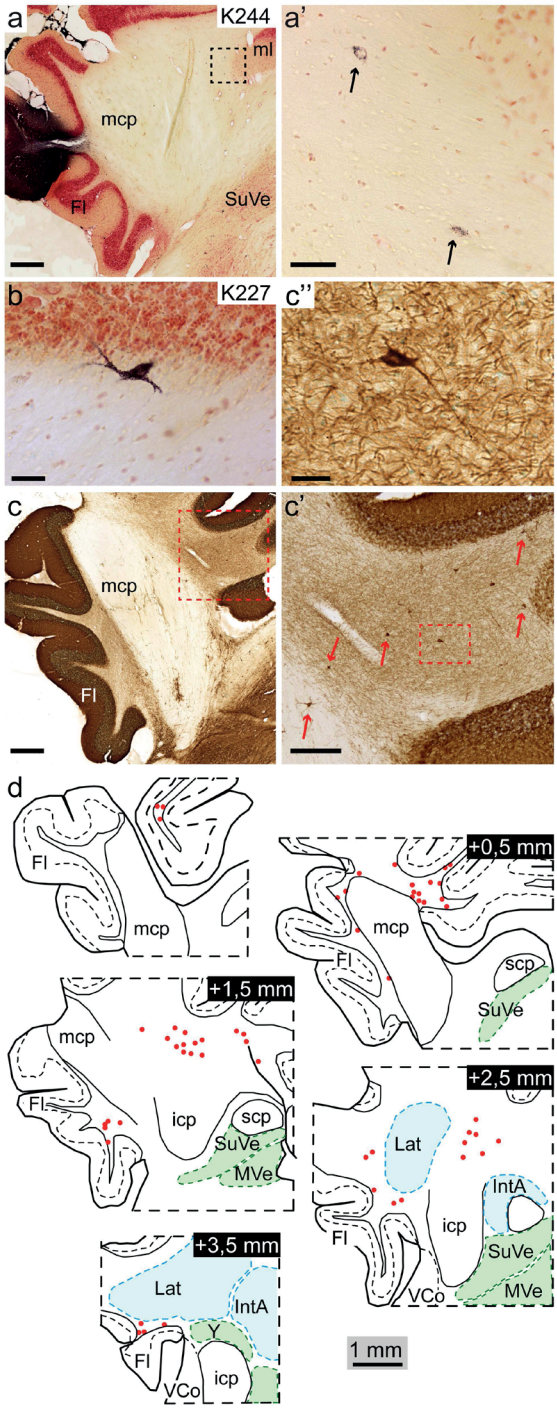

Figure 10. BIN neurons in rabbit. a, b: Low- (a) and high-magnification photomicrographs (a', b) illustrating retrogradely-labeled neurons in the white matter between the medial cerebellar peduncle (mcp) and the anterior vermis (arrows in a', b) following WGA-HRP injection in the rabbit flocculus (a). Images are from experimental animals (K244 and K227) from previously reported experiments[52]. c, d: GAD-immunoperoxidase staining reveals GAD+ neurons in the white matter mediocaudal of the mcp, while a few GAD+ neurons are present in the floccular white matter lateral of the mcp. In the plot in d, all GAD+ cells in white areas surrounding the mcp are plotted. The distribution and size of GAD+ neurons corresponded to the distribution of WGA-HRP tracing experiments. Scale bars: a and c, 500 µm; a', 50 µm; b and c'', 20 µm; c', 200µm.

To further explore the variability in distribution of BIN neurons across mammalian species we searched for potential BIN neurons in ferret cerebellum. Analysis of thionin and GAD stained section showed that as in primates and rabbit there are only a few GAD+ neurons in the white matter of the ferret flocculus. However, a cluster of GAD+ neurons, reminiscent of BIN neurons, was present in the white matter of the transition zone between the flocculus and the ventral paraflocculus (Fig. 11). Caudo-dorsally this cluster is bordered by the lateral cerebellar nuclei. Like BIN neurons the neurons are moderately-large in size and show elongated fusiform or polygonal morphologies with dendrites emanating from two sides. With about 1000 ($1.1 \pm 0.1 * 10^3$, mean ± SE, n=2) neurons per side, their number is compatible with BIN neurons in other species. Together the data indicate that BIN neurons also occur in rabbit and ferret cerebellum, but show different distributions than in rodent and primates.

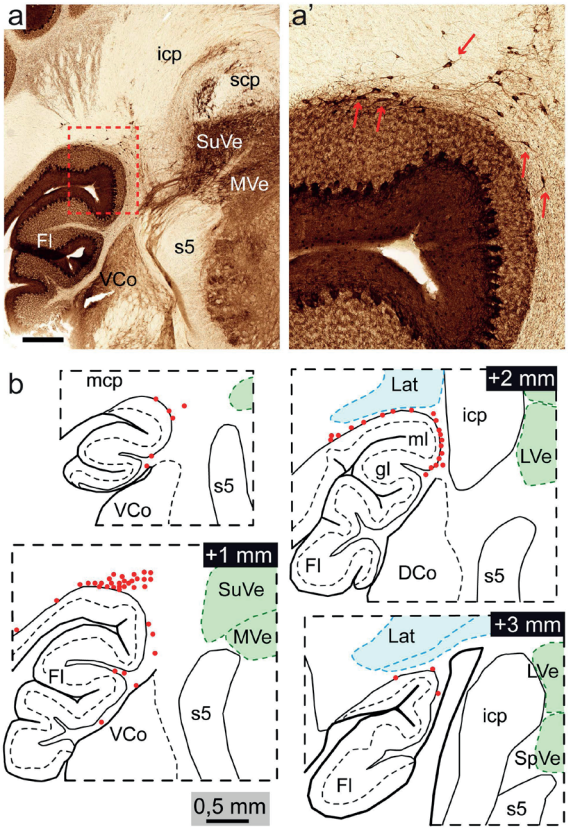

Figure 11. BIN neurons in ferret. Low-(a) and high-magnification (a') images and plots (b) of GAD-immunostaining in ferret flocculus illustrating a cluster of GAD+ neurons (red arrows in a', red dots in b) in the white matter facing the transition zone between the flocculus and the ventral paraflocculus. **Scale Bar:** a, 500 µm.

DISCUSSION

The BIN has been originally identified by Langer in macaque as a population of neurons that innervate the flocculus and the ventral paraflocculus (also designated floccular complex; [25], and is located in the basal white matter between the flocculus and the cerebellar nuclei [33,34]. Although this finding was confirmed by others [64], the BIN has been largely neglected in the literature. In addition, in some studies [65,66] the term BIN has been used for a group of neurons that does not overlap with the BIN originally defined by Langer [34]. In these studies, 'BIN' neurons were found to project to pontine nuclei [65] and to display saccade-related firing activity [66]. However, the cells explored in these studies were localized medial of group Y, whereas BIN neurons identified by retrograde tracing localize lateral of group Y (see Fig 1 of this study, and Fig. 3 in Langer, 1985). In a recent human brain Atlas [67], the term BIcb (basal interstitial nucleus of the cerebellum) has been assigned to a population of large neurons in the roof of the 4th ventricle neurons (see Fig. 13 in [67]. In this study, there is no reference to the study of Langer [34], and it is not clear whether the BIcb was intended to represent the human homologue of the macaque BIN [67]. On the basis of our data, we propose to reserve the term BIN (or BICb) for the population of neurons originally defined by Langer on the basis of retrograde tracing from the flocculus [33,34]. Our data indicate that these neurons represent a novel GABAergic cerebellar neuron that can be found in multiple mammalian species beyond macaque, including human, rat, mouse, rabbit and ferret (Table 2). Distinctive properties of BIN neurons are the following: they are moderately-sized GABAergic neurons localized in the white matter; they innervate floccular granule cells; and they receive excitatory input from the medullary reticular formation. BIN neurons represent a second source of inhibition of floccular granule cells, complementing inhibitory input from Golgi cells (Fig. 9h).

We found that BIN neurons in macaque stain positive for GAD and ChAT (Figs 1 and 2) and that ChAT staining can also be used to outline the BIN in human cerebellum (Fig. 3). ChAT staining did not label BIN neurons in the other species investigated, i.e. rat, mouse, rabbit and ferret, but in these species, we identified homologous populations of neurons based on the following criteria: their localization in the white matter, their size and elongated morphologies with dendrites emanating from the two ends, their retrograde labeling after tracer injection in the flocculus, and their immunoreactivity for GAD (Figs 4, 6, 10, 11). Our data indicate that the distribution of BIN neurons shows variability across species, varying from the floccular white matter in rat and mouse, to a relatively condensed distribution in the white matter dorso-medial of the flocculus in ferret, and more widespread distributions in rabbit and primates.

A search in Allen Brain Atlas to identify molecular markers that could further aid in the identification of BIN neurons uncovered the calcium binding protein Necab1 as a marker for BIN neurons in mouse cerebellum (Fig. 6). However, Necab1 is not expressed by BIN neurons in other species. The interspecies heterogeneity of ChAT and Necab1 expression is not against our tenet that BIN neurons represent a single class of neurons across species for two reasons: First, Necab1 is also absent in rat BIN neurons, which are highly similar to mouse BIN neurons in distribution and morphology. Second, interspecies heterogeneity in the expression of neurochemical markers also occurs in other populations of cerebellar neurons, in particular Golgi cells that differentially express ChAT, neurogranin and calretinin in closely related species [32,58,68-70]. In addition to Necab1, we found other proteins that might serve as neurochemical markers for BIN neurons, although the majority of these, like GlyT2, muscarinic M2 receptor, Lgi2, and acetylcholine esterase (AChE) are also expressed by Golgi cells (Figs 6, 7). In fact, our data show that also Necab1, while not being expressed by Golgi cells in the flocculus, is expressed in a subset of Golgi cells in most other lobules (Figs 6, 7). Instead mGluR2 is a marker that differentiates BIN neurons from Golgi cells, as it is not expressed in BIN neurons (Figs 2, 5, 6, 8) while being expressed by the majority of cerebellar Golgi cells and their nerve terminals [29,30,55,70]. Furthermore, in mouse, we found that BIN neurons do not express neurogranin (Fig. 7), another Golgi cell marker that is expressed in at least 2 subpopulations of Golgi cells in mouse cerebellum, including a subpopulation of Golgi cells (type 4 Golgi cells) that does not express mGluR2 and GlyT2 [30,69]. Importantly, by comparing the expression of a panel of Golgi cell markers between anterior vermis and the flocculus, we found that neurogranin+GlyT2-mGluR2- Golgi cells, while constituting 10-15% of the Golgi cells in the anterior vermis [30], are not present in the flocculus, (Fig. 7). These findings on the one hand point to differences in neurochemical identities between Golgi cells in the flocculus compared to the anterior vermis [30]; and on the other hand, support our notion that mGluR2 may represent a useful marker to differentiate BIN neurons from Golgi cells in the flocculus .

Recently, an ascending GABAergic/glycinergic inhibitory projection from the cerebellar nuclei to the cerebellar cortex has been reported [31]. These nucleo-cortical inhibitory neurons differ from BIN neurons in at least two aspects: They do not express Necab1 and they innervate Golgi cells rather granule cells [31]. It has been suggested that these inhibitory nucleo-cortical neurons also innervate the floccular granule cell layer (see Fig. 2A of [31]. However, we did not identify retrogradely labeled neurons in the cerebellar nuclei following CTB tracer injection in the flocculus. We, therefore, speculate that the floccular projections in the study of Ankri et al. (2015) derive from BIN neurons. The absence of inhibitory nucleo-cortical projections to the flocculus also is consistent with the absence of neurogranin+GlyT2-mGluR2- Golgi cells in the flocculus (Fig. 7), representing a major target of this projection [31]. Taken together, although BIN neurons show resemblance with

either Golgi cells or inhibitory nucleo-cortical neurons and probably derive from the same lineage, they are sufficiently distinct to consider them as a novel population of cerebellar neurons.

To characterize BIN axon terminals, we took advantage of their immunoreactivity for ChAT in macaque flocculus (Fig. 2) and we used AAV-GFP anterograde tracing in mice (Fig. 8). We found that BIN axon terminals to various degrees populate glomeruli in the floccular granule cell layer and complement mGluR2+ inhibitory input from Golgi cells. Electron microscopy of anterogradely labeled BIN axons in mouse provided direct demonstration that BIN axons innervate granule cell dendrites (Fig. 8d,e). Using confocal microscopy, we found examples of ChAT+ BIN axons innervating glomeruli with UBC brushes in macaque (Fig. 2i). So far, we did not obtain ultrastructural evidence of BIN axons making synaptic contacts with UBCs. We also used confocal microscopy to examine whether AAV-GFP traced BIN axons contact Golgi cells stained with antibodies against mGluR2 or muscarinic M2 receptor, but so far, we did not find conclusive examples of BIN axons contacting the cell body or dendrites of Golgi cells. Thus, granule cell dendrites represent a major target of BIN axons, while further work is needed to establish to what extent other granule cell layer neurons receive direct BIN input.

To obtain an idea about the relative contribution of inhibition by BIN axons in the floccular granule cell layer, we determined the proportion of ChAT+ inhibitory boutons in macaque flocculus, and the proportion of GFP+ inhibitory boutons in AAV- GFP anterograde tracing experiments in mice. These analyses indicated that at least 20% of inhibitory boutons in the floccular granule cell layer represent BIN axon terminals. Thus, in macaque flocculus about 20% of VIAAT+ boutons stain positive for ChAT, while in mice AAV-GFP injections resulted in GFP labelling of up to 20% of VIAAT+ boutons. However, the proportion of BIN axon terminals is likely to be higher in both macaque and mouse, in view of the presence of a population of ChAT- BIN neurons in macaque (Fig. 2a,b), and unlabeled BIN neurons in the AAV- GFP tracing experiments in mice. Analysis of the proportion of Golgi axon terminals on the basis of double labelling for VIAAT and mGluR2 metabotropic glutamate receptor indicated that about 60% of VIAAT+ axon terminals in the floccular granule cell layer is from mGluR2+ Golgi cells. Instead the proportion of mGluR2+ boutons is higher in other lobules (up to 95% in the anterior vermis; Fig. 8j,k), consistent with previous data indicating that 85-90% of Golgi cells are mGluR2+ [29,30] and that toxin-mediated selective ablation of mGluR2+ Golgi cells results in almost complete loss of GABAergic boutons in the granule cell layer [55]. The large proportion of mGluR2-VIAAT+ boutons in the floccular granule cell layer (about 40%) as compared to other lobules, at least in part can be explained by the presence BIN axons. mGluR2-VIAAT+ boutons also may derive from mGluR2- Golgi cells, but our data indicate that this type of Golgi cell does not occur

in the flocculus (see above). Purkinje cells may represent an additional source of inhibitory boutons in the granule cell layer [71] predominantly innervating Lugaro and globular cells [30], but double labelling for VIAAT and the Purkinje cell marker calbindin indicated that inhibitory boutons from Purkinje cells are rare in the floccular granule cell layer (<1% of VIAAT boutons). Taken together, our data indicate that about 60% of the VIAAT+ axon terminals in the floccular granule cell layer derive from mGluR2+ Golgi cells, while at least 20% and potentially up to 40% of the residual VIAAT+ axon terminals are from BIN neurons.

What could be the function of BIN neurons in the floccular circuitry? BIN axon terminals co-distribute with mGluR2+ Golgi cell axon terminals in the same glomeruli, and likely have complementary roles in controlling mossy fiber to granule cell signaling. Golgi cells receive excitatory granule cell and mossy fiber input and implement a local inhibitory feedback circuit that may control the precise timing and gain of granule cell firing [12,60,72]. The distinctive feature of Golgi cells is their local dense axonal plexus that provides inhibitory input primarily to nearby granule cells, although some Golgi cells may have more distant projections [60]. BIN neurons instead project to large portions of the flocculus, and only produce a few axon terminals per glomerulus. This wiring pattern indicates that BIN neurons have a more global inhibitory role over widely distributed granule cells (Fig. 9h). We also show that BIN neurons receive bilateral glutamatergic input from a population of neurons in the medullary gigantocellular reticular formation. These fibers innervate the cell body and proximal dendrites of BIN neurons, and likely play an important role in controlling the activity of BIN neurons. Importantly, our data also indicate that BIN neurons are not innervated by collaterals from climbing and mossy fiber collaterals that innervate the floccular cortex, although at this point we cannot exclude collateral projections on distal dendrites of BIN neurons. It had been anticipated by Langer that BIN neurons receive inhibitory input from floccular Purkinje cells [34]. However, anterograde tracing experiments in macaque have shown that BIN neurons do not receive input from the flocculus [73]. In accord with the idea that BIN neurons do not receive Purkinje cell input, our data indicate that BIN neurons are only innervated by calbindin-negative inhibitory boutons.

Together the data indicate that BIN neurons represent a diffuse inhibitory system of floccular granule cells that is controlled by a group of neurons in the medullary formation (Fig. 9h). Understanding the information conveyed by the medullary BIN afferents, will be critical for clarifying the role of the BIN neurons in the well-established role of the flocculus in eye movement control [22,24,25,74,75]. Importantly, future studies on the function of BIN neurons would benefit from experiments in multiple mammalian species to validate whether BIN neurons indeed represent a single class of prefloccular neurons with evolutionary conserved function.

REFERENCES

1. Voogd, J. & Glickstein, M. The anatomy of the cerebellum. *Trends Neurosci* **21**, 370-375 (1998).
2. Cerminara, N.L., Lang, E.J., Sillitoe, R.V. & Apps, R. Redefining the cerebellar cortex as an assembly of non-uniform Purkinje cell microcircuits. *Nat Rev Neurosci* **16**, 79-93 (2015).
3. Dean, P., Porrill, J., Ekerot, C.F. & Jorntell, H. The cerebellar microcircuit as an adaptive filter: experimental and computational evidence. *Nat Rev Neurosci* **11**, 30-43 (2010).
4. De Zeeuw, C.I.*, et al.* Spatiotemporal firing patterns in the cerebellum. *Nat Rev Neurosci* **12**, 327-344 (2011).
5. Gao, Z., van Beugen, B.J. & De Zeeuw, C.I. Distributed synergistic plasticity and cerebellar learning. *Nat Rev Neurosci* **13**, 619-635 (2012).
6. Palay, S.L. & Chan-Palay, V.E. *Cerebellar cortex: cytology and organization*, (Springer Verlag, Berlin, 1974).
7. Davie, J.T., Clark, B.A. & Hausser, M. The origin of the complex spike in cerebellar Purkinje cells. *J Neurosci* **28**, 7599-7609 (2008).
8. Jelitai, M.*, et al.* Dendritic excitation-inhibition balance shapes cerebellar output during motor behaviour. *Nat Commun* **7**, 13722 (2016).
9. Harvey, R.J. & Napper, R.M. Quantitative study of granule and Purkinje cells in the cerebellar cortex of the rat. *J Comp Neurol* **274**, 151-157 (1988).
10. Rancz, E.A.*, et al.* High-fidelity transmission of sensory information by single cerebellar mossy fibre boutons. *Nature* **450**, 1245-1248 (2007).
11. Jakab, R.L. & Hamori, J. Quantitative morphology and synaptology of cerebellar glomeruli in the rat. *Anat Embryol (Berl)* **179**, 81-88 (1988).
12. Valera, A.M.*, et al.* Stereotyped spatial patterns of functional synaptic connectivity in the cerebellar cortex. *Elife* **5**(2016).
13. Powell, K., Mathy, A., Duguid, I. & Hausser, M. Synaptic representation of locomotion in single cerebellar granule cells. *Elife* **4**(2015).
14. Sudhakar, S.K.*, et al.* Spatiotemporal network coding of physiological mossy fiber inputs by the cerebellar granular layer. *PLoS Comput Biol* **13**, e1005754 (2017).
15. Arenz, A., Bracey, E.F. & Margrie, T.W. Sensory representations in cerebellar granule cells. *Curr Opin Neurobiol* **19**, 445-451 (2009).
16. Chabrol, F.P.*, et al.* Synaptic diversity enables temporal coding of coincident multisensory inputs in single neurons. *Nat Neurosci* **18**, 718-727 (2015).
17. Huang, C.C.*, et al.* Convergence of pontine and proprioceptive streams onto multimodal cerebellar granule cells. *Elife* **2**, e00400 (2013).
18. Gao, Z.*, et al.* Excitatory Cerebellar Nucleocortical Circuit Provides Internal Amplification during Associative Conditioning. *Neuron* **89**, 645-657 (2016).
19. Witter, L. & De Zeeuw, C.I. Regional functionality of the cerebellum. *Curr Opin Neurobiol* **33**, 150-155 (2015).
20. Zhou, H.*, et al.* Cerebellar modules operate at different frequencies. *Elife* **3**, e02536 (2014).
21. De Zeeuw, C.I. & Ten Brinke, M.M. Motor Learning and the Cerebellum. *Cold Spring Harb Perspect Biol* **7**, a021683 (2015).
22. Ito, M. Cerebellar control of the vestibulo-ocular reflex--around the flocculus hypothesis. *Annu Rev Neurosci* **5**, 275-296 (1982).
23. Lisberger, S.G. Internal models of eye movement in the floccular complex of the monkey cerebellum. *Neuroscience* **162**, 763-776 (2009).
24. Schonewille, M.*, et al.* Zonal organization of the mouse flocculus: physiology, input, and output. *J Comp Neurol* **497**, 670-682 (2006).
25. Voogd, J., Schraa-Tam, C.K., van der Geest, J.N. & De Zeeuw, C.I. Visuomotor cerebellum in human and nonhuman primates. *Cerebellum* **11**, 392-410 (2012).
26. van Dorp, S. & De Zeeuw, C.I. Forward Signaling by Unipolar Brush Cells in the Mouse Cerebellum. *Cerebellum* (2015).
27. Sekerkova, G., Watanabe, M., Martina, M. & Mugnaini, E. Differential distribution of phospholipase C beta isoforms and diaglycerol kinase-beta in rodents cerebella corroborates the division of unipolar brush cells into two major subtypes. *Brain Struct Funct* **219**, 719-749 (2014).

28. Zampini, V.*, et al.* Mechanisms and functional roles of glutamatergic synapse diversity in a cerebellar circuit. *Elife* **5**(2016).
29. Neki, A.*, et al.* Metabotropic glutamate receptors mGluR2 and mGluR5 are expressed in two non-overlapping populations of Golgi cells in the rat cerebellum. *Neuroscience* **75**, 815-826 (1996).
30. Simat, M., Parpan, F. & Fritschy, J.M. Heterogeneity of glycinergic and gabaergic interneurons in the granule cell layer of mouse cerebellum. *J Comp Neurol* **500**, 71-83 (2007).
31. Ankri, L.*, et al.* A novel inhibitory nucleo-cortical circuit controls cerebellar Golgi cell activity. *Elife* **4**(2015).
32. Eyre, M.D. & Nusser, Z. Only a Minority of the Inhibitory Inputs to Cerebellar Golgi Cells Originates from Local GABAergic Cells. *eNeuro* **3**(2016).
33. Langer, T., Fuchs, A.F., Scudder, C.A. & Chubb, M.C. Afferents to the flocculus of the cerebellum in the rhesus macaque as revealed by retrograde transport of horseradish peroxidase. *J Comp Neurol* **235**, 1-25 (1985).
34. Langer, T.P. Basal interstitial nucleus of the cerebellum: cerebellar nucleus related to the flocculus. *J Comp Neurol* **235**, 38-47 (1985).
35. Zeilhofer, H.U.*, et al.* Glycinergic neurons expressing enhanced green fluorescent protein in bacterial artificial chromosome transgenic mice. *J Comp Neurol* **482**, 123-141 (2005).
36. Vong, L.*, et al.* Leptin action on GABAergic neurons prevents obesity and reduces inhibitory tone to POMC neurons. *Neuron* **71**, 142-154 (2011).
37. Siegers, J.Y.*, et al.* Novel avian-origin influenza A (H7N9) virus attachment to the respiratory tract of five animal models. *J Virol* **88**, 4595-4599 (2014).
38. van Riel, D.*, et al.* Decrease of virus receptors during highly pathogenic H5N1 virus infection in humans and other mammals. *Am J Pathol* **183**, 1382-1389 (2013).
39. Jaarsma, D.*, et al.* Light-microscopic distribution and parasagittal organisation of muscarinic receptors in rabbit cerebellar cortex. *J Chem Neuroanat* **9**, 241-259 (1995).
40. Ruigrok, T.J., Hensbroek, R.A. & Simpson, J.I. Spontaneous activity signatures of morphologically identified interneurons in the vestibulocerebellum. *J Neurosci* **31**, 712-724 (2011).
41. Ruigrok, T.J. Collateralization of climbing and mossy fibers projecting to the nodulus and flocculus of the rat cerebellum. *J Comp Neurol* **466**, 278-298 (2003).
42. Boele, H.J., Koekkoek, S.K., De Zeeuw, C.I. & Ruigrok, T.J. Axonal sprouting and formation of terminals in the adult cerebellum during associative motor learning. *J Neurosci* **33**, 17897-17907 (2013).
43. Paxinos, G. & Franklin, K.B.J. *The mouse brain in stereotaxic coordinates*, (Academic Press, London, 2001).
44. Wang, Q.*, et al.* Systematic comparison of adeno-associated virus and biotinylated dextran amine reveals equivalent sensitivity between tracers and novel projection targets in the mouse brain. *J Comp Neurol* **522**, 1989-2012 (2014).
45. Harris, J.A., Oh, S.W. & Zeng, H. Adeno-associated viral vectors for anterograde axonal tracing with fluorescent proteins in nontransgenic and cre driver mice. *Curr Protoc Neurosci* **Chapter 1**, Unit 1 20 21-18 (2012).
46. Ruigrok, T.J., Osse, R.J. & Voogd, J. Organization of inferior olivary projections to the flocculus and ventral paraflocculus of the rat cerebellum. *J Comp Neurol* **316**, 129-150 (1992).
47. Jaarsma, D., Dino, M.R., Cozzari, C. & Mugnaini, E. Cerebellar choline acetyltransferase positive mossy fibres and their granule and unipolar brush cell targets: a model for central cholinergic nicotinic neurotransmission. *J Neurocytol* **25**, 829-842 (1996).
48. Zhang, M.D.*, et al.* Comparative anatomical distribution of neuronal calcium-binding protein (NECAB) 1 and -2 in rodent and human spinal cord. *Brain Struct Funct* **221**, 3803-3823 (2016).
49. Singec, I.*, et al.* Neurogranin is expressed by principal cells but not interneurons in the rodent and monkey neocortex and hippocampus. *J Comp Neurol* **479**, 30-42 (2004).
50. Lein, E.S.*, et al.* Genome-wide atlas of gene expression in the adult mouse brain. *Nature* **445**, 168-176 (2007).
51. Kuijpers, M.*, et al.* Amyotrophic lateral sclerosis (ALS)-associated VAPB-P56S inclusions represent an ER quality control compartment. *Acta Neuropathol Commun* **1**, 24 (2013).
52. Tan, J., Epema, A.H. & Voogd, J. Zonal organization of the flocculovestibular nucleus projection in the rabbit: a combined axonal tracing and acetylcholinesterase histochemical study. *J Comp Neurol* **356**, 51-71 (1995).

53. Barmack, N.H., Baughman, R.W. & Eckenstein, F.P. Cholinergic innervation of the cerebellum of rat, rabbit, cat, and monkey as revealed by choline acetyltransferase activity and immunohistochemistry. *J Comp Neurol* **317**, 233-249 (1992).
54. Barmack, N.H., Baughman, R.W., Eckenstein, F.P. & Shojaku, H. Secondary vestibular cholinergic projection to the cerebellum of rabbit and rat as revealed by choline acetyltransferase immunohistochemistry, retrograde and orthograde tracers. *J Comp Neurol* **317**, 250-270 (1992).
55. Watanabe, D.*, et al.* Ablation of cerebellar Golgi cells disrupts synaptic integration involving GABA inhibition and NMDA receptor activation in motor coordination. *Cell* **95**, 17-27 (1998).
56. Jaarsma, D.*, et al.* Metabotropic glutamate receptors are associated with non-synaptic appendages of unipolar brush cells in rat cerebellar cortex and cochlear nuclear complex. *J Neurocytol* **27**, 303-327 (1998).
57. de Lacalle, S., Hersh, L.B. & Saper, C.B. Cholinergic innervation of the human cerebellum. *J Comp Neurol* **328**, 364-376 (1993).
58. Jaarsma, D.*, et al.* Cholinergic innervation and receptors in the cerebellum. *Prog Brain Res* **114**, 67-96 (1997).
59. Dugué, G.P., Dumoulin, A., Triller, A. & Dieudonné, S. Target-dependent use of co-released inhibitory transmitters at central synapses. *J Neurosci* **25**, 6490-6498 (2005).
60. Pietrajtis, K. & Dieudonné, S. Golgi Neurons. in *Handbook of the cerebellum and cerebellar disordersders* doi: 10.1007/1978-1094-1007-1333-1008_1034 (Springer, 2013).
61. Mapelli, L., Solinas, S. & D'Angelo, E. Integration and regulation of glomerular inhibition in the cerebellar granular layer circuit. *Front Cell Neurosci* **8**, 55 (2014).
62. Ohishi, H.*, et al.* Immunohistochemical localization of metabotropic glutamate receptors, mGluR2 and mGluR3, in rat cerebellar cortex. *Neuron* **13**, 55-66 (1994).
63. Hioki, H.*, et al.* Differential distribution of vesicular glutamate transporters in the rat cerebellar cortex. *Neuroscience* **117**, 1-6 (2003).
64. Nagao, S.*, et al.* Differences of the primate flocculus and ventral paraflocculus in the mossy and climbing fiber input organization. *J Comp Neurol* **382**, 480-498 (1997).
65. Gonzalo-Ruiz, A., Leichnetz, G.R. & Smith, D.J. Origin of cerebellar projections to the region of the oculomotor complex, medial pontine reticular formation, and superior colliculus in New World monkeys: a retrograde horseradish peroxidase study. *J Comp Neurol* **268**, 508-526 (1988).
66. Takikawa, Y., Kawagoe, R., Miyashita, N. & Hikosaka, O. Presaccadic omnidirectional burst activity in the basal interstitial nucleus in the monkey cerebellum. *Exp Brain Res* **121**, 442-450 (1998).
67. Ding, S.L.*, et al.* Comprehensive cellular-resolution atlas of the adult human brain. *J Comp Neurol* **524**, 3127-3481 (2016).
68. Bastianelli, E. Distribution of calcium-binding proteins in the cerebellum. *Cerebellum* **2**, 242-262 (2003).
69. Singec, I.*, et al.* Neurogranin expression by cerebellar neurons in rodents and non-human primates. *J Comp Neurol* **459**, 278-289 (2003).
70. Geurts, F.J., Timmermans, J., Shigemoto, R. & De Schutter, E. Morphological and neurochemical differentiation of large granular layer interneurons in the adult rat cerebellum. *Neuroscience* **104**, 499-512 (2001).
71. Guo, C.*, et al.* Purkinje Cells Directly Inhibit Granule Cells in Specialized Regions of the Cerebellar Cortex. *Neuron* **91**, 1330-1341 (2016).
72. Cesana, E.*, et al.* Granule cell ascending axon excitatory synapses onto Golgi cells implement a potent feedback circuit in the cerebellar granular layer. *J Neurosci* **33**, 12430-12446 (2013).
73. Nagao, S.*, et al.* Location of efferent terminals of the primate flocculus and ventral paraflocculus revealed by anterograde axonal transport methods. *Neurosci Res* **27**, 257-269 (1997).
74. De Zeeuw, C.I., Wylie, D.R., Stahl, J.S. & Simpson, J.I. Phase relations of Purkinje cells in the rabbit flocculus during compensatory eye movements. *J Neurophysiol* **74**, 2051-2064 (1995).
75. Voges, K.*, et al.* Mechanisms underlying vestibulo-cerebellar motor learning in mice depend on movement direction. *J Physiol* **595**, 5301-5326 (2017).

Chapter 5.2

Mechanisms underlying vestibulo-cerebellar motor learning in mice depend on movement direction

Kai Voges[1,2], Bin Wu[1], Laura Post[1], Martijn Schonewille[1#] and Chris I. De Zeeuw[1,3#]

[1] Department of Neuroscience, Erasmus MC, Rotterdam, the Netherlands
[2] SINAPSE, Singapore National University, Singapore
[3] Netherlands Institute for Neuroscience, Royal Netherlands Academy of Arts & Sciences Amsterdam, the Netherlands
[#]corresponding authors

Published on Journal of Physiology (2017)

ABSTRACT

Compensatory eye movements elicited by head rotation, also known as vestibulo-ocular reflex (VOR), can be adapted with the use of visual feedback. The cerebellum is essential for this type of movement adaptation, but its neuronal correlates remain to be elucidated. Here we show that the direction of vestibular input determines the magnitude of eye movement adaptation induced by mismatched visual input in mice, with larger changes during contraversive head rotation. Moreover, the location of the neural correlate of this changed behavior depends on the type of paradigm. Gain-increase paradigms induce increased simple spike (SS) activity in ipsilateral cerebellar Purkinje cells (PC), which is in line with eye movements triggered by optogenetic PC activation. In contrast, gain-decrease paradigms do not induce changes in SS activity, highlighting that the murine vestibulo-cerebellar cortical circuitry is optimally designed to enhance ipsiversive eye movements.

INTRODUCTION

As a result of the structure and connections of their receptors, afferents from the vestibular and visual system carry inherently direction-selective information[1,2]. In principle, this type of information may be relevant for cerebellar motor learning, such as goal-directed adaptation of reaching tasks of the limbs, smooth pursuit eye movements, or compensatory eye movements (CEMs)[3-8]. Sensory and motor information required for motor learning are conveyed to the cerebellar cortex through two main afferent systems[9]. These include the mossy fiber system, which modulates simple spike (SS) activity of Purkinje cells (PCs) via parallel fibers (PFs) and interneurons, and the climbing fiber system, which gives rise to the all-or-none complex spike (CS) activity of PCs[9]. The PF to PC synapse as well as the PF to molecular layer interneuron (MLI) synapse and MLI to PC synapse form major sites of cerebellar integration and plasticity[10,11], all of which are putatively controlled by the climbing fiber input[9]. Early, postsynaptic long-term depression (LTD) has been suggested as a possible mechanism[12,13] to adjust the efficacy of these synapses, but it is still under debate to what extent also postsynaptic long-term potentiation (LTP) contributes to a given behavior[8,14-18]. As spiking activity of the climbing fibers is highly direction-selective[19], the emerging hypothesis is that plasticity mechanisms contributing to learning are direction-selective too. Hence, cerebellar learning, in terms of mechanism and strength, may in principle also depend on the direction of sensory input and/or desired motor output. However, for adaptation of the vestibulo-ocular reflex (VOR), which is one of the most studied cerebellar motor learning tasks[20-23], the efficacy of direction-specific learning has not been assessed in detail yet and the quantitative relation between movement direction and adaptation still has to be studied in the same experiments[23-25]. More specifically, the contribution of both SS and CS activity of PCs to adaptation of the VOR remains enigmatic[25-29]. Based on previous studies in mutants in which various forms of plasticity and/or parts of the cerebellar cortical network are affected[9,15,16,30,31], one can make several predictions on potential direction-dependent plasticity mechanisms, even with data that have been collected following sinusoidal stimulations. Deficits in potentiation mechanisms in PCs robustly impair VOR gain-increase, but less so gain-decrease paradigms[15], whereas selective deficits in LTD at the parallel fiber to PC synapse do not appear to lead to obvious changes in any form of VOR adaptation[16]. Interestingly, in the related Purkinje cells (vertical-axis type or VA-type, see Methods) increasing SS activity and thus decreasing CS activity is known to correlate with naso-temporal eye movements, during both the VOR and optokinetic reflex (OKR) evoked by visual input[32-34]. Taken together, this would imply that the strongest training paradigms include those that occur when SS activity of PCs is enhanced and when the climbing fibers are inhibited, i.e. during contraversive head movements[28,33,35]. Hence, we hypothesize that gain-increase and gain-decrease trainings can both be optimally executed during contraversive head movements and that the levels of increase and decrease of both

SS and eye movement gain depend on the level of concomitant climbing fiber activity, with low climbing fiber activity leading to gain-increases and vice versa because of the windows of opportunity set by the synergistic forms of plasticity[9].

In the present study, we use direction-specific sigmoidal, rather than sinusoidal, visual and vestibular stimuli so as to assess the contribution of individual movement directions in vestibulo-cerebellar learning. By simultaneously monitoring eye movement performance and corresponding PC activity during VOR adaptation, we test our hypothesis that cerebellar learning is direction-dependent. We show that adaptation to the visual stimulus is more pronounced during contraversive head movements, both for gain-increase and gain-decrease VOR adaptation. The learned changes during contraversive head movements are reflected in the activity of PCs when we increase the amplitude of the VOR gain, but not when we decrease it. Finally, optogenetic stimulation of PCs confirms the presence of a quantitative, causal relationship between SS firing, movement direction and amplitude.

MATERIAL AND METHODS

Animals. Wildtype mice (n = 80; C57bl/6, Harlan) were prepared for eye movement recordings under general inhalation anesthesia (Isoflurane, in 100% O_2; 4% induction, 1.5-2.0% maintenance, Pharmachemie BV) with a magnetic pedestal that was attached to the frontal and parietal bones of the skull with dental cement (Charisma, Heraeus). After surgery, mice were allowed to recover for at least 5 days. After experiments animals were first anesthetized as described above and then euthanized by cervical dislocation. For optogenetic experiments, mice expressing Cre recombinase under the Purkinje cell specific L7 promotor (L7Cre)[36] were crossed with mice carrying floxed hChR2(H134R)-tdT (Ai27D) to obtain L7-Ai27D animals that express channelrhodopsin-2 H134R fused with TdTomato[37] in cerebellar Purkinje cells (n = 4; Jackson Laboratories, Bar Harbor, ME, USA).

Stimulation. Vestibular stimulation was delivered through a turntable (diameter 60 cm) with the head of the mouse fixed in the center and its body placed in a custom-made mouse restrainer. For visual stimulation a high-resolution (3800 x 1000 pixels) rear projection system was used. Three standard projectors (D3Series, Vivitek, The Netherlands) projected a blended and warped (Vioso, Presenter) image, consisting of a random dotted pattern (minimum shape size: 2°; colors: black and white) onto a dome shaped screen (radius: 35 cm; azimuth: 240°; elevation: -10 to +60°). Two sinusoidal functions were combined to generate a sigmoidal output for the vestibular stimulus (custom sequencer file, Spike2, CED). Mice were familiarized with the experimental setup 3 days prior to experiments by providing visual and vestibular stimulations for 30 minutes. Experiments

started with recordings of baseline CEMs – OKR, VVOR and VOR (stimulation amplitudes: 5°, 10°, 15°, 20°, 25°, 30°, with peak velocities 3.8, 7.9, 11.3, 14.6, 18.3 and 22.0°/s) – either in clockwise or counter clockwise direction. VOR gain adaptation experiments started on the next day, beginning with an initial VOR recording. VOR gain-increase and gain-decrease were induced by training mice in blocks (50 repeats, each stimulus cycle is 12 s = 10 min) consisting of out-of-phase or in-phase vestibular and visual input (both at 10° amplitude), respectively, and directly followed by probe trials (20 repeats, 4 min), consisting of VOR recordings in the dark (also at 10° amplitude). This block was repeated 5 or 6 times (i.e. massed training without intervals, total duration 74 or 88 min). VOR gain adaptation experiments combined with electrophysiological recordings started with an initial VOR recording, followed by a block of training sessions (2x10 repeats) and probe trials (1x10 repeats). This block was repeated 3 times (total duration 20 min). Out of the 32 cells 4 were stable only till the 3rd probe trial repeat, which was then taken as the last probe trial for further analysis.

Eye movement recordings. Eye movements were recorded and calibrated with a video camera-based system (ETL-200, iScan) as has been described previously[38]. Three infrared emitters (max. output 600 mW, dispersion angle 7°, peak wavelength 880 nm) were used to illuminate the eye: two from below that were fixed to the table and one from above, which was fixed to the camera and of which the corneal reflection was used as the reference point.

Electrophysiology. For details see Chapter 3. PCs (n = 67 from C57bl6 mice and n = 20 from L7-Ai27 mice) were identified by the presence of simple and complex spikes, and determined to be from a single unit by confirming that each complex spike was followed by a climbing fiber pause. To ensure recordings were made from PCs in floccular vertical-axis zones (visual stimulus rotation axis azimuth: 0°; elevation: 90°)[34] the phase locking of CSs was compared between sinusoidal stimulation around the vertical axis and horizontal axis (horizontal axis here refers to the axis at 45° azimuth from the rostro-caudal midline; with an elevation of 0°). If CSs showed strong phase locking while the visual stimulus moved temporo-nasally, the zone was identified as a vertical-axis zone. If phase locking was strongest during upward movement of the stimulus, the zone was identified as a horizontal-axis zone. For the cells that were stable after experiments (n = 16) a tuning curve with sinusoidal rotations in the vertical axis, horizontal axis and an intermediate angle (azimuth: 45°; elevation: 45°) was recorded and the coefficient of synchronization and the z-value were calculated.

Optogenetics. In L7-Ai27D (see above), an additional small craniotomy in the periotic capsule with a diameter of ~800 µm was performed. To form a cannula that gives access to

the caudal floccular complex, the tip of a plastic pipette (5 mm) was placed perpendicular to the bone and fixed with dental cement (Simplex Rapid; Kemdent). After a recovery period of at least 5 days, an optical fibre (200 µm × 5 mm, filter: 470 nm, driver: LEDD1B; Thorlabs, Ely, UK) was lowered between 4 and 5.5 mm into the cannula, and placed on the outside of the paraflocculus, directed towards the flocculus. To mimic eye movements and spiking patterns during visual stimulation, the LED was pulsed over a period of 2.25 s, with increasing frequencies (60, 80, 90, 100 and 120 Hz) and a duty cycle of 50%. Irradiance was varied between 0.12, 0.42, 0.72 and 1.8 mW mm^{-2} measured at the electrode tip prior to experiments (Optical power meter 1830-C, with sensor 883-SL; Newport, Irvine, CA, USA).

Analysis and Statistics. Gain was calculated as the ratio between stimulus amplitude and eye movement amplitude. Eye movement delay was calculated as the time shift between the velocity peak of the stimulus and the velocity peak of the eye movement. Extracellular recordings were spike sorted with SpikeTrain (Neurasmus BV). Using super-paramagnetic clustering SSs and CSs usually split up in two clusters at low temperatures, i.e. < 0.1[39]. Spikes during fast eye movement components were removed in a window of 40 ms prior to, to 80 ms post movement onset. Eye movement gains in the two directions were compared using a linear mixed model with the trial number as repeated measure, a diagonal covariance matrix and fixed effects for the trial number, the movement direction and uni- or bidirectional stimulation. Although this analysis method also allows for the comparison of mean values in between trials of one group resulting in a p-value for each repeat, here we give only the F and P value over all repeats. Spiking data had an additional repeated measure when spontaneous and stimulus evoked spiking frequencies or the initial and the secondary segment were compared. To compare depth of modulation of spiking data the spontaneous firing frequency was subtracted from the stimulus evoked firing frequency and a linear mixed model was setup, comparable to that for eye movement gains. Significance of correlations was tested with Spearman's rank correlation coefficient. All statistical analysis was done with SPSS (Version 21, IBM).

RESULTS

To evoke and adapt direction-specific compensatory eye movements we subjected mice to visual and vestibular stimuli around an earth-vertical axis with a sigmoidal position profile. In contrast to sinusoidal stimulation, a sigmoidal stimulus temporally separates the contribution of the individual movement directions and allows us to more directly correlate the spiking activity to eye movements. We recorded eye movements from the left eye and

simultaneously recorded single cell activity of PCs (total n = 87) from the left flocculus of mice (eye movements only n = 68; electrophysiology and eye movements n = 30).

Preferred directions for baseline visual compensatory eye movements

We first investigated to what extent normal, un-adapted eye movement reflexes reveal a preference for movement direction (Fig. 1*A*). Eye movements evoked by sigmoidal horizontal visual stimulation at amplitudes ranging from 5 to 30° (i.e. peak velocities 3.8 to 22.0°/s; n = 32 mice) showed a clear direction preference (see Fig. 1*B*). Independent of stimulus amplitude the preferred direction for visually-driven eye movements was the naso-temporal (n-t) direction (i.e. for the optokinetic reflex, OKR, and the visual vestibulo-ocular reflex, VVOR, but not VOR) (Fig. 1*C*). For the solely visually-driven OKR, gains decreased with increasing stimulus amplitude, yet eye movements in the n-t direction consistently yielded higher gains than those in the opposite direction (n = 39, mixed model: $p < 0.001$, $t = 4.81$) (Fig. 1*C*). Interestingly, the OKR peak velocity was delayed in the n-t direction with respect to that in the t-n direction ($p < 0.001$, $t = 7.05$) (Fig. 1*C*). Likewise, VVOR gain values showed a preference for n-t movements (n = 39, $p < 0.001$, $t = 8.66$) and delays of VVOR peak velocity in the n-t direction were also significantly longer than those in the t-n direction ($p < 0.001$, $t = 8.72$) (Fig. 1*C*). For the solely vestibularly driven VOR (Fig. 1*B* and *C*) gains were not significantly different for the two directions (n = 31, $p = 0.10$, $t = 1.64$), but in line with the VVOR data described above VOR delays were shorter for the eye movements in the t-n direction ($p < 0.001$, $t = 6.20$).

To ensure that the preferred direction was independent of the camera position we tested baseline CEMs with extreme camera positions, ± 10° towards nasal and temporal from the center position. Consistent with the data described above, gains were higher in the n-t direction for visually driven CEM, but not for VOR (Fig. 2*A*). These eye movement recordings were all obtained from the left eye. To confirm that directional preference is indeed naso-temporal and not a right-left preference, we subsequently also evaluated the direction selectivity in the right eye (n = 6) (Fig. 2*B*). Here, direction-selectivity largely reversed from right to left, to left to right, indicating that the preference is predominantly related to the preference for n–t eye movements (mixed model: VVOR, n vs. t: $p < 0.001$, $t = -2.11$).

Thus, in comparison to sinusoidal stimulation[26,33], the visually driven CEMs following sigmoidal stimulation showed similar eye movement-stimulation amplitude relations, with velocity profiles of OKR lagging behind, profiles of VVOR closely tuned to the velocity profile of the stimulus, and VOR velocity profiles leading that of the stimulation. Moreover, and most importantly, both types of visually driven CEMs (i.e. OKR and VVOR) showed higher gain values towards the ipsilateral visual field.

Preferred directions for PC activity

Next, we characterized the correlation of PC activity with different movement directions. To this end, floccular vertical-axis PCs (n = 27 cells; 11 mice) were identified by the presence of CSs and SSs (Fig. 3*A*), the consistent presence of a pause in SSs firing after a CS (i.e. climbing fiber pause), and optimal CS responses during a contraversive visual stimulus around the vertical axis (Fig. 3*B*-*C*)[19,33,34,40]. Vertical-axis PCs had an average baseline SS firing frequency of 63 ± 2 spikes/s at rest (Fig. *4A* and *B*).

The depth of modulation, i.e. the change in spike rate relative to baseline, of SSs was significantly greater during OKR and VVOR than that during VOR (SS depth of modulation OKR vs VOR: $p < 0.001$, $t = -5.346$; VVOR vs VOR: $p = 0.003$, $t = -3.586$), but for all three types of CEMs SS firing rate increased during n-t and decreased during t-n movements of the ipsilateral eye (Fig. 4*B* and *C*). Latencies of the maximum change in SS modulation with respect to the maximum change in stimulus velocity were not different for the two movement directions for any type of CEM (SS latency OKR n-t: -0.01 ± 0.09 s, t-n: -0.14 ± 0.09 s; VVOR n-t: 0.02 ± 0.07 s, t-n: -0.13 ± 0.11 s; VOR t-n: -0.07 ± 0.11 s, n-t: -0.16 ± 0.13 s; all $p > 0.2$) and maximum SS modulation generally preceded maximum velocity peak of eye movements (cf. Fig. 1*C*). Interestingly, for all paradigms, SS modulation during the first segment of the stimulus cycle (colored parts of stimulus traces in figures) was significantly greater than that of the second segment (OKR $p < 0.001$, $t = 9.52$; VVOR $p = 0.001$, $t = 4.34$; VOR $p = 0.042$, $t = -2.18$). Since the first half of the stimulation placed the ipsilateral eye at an eccentric position at the start of the second half of the visual and/or vestibular stimulation, these data suggest that absolute eye position influences PC SS activity, and hence all following data presented here are obtained during the first half of stimulation (Fig. 1*B* and 4*B*).

The reciprocal SS and CS activity of vertical-axis PCs during visual and/or vestibular sigmoidal stimulation showed significantly higher levels of modulation during OKR and VVOR than VOR (OKR vs VOR: $p < 0.001$, $t = 4.183$) (Fig. *4C*). Interestingly, the depth of CS modulation during OKR was not significantly different from that during VVOR (n-t: $p = 0.66$, $t = 0.45$; t-n: $p = 0.64$, $t = 0.48$), despite the fact that OKR gains and delays were significantly lower and longer, respectively, than those during VVOR (see Fig. 1*C*; gain: n-t $p < 0.001$, $t = -23.766$, t-n $p < 0.001$, $t = 4.182$; delay: n-t $p < 0.001$, $t = 7.663$ and t-n $p < 0.001$, $t = -21.841$). Latencies of CS peak modulation in the t-n direction were consistently shorter than in the n-t direction (OKR $p = 0.03$, $t = 2.18$; VVOR $p = 0.03$, $t = -2.21$), in line with the shorter delay in peak velocity of the eye movement (see Fig. 1*C*). During VOR the CS modulation pattern diverged even more from that of the SSs and revealed a bimodal spiking pattern, consisting of an initial increase followed by a decrease in firing when the ipsilateral eye moved into n-t direction and a reversed pattern in the t-n direction (in 10 out of 16 cells). Together, these data indicate that CS modulation during visuo-vestibular

sigmoidal stimulation encodes mainly retinal slip and in addition probably some vestibular and/or motor signals[33,40].

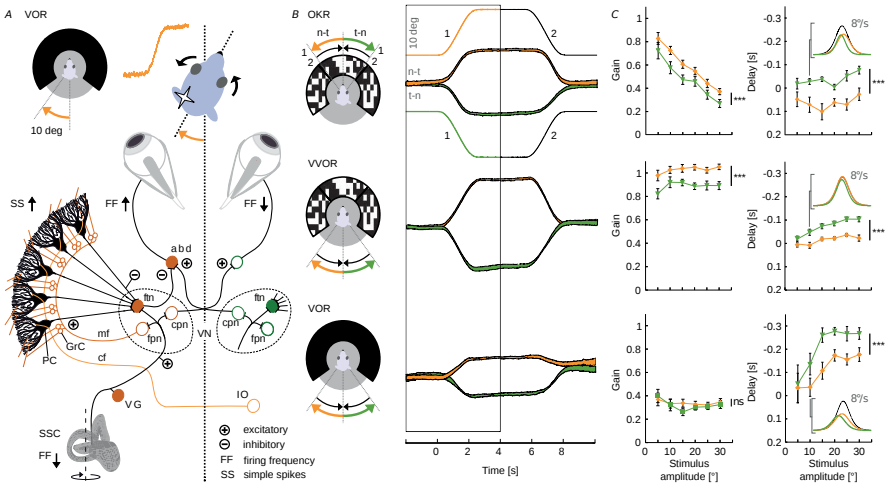

Figure 1. Baseline compensatory eye movements have a preferred direction. A, Rotating a head-fixed mouse in the dark in contraversive direction with respect to the recording side will evoke a compensatory eye movement into naso-temporal direction towards the ipsilateral visual field (top) via a three-neuron arc in the brainstem (bottom, filled orange symbols). Sensory information from the semi-circular canals (SCC), transferred by the vestibular ganglion cells (VG), reaches the vestibular nuclei (VN). Excitatory inputs drive flocculus projection neurons (fpn), flocculus target neurons (ftn) and commissural projection neurons (cpn). The PCs in the flocculus, which receive their input from the VN via mossy fibers (mf) to the granule cells (GrC) and after processing in the molecular layer, provide an inhibitory input to the VN, which in turn inhibit ipsilateral abducens neurons (abd); thus through a process of disinhibition PCs are expected to eventually facilitate a naso-temporal eye movement. The climbing fibers (cf) of the inferior olive (IO) provide the error signal to the contralateral PCs. B**,** CEMs following direction-selective stimulation. Icons (left) display eye movement (n-t orange, t-n green) and stimulus direction (arrow heads) for the visual (arrows top) and the vestibular (arrows bottom) stimulus. Numbers at the icon for OKR indicate the first and second stimulus segment. Note that visual stimulation evokes CEMs in the same direction as the stimulus, whereas vestibular stimulation-evoked movements are opposite to the direction of the stimulus. Right, stimulus (thin lines) and average eye movement traces recorded at a stimulation amplitude of 10° for naso-temporal (n-t) and temporo-nasal (t-n) eye movements. Analysis of eye movement was performed during the initial segment (black box, number 1). C**,** Gains of average eye movements (left) were significantly larger in the n-t direction (n=20) than in the t-n (n=19) direction for the visually driven OKR and VVOR, but not for the VOR over stimulation amplitudes ranging from 5 to 30° (peak velocities 3.8 to 22.0°/s). Delays (right) for the t-n direction were leading (i.e. have a more negative delay than) those of the other direction. Insets show example velocity profiles of n-t and t-n movements following 10° stimulation (black lines). Data are represented as mean ± SEM; population data (B middel panels) represent ± SEM.

Magnitude of VOR gain adaptation depends on movement direction

To test the hypothesis that the strength of gain adaptation depends on the direction of eye movements, we used the sigmoidal stimulus during visuovestibular mismatch training. Animals were trained to increase their VOR gain by rotating the visual stimulus out of

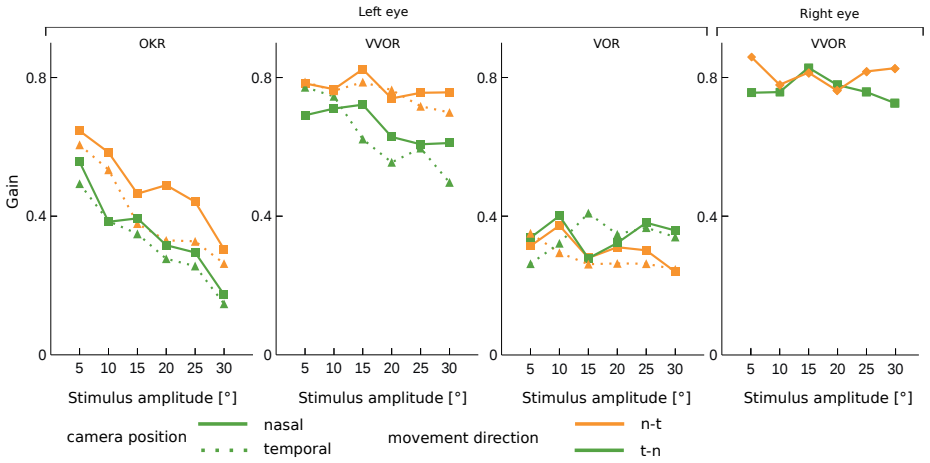

Figure 2. Relation eye movement gain, preferred direction, and camera position. To rule out the possibility that camera position relative to the eye might have resulted in asymmetric recording conditions, eye movements were measured at two additional camera positions, i.e. at +10° and -10° from the usual position. Independent of camera position, eye movements during visual stimulation were larger in the n-t direction. Moreover, here too gains did not show any direction dependence during vestibular stimulation in the dark, further assuring that differences in preferred direction are not related to the camera position. Data are shown as mean values.

phase (180°) with the vestibular stimulus and decrease their VOR gain by rotating both stimuli in phase (0°) (n = 35 mice) (Fig. 5*A*). Interestingly, out of phase trainings with eye movements in the n-t direction, i.e. contraversive vestibular and ipsiversive visual rotation, resulted in a prominent increase of eye movements during probe trials (n = 11, Δ-gain: n-t +0.37 ± 0.06; p = 0.04, f = 9.34), whereas increase trainings with movements in the t-n direction were not successful, with a trend towards gain decrease (n = 13, Δ-gain: t-n -0.1 ± 0.02; p = 0.1, f = 2.4; n-t vs. t-n: p < 0.001, t = -11.22) (Fig. 5*B*, top). Similar to VOR gain-increase, decrease training was more effective when the visual and vestibular stimulus rotated in phase to suppress eye movements in the n-t direction (n = 13, Δ-gain t-n -0.17 ± 0.02) than in the t-n direction (n = 13, Δ-gain n-t -0.04 ± 0.03; n-t vs. t-n: p = 0.001, t = 3.62). This effect was not dependent on the presence of visual feedback during the secondary segment of the stimulation (Fig. 6*A* and *B*), as the learned responses were similar when mice were subjected to only unidirectional visual training stimulation, with the table rotating back to the starting position in the dark (gain-increase n-t: 0.37 ± 0.08, t-n: 0.02 ± 0.04; p = 0.079, t = 1.761; gain-decrease n-t: -0.02 ± 0.03, t-n: -0.17 ± 0.02; p = 0.18, t = 1.34) (Fig. 3*B*, right). The decrease in gain was not the result of habituation[41,42], as "training" stimulation in the dark, without visual input, resulted in a minimal change in gain during n-t movements (Fig. 5*B*, bottom left, gray curve). This change was different from that in the preferred, contraversive direction (p < 0.001, t = 3.76), suggesting that habituation is relatively limited for sigmoidal stimulation.

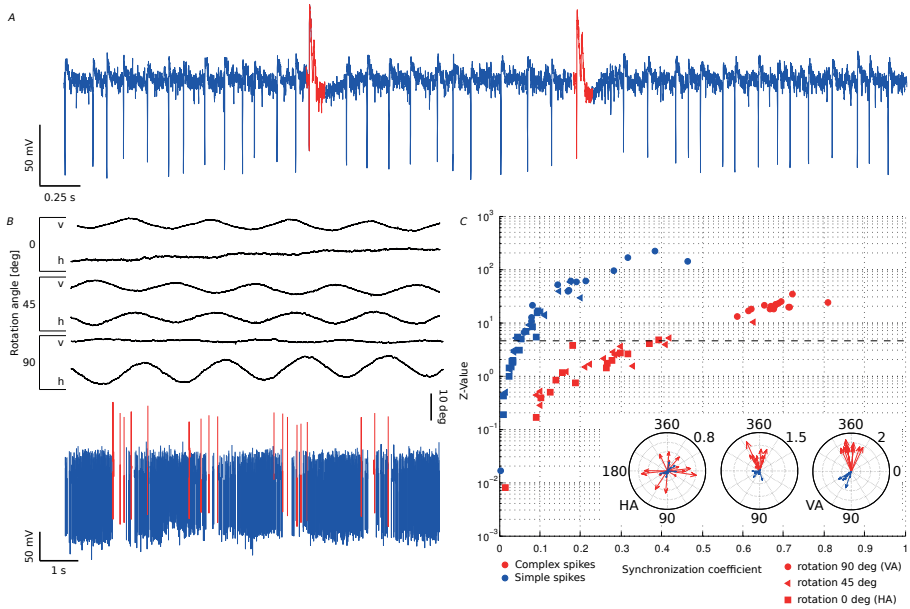

Figure 3. Identification of vertical-axis floccular PCs. A, In vivo extracellular recordings were obtained from cerebellar PCs during visual and/or vestibular stimulation in awake mice. Recordings were identified as a single unit by the consistent presence of a pause in SSs (blue) following each CS (red). B, Traces show examples of vertical axis (VA) and horizontal axis (HA) eye movements following visual stimulation around three different rotational axes (from top to bottom: HA, intermediate and VA). To separate VA-responsive PCs from HA-responsive and non-floccular PCs the activity of PCs in response to each stimulus was recorded and SSs (blue) and CSs (red) were identified (bottom). C, PCs showing significant ($p < 0.001$ for z-values > 4.6) synchronization with VA but not HA stimulus were identified with the use of circular statistics and used for further analysis. Insets: polar plots show a strong phase relation and depth of modulation for SSs and CSs during VA stimulation (right) but less so during intermediate or vertical axis stimulation (middle and left inset, respectively).

These results demonstrate for the first time that VOR gain adaptation in mice is direction-sensitive in that the adaptation is more pronounced during both increase ánd decrease trainings during contraversive vestibular input. This implicates that eye movements in the preferred, i.e. naso-temporal, direction are more prone to adapt, while at the same time the contralateral eye does not undergo obvious changes.

Gain-increase training leads to enhancement of SSs

The findings that compensatory eye movements and related SS modulation are both optimal in the n-t direction and that learning visuo-vestibular mismatch tasks is also optimal when the contraversive vestibular stimulus elicits eye movements in the n-t direction point towards preferred plasticity mechanisms that depend on movement direction (i.e. a principal learning direction). Lesions of the flocculus ablate the ability to adapt the VOR[43,44], but how floccular PCs contribute to VOR adaptation and how their activity changes during

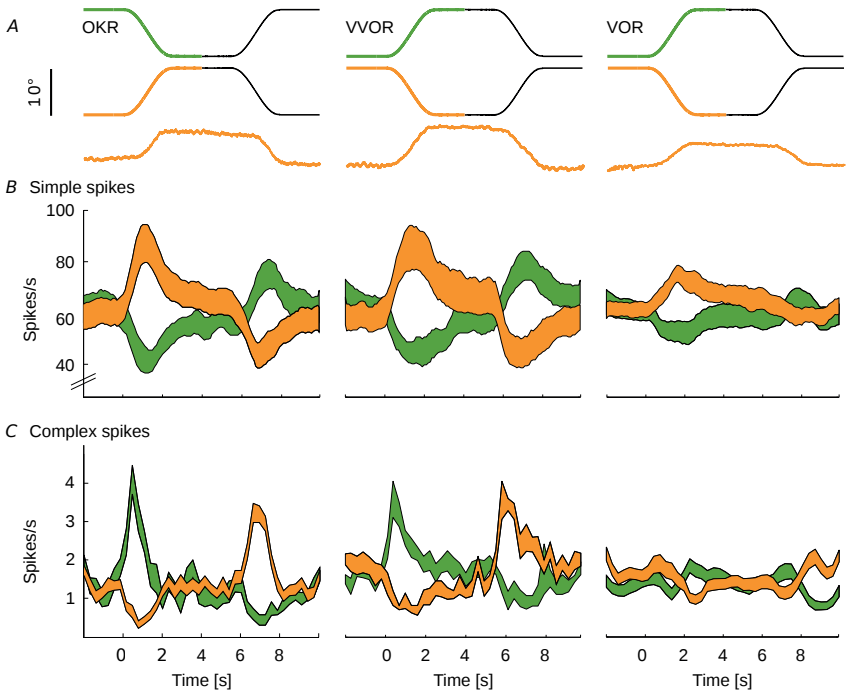

Figure 4. PCs spiking patterns reflect the direction of movement. A, Stimulus traces in the two movement directions (top, n-t orange, t-n green) and example eye movement traces (bottom, n-t direction). Note that data are sorted according to eye movement, rather than stimulus, direction. B and C, Average SS and CS firing during base line CEMs measured at a stimulation amplitude of 10°. PCs (total of 27) showed an increase or decrease of SS firing and the reciprocal CS pattern for the n-t and t-n direction, respectively. B, The SS firing pattern in one direction was a mirror image of the spiking pattern in the other direction in terms of depth of modulation and latency to peak modulation. C, Visually driven CS modulated stronger in the t-n direction with a bigger lead of peak modulation as compared to the n-t direction; the CSs during stimulation in t-n direction may explain why eye movement delays were shorter in this direction. CS activity during VOR showed a bimodal pattern with an initial increase followed by a decrease in the n-t and vice versa for the t-n direction. Data are represented as mean ± SEM; population data (B and C) represent ± SEM.

learning is still under debate. Therefore, we recorded single-unit PC activity during VOR gain adaptation (n = 32 cells; 17 mice).

VOR gain was increased in the identified principal learning direction by contraversive vestibular and ipsiversive visual rotation (10° amplitude each), resulting in n-t movements of the ipsilateral eye, which compensated fully for the stimulus amplitude (eye movement amplitudes ~19-20°) (middle panel Fig. 7*A*). In line with what has been previously shown in sinusoidal training paradigms[28,45], the SSs showed a substantial increase in firing rate during the initial segments of the individual training cycles, during which the eyes moved into the n-t direction (Fig. 7*B*). Concomitantly, CS firing rate decreased with a reciprocal pattern.

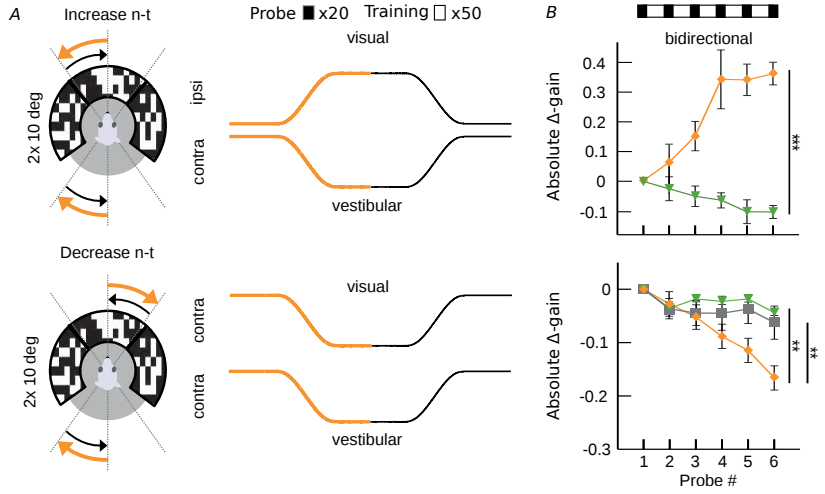

Figure 5. VOR gain-increase and gain-decrease training have a principal learning direction. A, Scheme of stimulation during gain-increase (vestibular and visual stimulus out-of-phase, top) and gain-decrease training (vestibular and visual stimulus in-phase, bottom). Icons depict stimulation (left) and stimulus traces (right) during training sessions with contraversive vestibular stimulation (n-t, orange, cf. Fig. 6A for unidirectional ipsiversive stimulation); during probe trials mice received vestibular stimulation in the dark in the respective direction. B, Changes in eye movement gain were measured during VOR probe trials (black boxes; 20 repeats = 4 min, top), caused by five gain-increase (n = 24; starting gain: 0.35 ± 0.02) (top panels) or gain-decrease (n = 26; starting gain: 0.35 ± 0.03) (bottom panels) training sessions (white boxes; 50 repeats = 10 min; total: 6x4mins + 5x10mins = 74 mins). Learning effect depended on the direction of stimulation, with significantly better learning in trainings based on contraversive (n-t, orange) than with ipsiversive (t-n, green) vestibular stimulation. Note that this difference was independent of whether the visual stimulus was presented bidirectionally, i.e. present during both ipsi- and contraversive vestibular input, or unidirectional, when the visual stimulus was presented only during the first segment of the vestibular stimulus, i.e. only during either ipsi- or contraversive input (Fig. 6). VOR habituation in the learning direction (gray line, bottom left), i.e. contraversive head rotations, is significantly different from VOR decrease in the same direction. Data are represented as mean ± SEM.

However, displaying close to perfect eye movement compensation, neither the behavioral responses nor the SS or CS spiking patterns changed over successive training sessions (n = 10, gain p = 0.97, f = 0.99; SS p = 0.9, f = 0.3; CS p = 0.9, f = 0.3) (Fig. 4*A* and *B*, right). In contrast, and as expected, over the successive VOR probe trials eye movement gain steadily and significantly increased (p = 0.004, f = 5.69) (Fig. 7*C*). Concomitantly, SS modulation also increased from 8 ± 1 to 20 ± 3 spikes/s (p = 0.004, f = -3.04), with a peak in modulation at the initial segments of the VOR probe cycle, which predominantly encoded velocity (Fig. 8*A* and *B*). During the stationary segment of the stimulus, after the eye had rotated to a temporal position, SS firing maintained a plateau level suggesting encoding of position; this level increased from 71 ± 4 spikes/s in the first trial to 85 ± 5 spikes/s in the last trial (Fig. 7*D*) (p = 0.045, t = -2.832). In contrast, CS modulation remained constant not only during training, but also during probe trials (training: p = 0.91 f = 0.299; probe: p = 0.98,

f = 0.51). During the secondary segment of the training stimulus, i.e. the rotation back to the initial position (Fig. 7*B*, black parts of stimulus traces) SSs and CSs modulated with the reversed unimodal pattern reflecting conditions during trainings in the non-learning direction (cf. Fig. 5). Purkinje cell recordings during unidirectional increase training (i.e. when the light was turned off during the second segment of the training cycles, see also Fig. 6*A*) revealed similar results (Fig. 9*A-D*) (n = 5, unidirectional vs. bidirectional: gain p = 0.11, t = 1.62; SS p = 0.38, t = 0.89; CS p = 0.1, t = 1.8), highlighting the facilitatory role of SS activity for gain-increase learning with contraversive head rotation.

Lower VOR gains after decrease training do not correlate with changes in PC simple spike activity

During VOR gain-decrease training in the principal learning direction the contraversive vestibular stimulus was combined with an in-phase visual stimulation (10° amplitude each) so as to suppress eye movements in the n-t direction (Fig. 10*A*). As could be predicted based on the minimized level of eye movements, SS modulation was largely absent during gain-decrease training sessions, showing a slightly bimodal pattern with no significant difference in SS peak firing rates compared to rest (n = 11, SS rest vs. stimulation: p = 0.746 t = -0.325) (Fig. 10*B*). Moreover, we observed no significant changes in eye movement gain or SS modulation across the successive training sessions (gain: p = 0.5, f = 0.9; SS p = 0.59, f = 0.75) (Fig. 5*B*). In contrast, during the intermittent probe trials VOR gain values steadily and significantly decreased (p < 0.001, f = 9.82) (Fig. 10*C*). However, we found no changes in SS firing during the probe trials over the course of the experiment (p = 0.92, f = 0.17) (Fig. 10*D*).

CS modulation during gain-decrease training sessions was also bimodal, but now with a significant peak-to-peak modulation (i.e. initial increase followed by a decrease; p < 0.001, t = 10.521), closely resembling the pattern of baseline VOR (Fig. 4*C*, Fig. 10*B* and Fig. 8*B* complex spikes during training). During the probe trials CS modulation was unchanged (p = 0.4 f = 1.1), but the baseline firing frequency showed a significant decrease (p = 0.025, f = 3.76) (Fig. 10*D*). This change in CS activity during the probe trials with bidirectional stimulation was also observed during probe trials after unidirectional training sessions with a concomitant change in gain, while SS activity did not change (n = 6, mixed model unidirectional: gain p = 0.003, f = 9.257, SS p = 0.9, f = 0.1, CS p = 0.02, f = 2.91) (Fig. 11*A-D*).

Causality and reversibility support a paradigm-dependent location of neuronal correlates

To find out whether the changes in SS modulation are sufficient to explain the differences in eye movement amplitude during VOR adaptation, we attempted to replicate the responses to a sigmoidal stimulus, using selective optogenetic manipulation of PCs in L7/

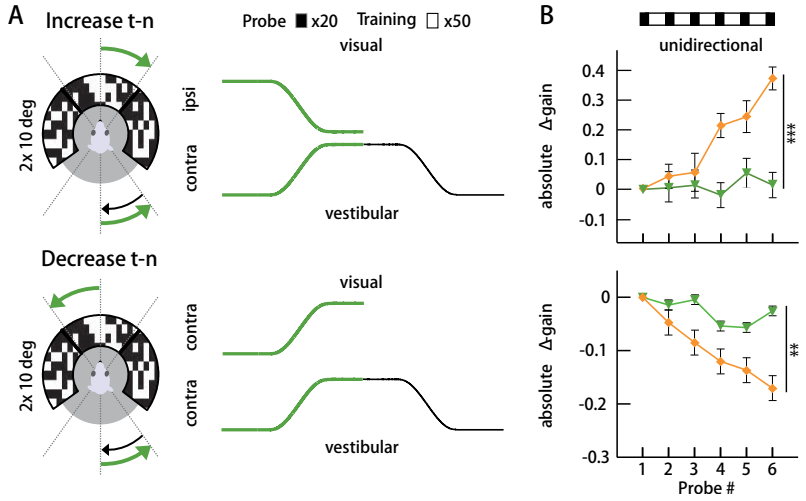

Figure 6. Unidirectional VOR gain adaptation. A, Schemes showing how we provided unidirectional stimulation during gain-increase (vestibular and visual stimulus out-of-phase, top) and gain-decrease training (vestibular and visual stimulus in-phase, bottom). Icons depict visual and vestibular stimulation (left) and stimulus traces (right) during training sessions with ipsiversive vestibular stimulation (t-n, green); during probe trials mice received vestibular stimulation in the dark in the respective direction. B, Changes in eye movement gain were measured during VOR probe trials (black boxes; 20 repeats = 4 min, top); these changes were induced by five gain-increase (top panels) or gain-decrease (bottom panels) training sessions (white boxes; 50 repeats = 10 min; total time 74 min (6x4mins+5x10mins). As during bidirectional stimulation, the learning effect depended on the direction of stimulation, with significantly better learning in trainings based on contraversive (n-t, orange) than with ipsiversive (t-n, green) vestibular stimulation.

cre-Ai27 mice in the dark without vestibular stimulation (n = 20 cells; 4 mice) (Fig. 12*A*). Unilateral stimulation of floccular PCs with blue light pulses resulted in SSs and CSs with a normal shape (Fig. 12*B* and Fig. 13). Increasing stimulus frequency induced concomitantly an increase in SS firing rate and naso-temporal eye movements (Fig. 12*C*), mimicking those evoked by natural vestibular or visual stimulation. The SS firing rate and pupil position changed proportionally to the light intensity (0.12, 0.42, 0.72, 1.8 mW/mm^2) (Fig. 12*D*). ADD LIGHT CONTROL EXPERIMENT HERE. The change in spike rate per degree of eye movement was significantly higher during optogenetic stimulation than that during VOR adaptation (7 ± 2 vs. 4 ± 3 spikes/s/°, respectively) (2-tailed t-test: p = 0.02, t = 2.52), possibly reflecting the fact that the basic drive from the primary vestibular afferents to the second-order vestibular neurons is present during VOR adaptation, but not during optogenetic stimulation (Fig. 1*A*) and/or that natural vestibular stimulation exerts bilateral effects while our optogenetic stimulation was provided unilaterally. In conjunction with the increase in SS activity following natural training stimulation, these data suggest that SS activity can code for gain-increase adaptation contributing to movement-direction selective learning.

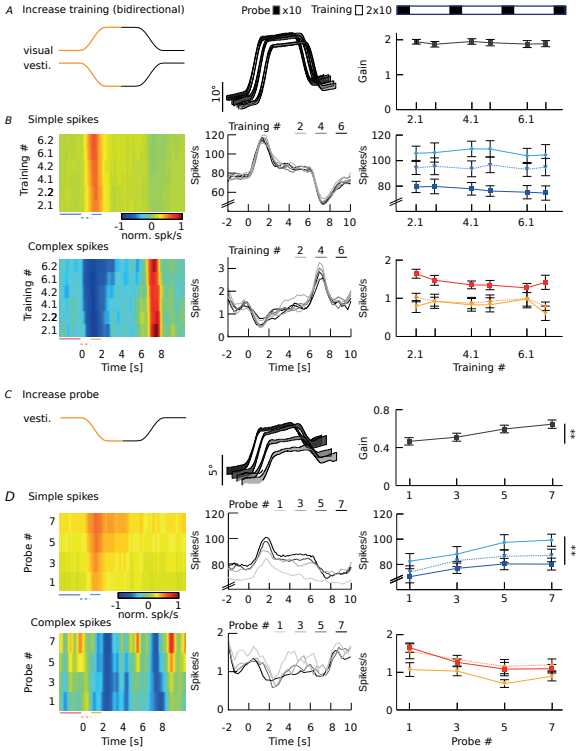

Figure 7. VOR gain-increase correlates with increased SS activity in probe trials. A, VOR gain-increase training was induced by simultaneous visual and vestibular stimulations moving in opposite directions. After an initial VOR baseline measurement including 10 stimulus cycles of 12 s each (2 min), we recorded from each cell during 3 consecutive training blocks (total duration 20 min). Each of these training blocks consisted of 2 visuovestibular mismatch training sessions and each session included 10 stimulus cycles (i.e. 2 x 2 min) and 1 VOR probe session including 10 stimulus cycles (i.e. 1 x 2 min). Only repeats with stable spiking activity were used for analysis. From the start of the gain-increase training the eye movements of the mice compensated close to optimally for the combined amplitude of the visual and vestibular stimulation and the gains during this visuovestibular mismatch stimulation did not change significantly over time (middle panel). Schematic drawing at the top right illustrates the order of 10 VOR probe trials in the dark (black boxes) and 20 visuovestibular training trials (white boxes) for 3 consecutive blocks. B, Heat maps of normalized SS and CS responses of an example PC during the training trials qualitatively (left) and average firing rates of all cells for each training block quantitatively (middle) representing unimodal and reciprocal SS and CS firing rates. Absolute firing rates (right) were determined for three intervals during the first segment of stimulation as indicated by colored lines below heatmaps of relative firing rate (left): The baseline before the stimulus (solid lines, SS dark blue and CS red) compared to the accelerating and decelerating half of the stimulus (dotted and solid line, SS light blue and CS light red, respectively). SS and CS activity were stable over the subsequent training sessions. C, As a result of the increase training sessions, eye movement amplitude in the probe trials (i.e. during vestibular stimulation in the dark only) increased from starting gains of ~0.4 to ~0.7 (right). D, Similar to B, but for probe trials. While CS activity was not affected, SS firing rate increased significantly, particularly during the decelerating phase of the initial segment and during the stationary segment of the stimulus, over the course of the training sessions (right). Data are represented as mean ± SEM; eye movement population data (middle panels) represent ± SEM and spiking data are mean values.

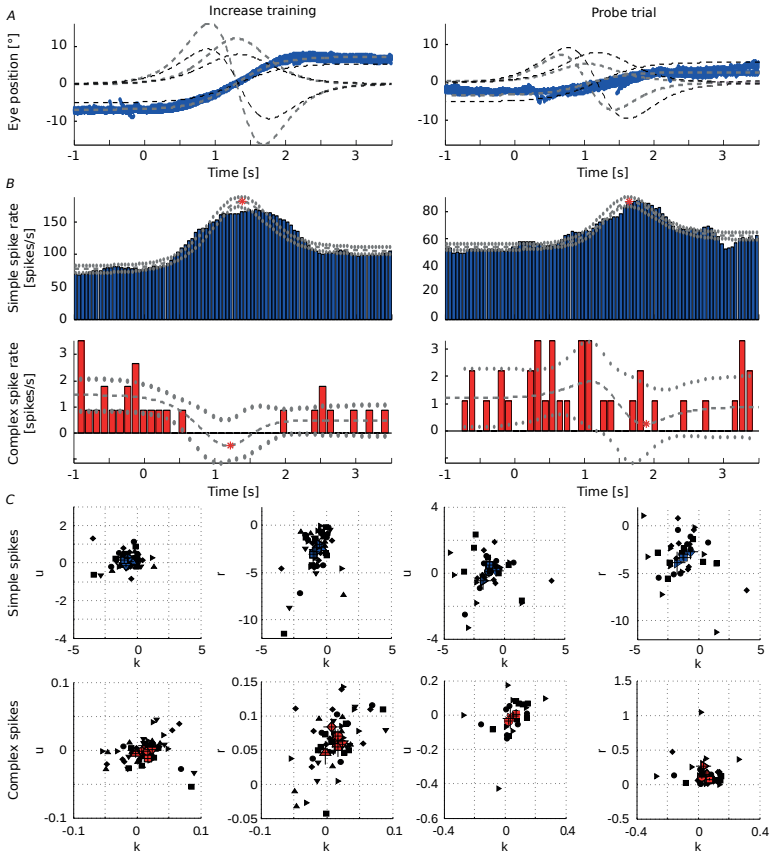

Figure 8. Regression of VA PC responses during increase training. A, Position, velocity and acceleration profiles of the initial segment of a sigmoidal vestibular stimulation (black) and the corresponding averaged eye movement responses of a single mouse (gray) during increase training (left) and during the first probe trial (right). Note that during the increase training (left panel) the added visual stimulation results in compensatory eye movements that are larger than that of the vestibular stimulus alone (right panel). B, Corresponding averaged SS (blue) and CS (red) activity profiles of a VA Purkinje cell during these initial segments of the training and probe trial; date were fitted using an inverse dynamics model of the eye movements (gray) (Materials & Methods formula 2). C, Results of all recorded PCs for position (k), velocity (r) and acceleration (u) components of SSs (top row) and CSs (bottom) during increase training (left) and probe trials (right). Data are represented as mean ± SEM.

Gain increases and gain decreases are reversible when induced with sinusoidal stimulation[46,47]. Interestingly the reversibility is asymmetric, implicating that the two paradigms depend on different processes[46], which could in fact be in different locations. Given that here with sigmoidal stimulation SS modulation was increased over consecutive probe trials following VOR gain-increase training, and that there was no significant change in SS activity upon VOR gain-decrease training in the probe trials, one could hypothesize that the learning abilities might ultimately be blocked due to saturation. Alternatively, the

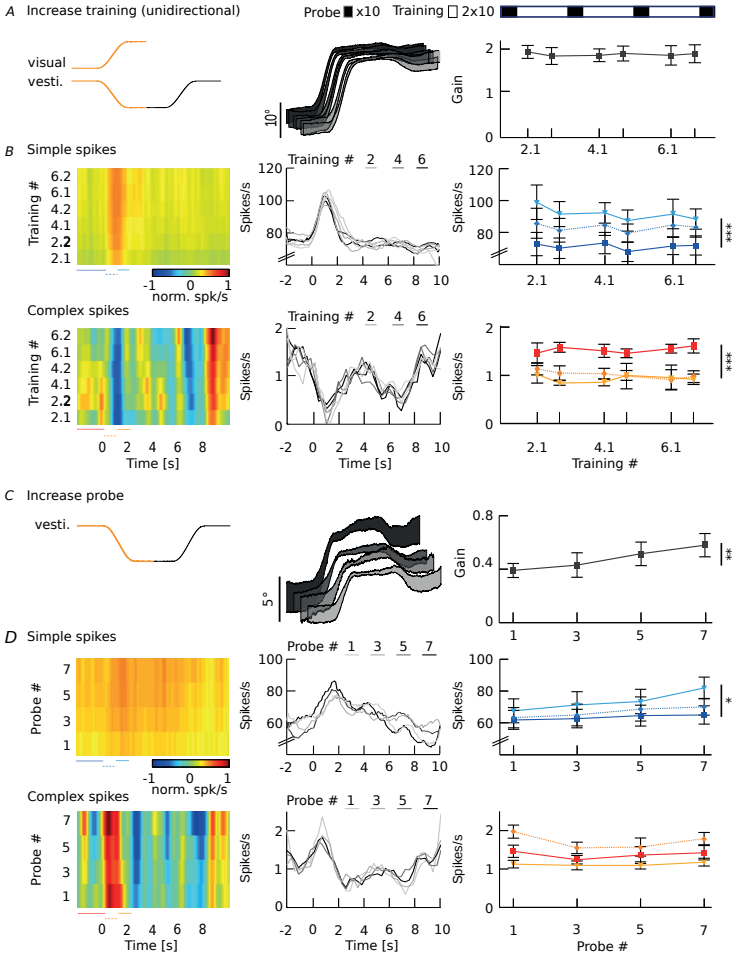

Figure 9. Eye movements and PC modulation during training and probe trials following unidirectional training. A, Stimulus and average eye movements during unidirectional increase training, which consisted of visual and vestibular stimuli moving in opposite directions during the initial segment of the stimulus and the vestibular stimulus rotating back without the visual stimulus present during the second segment (left). Eye movements compensated for the combined amplitude of the stimuli during the initial segment (middle) and gains did not change over time (right). B, Heat map of normalized SS and CS responses of a representative PC (left) and average firing rates for each training block (middle). Absolute firing rates (right) were determined for three intervals during the first segment of stimulation as indicated by colored lines below heat-maps of relative firing rate (left): The baseline before the stimulus (solid lines, SS dark blue and CS red) compared to the accelerating and decelerating half of the stimulus (dotted and solid line, SS light blue and CS light red, respectively). Note that a significant modulation was only present during the initial segment. C, Stimulus and average eye movements during probe trials. In probe trials, when the vestibular stimulus was delivered in the dark (left), eye movement amplitude significantly increased over the training sessions (middle, right). D, SS and CS responses of the same cell as in B (left) and on average for all cells (right) show that SS activity increases during vestibular stimulation over the course of gain-increase learning. Spike data on the left are mean values. Eye movement population data in the middle panels and spike data on the right represent mean ± SEM.

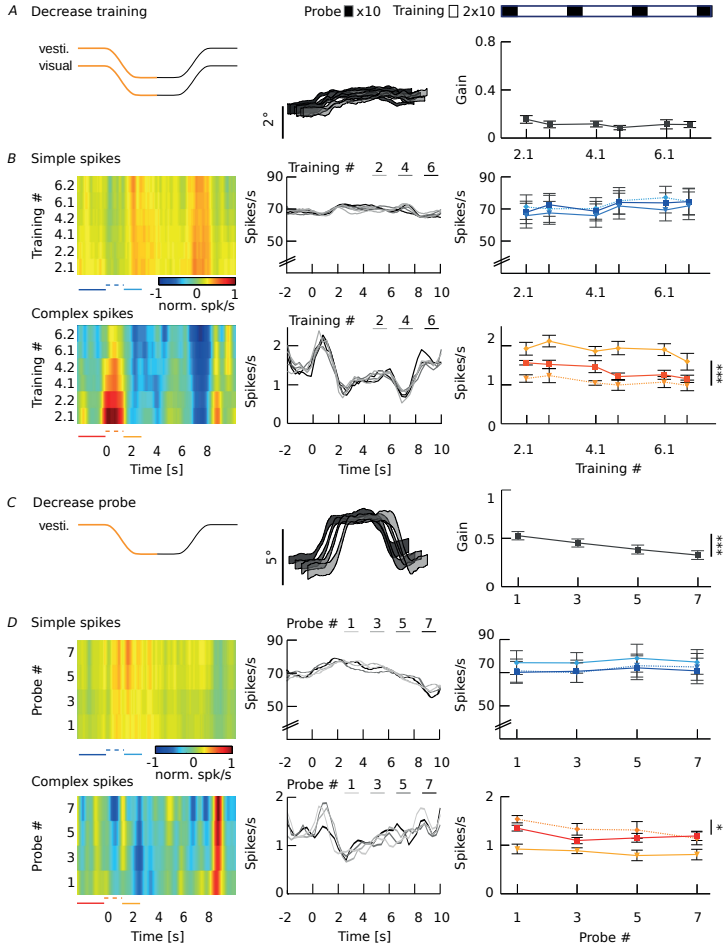

Figure 10. VOR gain-decrease affects CS activity during training sessions. A, VOR gain-decrease training was induced by simultaneous visual and vestibular stimulations that move in-phase (left panel), which resulted in minimized eye movements (middle panel) that did not change in gain over time (right panel). Order of VOR probe trials (black boxes lasting 8 minutes) and training sessions (white boxes lasting 12 minutes) is illustrated above the line plots. B, SS and CS activity, on average, did not change during the decrease training sessions. Insets in middle panels show graphical fit of the acceleration profile of the stimulus onto the bimodal average SS and CS modulation during the initial segment of the stimulus. Absolute firing rates (right) were determined for three intervals during the first segment of stimulation as indicated by colored lines below heatmaps of relative firing rate (left): The baseline before the stimulus (solid lines, SS dark blue and CS red) compared to the accelerating and decelerating half of the stimulus (dotted and solid line, SS light blue and CS light red, respectively). C, Vestibular stimulus and average eye movements during probe trials in the dark (left panel). Eye movement amplitude decreased over subsequent training sessions (middle panel), with gains starting from ~0.4 and significantly decreasing to ~0.26 (right panel). D, Same PC as in B (left panels) and group averages (middle panels) showing that gain-decrease was reflected in CS activity, but not in SS activity (right panels). Spike data on the left are mean values. Eye movement population data in the middle panels and spike data on the right represent mean ± SEM.

gain-decrease training could actively extinguish the changes acquired during gain-increase training, in effect at least in part 'cleaning the sheet' for new trainings. To test this we performed an additional set of behavioral experiments, in which mice (n = 6) were first subjected to VOR gain-increase training, immediately followed by a decrease training, both in the principal learning direction. The first block of decrease training ablated the effect of 7 blocks of increase training (total of 98 min), significantly reducing VOR gains to baseline levels (first vs. second probe trial: $p = 0.039$, $t = 2.47$) and below (baseline vs. last decrease probe trial: $p = 0.034$, $t = -2.564$) (Fig. 14*A*). During the remaining decrease training eye movement gains further decreased, comparable to the effect of VOR gain-decrease training alone (Fig. 5*B*). To assess SS dynamics during this extinction we next recorded PC activity related to the decrease training (n = 8) after the mice had received an increase training (Fig. 14*B*). While eye movement gains, like before, decreased rapidly after the first decrease training, SS modulation depth declined more gradually from a potentiated peak firing rate back to baseline levels (first vs. second probe: $p = 0.64$, $t = -0.48$; all probes: $p = 0.03$, $f = 3.88$) (Fig. 14*B*) than could be expected based upon the rapid changes in eye movement gain at the initial stage. This partial discrepancy between behavior and neuronal signals may reflect the differential loci for un-learning VOR gain-increase and learning VOR gain-decrease, which is also suggested by the absence of a change in SS rate following VOR gain-decrease training alone.

DISCUSSION

Directionality is an inherent feature of the compensatory eye movement system and manifests itself in the lateralization of the cerebellum and the mirrored preferred axes of modulation for climbing fiber activity of PCs in the various zones of both flocculi[34,48]. To test the hypothesis that cerebellar learning depends on movement direction, we investigated to what extent compensatory eye movements and VOR gain-increase and gain-decrease adaptation are direction-specific. Behavioral results showed that visual input generated a direction-selective difference in eye movement gains and delays, with larger gains and longer delays for eye movements in the naso-temporal (n-t) direction. Learning efficacy was optimal when the vestibular stimulus moved contraversively, which coincides with the preferred n-t movement direction for visually driven compensatory eye movements. In addition, our electrophysiological data showed that SS activity during probe trials could only be correlated with eye movements during VOR gain-increase adaptation in the n-t direction. Moreover, albeit in a reciprocal fashion, CS activity during probe trials was also best correlated with eye movements during VOR gain-decrease adaptation in the same preferred direction (Fig. 15*A*). Indeed, together these results point towards a principal learning direction for eye movement adaptation.

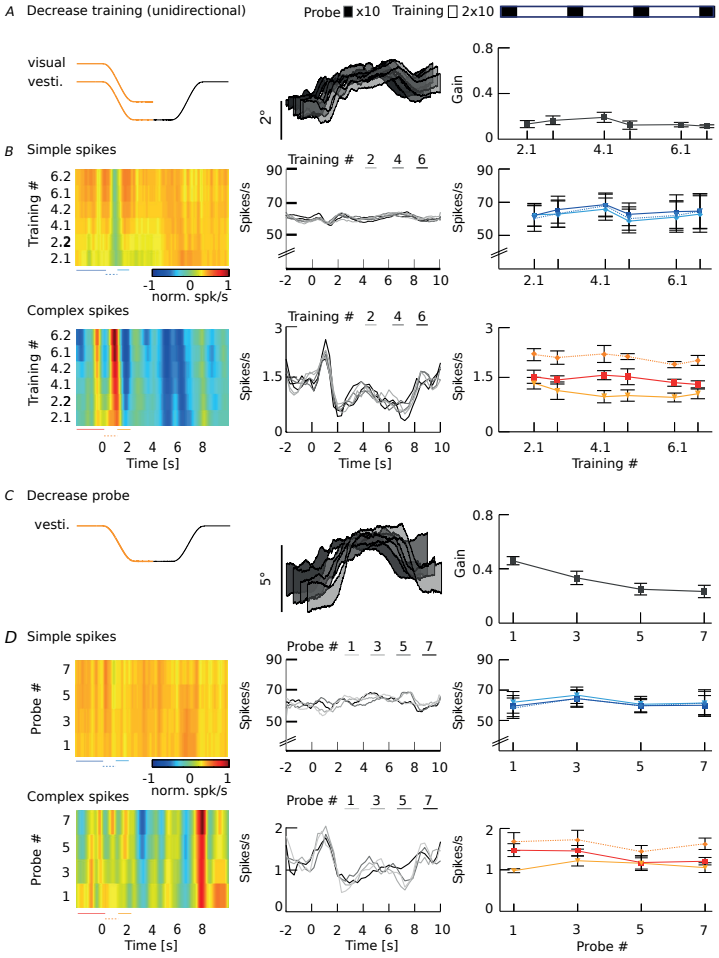

Figure 11. Eye movements and PC modulation during training and probe trials following unidirectional decrease training. A, Stimulus and average eye movements during unidirectional decrease training consisting of visual and vestibular stimuli moving in phase during the initial segment of the stimulus and the vestibular stimulus rotating back without the visual stimulus present during the second segment (left). Eye movements were minimized as a result of the stimuli during the initial segment (middle) and these gains did not change over time (right). B, Heat map of normalized SS and CS responses of a representative PC (left) and average firing rates for each training block (middle). Absolute firing rates (right) were determined for three intervals during the first segment of stimulation as indicated by colored lines below heatmaps of relative firing rate (left): The baseline before the stimulus (solid lines, SS dark blue and CS red) compared to the accelerating and decelerating half of the stimulus (dotted and solid line, SS light blue and CS light red, respectively). SS responses were largely absent, whereas CSs showed a similar bimodal pattern as seen in bidirectional training (Fig. 10). C, Stimulus and average eye movements during probe trials. In probe trials, when the vestibular stimulus is delivered in the dark (left), eye movement amplitude significantly decreased over the training sessions (middle, right). D, SS and CS responses of the same cell as in B (left); on average the cells (middle, right) show no changes in SS or CS activity over time. Eye movement population data in the middle panels and spike data on the right represent mean ± SEM.

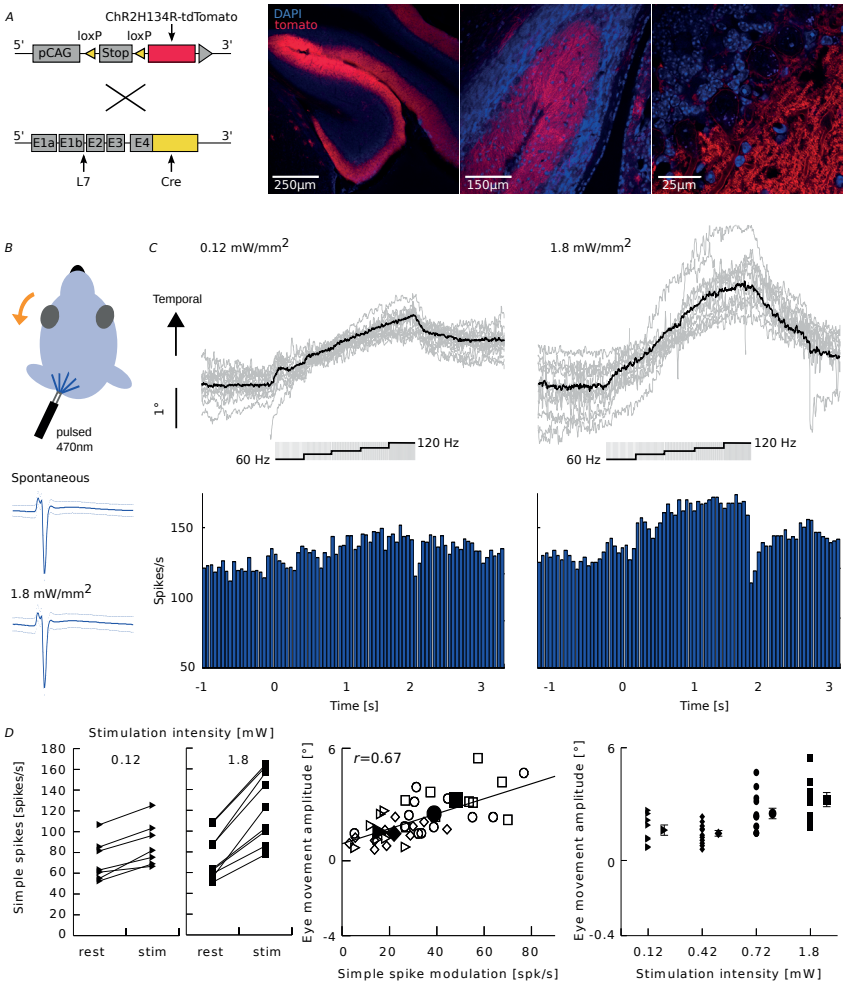

Figure 12. Interactions between SS activity and direction and amplitude of eye movements. A, Purkinje cell-specific Cre (L7-Cre) and Cre-recombinase-dependent channelrhodopsin expressing (Ai27D) mice were crossed to generate mice in which the firing activity of Purkinje cells can be increased by a light stimulus (left). Confocal images of sagittal cerebellar slices of the flocculus-parafloccular complex showed reliable expression of channelrhodopsin (red) in PCs. Blue indicates DAPI staining. B, Selective optogenetic stimulation of PCs in the flocculus with blue light (pulsed 470nm; five steps: 60, 80, 90, 100, 120 Hz for 400 ms each) resulted in temporal eye movements (top). SS shapes did not differ between spontaneous and evoked activity (bottom). C, Example eye movement traces (top, n = 10, black line = average) following repeated optogenetic stimulation (gray box) mimicking the naturally evoked response, raster plot (middle) and PSTH (bottom) of the SS response due to low (left) and high (right) light intensities (Fig. 13 for CS). D, Increasing intensities resulted in increases in SS firing rates of individual cells (left) and accompanying ipsiversive eye movements (right). Optogenetically evoked changes in SS firing correlate with changes in eye movements (middle) in terms of direction and eye movement per spike, indicating a causal relationship (triangles, diamonds, circles and squares indicate 0.12, 0.42, 0.72 and 1.8 mW/mm^2, respectively, filled symbols represent mean values). Note that optogenetic stimulation also evoked eye movements in the vertical plane (Fig. 13).

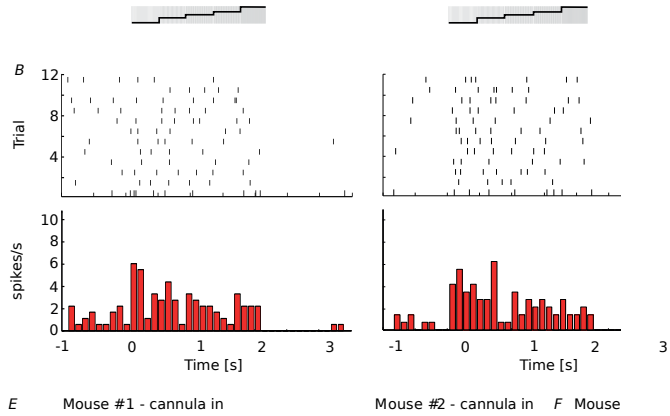

Figure 13. Optogenetic stimulation of floccular PCs and corresponding eye movements. A, Examples of horizontal (middle) eye movements evoked by stimulation traces (bottom) at different light intensities. Stimulation traces consisted of light pulses with increasing frequencies (60, 80, 90, 100, 120 Hz; 50% duty cycle; 450 ms duration each). Eye movements increased in amplitude with increasing light intensity and were typically diagonal, consisting of a temporal and ventral component. B, Raster plots and PSTHs of CS activity corresponding to the eye movements in A. C, Average CS shapes and 95% confidence interval of the cell in B during stimulation and interstimulus intervals. Shapes of the two spike types were not different during these periods, suggesting that the optogenetically evoked CSs are electrophysiologically similar to spontaneous CSs (for SS cf. Fig. 6B). D, Linear regression of the eye movement onto PC cell firing showed a strong correlation with the position component (k) for the four light intensities of both SS and CS firing (0.12 mW, position k: SS = 19.7 ± 4.9, CS = -1.2 ± 0.5, velocity r: SS = 1.2 ± 2.2, CS = -0.9 ± 0.3; 1.8 mW, position k: SS = 16.5 ± 2.6, CS = -1.6 ± 0.5, velocity r: SS = -2 ± 1.5, CS = -0.5 ± 0.2). Using a linear fit of the eye movements the constant velocity term represents the offset of spiking, whereas the acceleration term was zero and did not contribute.

To the best of our knowledge this is the first study correlating SS and CS activity to eye movement adaptation using sigmoidal trainings and probe trials during complete cycles of learning. This experimental setup allowed quantitative identification of learning rules and direction selectivity for both gain-increase and gain-decrease[25,27]. Interestingly, gain-increase training was exclusively successful when the visual stimulus moved the eye into the preferred n-t direction, minimizing the activity of the climbing fibers. These data are in line with our working hypothesis that potentiation rather than depression mechanisms drive VOR learning[15,16,18], since LTP at the parallel fiber to PC synapse and enhancement of PC intrinsic plasticity are facilitated by a reduction in climbing fiber activity[9]. Importantly, our optogenetic experiments demonstrated that the increase in SS activity is not only necessary but also sufficient to increase the gain (Fig. 12 and Fig. 15*B*). Likewise, the shorter delays for eye movements in the temporo-nasal (t-n) direction may be related to the rapidly and synchronously activated CSs during contraversive movements, as a lack of olivary gap junctions induces a short delay during such visual compensatory eye movements[49].

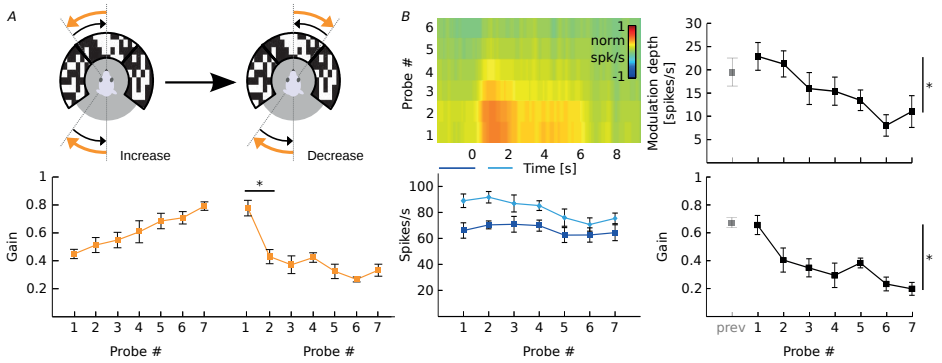

Figure 14. Neuronal correlates for VOR adaptation involve the cerebellar cortex and targets downstream of PCs. A, VOR gain-decrease training can reverse adapted changes in eye movement gain due to increase training. Icons (top) depict the paired paradigm. Note the sharp drop in gain after the first decrease training block (bottom). Data from behavioral experiments. B, Heat map of simple spike activity of an example cell (left top) showing that the increase in SS firing after gain-increase training returns to near baseline levels during decrease training (compare to Fig. 4D and Fig. 5D). Averaged firing rates of all recorded cells (n = 8) prior to (dark blue) and during (light blue) stimulation (left bottom). Eye movement gains, as in A, decreased with an initial fast drop followed by a slower decrease (right bottom), whereas the depth of simple spike modulation (right top) returned more gradually to baseline levels (gray data point indicating depth of modulation after increase training, cf. Fig. 7D). Data are represented as mean ± SEM.

Other forms of plasticity in the cerebellar cortex may also influence SS activity of PCs and thereby gain-increase learning[9]. These include for example those engaging the molecular layer interneurons, which directly control the rate and regularity of SS activity[9,50]. The inhibitory interneurons as well as the plasticity mechanisms that control their activity are probably also relevant for the inversion of the vestibular signal that occurs between the vestibular organs and the Purkinje cells[50]. Contraversive head rotation decreases activity in the vestibular ganglion neurons, but correlates with an increased firing rate in Purkinje cells (Fig. 1*A*). Hence, suppression of the inhibitory input, which is indeed facilitated during the absence of climbing fiber activity[9], may contribute to VOR gain-increase learning, whereas the absence of effects on SS firing rate during gain-decrease training suggests that changes in inhibition in this form of adaptation are absent or nullified by concomitant changes in excitatory input or intrinsic properties. In line with this, mutant mice lacking GABA2 receptor subunits at their molecular layer interneuron to PC synapse or mutants lacking the potassium chloride transporter KCC2 specifically in their PCs, both of which suffer from impaired inhibition onto their PC, show virtually normal gain-decrease training, whereas gain-increase learning and phase reversal learning are strongly affected[9,26,51]. Thus, the changes in SS firing that we observed during gain-increase training may be potentially enhanced by net changes of inputs from both excitatory and inhibitory inputs[35,52], but their functional impact during gain-decrease learning appears rather limited.

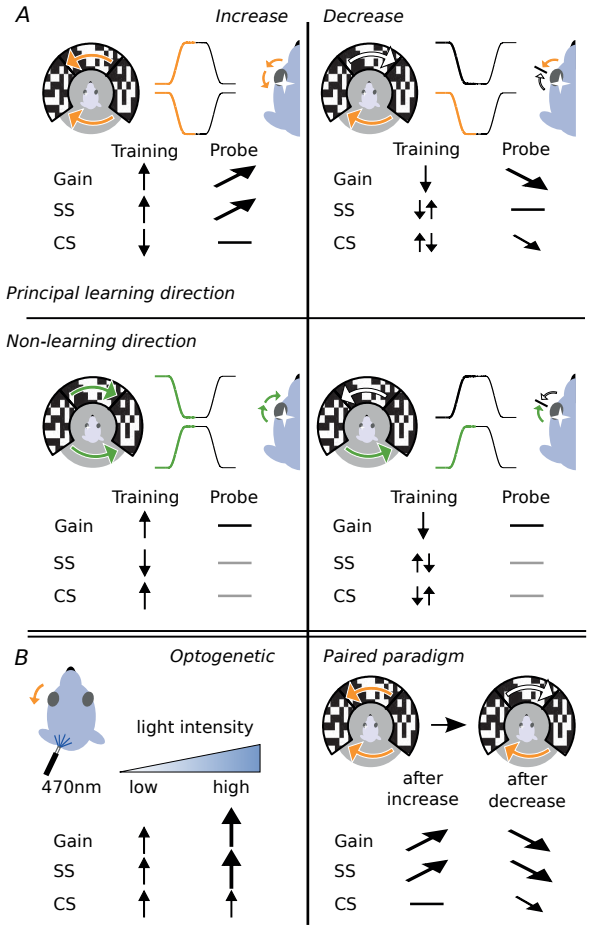

Figure 15. VOR adaptation and its neural correlates are paradigm and direction specific. A, VOR adaptation and related spiking changes during gain-increase (left) and gain-decrease (right) adaptation paradigms in the principal (top) and non-learning (bottom) direction. The gain of the VOR evoked by contraversive rotation could be adapted, increased or decreased, whereas that evoked by ipsiversive rotation could not. During gain-increase training in the principal learning direction simple spike and complex spike rates increased and decreased, respectively, and the simple spike firing rate during probe trials after training increased significantly, in line with the VOR gain. Conversely, complex spike and simple spike modulation during gain-decrease training was more complex, revealing a bimodal CS pattern during training and a CS reduction during the probe trials, whereas simple spike rates did not change over time in probe trials. B, Ipsilateral optogenetic stimulation and simultaneous recordings of PCs in the flocculus evoked an increase in SS and CS firing and naso-temporal eye movements. Increasing light intensities led to increasing PC activity and eye movement amplitudes, effectively simulating the behavioral and neuronal changes observed due to visuovestibular mismatch, gain-increase training (left). A paired paradigm showed that simple spike activity potentiated by gain-increase training, unlike that in naïve mice, can be actively suppressed by gain-decrease training. This discrepancy and the rapid drop in eye movement gain compared to the gradual decrease in simple spike activity point towards the potential involvement of downstream areas in the decrease of eye movement gain, e.g. the vestibular nuclei.

A dichotomy between gain increase and decrease has been suggested before, but the evidence for the underlying locations and processes is inconclusive[15,16,18,29,30]. Presumably, plasticity in the vestibular nuclei downstream contributes substantially to gain-decrease learning[53-55]. Indeed, the gain-decrease paradigm did not result in persistent changes in SS activity but only in changes in CS activity that may influence plasticity in the vestibular and cerebellar nuclei[56,57] (Fig. 15*A*). These data are in line with the observation that mutants, in which the majority of granule cell output is impaired and both LTD and LTP are impaired, can still successfully complete the gain-decrease, but not the gain-increase, paradigm[31]. In addition, plasticity at the level of vestibular nuclei during gain-decrease learning may also explain why gain-increase effects are rather specific for the training frequency[58], whereas gain-decrease appears to be more generalized over a wider range of vestibular input frequencies[59]. Finally, the current data are also in line with the behavioral and spike activity phenotypes of various mutants during phase reversal of the VOR, which requires initially an extension of the gain-decrease paradigm followed by an increase in gain, ultimately moving the eye opposite to the natural reflex[28,60].

The notion that changes in SS activity of floccular PCs could be directly responsible for the adaptive response during VOR adaptation has been put forward before[25,61], as has a contribution of the vestibular nuclei[62], but here we show for the first time that this activity as well as the level of learning is related to the direction of the eye movement. Optogenetically driven floccular SS activity during contraversive, but not ipsiversive, vestibular input indeed resulted in a higher VOR gain[25]. In contrast, climbing fiber activation during contraversive head movement had no effect[25], arguing against a role for climbing fiber - dependent plasticity during VOR gain-decrease, which is in line with our observations. Kimpo et al.[27], on the other hand, observed an effect on PC activity during a gain-increase training paradigm that was supposed to occur during ipsiversive head movements while climbing fibers are activated. However, eye movement behavior was not recorded during these PC recordings and the current data raise doubt as to whether the gain-increase adaptation fully occurred. It should be noted that, unlike the current study, the majority of previous studies used continuous sinusoidal vestibular input that hampers analysis of direction-specific components and/or that they did not combine behavioral analysis with simultaneous PC recordings.

Our experiments in which we investigated gain-decrease training following gain-increase training, i.e. the decrease in gain occurred following an initial enhancement of SS firing rates (Fig. 15*B*), revealed that gain-decrease adaptation and changes in SS modulation follow different dynamics, even when both eye movement gain and SS activity are bound to decrease. While the gain had already dropped to baseline levels after one training session, SS modulation gradually declined over several training sessions, but never dropped

below baseline, once more indicating that the locus for VOR gain-decrease learning resides partly somewhere downstream of PC output. Nevertheless, proper PC activity may also be required for successful VOR gain-decrease training, as it is impaired after flocculectomy[41].

It is interesting to note that other laterally eyed animals such as zebrafish show a similar pronounced asymmetry in directional sensitivity of their optic system[63]. Moreover, even though direction-selectivity remains to be investigated at a more detailed level, several findings point towards similar mechanisms in frontal eyed animals. For example in non-human and human primates, unidirectional rotations around the vertical axis also resulted in asymmetric gain changes towards the adapted, but not un-adapted side[23,24]. Rotations around the horizontal axis in humans appear to have a direction-specific preference for downward movements[64-66] that may coincide with increased SS activity in floccular horizontal-axis zones[21,67]. It would be interesting to find out to what extent floccular PC activity is also concomitantly and selectively enhanced in frontal eyed animals during ipsiversive eye movements. If this correlation holds throughout all vertebrate species, one might hypothesize that such control systems provide evolutionary advantageous control over explorations of the ipsilateral visual field and concomitantly ipsilateral motor control, such as limb movements. After all, with such a configuration the cerebral cortical control systems involved, i.e. frontal eye fields, primary and secondary visual cortices as well as the cortical areas involved in limb control, all develop on the same side of the brain, offering optimal opportunities for integration from a neuro-anatomical point of view.

The asymmetry in learning mechanisms for different directions might depend partly on the different types of cerebellar zones involved. PCs in floccular zones are predominantly, if not exclusively, zebrin-positive and thus have a relatively low SS firing rate[14,68,69]. Thereby, they are probably more prone to be potentiated by their parallel fiber input[70]. In contrast, PCs in the zebrin-negative zones, such as those controlling eyeblink conditioning[71], have relatively high SS firing rates and are probably more prone to be suppressed[72,73]. Interestingly, in cerebellum-dependent eyeblink conditioning the learning related changes that occur in PCs are indeed in the opposite direction, i.e. SS firing is suppressed in a time-locked fashion to the conditioned eyeblink response[73-75]. Together these studies and the current results suggest that potentiation and suppression of SS activity could be module-dependent, as a general feature intrinsic to cerebellar functioning[76].

REFERENCES

1. Ezure, K. & Sasaki, S. Frequency-response analysis of vestibular-induced neck reflex in cat. I. Characteristics of neural transmission from horizontal semicircular canal to neck motoneurons. *J Neurophysiol* **41**, 445-458 (1978).
2. Lopez-Barneo, J., Darlot, C., Berthoz, A. & Baker, R. Neuronal activity in prepositus nucleus correlated with eye movement in the alert cat. *J Neurophysiol* **47**, 329-352 (1982).

3. Robinson, D.A. Adaptive gain control of vestibuloocular reflex by the cerebellum. *J Neurophysiol* **39**, 954-969 (1976).
4. Distler, C. & Hoffmann, K.P. Development of the optokinetic response in macaques: a comparison with cat and man. *Ann N Y Acad Sci* **1004**, 10-18 (2003).
5. Smith, M.A. & Shadmehr, R. Intact ability to learn internal models of arm dynamics in Huntington's disease but not cerebellar degeneration. *J Neurophysiol* **93**, 2809-2821 (2005).
6. Tseng, Y.W., *et al.* Sensory prediction errors drive cerebellum-dependent adaptation of reaching. *J Neurophysiol* **98**, 54-62 (2007).
7. Cahill, H. & Nathans, J. The optokinetic reflex as a tool for quantitative analyses of nervous system function in mice: application to genetic and drug-induced variation. *PLoS One* **3**, e2055 (2008).
8. Medina, J.F. & Lisberger, S.G. Links from complex spikes to local plasticity and motor learning in the cerebellum of awake-behaving monkeys. *Nat Neurosci* **11**, 1185-1192 (2008).
9. Gao, Z., van Beugen, B.J. & De Zeeuw, C.I. Distributed synergistic plasticity and cerebellar learning. *Nat Rev Neurosci* **13**, 619-635 (2012).
10. Lev-Ram, V., Wong, S.T., Storm, D.R. & Tsien, R.Y. A new form of cerebellar long-term potentiation is postsynaptic and depends on nitric oxide but not cAMP. *Proc Natl Acad Sci U S A* **99**, 8389-8393 (2002).
11. Coesmans, M., Weber, J.T., De Zeeuw, C.I. & Hansel, C. Bidirectional parallel fiber plasticity in the cerebellum under climbing fiber control. *Neuron* **44**, 691-700 (2004).
12. Ito, M. Cerebellar control of the vestibulo-ocular reflex--around the flocculus hypothesis. *Annu Rev Neurosci* **5**, 275-296 (1982).
13. Ito, M. & Kano, M. Long-lasting depression of parallel fiber-Purkinje cell transmission induced by conjunctive stimulation of parallel fibers and climbing fibers in the cerebellar cortex. *Neurosci Lett* **33**, 253-258 (1982).
14. Hansel, C., *et al.* alphaCaMKII Is essential for cerebellar LTD and motor learning. *Neuron* **51**, 835-843 (2006).
15. Schonewille, M., *et al.* Purkinje cell-specific knockout of the protein phosphatase PP2B impairs potentiation and cerebellar motor learning. *Neuron* **67**, 618-628 (2010).
16. Schonewille, M., *et al.* Reevaluating the role of LTD in cerebellar motor learning. *Neuron* **70**, 43-50 (2011).
17. Peter, S., *et al.* Dysfunctional cerebellar Purkinje cells contribute to autism-like behaviour in Shank2-deficient mice. *Nat Commun* **7**, 12627 (2016).
18. Gutierrez-Castellanos, N., *et al.* Motor Learning Requires Purkinje Cell Synaptic Potentiation through Activation of AMPA-Receptor Subunit GluA3. *Neuron* **93**, 409-424 (2017).
19. Simpson, J.I. & Alley, K.E. Visual climbing fiber input to rabbit vestibulo-cerebellum: a source of direction-specific information. *Brain Res* **82**, 302-308 (1974).
20. Lisberger, S.G. & Fuchs, A.F. Role of primate flocculus during rapid behavioral modification of vestibuloocular reflex. II. Mossy fiber firing patterns during horizontal head rotation and eye movement. *J Neurophysiol* **41**, 764-777 (1978).
21. Hirata, Y. & Highstein, S.M. Analysis of the discharge pattern of floccular Purkinje cells in relation to vertical head and eye movement in the squirrel monkey. *Prog Brain Res* **124**, 221-232 (2000).
22. Ito, M. Cerebellar circuitry as a neuronal machine. *Prog Neurobiol* **78**, 272-303 (2006).
23. Ushio, M., Minor, L.B., Della Santina, C.C. & Lasker, D.M. Unidirectional rotations produce asymmetric changes in horizontal VOR gain before and after unilateral labyrinthectomy in macaques. *Exp Brain Res* **210**, 651-660 (2011).
24. Migliaccio, A.A. & Schubert, M.C. Unilateral adaptation of the human angular vestibulo-ocular reflex. *J Assoc Res Otolaryngol* **14**, 29-36 (2013).
25. Nguyen-Vu, T.D., *et al.* Cerebellar Purkinje cell activity drives motor learning. *Nat Neurosci* **16**, 1734-1736 (2013).
26. Wulff, P., *et al.* Synaptic inhibition of Purkinje cells mediates consolidation of vestibulo-cerebellar motor learning. *Nat Neurosci* **12**, 1042-1049 (2009).
27. Kimpo, R.R., *et al.* Gating of neural error signals during motor learning. *Elife* **3**, e02076 (2014).
28. Badura, A., Clopath, C., Schonewille, M. & De Zeeuw, C.I. Modeled changes of cerebellar activity in mutant mice are predictive of their learning impairments. *Sci Rep* **6**, 36131 (2016).

29. Titley, H.K. & Hansel, C. Asymmetries in Cerebellar Plasticity and Motor Learning. *Cerebellum* **15**, 87-92 (2016).
30. Boyden, E.S.*, et al.* Selective engagement of plasticity mechanisms for motor memory storage. *Neuron* **51**, 823-834 (2006).
31. Galliano, E.*, et al.* Silencing the majority of cerebellar granule cells uncovers their essential role in motor learning and consolidation. *Cell Rep* **3**, 1239-1251 (2013).
32. Graf, W., Simpson, J.I. & Leonard, C.S. Spatial organization of visual messages of the rabbit's cerebellar flocculus. II. Complex and simple spike responses of Purkinje cells. *J Neurophysiol* **60**, 2091-2121 (1988).
33. De Zeeuw, C.I., Wylie, D.R., Stahl, J.S. & Simpson, J.I. Phase relations of Purkinje cells in the rabbit flocculus during compensatory eye movements. *J Neurophysiol* **74**, 2051-2064 (1995).
34. Schonewille, M.*, et al.* Zonal organization of the mouse flocculus: physiology, input, and output. *J Comp Neurol* **497**, 670-682 (2006).
35. Badura, A.*, et al.* Climbing fiber input shapes reciprocity of Purkinje cell firing. *Neuron* **78**, 700-713 (2013).
36. Barski, J.J., Dethleffsen, K. & Meyer, M. Cre recombinase expression in cerebellar Purkinje cells. *Genesis* **28**, 93-98 (2000).
37. Madisen, L.*, et al.* A toolbox of Cre-dependent optogenetic transgenic mice for light-induced activation and silencing. *Nat Neurosci* **15**, 793-802 (2012).
38. Stahl, J.S., van Alphen, A.M. & De Zeeuw, C.I. A comparison of video and magnetic search coil recordings of mouse eye movements. *J Neurosci Methods* **99**, 101-110 (2000).
39. Quiroga, R.Q., Nadasdy, Z. & Ben-Shaul, Y. Unsupervised spike detection and sorting with wavelets and superparamagnetic clustering. *Neural Comput* **16**, 1661-1687 (2004).
40. Winkelman, B.H.*, et al.* Nonvisual complex spike signals in the rabbit cerebellar flocculus. *J Neurosci* **34**, 3218-3230 (2014).
41. Nagao, S. Effects of vestibulocerebellar lesions upon dynamic characteristics and adaptation of vestibulo-ocular and optokinetic responses in pigmented rabbits. *Exp Brain Res* **53**, 36-46 (1983).
42. Gutierrez-Castellanos, N.*, et al.* Impact of aging on long-term ocular reflex adaptation. *Neurobiol Aging* **34**, 2784-2792 (2013).
43. Kassardjian, C.D.*, et al.* The site of a motor memory shifts with consolidation. *J Neurosci* **25**, 7979-7985 (2005).
44. Shutoh, F.*, et al.* Memory trace of motor learning shifts transsynaptically from cerebellar cortex to nuclei for consolidation. *Neuroscience* **139**, 767-777 (2006).
45. Raymond, J.L. & Lisberger, S.G. Neural learning rules for the vestibulo-ocular reflex. *J Neurosci* **18**, 9112-9129 (1998).
46. Boyden, E.S., Katoh, A. & Raymond, J.L. Cerebellum-dependent learning: the role of multiple plasticity mechanisms. *Annu Rev Neurosci* **27**, 581-609 (2004).
47. Broussard, D.M., Titley, H.K., Antflick, J. & Hampson, D.R. Motor learning in the VOR: the cerebellar component. *Exp Brain Res* **210**, 451-463 (2011).
48. Wylie, D.R., De Zeeuw, C.I., DiGiorgi, P.L. & Simpson, J.I. Projections of individual Purkinje cells of identified zones in the ventral nodulus to the vestibular and cerebellar nuclei in the rabbit. *J Comp Neurol* **349**, 448-463 (1994).
49. Kistler, W.M.*, et al.* Analysis of Cx36 knockout does not support tenet that olivary gap junctions are required for complex spike synchronization and normal motor performance. *Ann N Y Acad Sci* **978**, 391-404 (2002).
50. Miyashita, Y. & Nagao, S. Contribution of cerebellar intracortical inhibition to Purkinje cell response during vestibulo-ocular reflex of alert rabbits. *J Physiol* **351**, 251-262 (1984).
51. Seja, P.*, et al.* Raising cytosolic Cl- in cerebellar granule cells affects their excitability and vestibulo-ocular learning. *EMBO J* **31**, 1217-1230 (2012).
52. Barmack, N.H. & Yakhnitsa, V. Modulated discharge of Purkinje and stellate cells persists after unilateral loss of vestibular primary afferent mossy fibers in mice. *J Neurophysiol* **110**, 2257-2274 (2013).
53. Gittis, A.H. & du Lac, S. Intrinsic and synaptic plasticity in the vestibular system. *Curr Opin Neurobiol* **16**, 385-390 (2006).

54. McElvain, L.E., Bagnall, M.W., Sakatos, A. & du Lac, S. Bidirectional plasticity gated by hyperpolarization controls the gain of postsynaptic firing responses at central vestibular nerve synapses. *Neuron* **68**, 763-775 (2010).
55. Jamali, M., Chacron, M.J. & Cullen, K.E. Self-motion evokes precise spike timing in the primate vestibular system. *Nat Commun* **7**, 13229 (2016).
56. Pugh, J.R. & Raman, I.M. Potentiation of mossy fiber EPSCs in the cerebellar nuclei by NMDA receptor activation followed by postinhibitory rebound current. *Neuron* **51**, 113-123 (2006).
57. De Zeeuw, C.I., *et al.* Spatiotemporal firing patterns in the cerebellum. *Nat Rev Neurosci* **12**, 327-344 (2011).
58. Lisberger, S.G., Miles, F.A. & Optican, L.M. Frequency-selective adaptation: evidence for channels in the vestibulo-ocular reflex? *J Neurosci* **3**, 1234-1244 (1983).
59. Kimpo, R.R., *et al.* Distinct patterns of stimulus generalization of increases and decreases in VOR gain. *J Neurophysiol* **94**, 3092-3100 (2005).
60. Clopath, C., Badura, A., De Zeeuw, C.I. & Brunel, N. A cerebellar learning model of vestibulo-ocular reflex adaptation in wild-type and mutant mice. *J Neurosci* **34**, 7203-7215 (2014).
61. Blazquez, P.M., *et al.* Cerebellar signatures of vestibulo-ocular reflex motor learning. *J Neurosci* **23**, 9742-9751 (2003).
62. Lisberger, S.G. Neural basis for motor learning in the vestibuloocular reflex of primates. III. Computational and behavioral analysis of the sites of learning. *J Neurophysiol* **72**, 974-998 (1994).
63. Feierstein, C.E., Portugues, R. & Orger, M.B. Seeing the whole picture: A comprehensive imaging approach to functional mapping of circuits in behaving zebrafish. *Neuroscience* **296**, 26-38 (2015).
64. Akao, T., *et al.* Directional asymmetry in vertical smooth-pursuit and cancellation of the vertical vestibulo-ocular reflex in juvenile monkeys. *Exp Brain Res* **182**, 469-478 (2007).
65. Bonnet, C., *et al.* Horizontal and vertical eye movement metrics: what is important? *Clin Neurophysiol* **124**, 2216-2229 (2013).
66. Ke, S.R., Lam, J., Pai, D.K. & Spering, M. Directional asymmetries in human smooth pursuit eye movements. *Invest Ophthalmol Vis Sci* **54**, 4409-4421 (2013).
67. Hirata, Y. & Highstein, S.M. Plasticity of the vertical VOR: a system identification approach to localizing the adaptive sites. *Ann N Y Acad Sci* **978**, 480-495 (2002).
68. Fujita, H., *et al.* Detailed expression pattern of aldolase C (Aldoc) in the cerebellum, retina and other areas of the CNS studied in Aldoc-Venus knock-in mice. *PLoS One* **9**, e86679 (2014).
69. Zhou, H., *et al.* Cerebellar modules operate at different frequencies. *Elife* **3**, e02536 (2014).
70. Wang, X., Chen, G., Gao, W. & Ebner, T.J. Parasagittally aligned, mGluR1-dependent patches are evoked at long latencies by parallel fiber stimulation in the mouse cerebellar cortex in vivo. *J Neurophysiol* **105**, 1732-1746 (2011).
71. Mostofi, A., *et al.* Electrophysiological localization of eyeblink-related microzones in rabbit cerebellar cortex. *J Neurosci* **30**, 8920-8934 (2010).
72. Wadiche, J.I. & Jahr, C.E. Patterned expression of Purkinje cell glutamate transporters controls synaptic plasticity. *Nat Neurosci* **8**, 1329-1334 (2005).
73. ten Brinke, M.M., *et al.* Evolving Models of Pavlovian Conditioning: Cerebellar Cortical Dynamics in Awake Behaving Mice. *Cell Rep* **13**, 1977-1988 (2015).
74. Jirenhed, D.A., Bengtsson, F. & Hesslow, G. Acquisition, extinction, and reacquisition of a cerebellar cortical memory trace. *J Neurosci* **27**, 2493-2502 (2007).
75. Wetmore, D.Z., *et al.* Bidirectional plasticity of Purkinje cells matches temporal features of learning. *J Neurosci* **34**, 1731-1737 (2014).
76. De Zeeuw, C.I. & Ten Brinke, M.M. Motor Learning and the Cerebellum. *Cold Spring Harb Perspect Biol* **7**, a021683 (2015).

Chapter 7

Dysfunctional cerebellar Purkinje cells contribute to autism-like behaviour in Shank2-deficient mice

Saša Peter[1,2,7,*], Michiel M. ten Brinke[2,7], Jeffrey Stedehouder[3], Claudia M. Reinelt[4], Bin Wu[2], Haibo Zhou[2], Kuikui Zhou[2], Henk-Jan Boele[2], Steven A. Kushner[3], Min Goo Lee[5], Michael J. Schmeisser[4,6], Tobias M. Boeckers[4], Martijn Schonewille[2], Freek E. Hoebeek[2] and Chris I. De Zeeuw[1,2,*]

[1] Netherlands Institute for Neuroscience, Amsterdam, Netherlands
[2] Department of Neuroscience, Erasmus MC, Rotterdam, Netherlands
[3] Department of Psychiatry, Erasmus MC, Rotterdam, Netherlands
[4] Institute for Anatomy and Cell Biology, Germany
[5] Yonsei University College of Medicine, Korea
[6] Department of Neurology, Ulm, Germany
[7] Co-first authors
[*] Correspondence

Published on Nature communications (2016)

ABSTRACT

Loss-of-function mutations in the gene encoding the postsynaptic scaffolding protein *SHANK2* are a highly penetrant cause of autism spectrum disorders (ASD) including cerebellum-related motor problems. Recent studies have implicated cerebellar pathology in etiology of ASD. Here, we evaluate the possibility that cerebellar Purkinje cells represent a critical locus of ASD pathophysiology in *Shank2*-related ASD. Absence of *Shank2* impairs both Purkinje cell intrinsic plasticity and induction of long-term potentiation at the parallel fiber to Purkinje cell synapse. Moreover, inhibitory input onto Purkinje cells is significantly enhanced, most prominently in the posterior lobe where simple spike regularity is most affected. Using Purkinje cell-specific *Shank2*-knockouts, we replicate alterations of simple spike regularity *in vivo* and establish cerebellar-dependence of ASD-like behavioural phenotypes in motor learning and social interaction. These data highlight the importance of *Shank2* for Purkinje cell function, and support a model by which cerebellar pathology is prominent in certain forms of ASD.

INTRODUCTION

Autism spectrum disorders (ASD) are neurodevelopmental disease entities primarily defined by deficits in social interaction and repetitive behaviour [1]. In addition, individuals with autism often suffer from motor skill deficiencies [2], many of which manifest early in the disease [3]. The aetiology of ASD is complex with reported pathophysiological alterations encompassing multiple brain regions, including the cerebellum [1]. Cerebellum-related motor symptoms of ASD patients have been observed by impairments in eyeblink conditioning [4,5], eye movement abnormalities [6,7], general motor learning deficits [8,9] as well as balance and postural difficulties [10,11]. Patients with cerebellar lesions emerging later in development are often diagnosed with cerebellar cognitive affective syndrome, a condition characterized by deficits in language, executive function and impaired emotions which overlaps considerably with symptoms in ASD [12]. Anatomical evidence for cerebellar involvement in ASD includes a decrease in the number of Purkinje cells (PCs) by post-mortem brain histopathological examination [13,14] and functional connectivity between the cerebellum, and frontoparietal and sensorimotor regions in resting-state fMRI studies of ASD [15]. Moreover, the cerebellum is among the most prominent brain regions demonstrating high co-expression of ASD-associated genes [16].

Emerging data indicate that neurodevelopmental disorders including ASD result from dysfunctional synaptic networks [17,18]. The postsynaptic density (PSD) in particular represents a critically important proteomic hub for a considerable proportion of neurodevelopmental disease-causing mutations, including ASD [19]. A prominent example is the Shank family of postsynaptic scaffolding proteins, which has gained wide attention because of their strong link to ASD [20-24]. To date, two studies have independently reported generating *Shank2* knockout (KO) mice with ASD-like behaviour and abnormal hippocampal processing [25,26]. However, in addition to the forebrain, *Shank2* is also highly expressed in cerebellar PCs [27,28]. Moreover, patients with *Shank2*-related ASD exhibit motor impairments consistent with cerebellar dysfunction [29]. However, the causal influence of cerebellar dysfunction on *Shank2*-related ASD has never been established.

We therefore used both global germ-line *Shank2* knock-out (KO; *Shank2*$^{-/-}$) and PC-specific *Shank2* KO (*L7-Shank2*$^{-/-}$) mouse models to investigate the causal influence of *Shank2* on cerebellar function and ASD-related behaviours. Notably, *Shank2*$^{-/-}$ mice have impairments in plasticity at the parallel fiber (PF) to PC synapse, increased inhibitory input onto PCs, and significant irregularities in PC simple spike activity. Moreover, *L7-Shank2*$^{-/-}$ mice show deficits in social interaction and exhibit task-specific repetitive behaviour. Together, these results provide novel insight into the pathophysiological mechanisms by which *Shank2* mutations cause impairments in cerebellar function that may contribute to ASD.

RESULTS

Reduction of functional cerebellar AMPAR in Shank2$^{-/-}$ mice

A divergent role of the *Shank2* scaffolding protein has been hypothesized for PSD function and cellular morphology [30]. To evaluate the morphology of *Shank2*-deficient postsynaptic specializations along PC dendrites, we quantified the structural characteristics of dendritic spines and PSDs in the distal molecular layer of global *Shank2*$^{-/-}$ mice using Golgi-Cox staining of PC dendrites and electron microscopy (Fig. 1). Neither spine density (WT: 1.93±0.74 spines/µm dendrite; *Shank2*$^{-/-}$: 1.82±0.67 spines/µm dendrite; P=0.2, Mann-Whitney U-test (MWU-test), nor the length (WT: 1.34±0.77 µm; *Shank2*$^{-/-}$: 1.32±0.50 µm; P=0.4, MWU-test) or width of individual spines (WT: 0.72±0.45 µm; *Shank2*$^{-/-}$: 0.71±0.32 µm; P=0.9, MWU-test) was significantly affected (Fig. 1a). In addition, the length (WT: 313.3±97.1 nm; *Shank2*$^{-/-}$: 305.3±96.2 nm; P=0.3) and thickness of PSDs (WT: 26.2±6.0 nm; *Shank2*$^{-/-}$: 26.0±5.3 nm; P=0.9) were similar between genotypes (Fig. 1b,c). In contrast, biochemical analysis of cerebellar synaptosomes indicated that global *Shank2*$^{-/-}$ mice have lowered expression of AMPA receptor subunits GluA1 (WT: 1.00±0.37; *Shank2*$^{-/-}$: 0.63±0.23; P=0.041) (Fig. 1d) and GluA2 (WT: 1.00±0.32; *Shank2*$^{-/-}$: 0.58±0.11; P=0.014). In addition, we looked into the ASD pathology related cell adhesion molecule neuroligin 3 (Nlgn3), which has been shown to interact with Shank proteins [19], but found no significant difference in its expression (WT: 1.00±0.37; *Shank2*$^{-/-}$ 0.84±0.33; P=0.4). Together, these findings indicate that *Shank2* is not crucial for the morphological differentiation of PC dendritic spines and PSDs, but instead may play an important role in the maintenance of cerebellar GluA1 and GluA2 levels.

Normal baseline excitability in Shank2$^{-/-}$ Purkinje cells

Considering that we found a reduction of cerebellar AMPA receptor expression in global *Shank2*$^{-/-}$ mice, we next examined neurotransmission at the PF-PC synapse using *ex vivo* whole-cell recordings (at 21±1°C) (**Fig. 2a**). PF-PC EPSCs, which were obtained in WT and *Shank2*$^{-/-}$ under comparable conditions (holding current: WT: -389±102 pA; *Shank2*$^{-/-}$ -388±114 pA, P=1; PC input resistance: WT: 67.2±16.8 MΩ; *Shank2*$^{-/-}$: 69.1±12.4 MΩ; P=0.8; **Fig. 2b,c**), revealed no significant differences in rise time (WT: 2.1±0.7 ms; *Shank2*$^{-/-}$: 1.7±0.6 ms; P=0.2) or decay time (WT: 9.7±0.8 ms; *Shank2*$^{-/-}$: 9.3±0.3 ms; P=0.3) (**Fig. 2d,e**). Moreover, evoking PF-EPSCs using stimulation currents varying from 3 to 15 µA resulted in similar event amplitudes (P=0.9, repeated-measures ANOVA) (**Fig. 2f,g**) and applying inter-stimulus intervals varying from 50 to 200 ms evoked comparable levels of paired-pulse facilitation (P=0.2, repeated-measures ANOVA) (**Fig. 2h**), indicating that baseline PF-PC synaptic transmission is unaltered by the lack of *Shank2*. Next, we evaluated whether the loss of *Shank2* affected neurotransmission at the climbing fiber (CF) to PC synapse. CF stimulation induced PC complex spikes in WT and *Shank2*$^{-/-}$. These

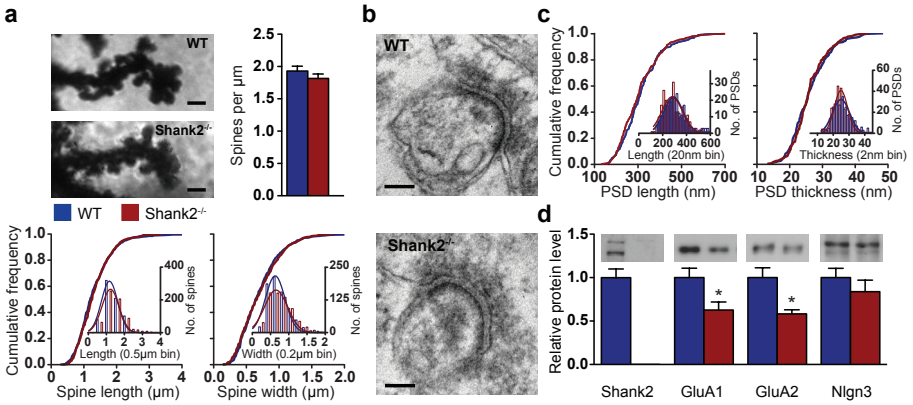

Figure 1. Reduction of AMPA receptor subunits in Shank2$^{-/-}$ cerebellar synaptosomes, but no changes in spine and PSD morphology in the distal molecular layer (DML). (a) Representative images (Golgi-Cox staining) of distal Purkinje cell dendrites in the DML, quantification of spine density (WT, n=97/4, dendrites/mice; Shank2$^{-/-}$, n=89/4, P=0.2, MWU-test) and cumulative frequency plots of spine length (P=0.4, MWU-test) and thickness (P=1, MWU-test) in WT (n=748/4 spines/mice) and Shank2$^{-/-}$ mice (n=639/4) as indicated. Scale bar: 1 µm. (b,c) Representative images (electron microscopy) of spine synapses in the DML and cumulative frequency plots of PSD length (WT, n=226/4, PSDs/mice; Shank2$^{-/-}$, n=243/4, P=0.3) and thickness (WT, n=223/4; Shank2$^{-/-}$, n=233/4, P=0.9) as indicated. Scale bar: 100 nm. (d) Biochemical analysis of Shank2 (WT, n=12 synaptosomes; Shank2$^{-/-}$, n=6), GluA1 (WT, n=12 synaptosomes; Shank2$^{-/-}$, n=6, P=0.041) GluA2 (WT, n=11; Shank2$^{-/-}$, n=5, P=0.014), and Nlgn3 (WT, n=12; Shank2$^{-/-}$, n=6, P=0.4) in cerebellar synaptosomes from WT and Shank2$^{-/-}$ mice as indicated. Data in bar graphs are presented as mean ± SEM; single asterisks indicates $p < 0.05$. Two-sided t-tests were used, unless stated otherwise.

waveforms showed no significant differences in the amplitude of the initial Na^+-spike (WT: 51.8±6.4 mV; *Shank2*$^{-/-}$: 48.5±5.9 mV, P=0.3) and in the number of subsequent Ca^{2+}-spikelets (WT: 1.6±0.5; *Shank2*$^{-/-}$: 2.0±0.7; P=0.2) or the amplitude of Ca^{2+}-spikelets (WT: 31.8±11.9 mV; *Shank2*$^{-/-}$: 33.9±6.4 mV, P=0.7). Moreover, at P9-10 virtually all PCs of both WT and *Shank2*$^{-/-}$ were innervated by multiple CFs, while at P25-35 all converted into mono-innervation (number of CF responses P9-10: WT: 2.0±0.5; *Shank2*$^{-/-}$: 2.3±0.5; P=0.2; P25-35: WT: 1.0±0.0; *Shank2*$^{-/-}$: 1.0±0.0; P=1, MWU-test) . Finally, the characteristic paired-pulse depression of CF-PC synaptic transmission showed no differences throughout the tested developmental stages (P9-10: WT: 0.59±0.14; *Shank2*$^{-/-}$: 0.54±0.11; P=0.5; P25-35: WT: 0.75±0.11; *Shank2*$^{-/-}$: 0.77±0.1; P=0.6), together indicating that the CF to PC input in *Shank2*$^{-/-}$ mice is not only normal in its baseline characteristics but also with respect to developmental elimination [31].

To examine PC kinetics, we evoked action potentials (APs) using depolarizing current steps at near-physiological temperature (33±1°C) (**Fig. 2i**). Evoked APs showed comparable thresholds (WT: -51.4±3.9 mV; *Shank2*$^{-/-}$: -51.0±3.5 mV; P=0.8), amplitudes (WT: 39.8±5.8 mV; *Shank2*$^{-/-}$: 35.9±5.8 mV; P=0.1) and half-widths (WT: 0.29±0.02 ms; *Shank2*$^{-/-}$:

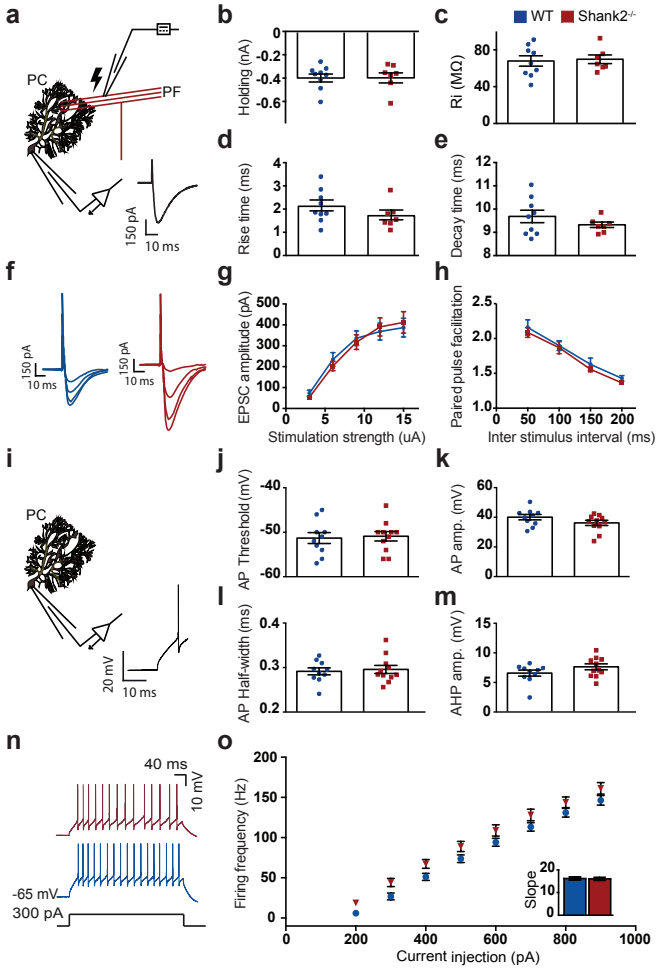

Figure 2. No changes in excited synaptic and intrinsic properties in Shank2$^{-/-}$ Purkinje cells ex vivo. (a) Recording configuration for voltage clamp recordings of PF-PC synaptic transmission. Inset: an example PF-EPSC. (b-e) With comparable holding current (at -65mV) (P=1) and input resistance (Ri) (P=0.8), PC EPSC rise time (P=0.2) and EPSC decay time (P=0.3) are not different between WT (n=9/6, cells/animals) and Shank2$^{-/-}$ (n=7/6). (f) Example EPSCs in response to 3, 6, 9, 12, and 15 uA stimulation. (g,h) Varying stimulation strength (P=0.9, repeated-measures ANOVA) and inter-stimulus interval (P=0.2, repeated-measures ANOVA) evoked comparable EPSC amplitude or facilitation (WT, n=11/3; Shank2$^{-/-}$ 15/3). (i) Recording configuration for whole cell recording. Inset: an example action potential. (j-m) Action potential threshold (P=0.8), amplitude (P=0.1), half-width (P=0.7), and afterhyperpolarization (P=0.2) were not different (WT, n=10/6; Shank2$^{-/-}$, n=11/6). (n) Example traces of intrinsic Purkinje cell excitability as apparent from action potential firing evoked by 300 pA current injections. (o) No difference in evoked firing frequency relative to various levels of current injections (WT, n=10/5; Shank2$^{-/-}$, n=11/5, P=0.1, repeated-measures ANOVA). Inset barplot shows average slope of firing rate per current step (P=1). Data are represented as mean ± SEM. Two-sided t-tests were used, unless stated otherwise.

0.30±0.03 ms; P=0.7), as well as after-hyperpolarization amplitudes (WT: 6.5±1.6 mV; *Shank2*$^{-/-}$: 7.5±1.7 mV; P=0.2) (**Fig. 2j-m**). In addition, PC intrinsic excitability was normal [32] in that current step injections of increasing amplitude resulted in a linear current-to-firing frequency relationship (P=0.1, repeated-measures ANOVA) (**Fig. 2n,o**) with a similar slope (WT: 16.2±2.2 Hz; *Shank2*$^{-/-}$: 16.1±2.3 Hz; P=1.0) (**Fig. 2o**). Together, these findings indicate that both the baseline transmission at PC excitatory synapses and PC intrinsic excitability remain intact in global *Shank2*$^{-/-}$ mice.

Increased sIPSCs and spiking irregularity in Shank2$^{-/-}$ PCs

To investigate inhibition of PCs in global *Shank2*$^{-/-}$ mice, we recorded spontaneous inhibitory postsynaptic currents (sIPSCs). Since PC activity can be related to the presence or absence of the glycolytic enzyme aldolase-c (referred to as zebrin) [33], we recorded from the predominantly zebrin-negative anterior lobules I-V as well as the predominantly zebrin-positive posterior lobule X of the cerebellar cortex (**Fig. 3a,b**). In both regions, we observed an increase in the frequency (lobules I-V: WT: 8.3±5.9 Hz; *Shank2*$^{-/-}$: 12.2±5.4 Hz; P=0.0295; lobule X: WT: 14.2±7.0 Hz; *Shank2*$^{-/-}$: 21.5±8.8 Hz; P=0.0079) (**Fig. 3c,e**), but not in the amplitude (for lobules I-V, WT: 53.2±24.4 pA; *Shank2*$^{-/-}$: 65.2±29.5 pA; P=0.1; for lobule X, WT: 58.9±19.0 pA; *Shank2*$^{-/-}$: 64.0±24.7 pA; P=0.5), of sIPSCs (**Fig. 3d,f**). Importantly, *Shank2*$^{-/-}$ sIPSC frequency was higher in lobule X than in the anterior lobe (P=0.0002). Given that inhibition decreases the firing frequency of PCs, but increases their irregularity [34,35], we hypothesized that the increased frequency of sIPSCs in *Shank2*$^{-/-}$ would translate into an overall decrease of *in vivo* simple spike (SS) activity but with an increased irregularity (**Fig. 3g,h**). The global *Shank2*$^{-/-}$ mice did indeed exhibit a decrease in firing frequency in lobules I-V (WT: 88.2±18.7 Hz; *Shank2*$^{-/-}$: 76.3±11.8 Hz; P=0.0096) (**Fig. 3i**), but notably not in lobule X (WT: 52.6±12.7 Hz; *Shank2*$^{-/-}$: 50.3±12.9 Hz; P=0.6) (**Fig. 3l**). Conversely, and consistent with the relative magnitude of the change in sIPSC frequency, the irregularity of PC SS firing was increased in lobule X (CV: WT, 0.30±0.08; *Shank2*$^{-/-}$, 0.38±0.09, P=0.0086; CV2: WT, 0.29±0.07; *Shank2*$^{-/-}$, 0.40±0.11, P=0.0003), but not in lobules I-V (CV: WT, 0.48±0.06; *Shank2*$^{-/-}$, 0.49±0.12, P=0.7; CV2: WT, 0.45±0.04; *Shank2*$^{-/-}$, 0.48±0.08, P=0.1) (**Fig. 3j-n**). The complex spike frequency and the pause in SS firing following each complex spike was similar between global *Shank2*$^{-/-}$ mice and their WT littermates in both the anterior (WT: frequency 1.28±0.29 Hz; pause 9.11±1.98 ms; *Shank2*$^{-/-}$: 1.32±0.24 Hz; 10±2.9 ms; P=0.7 and P=0.2, respectively) and posterior lobules (WT: frequency 0.67±0.19 Hz; pause 19.7±5.5 ms; *Shank2*$^{-/-}$: frequency 0.84±0.37 Hz; pause 17.61±5.29 ms; P=0.1 and P=0.2, respectively). Thus, in the absence of *Shank2*, the zebrin-positive lobule X selectively exhibits a highly irregular pattern of PC simple spike firing, which is consistent with a relative increase of inhibitory input onto lobule X PCs.

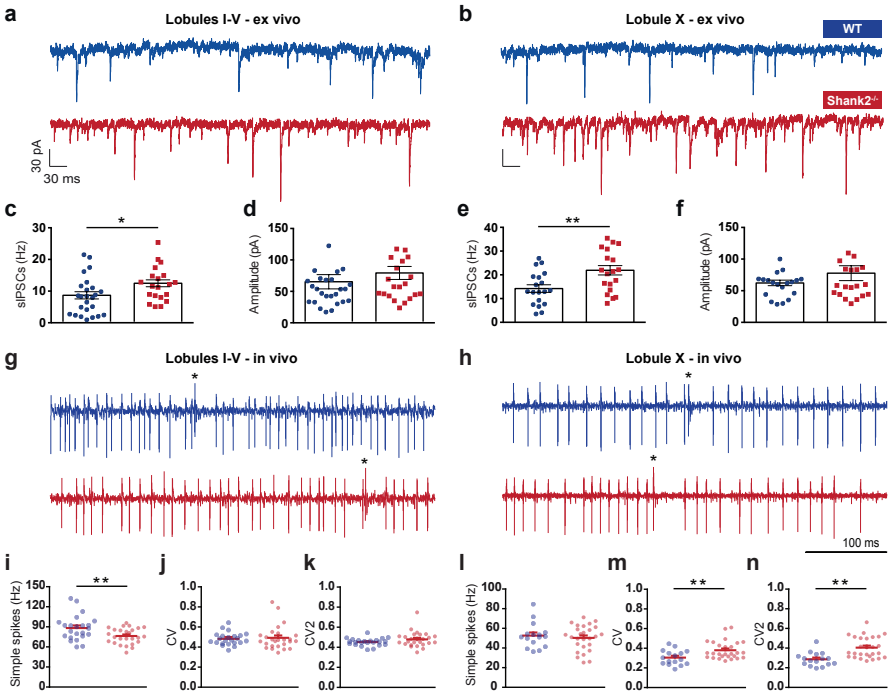

Figure 3. Increased spontaneous inhibitory events and higher simple spike irregularity in Shank2$^{-/-}$ Purkinje cells. (a, b) Example of spontaneous firing inhibitory post synaptic currents (sIPSCs) in lobules I-V and X. (c,e) A higher frequency of sIPSCs is found in both anterior (I-V) (P=0.0295) and posterior (X) lobules (P=0.0079) in Shank2$^{-/-}$ PCs (anterior: WT, n=25/3, cells/animals; Shank2$^{-/-}$, n=20/3; posterior: WT, n=19/3; Shank2$^{-/-}$, n=19/3). (d, f) There were no significant differences in sIPSC amplitudes anteriorly (P=0.1) or posteriorly (P=0.5). (g,h) Extracellular traces of PCs recorded in anterior (left) and posterior (right) lobules in the cerebellum, in WT and Shank2$^{-/-}$. Asterisks denote complex spikes. (i,j,k) Simple spike (SS) firing frequency was significantly lower (P=0.0096) in Shank2$^{-/-}$ (n=26/3) compared to wildtype (n = 23/3), whereas the coefficient of variation (CV) (P=0.7) and CV2 (P=0.1) did not differ. (l,m,n) In posterior lobule X, while SS firing frequency was similar (P=0.6), CV (P=0.0086) and CV2 (P=0.0003) were significantly higher in Shank2$^{-/-}$ (n=27/3) compared to WT (n = 16/3). Data are represented as mean ± SEM. Single and double asterisks indicate P<0.05 and P<0.01, respectively. Two-sided t-tests were used, unless stated otherwise.

Impaired synaptic and intrinsic plasticity in Shank2$^{-/-}$ PCs

Given that *Shank2* functions as a PSD scaffolding protein of postsynaptic receptors [17,30] for which we observed decreased expression of both GluA1 and GluA2 in cerebellar synaptosomes of *Shank2*$^{-/-}$ mice (**Fig. 1**), we reasoned that PC synaptic plasticity might also be affected [25,26]. Induction of long-term potentiation (LTP) (33±1˚C; 1 Hz, 5 min PF-tetanus) (**Fig. 4a**) reliably increased PF-EPSC amplitudes in WT PCs (121.1±19.8% at t=40 min; P=0.003, repeated-measures ANOVA), but not in those of global *Shank2*$^{-/-}$ mice (91.8±14.2% at t=40; P=0.3, repeated-measures ANOVA) (**Fig. 4b**). In contrast, both WT and global *Shank2*$^{-/-}$ mice exhibited robust long-term depression (LTD) of PF-EPSCs

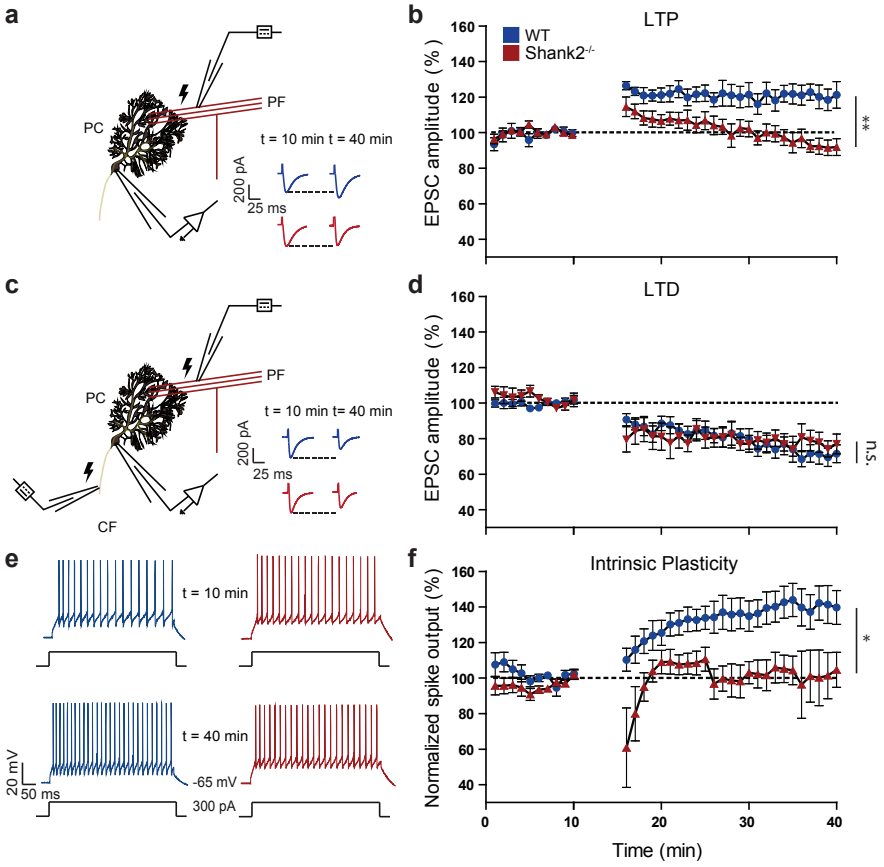

Figure 4. Impaired synaptic and intrinsic plasticity in Shank2$^{-/-}$ ex vivo. (a) Recording configuration for PF-LTP experiments. Inset: example of 5 averaged EPSCs for WT (blue) and Shank2$^{-/-}$ (red) before LTP induction (at 10 minutes) and after LTP induction (at 40 min). (b) LTP experiment with 5 min PF stimulation at 1Hz inducing LTP in WTs (n=7/6, cells/animals, P=0.0027) but not in Shank2$^{-/-}$ PCs (n=12/6, P=0.3), which is reflected in the difference between genotypes (P=0.0066). (c) Recording configuration for PF-LTD experiments. Inset: example traces as in a. (d) LTD is induced in both WT (n=9/6, P<0.0001) and Shank2$^{-/-}$ (n=7/6, P=0.0009) PCs, to a similar degree (P=1). (e) Example of traces for intrinsic plasticity with current injections of 300 pA. (f) LTP induction protocol induced enhanced spike output in WT PCs (n=5/4, P=0.0053), but not in Shank2$^{-/-}$ PCs (n=5/4, P=0.5), as reflected in their difference (P=0.0201). Data are represented as mean ± SEM. Single and double asterisks indicate P<0.05 and P<0.01, respectively. All tests were repeated-measures ANOVAs.

following co-activation (1 Hz) of PFs and CFs (WT: 71.4±14.9%; P<0.0001; *Shank2*$^{-/-}$: 76.9±14.6%; P=0.0009, repeated-measures ANOVA) (**Fig. 4c,d**). Since LTP has been reported to facilitate adaptation of intrinsic properties, driving spike activity [32], we next examined PC intrinsic plasticity before and after PF-LTP induction (**Fig. 4e**). Whereas WT mice readily demonstrated a potentiation of intrinsic excitability (139.7±21.3% at t=40 min; P=0.005, repeated-measures ANOVA), intrinsic plasticity was markedly impaired in

global *Shank2*$^{-/-}$ mice (104.6±22.2% at t=40 min; P=0.5, repeated-measures ANOVA) (**Fig. 4f**). These results suggest that *Shank2* is a critical modulator of both synaptic and intrinsic plasticity in Purkinje cells.

Expression of Shank2 in L7-Shank2$^{-/-}$ mice

To explore the behavioural impact of the lack of *Shank2* in PCs, we generated a PC-specific knockout of *Shank2 (*see methods section) using the floxed version of the *Shank2*$^{-/-}$ mutants [25] and the L7-vector [32]. Immunocytochemical analysis with the SA5193 rabbit primary *Shank2* antibody [25,36] confirmed that *Shank2*$^{-/-}$ was specifically deleted in PCs in the PC-specific *L7-Shank2*$^{-/-}$ mice, but not in WT littermates, whereas it was ubiquitously deleted in the global *Shank2*$^{-/-}$ (**Fig. 5**). Importantly, PC-specific deletion of *Shank2* had no discernible impact on cellular zebrin identity, or on the zonal patterns of zebrin staining across cerebellar modules.

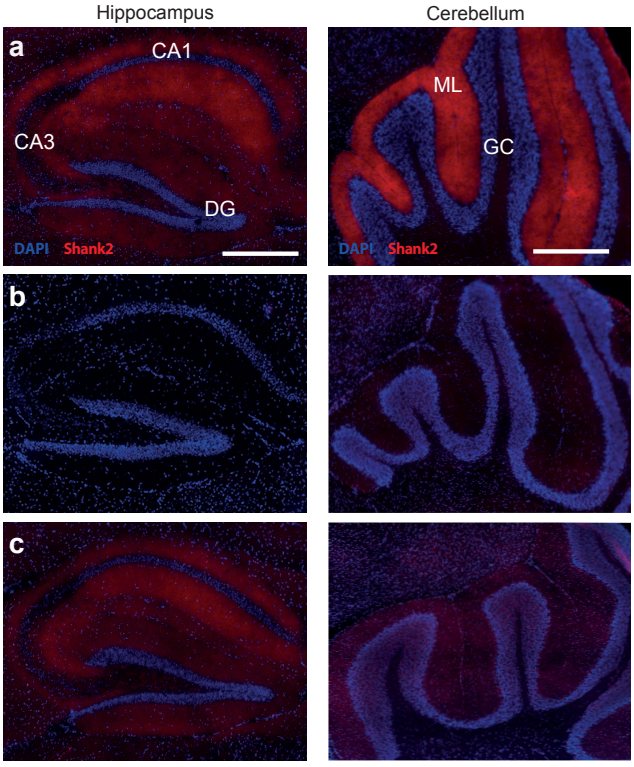

Figure 5. Immunohistological staining of the Shank2 protein in Shank2$^{-/-}$ and L7-Shank2$^{-/-}$ hippocampus and cerebellum. (a) Sagittal cryosection of hippocampal Shank2 (red) and nucleus staining (DAPI; blue) in a WT (left) L7-Shank2$^{-/-}$. Scale bar: 500 µm. Sagittal cryosection of cerebellar Shank2 staining (right). Scale bar: 200 µm. (b) Staining for Shank2 in the hippocampus and cerebellum of the global Shank2$^{-/-}$ shows absence of expression. (c) The L7-Shank2$^{-/-}$ shows expression in the hippocampus , but not in the molecular layer of the cerebellum.

Impaired motor learning in L7-Shank2$^{-/-}$ mice

Given the variety of electrophysiological aberrations in PCs in the global *Shank2*$^{-/-}$, we next examined motor behavior in the PC-specific *L7-Shank2*$^{-/-}$ mice. Unlike the hyperactivity exhibited by global *Shank2*$^{-/-}$ mice in an open field [25,26], mice with PC-specific deletion of *Shank2* exhibited no evidence of hyperactivity in the open field test compared to their WT littermates (velocity: WT: 12.28±2.79 cm/s; *L7-Shank2*$^{-/-}$: 13.24±2.61 cm/s ; P=0.3; distance moved: WT: 7.37±1.68 m; *L7-Shank2*$^{-/-}$: 7.94±1.57 m; P=0.3). The lack of hyperactivity was confirmed using the PhenoTyper Box (Noldus), in which free exploration was quantified over a 30 min-period in a homecage-like environment (velocity: WT: 6.7±1.1 cm/s; *L7-Shank2*$^{-/-}$: 6.3±1.3 cm/s; P=0.5, distance moved: WT: 384.6±68.8 cm; *L7-Shank2*$^{-/-}$: 371.7±79.7 cm; P=0.5, repeated-measures ANOVA). Moreover, during the ErasmusLadder test [37] motor performance was similar between genotypes, including the efficiency and timing of steps (2nd day efficiency, WT: 33.1±20.0%; *L7-Shank2*$^{-/-}$: 47.1±15.4 cm; P=0.3; 2nd day timing: WT: 359.2±84.2 ms; *L7-Shank2*$^{-/-}$: 330.7±49.4 ms; P=0.8, repeated-measures ANOVA) . Finally, the amplitude (gain) and timing (phase) of baseline optokinetic (OKR) (OKR gain, P=0.6, OKR phase, P=0.9, repeated-measure ANOVA) and vestibulo-ocular reflexes (VOR) (VOR gain, P=0.4, VOR phase, P=0.2, repeated-measure ANOVA) were also similar, further highlighting that motor performance is normal in *L7-Shank2*$^{-/-}$ mutants.

In contrast, motor learning was consistently affected in a variety of cerebellar motor learning tasks (**Fig. 6**). Using a conditioning task within the ErasmusLadder, in which mice were presented with a tone preceding the elevation of an obstructive rung at a 200 ms interval [37], *L7-Shank2*$^{-/-}$ mice were unable to successfully avoid the obstacle (*L7-Shank2*$^{-/-}$ versus WT: P=0.018, repeated-measures ANOVA) (**Fig. 6a,b**). Furthermore, *L7-Shank2*$^{-/-}$ mice failed to acquire the normal increase in VOR gain (*L7-Shank2*$^{-/-}$ versus WT: P=0.006, repeated-measures ANOVA) or shift in VOR phase (2nd day; P=0.047, 3rd P=0.0013, 4th P<0.0001, 5th P=0.0003, repeated-measures ANOVA) following visuovestibular mismatch training [38] (**Fig. 6c-f**). Finally, *L7-Shank2*$^{-/-}$ mice exhibited a significant impairment of Pavlovian eyeblink-conditioning [39] using a light pulse as the conditioning stimulus (CS) and a corneal air puff as the unconditioned stimulus at a 250 ms interval (conditioned response or CR rate: P=0.0013; CR amplitude: P=0.0009; repeated-measures ANOVA) (**Fig. 6g-i**). These findings indicate that *L7-Shank2*$^{-/-}$ mice have normal baseline motor performance, but prominent impairments in motor learning.

Irregular in vivo PC simple spikes in L7-Shank2$^{-/-}$ mice

To investigate whether the changes in electrophysiological properties observed in PCs of the global *Shank2*$^{-/-}$ mice may contribute to the behavioural phenotypes observed, we tested to what extent the changes in simple spike activity also occurred in the *L7-Shank2*$^{-/-}$ mice. We first recorded extracellular single units *in vivo* from the largely zebrin-negative lobules

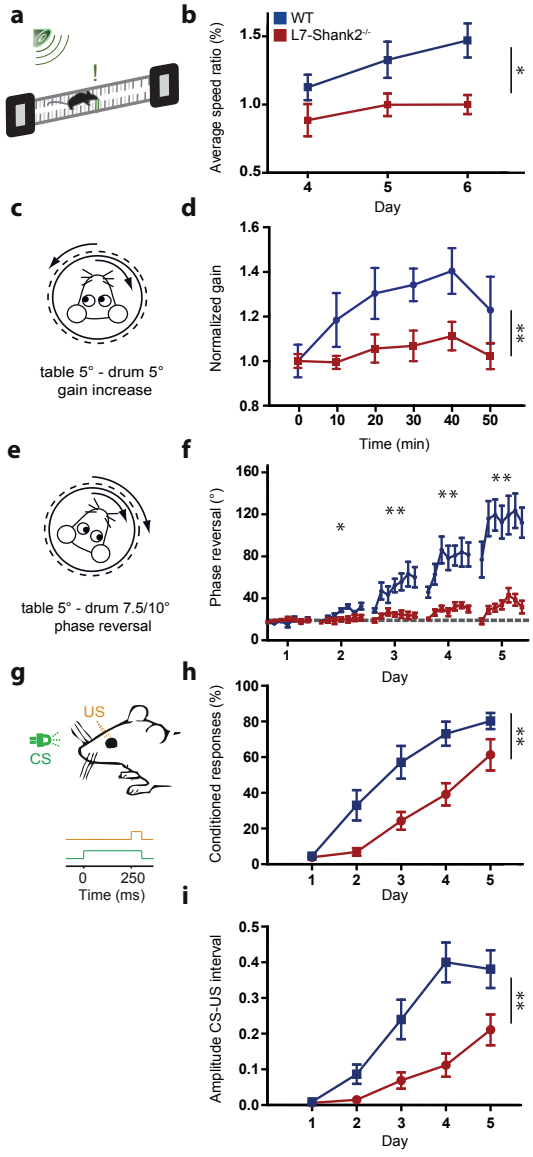

Figure 6. L7-Shank2$^{-/-}$ mice show impaired motor learning. (a, b) After three days of training, WT (n=9) but not L7-Shank2$^{-/-}$ mice (n=6) (P=0.018) learned to increase their speed during a conditioned ErasmusLadder test using tone-cued rung displacements. (c,d) In vestibulo-ocular reflex (VOR) gain increase training, L7-Shank2$^{-/-}$ mice (n=8) were not able to adapt their gain like WTs did (n=7) (P=0.006). (e,f) L7-Shank2$^{-/-}$ mutants (n=9) did not adapt their VOR phase following a reversal training paradigm, whereas WT (n=9) did (2nd day, P=0.047; 3rd, P=0.0013; 4th, P<0.0001; 5th, P=0.0003). (g,h,i) Impaired percentage (P=0.0013) and amplitude (P=0.0009) of conditioned responses (CRs) in L7-Shank2$^{-/-}$ mice (n=10) compared to WT (n=11) in an eyeblink conditioning paradigm (200 paired trials daily). Data are represented as mean ± SEM. Single and double asterisks indicate P<0.05 and P<0.01, respectively. All tests were repeated-measures ANOVAs.

I-V (**Fig. 7a-d**) and the predominantly zebrin-positive lobules IX-X (**Fig. 7e-h**). Importantly, the recordings in the *L7-Shank2*$^{-/-}$ mice fully reproduced the increases in CV (WT, 0.35±0.07; *L7-Shank2*$^{-/-}$, 0.49±0.09; P<0.0001) and CV2 (WT, 0.36±0.06; *L7-Shank2*$^{-/-}$, 0.47±0.06; P<0.0001) (Fig. 7**g,h**) that were found in the posterior lobules of the global *Shank2*$^{-/-}$ **(Fig. 3i-n)**, confirming the higher SS irregularity. In addition, the *L7-Shank2*$^{-/-}$ mice also showed signs of SS irregularity in the anterior lobules in that their CV2 was also significantly increased (WT, 0.43±0.04; *L7-Shank2*$^{-/-}$, 0.47±0.04; P=0.0092) (**Fig. 7c,d**). The

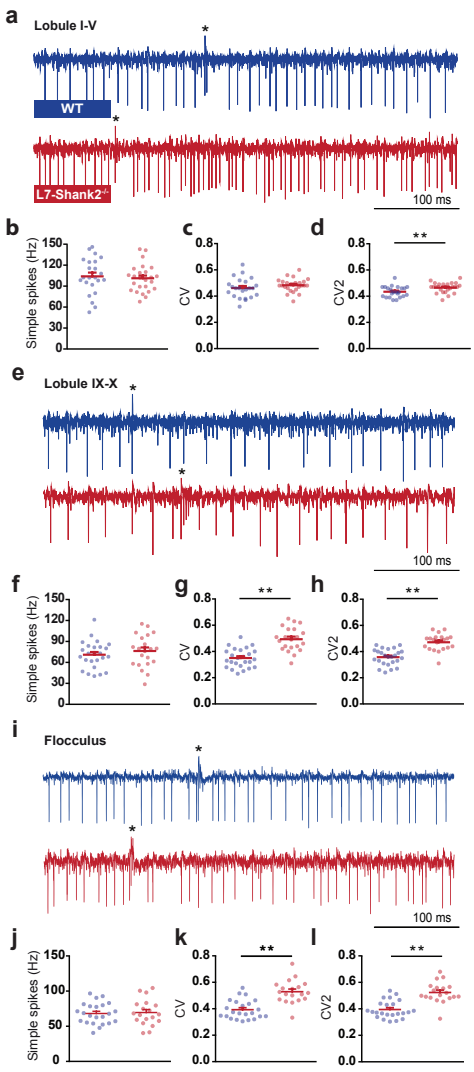

Figure 7. In vivo simple spike firing characteristics in L7-Shank2$^{-/-}$ Purkinje cells. (a) Extracellular PC traces recorded from anterior lobules (I-V) in WT (top) and L7-Shank2$^{-/-}$ (bottom) mice. (b,c,d) Firing characteristics in the anterior lobules reveal a difference in CV2 (P=0.0092) between L7-Shank2$^{-/-}$ (n=25/3, cells/animals) and WT (n=23/3). (e) Example PC traces from posterior lobules (IX-X). (f,g,h) PCs from the posterior cerebellum in L7-Shank2$^{-/-}$ (n=21/3) showed significantly higher CV (P<0.0001) and CV2 (P<0.0001) values compared to WT (n=25/3). (i) Example PC traces from posteriorly located flocculus, which is responsible for VOR learning. (j,k,l) Again, L7-Shank2$^{-/-}$ (n=19/2) shows significantly higher CV (P<0.0001) and CV2 (P<0.0001) values than WT (n=23/2). Double asterisks denote P<0.01. All tests were two-sided t-tests.

L7-Shank2$^{-/-}$ SS mice activity did not show higher firing frequencies in either the anterior (WT: 104.4±25.8 Hz; *L7-Shank2*$^{-/-}$: 101.2±19.7 Hz; P=0.6) or posterior (WT: 70.9±19.5 Hz; *L7-Shank2*$^{-/-}$: 76.3±23.4 Hz; P=0.4) lobules (**Fig. 7b,f**). Finally, we also recorded SS activity of PCs in the flocculus of the vestibulocerebellum, because they are known to directly control VOR adaptation [34] (**Fig. 7i-l**). In PCs that were identified to be related to VOR-adaptation by their response to motion around the vertical axis in space, we again found a significant increase in SS irregularity (CV: WT, 0.39±0.07; *L7-Shank2*$^{-/-}$, 0.53±0.08; P<0.0001; CV2: WT, 0.39±0.07; *L7-Shank2*$^{-/-}$, 0.52±0.08; P<0.0001), while their overall firing frequency was unaffected (WT: 68.2±15.0 Hz; *L7-Shank2*$^{-/-}$: 69.6±18.8 Hz; P=0.8)

(**Fig. 7j-l**). Moreover, *L7-Shank2*$^{-/-}$ showed a bigger difference with WT in SS irregularity in the posterior lobules (40.0% and 30.6% higher CV and CV2, respectively) compared to that in the anterior lobules (4.4% and 9.3% higher CV and CV2, respectively). No significant differences were observed in the duration of the complex spike-induced simple spike pause or the complex spike firing frequency in any of the recorded lobules (P>0.2 in all cases). Together, *L7-Shank2*$^{-/-}$ mice demonstrate the critical importance of *Shank2* in PCs for maintaining SS regularity.

Reduced cognitive functioning in L7-Shank2$^{-/-}$ mice

We next examined social and repetitive ASD-like behaviours in the PC-specific *L7-Shank2*$^{-/-}$ mice. The three-chamber social interaction task is a widely used social interaction paradigm for evaluating ASD-like behaviour in mouse models of autism [25,26]. WT mice exhibited a normal preference for the chamber in which the stranger mouse (S1) was present, compared to the empty chamber (P=0.0002, MWU-test) (**Fig. 8a**). In contrast, *L7-Shank2*$^{-/-}$ mice had no preference for either S1 or the empty chamber (P=0.7, MWU-test) (**Fig. 8b**). Comparing the preference index (stranger-empty) between WT and *L7-Shank2*$^{-/-}$ mice revealed a significantly decreased preference of *L7-Shank2*$^{-/-}$ mice for the stranger mouse (P=0.0213) (**Fig. 8c**), indicating their social interaction deficits. With the introduction of a second stranger in the previously empty chamber, WT mice again demonstrated an increased preference for the novel stranger (S2), this time compared to the familiar mouse (S1) (P=0.0001, MWU-test) (**Fig. 8d**), whereas *L7-Shank2*$^{-/-}$ mice showed no preference for either the familiar or the novel stranger mice (P=0.1, MWU-test) (**Fig. 8e**). Comparing the preference index (S2-S1) between WT and *L7-Shank2*$^{-/-}$ confirmed the impairment of social interaction in *L7-Shank2*$^{-/-}$ mice (P=0.0136) (**Fig. 8f**). Because of previously reported compulsive grooming [25] and jumping [26] in global *Shank2*$^{-/-}$ mice, we next examined repetitive behaviour. We observed no significant differences between WT and *L7-Shank2*$^{-/-}$ mice in the percentage of buried marbles in the marble-burying task (P=1.0) (**Fig. 8g**) or in the duration of grooming over a 15 min-period (P=0.054) (**Fig. 8h**). However, the *L7-Shank2*$^{-/-}$ mice did show an increase of repetitive behaviour in the T-maze through an increased perseveration, highlighting a reduction in cognitive flexibility (P=0.0023, MWU-test) (**Fig. 8i**). Finally, we observed no significant difference in anxiety (P=0.7, χ^2-test) or olfactory sensitivity (P=0.6) of *L7-Shank2*$^{-/-}$ mice that could have potentially biased the social behaviour assessments. Together, these results indicate that *L7-Shank2*$^{-/-}$ mice exhibit ASD-like social impairments and task-specific repetitive behaviour.

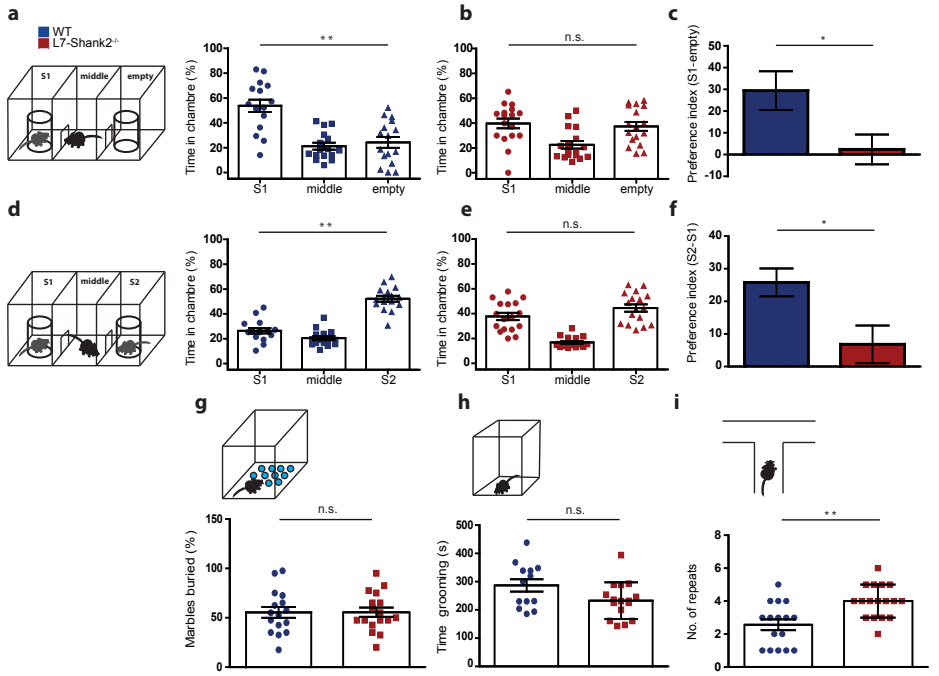

Figure 8. L7-Shank2$^{-/-}$ mice show social impairment and signs of task-specific repetitive behaviour. (a) Three-chamber social interaction evaluated by relative time spent in each chamber. WTs (n=16) prefer to spend time in the room with the stranger 1 mouse (S1), compared to the empty room (P=0.0002, MWU-test). (b) This was not the case for L7-Shank2$^{-/-}$ (n=17) mice (P=0.7, MWU-test). (c) The preference index (S1-empty) confirms the difference between genotypes (P=0.021). (d) Following the introduction of a second stranger (S2), WTs (n=16) prefer to spend time in the chamber with S2 compared to that with S1 (P=0.0001, MWU-test). (e) The L7-Shank2$^{-/-}$ mice (n=17) did not show a preference for newly introduced S2 (P=0.1, MWU-test). (f) The S1-S2 preference index indicates that WTs prefer S2 more than L7-Shank2$^{-/-}$ do (P=0.013). (g) No difference was found in a marble burying task indicative of anxious and/or repetitive behaviour (WT, n=16; L7-Shank2$^{-/-}$, n=17, P=1.0). (h) L7-Shank2$^{-/-}$ (n=16) seemed to trend towards less grooming than WTs (n=13) (P=0.054). (i) T-maze paradigm showed less consecutive alternations in L7-Shank2$^{-/-}$ (n=17) compared to WT (n=16) (P=0.0023, MWU-test) indicating repetitive decision-making. Data are presented as mean ± SEM. Single and double asterisks indicate P<0.05 and P<0.01, respectively. Two-sided t-tests were used, unless stated otherwise.

DISCUSSION

Severe loss-of-function mutations in *SHANK2* have been firmly established as conferring a high genetic risk for ASD and intellectual disability [20,22,29]. Children with disruptive *SHANK2* mutations exhibit motor impairments, language delay and cerebellar dysfunction including dysmetria and dysdiadochokinesis [29]. Considering the increasing evidence for cerebellar involvement in ASD [40], we investigated anatomical, molecular and physiological consequences of global *Shank2* ablation in the cerebellum. In addition, we analyzed

L7-Shank2$^{-/-}$ mice with cerebellar PC-specific deletion of *Shank2* to evaluate the extent to which the ASD-related behavioural findings in global *Shank2*$^{-/-}$ mice can be attributed to cerebellar dysfunction.

In recent years, several genetic mouse models for ASD have been used for the study of cerebellar abnormalities. The first study to implement a Purkinje cell-specific model related to ASD involved the deletion of FMR1, the fragile X mental retardation 1 protein [41]. In this study, the authors reported eye-blink abnormalities and increased LTD in both global and Purkinje cell-specific deletion of FMR1. Furthermore, global Nlgn3-KO mutants exhibited deficits in cerebellum-related motor performance as assessed by the ErasmusLadder [42]. A more recent model examining the 15q11-13 duplication ASD syndrome demonstrated impaired cerebellar synaptic plasticity and motor learning deficits as assessed by eye-blink conditioning [43]. Perhaps the most definitive study implicating cerebellar dysfunction as etiologic for ASD-like behaviour involved a Purkinje cell-specific deletion of *Tsc1* [44]. This study was the first to demonstrate that Purkinje cell-specific deletion of an ASD-associated gene results in ASD-like behaviour. Finally, a very recent study using multiple mouse models of syndromic ASD found a consistent pattern of impaired sensorimotor integration [45]. These studies have established the foundation by which the cerebellar synaptic pathophysiology underlying ASD can be mechanistically investigated [18].

Given the general importance of *Shank2* in the regulation of neuronal plasticity [25,26], we investigated both synaptic and intrinsic plasticity of cerebellar Purkinje cells **(Fig. 4)**. Our results indicate that *Shank2* is crucial for PF-PC LTP, but not LTD. Additionally, we show that *Shank2* is important for intrinsic plasticity of neuronal excitability [46]. In contrast to a recent study of the 15q11-13 duplication ASD syndrome in which PC synaptic plasticity deficits were limited to LTD [43], our results now highlight LTP impairments as a candidate mechanism underlying the cerebellar pathophysiology of ASD. *Shank2* is a dedicated scaffolding protein, which has a major role in the regulation of glutamate receptor integration, synaptic transmission and plasticity [17,47]. Future molecular and functional studies will have to elucidate the exact mechanisms by which *Shank2* mediates plasticity in the Purkinje cell, but it may well include a suboptimal integration of GluR subunits as the expression levels of GluA1 and GluA2 were both reduced in the *Shank2*$^{-/-}$ mice. Since GluR subunit levels were analysed in synaptosomes from whole cerebella, it remains to be further investigated to what extent these changes are limited to the PF to PC synapse.

Because of the cerebellar physiological impairments and the previously reported motor hyperactivity in *Shank2*$^{-/-}$ mice [25,26], we examined activity levels during both baseline exploration and motor learning. To our surprise we did not find motor performance abnormalities in the PC-specific *L7-Shank2*$^{-/-}$ mice during various assessments including five separate

locomotion and eye movement tests. However, we did observe substantial impairments of cerebellar motor learning including conditioning of locomotion and eyeblink responses as well as adaptation of compensatory eye movements (**Fig. 6**). It might seem counterintuitive that baseline motor performance can be intact while the capacity for motor learning is reduced, but this combination has been observed in many different mutant lines over the last few decades [48]. Most likely, it reflects the indispensable role of PC plasticity for the acquisition of new behaviours within relatively short periods of time as occurs during the experimental training paradigms (i.e. in the order of hours) and the ability of the motor performance control system to compensate upstream and/or downstream of the affected synapse when prolonged adaptation periods are available as occurs during postnatal development (i.e. in the order of weeks) [49]. The potential causality of the identified electrophysiological abnormalities as underlying the motor learning impairments is strengthened by our independent findings in another Purkinje cell-specific mouse mutant (L7-PP2B$^{-/-}$), in which also both synaptic LTP and intrinsic plasticity were affected [32]. Together, these phenotypes point towards a PC-dependent contribution to the behavioural motor impairments frequently observed in ASD.

In addition to changes in plasticity, we also found that inhibition of PCs was enhanced in the global *Shank2*$^{-/-}$ mutants. Since reduced inhibition of PCs increases regularity of SS activity [34], we hypothesized that PCs of the global *Shank2*$^{-/-}$ mutants should have a higher level of irregularity of SS firing **(Fig. 3)**. Indeed, this hypothesis was not only consistent with the *in vivo* extracellular recordings in lobule X of the global *Shank2*$^{-/-}$, but also confirmed in three different areas (Lobules I-V, Lobules IX-X and the flocculus) of the *L7-Shank2*$^{-/-}$ mice (**Fig. 7**). Moreover, this correlation was also in line with the fact that the differences in sIPSCs, CV and CV2 had bigger effect sizes in the posterior lobules than the anterior lobules.

The increased frequency of inhibition in the global *Shank2*$^{-/-}$ did not occur concomitantly with increased amplitude of sIPSCs postsynaptically at PCs, indicating that the observed effect could be of pre-synaptic origin. The PC irregularity in the *L7-Shank2*$^{-/-}$ would then have to originate from a pre-synaptic effect of the postsynaptic absence of *Shank2*. Indeed, recent evidence indicates the possibility of Shank-mediated transsynaptic signalling through transmembrane proteins affecting both post and pre-synaptic processes important for vesicle release probability [50]. This type of transsynaptic signalling could manipulate the inhibitory input to PCs either directly or indirectly, e.g. through altered glutamate spillover from the climbing fiber to Purkinje cell synapse [51]. Future research aimed at pinpointing the sites relevant to the effects described above should thus focus not only on Purkinje cell specific mouse mutants, but also on those in which their afferents are specifically affected [52,53]. In doing so, important consideration in studies implementing cell-specific deletions should be given to germline analyses, given the sensitivity of the *L7*-cre [44,54] and *Shank2* lines [55,56].

We observed a significant decrease in SS frequency in the anterior lobules of global *Shank2*$^{-/-}$ mice, but not in their posterior lobules, nor in the anterior or posterior lobules of *L7-Shank2*$^{-/-}$ mice. We believe that this inconsistency may reflect the fact that the spontaneous SS firing frequency of PCs is probably largely due to their intrinsic properties rather than the synaptic efficacy of their inhibitory or excitatory inputs [33]. Indeed, blocking inhibitory or excitatory synaptic input to PCs by deleting their GABA-A-gamma2 receptor-subunits or abolishing voltage gated calcium channels at their parallel fiber input primarily affects the regularity of SS firing, rather than their firing frequency [34,53]. Thus, the consistent irregularity of SS in PCs, particularly in the posterior lobe, of the *Shank2*$^{-/-}$ mutants underlines the putative importance of precise SS regularity for behavioural output [48]. Although abnormalities in the anterior and posterior lobules have both been proposed as relevant sites of cerebellar pathology in ASD [57], our converging data obtained in the posterior lobe suggest that the mechanisms governing the regularity of SS firing reveal a common biological vulnerability in the etiology of ASD.

Here, we report impaired social and task specific repetitive behaviour due to the Purkinje cell-specific deletion of *Shank2* (**Fig. 8**). This result is particularly interesting as, to our knowledge, it is the first Purkinje cell-specific mouse model for a non-syndromic form of autism in which ASD-like behaviour has been established. The impaired social behaviour, late-onset ataxia and reduced excitability of Purkinje cells previously observed in L7-Tsc1 mice [44] were due to the absence of a protein that inhibits mTOR signalling through which the translation of a wide variety of proteins is regulated. In contrast, we here show that disruption of the synapse through the absence of a single postsynaptic scaffolding protein in the Purkinje cell is sufficient to show impaired ASD-related motor learning and social behavioural impairments. In addition to the social impairments, we found signs of enhanced repetitive behaviour in the T-maze paradigm, but not the marble burying task or grooming tasks. Since the T-maze task reveals the level of cognitive inflexibility following decision making over consecutive trials rather than the level of repetitious behaviour dominated by high-frequency motor activity that characterizes the other two tasks and that may well be confounded by deficits in cerebellar motor learning, these results highlight the importance of the Purkinje cell synaptic function for ASD beyond the classically ascribed motor-related behaviour.

One of the main challenges remaining is to mechanistically explain the contribution of impaired Purkinje cell physiology to the observed ASD behavioural phenotypes. As previously mentioned, the Shank family of postsynaptic scaffolding proteins has many different interacting proteins in the postsynaptic density through which they could contribute to the functional establishment of regulatory mechanisms for plasticity. The translational challenge from synapse to behaviour brings about two main questions: How does an impaired

Purkinje cell mediate ASD-related behaviour? And how might Purkinje cell impairments lead to abnormal brain function beyond the cerebellum with regards to neurodevelopmental critical periods? The first question has been extensively addressed by the accumulating evidence regarding the contribution of ASD-related cerebellar dysfunction to impaired motor learning, as apparent from the eye movement adaptation, ErasmusLadder, and eyeblink conditioning findings examined here and by other investigators [45]. It is indeed possible that the increased inhibition and irregularity of SS firing, in addition to impaired cerebellar plasticity mechanisms, may contribute to social and repetitive behaviour-related phenotypes in ASD. We believe that the answer to how the cerebellum can essentially contribute to socially impaired behaviour could reside in various mechanisms. The idea that disruption of a certain brain area during development could affect the development and consequently the function of other inter-connected areas, also termed developmental diaschisis, has recently been put forward as a prime mechanism for the cerebellum in its ability to influence other cortical areas in critical developmental periods [58]. In the future, the latter hypothesis can for example be tested with Purkinje cell specific *Shank2* ablation at different stages during development using inducible mouse models, as has recently been employed for other ASD-related genes [24,59]. These experiments will help to further elucidate the mechanisms by which differential genes, such as *Shank2*, regulate cerebellar function and ultimately ASD-like behaviour.

METHODS

Experiments and analyses were performed with the experimenters blinded to the genotype. Mice used were global germ-line *Shank2*$^{-/-}$ and their littermate WTs all bred on a mixed C57BL6/N and C57BL6/J background. The generation of these mice has previously been described in detail [25,26]. The *L7-Shank2*$^{-/-}$ was generated by crossing Purkinje specific L7(Pcp2)-Cre [54] with *Shank2*$^{flxd/flxd}$ [25]. Genotyping was performed on postnatal day (P)7-10 using primers 1700 S (TCCATGGTT TCGCGAGAGCG), 1842 AS (TCCCTATTGGGACG-CAGTGG) and 2394 AS (CAGCATCATGACAATGTCTCCA).

Primary antibodies. The anti-*Shank2* SA5193 antibody has been characterized previously [25] the following antibodies were from commercial suppliers: anti-GluA1 (Cat. No. 182 003), anti-GluA2 (Cat. No. 182 103), anti-Nlgn3 (Cat. No. 129 113) (all Synaptic Systems, Goettingen, Germany), anti-β3-Tubulin (Cat. No. MRB-435P) (Covance, Brussels, Belgium) and Aldolase C (Cat. No. 12065) (Santa Cruz, Dallas, U.S.A.)

Golgi stainings. Adult mouse cerebella were dissected and prepared using the FD Rapid GolgiStain Kit (NeuroTechnologies, Vilnius, Lithuania). Serial coronal sections of 150 µm

were collected from WTs and global *Shank2*$^{-/-}$ mice and Z-stack images were taken using an upright Axioscope (Carl Zeiss, Jena, Germany). Distal dendrites of Purkinje cells were traced for spine analysis.

Electron microscopy, Immunohistochemistry, Electrophysiology and revevant behavioral tests. For details refer to previous Chapters.

Data analysis. In the text, mean ± SD values are presented, in the figures SEM-values are reported, and p-values smaller than 0.05 are considered significantly different. Two-sided Student's *t*-tests were performed, unless stated otherwise. Additionally, since the L7-Cre line was shown to reveal germline deletions and since the potential impact of cerebellar Purkinje cells on general cognitive tests is widely debated[62,63], we have checked for heterozygous germline deletions in our L7-Shank2 mice and statistically excluded the possibility they could have influenced our conclusions on the non-cerebellar paradigms.

REFERENCES

1. Chen, J.A.*, et al.* The Emerging Picture of Autism Spectrum Disorder: Genetics and Pathology. *Annual Review of Pathology: Mechanisms of Disease* 10, 111-144 (2015).
2. Kanner, L. Autistic disturbances of affective contact. *Nervous child* 2, 217-250 (1943).
3. Zwaigenbaum, L., Bryson, S. & Garon, N. Early identification of autism spectrum disorders. *Behavioural brain research* 251, 133-146 (2013).
4. Sears, L.L., Finn, P.R. & Steinmetz, J.E. Abnormal classical eye-blink conditioning in autism. *Journal of autism and developmental disorders* 24, 737-751 (1994).
5. Oristaglio, J.*, et al.* Children with autism spectrum disorders show abnormal conditioned response timing on delay, but not trace, eyeblink conditioning. *Neuroscience* 248, 708-718 (2013).
6. Takarae, Y.*, et al.* Pursuit eye movement deficits in autism. *Brain* 127, 2584-2594 (2004).
7. Schmitt, L.M., Cook, E.H., Sweeney, J.A. & Mosconi, M.W. Saccadic eye movement abnormalities in autism spectrum disorder indicate dysfunctions in cerebellum and brainstem. *Molecular autism* 5, 47 (2014).
8. Marko, M.K.*, et al.* Behavioural and neural basis of anomalous motor learning in children with autism. *Brain* 138, 784-797 (2015).
9. Mostofsky, S.H., Goldberg, M.C., Landa, R.J. & Denckla, M.B. Evidence for a deficit in procedural learning in children and adolescents with autism: implications for cerebellar contribution. *Journal of the International Neuropsychological Society* 6, 752-759 (2000).
10. Memari, A.H., Ghanouni, P., Shayestehfar, M. & Ghaheri, B. Postural control impairments in individuals with autism spectrum disorder: a critical review of current literature. *Asian journal of sports medicine* 5(2014).
11. Stins, J.F.*, et al.* Attentional and sensory contributions to postural sway in children with autism spectrum disorder. *Gait & Posture* (2015).
12. Schmahmann, J.D. The role of the cerebellum in cognition and emotion: personal reflections since 1982 on the dysmetria of thought hypothesis, and its historical evolution from theory to therapy. *Neuropsychology review* 20, 236-260 (2010).
13. Allen, G. The cerebellum in autism. *Clinical Neuropsychiatry* 2, 321-337 (2005).
14. Bailey, A.*, et al.* A clinicopathological study of autism. *Brain* 121, 889-905 (1998).

15. Stoodley, C.J. Distinct regions of the cerebellum show gray matter decreases in autism, ADHD, and developmental dyslexia. *Frontiers in systems neuroscience* 8(2014).
16. Menashe, I.*, et al.* Co-expression profiling of autism genes in the mouse brain. *PLoS computational biology* 9, e1003128 (2013).
17. Grabrucker, A.M., Schmeisser, M.J., Schoen, M. & Boeckers, T.M. Postsynaptic ProSAP/Shank scaffolds in the cross-hair of synaptopathies. *Trends in cell biology* 21, 594-603 (2011).
18. Zoghbi, H.Y. & Bear, M.F. Synaptic dysfunction in neurodevelopmental disorders associated with autism and intellectual disabilities. *Cold Spring Harbor perspectives in biology* 4, a009886 (2012).
19. Bourgeron, T. From the genetic architecture to synaptic plasticity in autism spectrum disorder. *Nature Reviews Neuroscience* 16, 551-563 (2015).
20. Leblond, C.S.*, et al.* Genetic and functional analyses of SHANK2 mutations suggest a multiple hit model of autism spectrum disorders. *PLoS Genet* 8, e1002521 (2012).
21. Durand, C.M.*, et al.* Mutations in the gene encoding the synaptic scaffolding protein SHANK3 are associated with autism spectrum disorders. *Nat Genet* 39, 25-27 (2007).
22. Berkel, S.*, et al.* Mutations in the SHANK2 synaptic scaffolding gene in autism spectrum disorder and mental retardation. *Nature genetics* 42, 489-491 (2010).
23. Sato, D.*, et al.* SHANK1 Deletions in Males with Autism Spectrum Disorder. *Am J Hum Genet* 90, 879-887 (2012).
24. Mei, Y.*, et al.* Adult restoration of Shank3 expression rescues selective autistic-like phenotypes. *Nature* 530, 481-484 (2016).
25. Schmeisser, M.J.*, et al.* Autistic-like behaviours and hyperactivity in mice lacking ProSAP1/Shank2. *Nature* 486, 256-260 (2012).
26. Won, H.*, et al.* Autistic-like social behaviour in Shank2-mutant mice improved by restoring NMDA receptor function. *Nature* 486, 261-265 (2012).
27. Böckers, T.M.*, et al.* Differential expression and dendritic transcript localization of Shank family members: identification of a dendritic targeting element in the 3' untranslated region of Shank1 mRNA. *Molecular and Cellular Neuroscience* 26, 182-190 (2004).
28. Boeckers, T.M.*, et al.* Proline-rich synapse-associated proteins ProSAP1 and ProSAP2 interact with synaptic proteins of the SAPAP/GKAP family. *Biochemical and biophysical research communications* 264, 247-252 (1999).
29. Leblond, C.S.*, et al.* Meta-analysis of SHANK mutations in autism spectrum disorders: a gradient of severity in cognitive impairments. *PLoS genetics* 10, e1004580 (2014).
30. Sala, C.*, et al.* Shank synaptic scaffold proteins: keys to understanding the pathogenesis of autism and other synaptic disorders. *Journal of neurochemistry* (2015).
31. Hashimoto, K. & Kano, M. Functional differentiation of multiple climbing fiber inputs during synapse elimination in the developing cerebellum. *Neuron* 38, 785-796 (2003).
32. Schonewille, M.*, et al.* Purkinje cell-specific knockout of the protein phosphatase PP2B impairs potentiation and cerebellar motor learning. *Neuron* 67, 618-628 (2010).
33. Zhou, H.*, et al.* Cerebellar modules operate at different frequencies. *eLife*, e02536-e02536 (2014).
34. Wulff, P.*, et al.* Synaptic inhibition of Purkinje cells mediates consolidation of vestibulo-cerebellar motor learning. *Nature neuroscience* 12, 1042-1049 (2009).
35. Häusser, M. & Clark, B.A. Tonic synaptic inhibition modulates neuronal output pattern and spatiotemporal synaptic integration. *Neuron* 19, 665-678 (1997).
36. Boeckers, T.M.*, et al.* Proline-rich synapse-associated protein-1/cortactin binding protein 1 (ProSAP1/CortBP1) is a PDZ-domain protein highly enriched in the postsynaptic density. *The Journal of neuroscience* 19, 6506-6518 (1999).
37. Veloz, M.F.V.*, et al.* Cerebellar control of gait and interlimb coordination. *Brain Structure and Function*, 1-24 (2014).
38. De Zeeuw, C.I. & Ten Brinke, M.M. Motor Learning and the Cerebellum. *Cold Spring Harbor perspectives in biology* 7, a021683 (2015).

39. ten Brinke, M.M., *et al.* Evolving Models of Pavlovian Conditioning: Cerebellar Cortical Dynamics in Awake Behaving Mice. *Cell Rep* 13, 1977-1988 (2015).
40. Becker, E.B. & Stoodley, C.J. Autism spectrum disorder and the cerebellum. *International review of neurobiology* 113, 1 (2013).
41. Koekkoek, S.K.E., *et al.* Deletion of FMR1 in Purkinje cells enhances parallel fiber LTD, enlarges spines, and attenuates cerebellar eyelid conditioning in Fragile X syndrome. *Neuron* 47, 339-352 (2005).
42. Baudouin, S.J., *et al.* Shared synaptic pathophysiology in syndromic and nonsyndromic rodent models of autism. *Science* 338, 128-132 (2012).
43. Piochon, C., *et al.* Cerebellar plasticity and motor learning deficits in a copy-number variation mouse model of autism. *Nature communications* 5(2014).
44. Tsai, P.T., *et al.* Autistic-like behaviour and cerebellar dysfunction in Purkinje cell Tsc1 mutant mice. *Nature* 488, 647-651 (2012).
45. Kloth, A.D., *et al.* Cerebellar associative sensory learning defects in five mouse autism models. *eLife* 4, e06085 (2015).
46. Belmeguenai, A., *et al.* Intrinsic plasticity complements long-term potentiation in parallel fiber input gain control in cerebellar Purkinje cells. *The Journal of neuroscience* 30, 13630-13643 (2010).
47. Jiang, Y.-h. & Ehlers, M.D. Modeling Autism by< i> SHANK</i> Gene Mutations in Mice. *Neuron* 78, 8-27 (2013).
48. De Zeeuw, C.I., *et al.* Spatiotemporal firing patterns in the cerebellum. *Nature Reviews Neuroscience* 12, 327-344 (2011).
49. van Alphen, A.M. & De Zeeuw, C.I. Cerebellar LTD facilitates but is not essential for long-term adaptation of the vestibulo-ocular reflex. *Eur J Neurosci* 16, 486-490 (2002).
50. Arons, M.H., *et al.* Autism-associated mutations in ProSAP2/Shank3 impair synaptic transmission and neurexin-neuroligin-mediated transsynaptic signaling. *J Neurosci* 32, 14966-14978 (2012).
51. Szapiro, G. & Barbour, B. Multiple climbing fibers signal to molecular layer interneurons exclusively via glutamate spillover. *Nat Neurosci* 10, 735-742 (2007).
52. Badura, A., *et al.* Climbing fiber input shapes reciprocity of Purkinje cell firing. *Neuron* 78, 700-713 (2013).
53. Galliano, E., *et al.* Silencing the majority of cerebellar granule cells uncovers their essential role in motor learning and consolidation. *Cell reports* 3, 1239-1251 (2013).
54. Barski, J.J., Dethleffsen, K. & Meyer, M. Cre recombinase expression in cerebellar Purkinje cells. *genesis* 28, 93-98 (2000).
55. Schmidt-Supprian, M. & Rajewsky, K. Vagaries of conditional gene targeting. *Nat Immunol* 8, 665-668 (2007).
56. Kobayashi, Y. & Hensch, T.K. Germline recombination by conditional gene targeting with Parvalbumin-Cre lines. *Front Neural Circuits* 7, 168 (2013).
57. Mosconi, M.W., *et al.* The role of cerebellar circuitry alterations in the pathophysiology of autism spectrum disorders. *Front Neurosci* 9, 296 (2015).
58. Wang, S.S.H., Kloth, A.D. & Badura, A. The cerebellum, sensitive periods, and autism. *Neuron* 83, 518-532 (2014).
59. Silva-Santos, S., *et al.* Ube3a reinstatement identifies distinct developmental windows in a murine Angelman syndrome model. *J Clin Invest* 125, 2069-2076 (2015).
60. Coesmans, M., Weber, J.T., De Zeeuw, C.I. & Hansel, C. Bidirectional parallel fiber plasticity in the cerebellum under climbing fiber control. *Neuron* 44, 691-700 (2004).
61. van Woerden, G.M., *et al.* betaCaMKII controls the direction of plasticity at parallel fiber-Purkinje cell synapses. *Nat Neurosci* 12, 823-825 (2009).
62. Galliano, E., *et al.* Synaptic transmission and plasticity at inputs to murine cerebellar Purkinje cells are largely dispensable for standard nonmotor tasks. *J Neurosci* 33, 12599-12618 (2013).
63. Rochefort, C., *et al.* Cerebellum shapes hippocampal spatial code. *Science* 334, 385-389 (2011).